REPORT NO. FAA-75-6
FAA-RD-75-40

ATCRBS ANTENNA MODIFICATION KIT

E. M. Newman
P. Kendrick

Hazeltine Corporation
Greenlawn NY 11740

JUNE 1976

FINAL REPORT

Prepared for
U.S. DEPARTMENT OF TRANSPORTATION
FEDERAL AVIATION ADMINISTRATION
Systems Research and Development Service
Washington DC 20591

Technical Report Documentation Page

1. Report No.	2. Government Accession No.	3. Recipient's Catalog No.
FAA-RD-75-40		

4. Title and Subtitle	5. Report Date
ATCRBS ANTENNA MODIFICATION KIT	June 1976
	6. Performing Organization Code
	8. Performing Organization Report No.
7. Author(s)	DOT-TSC-FAA-75-6
E. M. Newman, P. Kendrick	
9. Performing Organization Name and Address	10. Work Unit No. (TRAIS)
Hazeltine Corporation *	FA519/R6112
Greenlawn NY 11740	11. Contract or Grant No.
	DOT-TSC-598
	13. Type of Report and Period Covered
12. Sponsoring Agency Name and Address	Final Report
U.S. Department of Transportation	Aug.1973 to Mar. 1974
Federal Aviation Administration	
Systems Research and Development Service	14. Sponsoring Agency Code
Washington. DC 20591	

15. Supplementary Notes

*Under contract to: U.S. Department of Transportation
Transportation Systems Center
Kendall Square
Cambridge MA 02142

16. Abstract

This report describes the design, fabrication and test results of an improved ATCRBS (Air Traffic Control Radar Beacon System) array antenna for mounting on the reflector of an ASR radar antenna.

The antenna consists of a 4-foot high by 26-foot wide array with 252 dipole radiating elements. The structure of the antenna utilizes a specially designed tuned reflector to provide a physically open ground plane which minimizes wind loading while maintaining low backlobe levels. A companion 4-foot high omni antenna, intended for mounting on a pole next to the array, was fabricated and tested, and is also described.

The work was performed under the cognizance of the Air Traffic Control Product Line of Hazeltine, with technical direction by the Wheeler Laboratory antenna group.

17. Key Words	18. Distribution Statement
Antenna Radar Beacon Tuned Reflector Air Traffic Control	DOCUMENT IS AVAILABLE TO THE PUBLIC THROUGH THE NATIONAL TECHNICAL INFORMATION SERVICE, SPRINGFIELD, VIRGINIA 22161

19. Security Classif. (of this report)	20. Security Classif. (of this page)	21. No. of Pages	22. Price
Unclassified	Unclassified	186	

Form DOT F 1700.7 (8-72) Reproduction of completed page authorized

PREFACE

The Open Array Antenna development was performed by the Hazeltine Corporation of Greenlawn, New York under contract to the Department of Transportation, Transportation Systems Center, (DOT/TSC) of Cambridge, Massachusetts and was part of their Air Traffic Control Radar Beacon System (ATCRBS) improvement program.

A prime objective of that program was the improvement of the ATCRBS Antenna performance by reducing the vertical lobing problem of the existing antennas. The Hazeltine approach was the development of a direct replacement for the ATCRBS Linear Array Antenna presently being used in the terminal and enroute installations. Although the antenna developed for this prupose can be used for either installation, the work described in this report chiefly addresses the problems associated with the Terminal Antenna.

The Open Array Technique used in this development allowed the use of a larger vertical aperture antenna by minimizing the mechanical penalties of weight, overturning moment, and running torque requirements associated with large area antennas. The results have indicated the feasibility of this technique and Hazeltine acknowledges the assistance and encouragement of the Transportation Systems Center and the Federal Aviation Administration throughout the program.

METRIC CONVERSION FACTORS

Approximate Conversions to Metric Measures

Symbol	When You Know	Multiply by	To Find	Symbol
		LENGTH		
in	inches	2.5	centimeters	cm
ft	feet	30	centimeters	cm
yd	yards	0.9	meters	m
mi	miles	1.6	kilometers	km
		AREA		
in^2	square inches	6.5	square centimeters	cm^2
ft^2	square feet	0.09	square meters	m^2
yd^2	square yards	0.8	square meters	m^2
mi^2	square miles	2.6	square kilometers	km^2
	acres	0.4	hectares	ha
		MASS (weight)		
oz	ounces	28	grams	g
lb	pounds	0.45	kilograms	kg
	short tons (2000 lb)	0.9	tonnes	t
		VOLUME		
tsp	teaspoons	5	milliliters	ml
Tbsp	tablespoons	15	milliliters	ml
fl oz	fluid ounces	30	milliliters	ml
c	cups	0.24	liters	l
pt	pints	0.47	liters	l
qt	quarts	0.95	liters	l
gal	gallons	3.8	liters	l
ft^3	cubic feet	0.03	cubic meters	m^3
yd^3	cubic yards	0.76	cubic meters	m^3
		TEMPERATURE (exact)		
°F	Fahrenheit temperature	5.9 (after subtracting 32)	Celsius temperature	°C

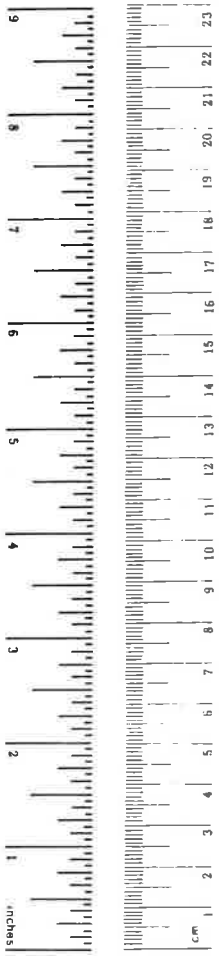

Approximate Conversions from Metric Measures

Symbol	When You Know	Multiply by	To Find	Symbol
		LENGTH		
mm	millimeters	0.04	inches	in
cm	centimeters	0.4	inches	in
m	meters	3.3	feet	ft
m	meters	1.1	yards	yd
km	kilometers	0.6	miles	mi
		AREA		
cm^2	square centimeters	0.16	square inches	in^2
m^2	square meters	1.2	square yards	yd^2
km^2	square kilometers	0.4	square miles	mi^2
ha	hectares (10,000 m^2)	2.5	acres	
		MASS (weight)		
g	grams	0.035	ounces	oz
kg	kilograms	2.2	pounds	lb
t	tonnes (1000 kg)	1.1	short tons	
		VOLUME		
ml	milliliters	0.03	fluid ounces	fl oz
l	liters	2.1	pints	pt
l	liters	1.06	quarts	qt
l	liters	0.26	gallons	gal
m^3	cubic meters	35	cubic feet	ft^3
m^3	cubic meters	1.3	cubic yards	yd^3
		TEMPERATURE (exact)		
C	Celsius temperature	9.5 (then add 32)	Fahrenheit temperature	°F

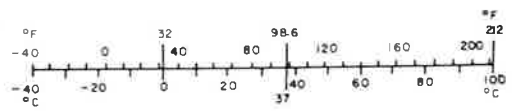

CONTENTS

CONTENTS (Cont)

APPENDIXES

ILLUSTRATIONS

ILLUSTRATIONS (Cont)

TABLES

1. INTRODUCTION

1.1 DESIGN OBJECTIVES

1.1.1 Basic Objective

The basic objective of the ATCRBS Antenna Modification Kit program was to design, fabricate and test an improved performance replacement for the existing beacon antenna in order to enhance overall system operational reliability. The present beacon antenna and similar linear arrays have serious performance limitations because of their limited vertical aperture. The ground in front of the antenna is strongly illuminated because the small vertical aperture results in a broad vertical pattern. As a result, at many sites located in flat open areas, there is very significant vertical lobing, which causes signal loss and/or excess interrogations. In addition, in order to avoid signal loss in the deep nulls, the power and sensitivity must be increased, thus resulting in more false reflected targets from nearby buildings, fences, and hilly terrain.

The ideal elevation pattern would be one which is zero for all angles below the horizon, then rises to maximum gain over a sector extending from the horizon up to the maximum elevation angle at which coverage is required. Unfortunately, this abrupt increase in gain at the horizon requires a very large vertical aperture. In practice, the vertical aperture is limited by mechanical and cost constraints. Since the open array antenna is intended to be mounted on the ASR, the maximum height was limited to 4 feet because of the wind loads imposed on the ASR reflector by the array. Figure 1-1 shows a comparison of the measured elevation patterns of a present ATCRBS antenna and the open array antenna. Note that the open array antenna pattern cuts off more sharply below the horizon and that much less power is radiated toward the ground.

The effect of this sharp cutoff on the vertical lobing is shown in figure 1-2, a plot of the free space patterns from 0 to +15 degrees elevation with the limits of the lobing calculated for flat earth with dry sandy loam soil. This is perhaps the worst case, but unfortunately it is approximately the situation at many ASR sites. A significant increase of the signal strength in lobing minima is provided by the open array antenna at the critical low elevation angles. This will substantially alleviate the problem

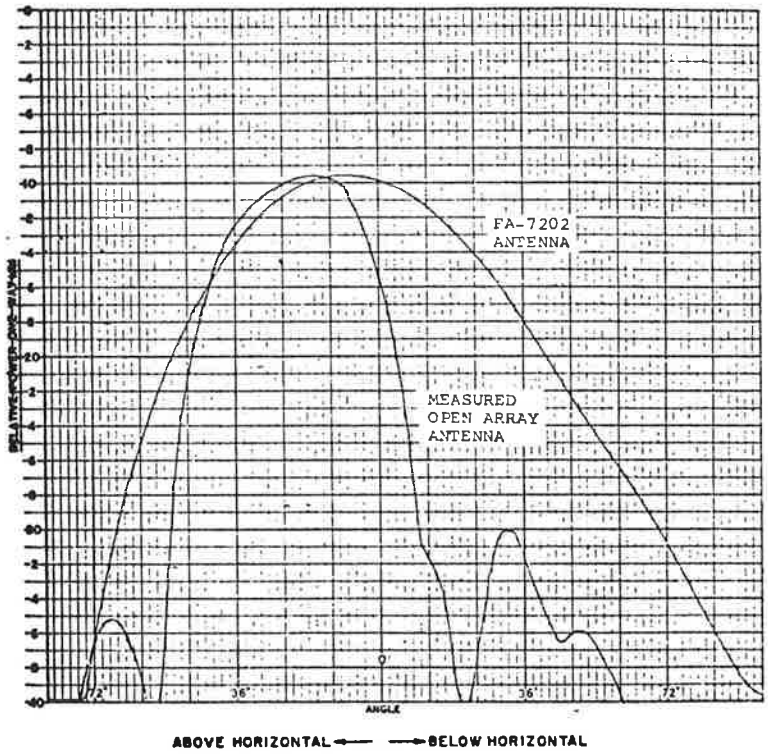

Figure 1-1. Comparison of Elevation Patterns

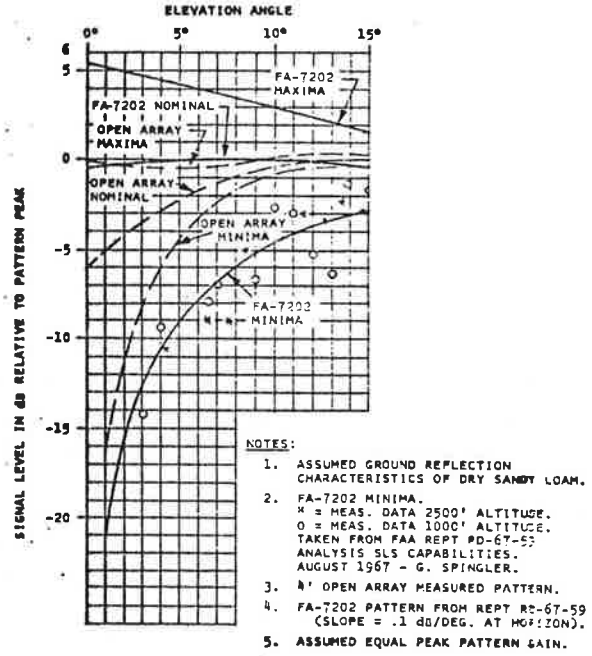

Figure 1-2. Vertical Lobing Envelopes

of missed targets caused by signal loss in the vertical lobing minima. A corresponding significant decrease in the lobing maxima will reduce the beacon system interference problem occurring when several interrogators are in the same region. Another major benefit that will result from the sharp cutoff elevation pattern of the open array is a major reduction of false targets that are caused by reflecting objects near or below the horizon. Additional benefits will be a major reduction of multiple, in-line targets caused by reply reflections from distant rising ground, and a major reduction of azimuth splits and angle errors caused by reflections from hilly terrain or laterally sloping ground.

1.1.2 Detailed Objectives

Significant detailed objectives of the development program included the following:

Direct replacement for the present antenna (size, weight and wind loads comparable)

21 dB gain minimum

Low azimuth sidelobes (-25 dB nominal relative to peak at same elevation angle)

Backlobe more than 21 dB down

Independent optimum sum and difference patterns for monopulse operation

Operating conditions including 85-knot winds and 1-1/2 inches of radial ice

Survival conditions including 130-knot winds and 1-1/2 inches of radial ice

Companion omni antenna with same elevation pattern

1.2 ANTENNA DESCRIPTION

The ATCRBS antenna modification consists of a 4-foot high omni antenna and a 4-foot by 26-foot open array antenna which mounts on top of the existing ASR reflector. Both antennas are shown

installed at NAFEC, Atlantic City, N.J., in figure 1-3. The open array antenna consists of 36 columns of dipoles with a total of 252 radiating elements. The dipoles are mounted on 2-inch diameter tubes which house the coaxial feed cables. Tuned reflector rods, used to suppress backlobe radiation, are mounted between the columns of dipoles, as shown in figure 1-4. The rf power dividing networks are housed in a channel at the bottom of the antenna. A backup structure provides additional support for mounting the open array on the ASR reflector. The omni antenna consists of one column of six double-dipole printed circuit elements (figure 1-5) housed in a cylindrical radome (figure 1-6). The elevation feed network for the omni antenna is mounted in an enclosure below the radiating column. Semi-rigid cables connect the six dipole elements to the elevation network.

1.3 PERFORMANCE ACHIEVED AND LIMITATIONS

1.3.1 Electrical Performance

The electrical performance of the open array antenna and the omni antenna was measured on Hazeltine's 1000-foot test range at Smithtown, N.Y. To ensure the validity of the open array measurements made on the relatively short Smithtown range, the open array was also tested on ESSCO's 2000-foot antenna test range in Concord, Mass. The two ranges showed excellent agreement in the measured data. A description of the test ranges and detailed test results can be found in paragraph 2.3. A summary of all the antenna performance measurements and the associated design specifications (Appendix B) is listed in table 1-1. A review of the data shows that the specifications were exceeded in most instances and the intent of the specifications was satisfied in all instances.

1.3.2 Mechanical Evaluation

The open array structure was mechanically designed for continuous exposed operation, including operation with 1.5 inches of radial ice at wind velocities of 85 knots. The type tests, described in paragraph 2.4, have demonstrated that the antenna can operate without electrical degradation under these conditions. Calculations contained in the Phase I study report demonstrate that the array can survive conditions of 1.5 inches of radial ice and 130-knot wind velocities. The study also concluded that under a combination

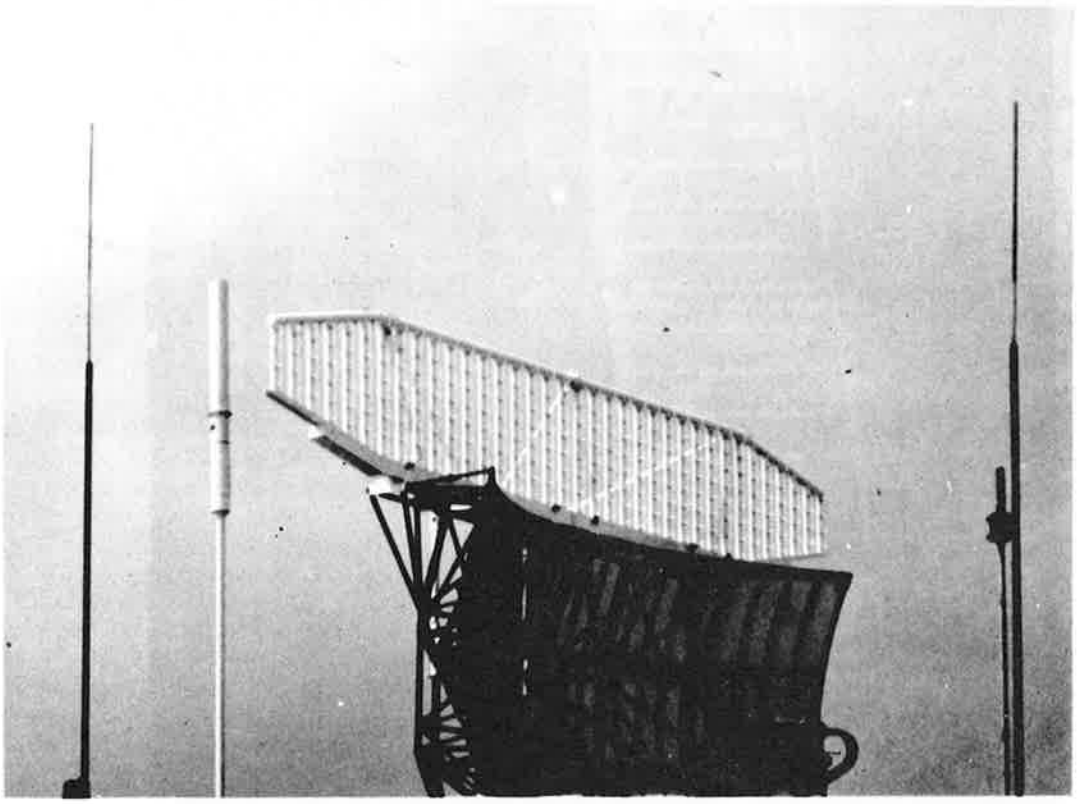

Figure 1-3. Open Array and Omni Antennas Installed

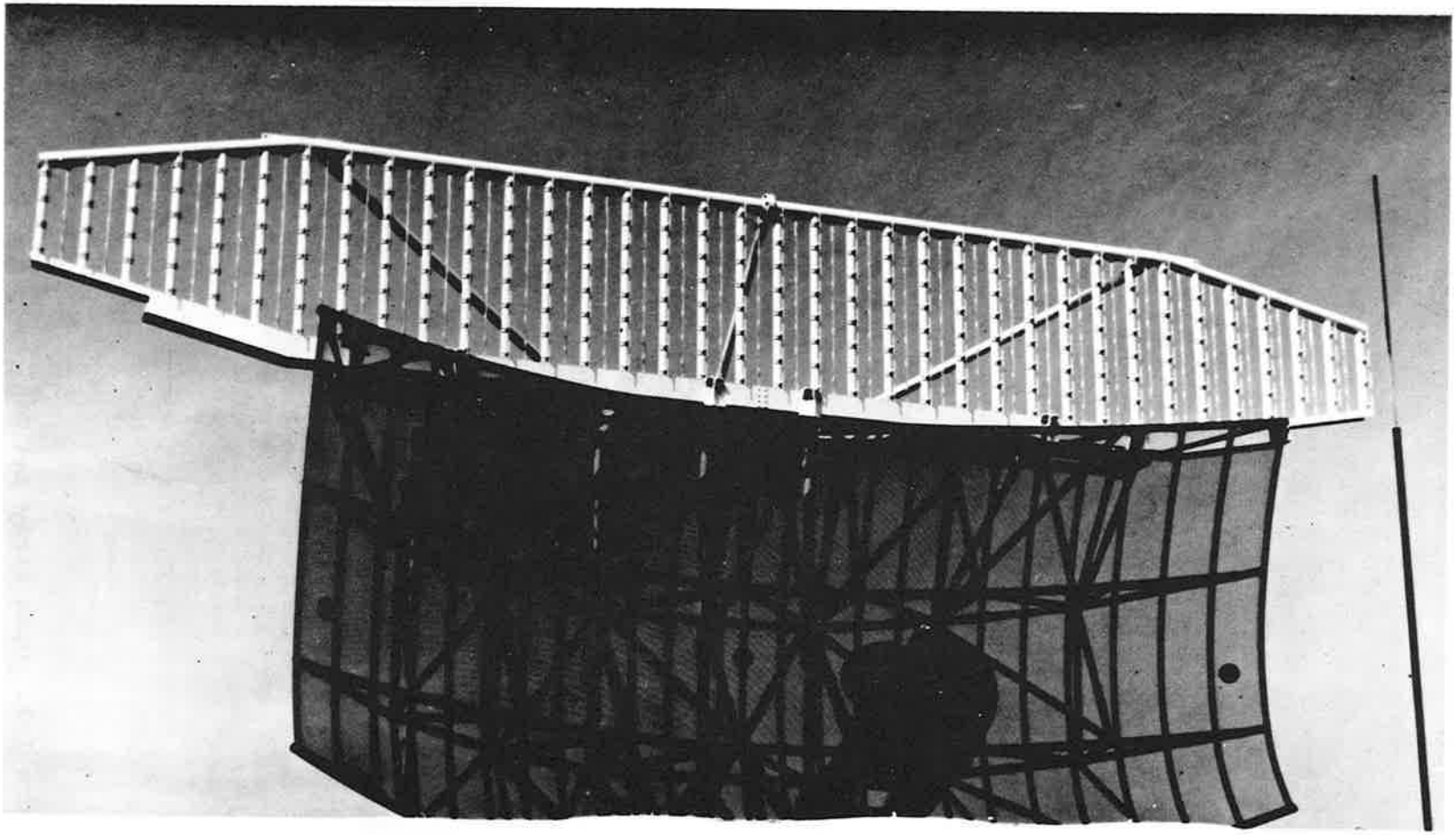

Figure 1-4. Open Array Antenna

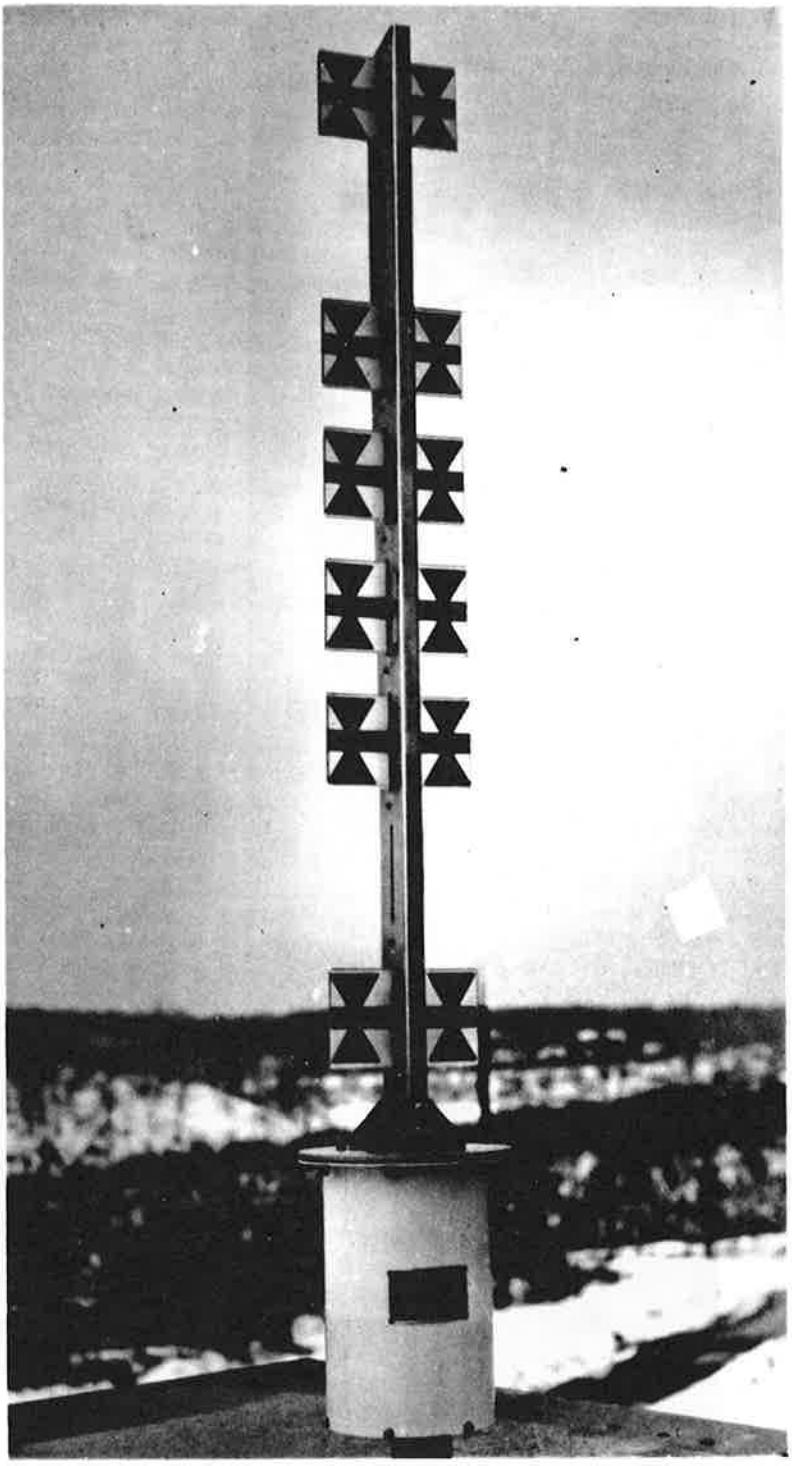

Figure 1-5. Omni Antenna without Radome

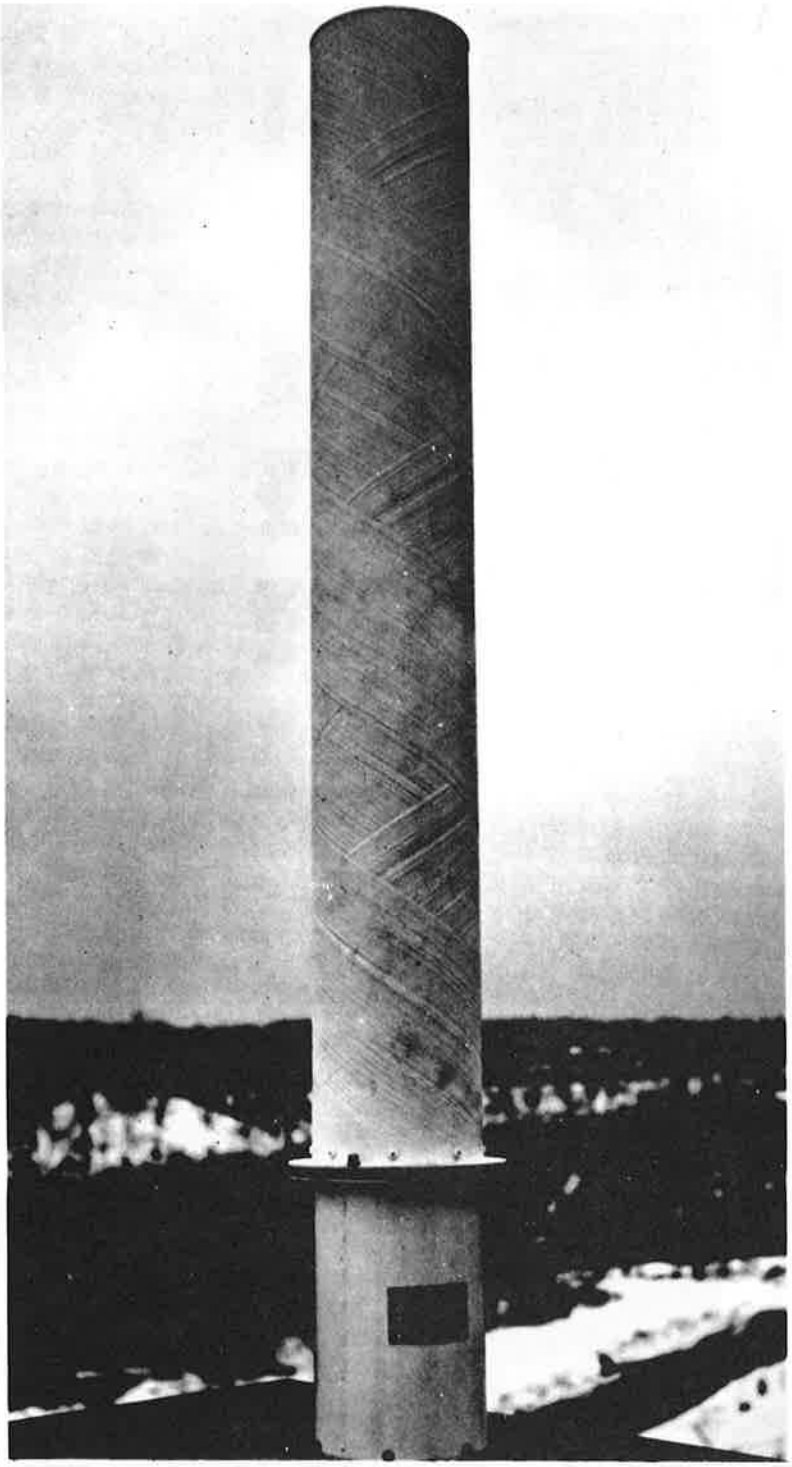

Figure 1-6. Omni Antenna with Radome

of winds greater than 65 knots and simultaneous ice loading greater than 1 inch of radial ice, the loads imposed on the ASR reflector would be greater than normal. The degradation of radar performance under these conditions was considered acceptably small. The open array antenna met all mechanical design goals with the exception of weight. The weight of the completed antenna was approximately 120 pounds greater than the design goal of 380 pounds. This increase is considered insignificant in comparison with the considerable weight of ice which the ASR reflector alone must be capable of supporting.

TABLE 1-1. SUMMARY OF ATCRBS MOD KIT PERFORMANCE

Parameter	Ref Para Appendix B	Design Goal	Measured
Directional Pattern			
Gain	1.4.1	21.0 dB	22.9 dB at 1030 MHz 23.1 dB at 1090 MHz (including filter loss)
Azimuth Beamwidth 1030 MHz			
Horizon (3 dB)	1.4.2	2.1° to 2.6°	2.45°
Horizon (10 dB)	1.4.2	<4.5°	4.3°
From -2° to +25°	1.4.2	Horizon ±15%	+13%
Azimuth Beamwidth 1090 MHz			
Horizon (3 dB)	1.4.6	2.1° to 2.6°	2.3°
Horizon (10 dB)	1.4.6	<4.5°	4.0°
From -2° to +25°	1.4.6	Horizon ±15%	+9%
Azimuth Sidelobe 1030 and 1090 MHz (referenced to peak at the same elevation angle)			
-2° to 0° elevation	1.4.2, 1.4.6	-15 dB	-25 dB
0° to 5° elevation	1.4.2, 1.4.6	-21 dB	-25 dB
+5° to +25° elevation	1.4.2, 1.4.6	-25 dB	-25 dB
Azimuth backlobes	1.4.2, 1.4.6	-21 dB	-21 dB
Elevation Pattern 1030, 1090 MHz			
Beam nose	1.4.4, 1.4.6	+13°	+14° (1030)
Min power +1° to +5° elevation	1.4.4, 1.4.6	-5 dB	-4.6 dB
Max power -1° elevation	1.4.4, 1.4.6	-7.5 dB	-6.6 dB
Max power <-9° elevation	1.4.4, 1.4.6	-20 dB	-19 dB
Ripple +5° to +30° elevation		3.0 dB	2.0 dB
Directional Beam Skew			
Lower 3 dB point to +25°	1.4.5	±0.3°	±0.1°
Directional Beam Squint			
1030/1090			
Lower 3 dB point to +25°	1.4.8	±0.2°	.05°
Cross Polarization Radiation			
1030/1090			
-2° to +25°	1.4.3, 1.4.7	<-15 dB	-30 dB (1030) -25 dB (1090)
VSWR			
Sum		1.5:1	1.42 (1030) 1.58 (1090) (with filter)
Diff		1.5:1	1.27 (1030) 1.08 (1090) (without filter)
EMI Filter			
Insertion loss 1015 to 1105 MHz	1.6	<1.0 dB	0.9 dB
Attenuation 1250 to 11000 MHz	1.6	>50 dB	-50 dB except -40 dB at 1550 MHz
Omni Antenna			
Omnidirectional pattern uniformity		±1.75 dB	±2 dB
Elevation pattern relative to directional	1.4.9	±2 dB	±2 dB
Cross polarization		<-15 dB	-15.5 dB
VSWR		1.5:1	1.27 (1030) (with filter)
Gain			4.4 dB (with filter)

2. OPEN ARRAY ANTENNA

2.1 MECHANICAL DESIGN

2.1.1 Main Antenna Structures

The open array antenna (figure 1-4) consists of a 4-foot high by 26-foot long dipole array with an associated backup structure. The dipole array structure contains 36 vertical 2-inch diameter aluminum tubes on 9-inch centers, which form the load-supporting members between the main horizontal supports. The vertical tubes are used to mount the individual dipole radiating elements and also function as part of the electrical ground plane of the antenna. Located on each side of the dipole mounting tubes are 35 vertical fiberglass-enclosed tuned reflector rods, which comprise the remainder of the electrical ground plane. These rods are fastened to the main horizontal supports. The main horizontal supports consist of a 3-inch diameter thin-walled aluminum tube on the top of the antenna, and a 4-inch by 1.72-inch by 0.32-inch structural channel on the bottom of the antenna. An aluminum sheetmetal enclosure housing the rf components is attached to the bottom channel. Both the top tubular support and the bottom channel have mounting flanges welded to them. The six flanges on the bottom channel allow for easy attachment of the open array antenna to the standard ASR reflector's ATCRBS antenna mounting points. Four of these six flanges are also used as support points for the backup structure, which also attaches to three flanges on the top tubular support. The backup structure itself, as shown in figure 2-1, contains three adjustable struts which connect to the three central trusses of the ASR. They are joined to a common horizontal 2-inch by 1/8-inch-wall tube which in turn has four members, also 2-inch by 1/8-inch-wall tubes, connecting to the bottom channel of the open array. The backup structure is completed by four diagonal members, one each to the top and bottom horizontal supports of the open array 8.3 feet left and right of the centerline, and by a 2-inch by 1/8-inch-wall centerline support from the top of the open array to the common horizontal member.

2.1.2 Mounting Arrangement

The open array antenna is mounted to the ASR reflector in nine places, as shown in figure 2-1. The tubular backup structure transmits overturning loads down to the strongest part of the

Figure 2-1. Open Array Antenna, Rear View

radar reflector truss. The three main struts which clamp to the trusswork are adjustable in length so that the tilt angle of the antenna relative to the radar can be varied. There are six mounting feet on the bottom of the open array antenna which are bolted to the existing mounting points for the "hogtrough" antenna. The feet locations are adjustable over a limited range to avoid interference problems with different radar reflectors. The feet are shimmed as required at installation to level the open array antenna. No modification is required to the ASR reflector itself. The overall 4-foot by 26-foot structure is designed to be separable into three sections; two 13-foot halves and the backup structure. This facilitates fabrication as well as transportation and installation of the antenna. It was found during testing of the open array antenna that the three sections could be conveniently handled by four men without the use of special equipment.

2.1.3 Weight Analysis

The mechanical design had as a major objective the achievement of the maximum strength-to-weight ratio necessary to meet both the operating and non-operating structural requirements. Lightweight materials were used throughout the antenna. The structural members were made of Aluminum Alloy 6061-T6. This alloy exhibits especially good strength-to-weight ratios and can be easily welded. The networks were designed using microwave printed circuit boards with an aluminum support plate for rigidity. The tuned reflectors used fiberglass tubes with aluminum rod segments inside. The weight breakdown of the antenna and its components is presented in table 2-1.

TABLE 2-1. WEIGHT BREAKDOWN, OPEN ARRAY ANTENNA (Pounds)

Dipoles		22
Cables		50
Elevation, Azimuth Networks		45
Tuned Reflectors		15
Structure & Enclosure		210
Mounting Flanges & Hardware		20
	Subtotal	362
Support Structure Main Weldment		54
6 Interface Brackets		60
3 Main Vertical Struts		24
	Subtotal	138
	Total	500

2.1.4 Dipole Construction

Details of the electrical design of the dipoles are presented in paragraph 2.2.2. Each dipole physically consists of an element and an rf connector encapsulated in epoxy resin. The dipole arms are reinforced with a fiberglass tube before they are potted using the injection moulding process. This method, which involves injection of epoxy under pressure into the mold, eliminates voids and surface imperfections. The dipole elements are mounted to contoured aluminum flanges, which in turn are fastened to the 2-inch diameter vertical tubes with two screws. This facilitates easy replacement should a dipole element malfunction or be damaged. The rf cables connecting the dipoles to their associated elevation networks (located in the aluminum enclosure attached to the bottom channel) are routed through the 2-inch diameter aluminum tubes. The dipole feed cables are coiled in the web area of the bottom channel before connection to the elevation networks, resulting in efficient space utilization and an organized packaging arrangement. A completed dipole element is shown in figure 2-2.

2.1.5 Elevation Network Construction

There are 36 elevation networks mounted in the aluminum enclosure attached to the bottom channel of the antenna, one for each of the 36 columns of dipoles. Each network is mounted to the side of the enclosure below the dipole column it feeds, whenever possible. Since the enclosure does not extend the entire length of the antenna, some networks are offset from the columns they feed. The networks themselves are stripline devices measuring 9 inches long, 3 inches wide and 3/8 inch thick. An aluminum plate is fixed to one side of the stripline for added rigidity and secure mounting. Protruding from each network are eight type SMA connectors for connection of the dipole feed cables, and one type TNC connector for connection of the feed cable from the azimuth network. Details of the electrical design of the elevation networks are presented in paragraphs 2.2.3 through 2.2.5. A completed elevation network is shown in figure 2-3.

2.1.6 Azimuth Network Construction

The azimuth distribution networks are stripline devices similar in construction to the elevation networks. They are 35 inches long, 3 inches wide and 3/8 inch thick. Twenty type TNC connectors are located on one side for connection of the rf power input cables and the feed cables to the elevation networks. The two

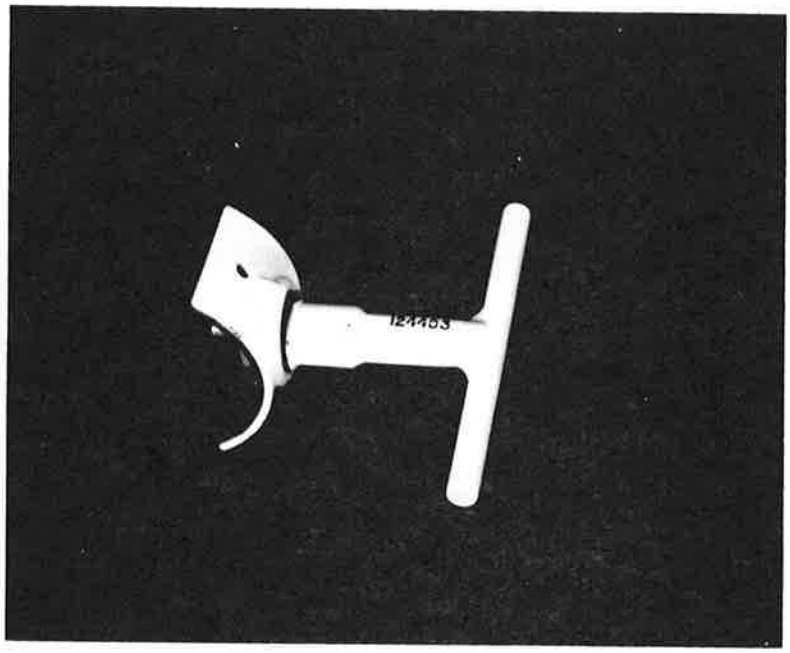

Figure 2-2. Open Array Dipole Element

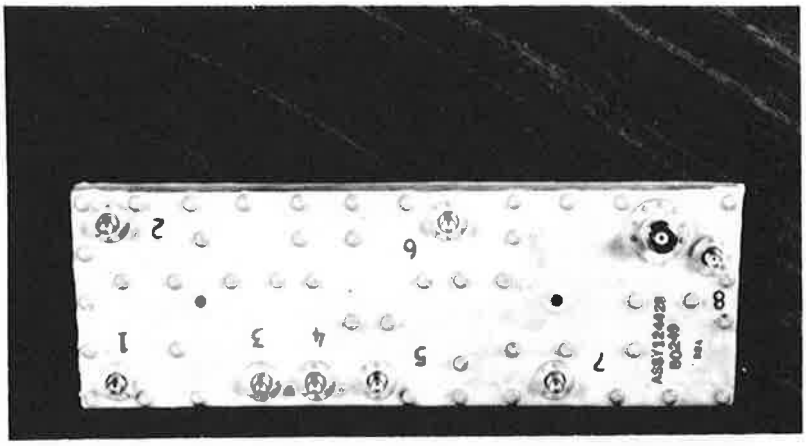

Figure 2-3. Elevation Network

azimuth networks used in the antenna are mounted in the enclosure at the bottom of the antenna. Details of the electrical design of the azimuth networks are presented in paragraphs 2.2.3, 2.2.4, and 2.2.6.

2.1.7 Enclosure Construction

As noted in paragraph 2.1.1, the aluminum sheetmetal enclosure attached to the bottom channel of the antenna is used to house the various rf components. Access panels for maintenance are located along the bottom of the enclosure, and allow for the installation and servicing of the rf components located inside. The central area of the enclosure has two protrusions on the back. The first protrusion extends 7 inches outward from the rear of the channel for 7 inches on each side of the centerline. The second protrusion extends 3 inches outward from the rear for 47 inches on each side of the centerline. The first protrusion houses the hybrids, couplers and feed connectors, and the second protrusion houses the azimuth networks. The elevation networks are mounted to the side of the enclosure. The foamflex feed cables from the azimuth networks to the elevation networks are also routed through the enclosure.

2.1.8 Tuned Reflector Construction

The 35 tuned reflector rods, along with the 2-inch diameter dipole mounting columns, make up the electrical ground plane of the antenna. These rods are designed to reflect the signal radiated towards the rear of the antenna by the dipoles, while simultaneously maximizing the antenna area that is left open to the wind. To achieve both goals, the reflector rods are tuned to obtain maximum reflection in a minimum physical diameter. Tuning of the reflector rods is accomplished by constructing them of metal segments separated by gaps, as shown in the simplified diagram of figure 2-4. This structure, at resonance, appears as a short circuit to an incident wave. The actual structure used in the antenna is shown in figure 2-5. The metal rod segments are 1/4-inch diameter aluminum rods. These rods are separated by dielectric disk spacers and stacked within a thin-walled dielectric sleeve. The entire column is compressed by a spring to eliminate air gaps. This assembly is then epoxied at each end inside a fiberglass tube, with dielectric spacers located midway along each rod segment to maintain the desired air gap. The fiberglass tube functions as a dielectric shield against the detuning effects of water and ice. The completed tuned reflector rod has a diameter of 0.625 inch and is attached by means of flanges to the antenna's 3-inch diameter top support and 4-inch bottom channel.

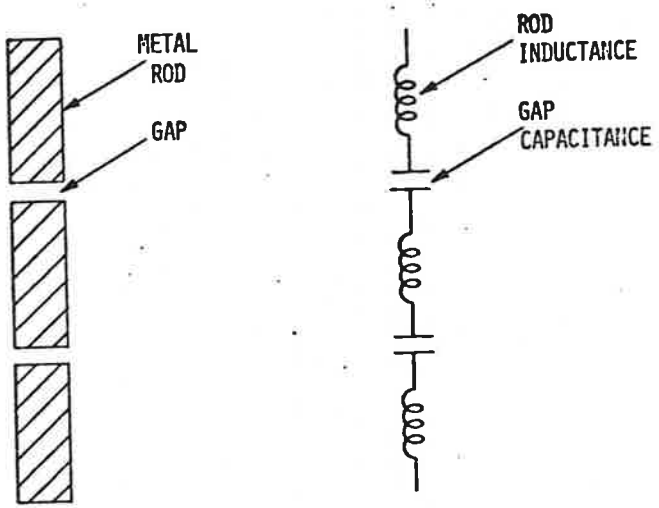

Figure 2-4. Tuned Reflector, Simplified Diagram

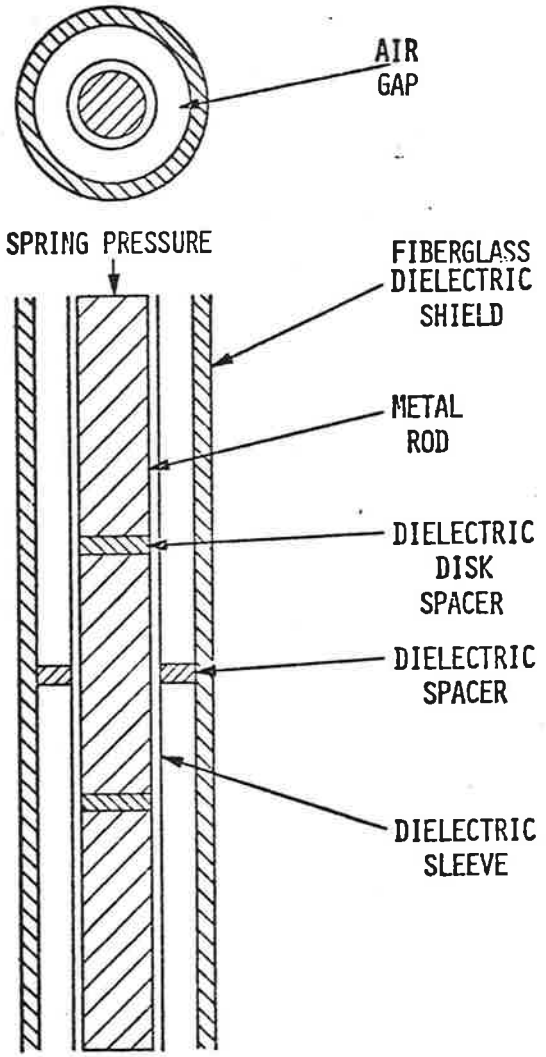

Figure 2-5. Tuned Reflector, Actual Construction

2.1.9 Vortex Shedding Analysis

An analysis of the induced vibration caused by vortex shedding on the 0.625-inch diameter tuned reflectors was performed. The major conclusions resulting from this study are that, although resonant stresses and deflections result from this phenomena, no significant effect on the structure or performance of the antenna will occur. The results and approach of the analysis are presented here. A more complete calculation is contained in the Phase I report. The resonant frequency of the tuned reflector is calculated first by treating it as fixed-end beam. By equating the natural frequency of the tuned reflector to the vortex shedding induced frequency, the critical wind velocity can be determined. The resulting calculated critical wind velocity of 7 knots, which produces resonant vibration, is well within the operational range. However, this presents neither a deflection nor a working stress problem. This is because the exciting force induced by vortex shedding is of relatively small magnitude. The fixed-end reflector could, therefore, be excited with the calculated force of $F_x = 0.029$ lb. sin ωt. With a reflector weight of 0.4 pound, the acceleration and amplitude of deflection of the reflector is 0.0003 inch. Assuming a very conservative transmissibility of 100 maximum through the reflector, a double amplitude of 0.061 inch will exist at mid-span, along with a 7.2 "G" acceleration. The corresponding stress at this point would be 562 psi. The stress of 562 psi induced by the vortex shedding phenomena is extremely low in this case, and results in a safety factor of 28 in the fiberglass reflector. The rod deflection of 0.03 inch is within the acceptable limits necessary for electrical performance. To ensure that vortex shedding does not present a problem at the higher harmonics of the fundamental frequency, calculations similar to the above were conducted with the results showing that higher stresses but lower reflector deflection would occur.

For example, the fourth harmonic of the reflector would have a natural frequency of 400 Hz which corresponds to a critical wind velocity of 60 knots. The vortex shedding force would be 2.17 pounds, or 5.4 "G"'s. Assuming a conservative transmissibility of 20, a 108 "G" acceleration and 0.0064-inch deflection occurs in each quarter length of the reflector. This stresses the rod to 1900 psi, which results in an adequate safety factor of 8.25. For the maximum survival specification of 130-knot winds, the respective vortex-induced frequency would be the fifth harmonic. The natural frequency of the reflector would be 826 Hz. The vortex shedding force would be 9.3 pounds or 23.2 "G"'s. Using

a transmissibility of 5 for this harmonic, the deflection and stress would calculate to 0.0003 inch and 5730 pounds, respectively, at each sixth length of the reflector. This results in a 2.8 safety factor. In conclusion, as wind velocity increases, vortex shedding critical frequencies increase and excite the tube at harmonics of its fundamental frequency. At each of these harmonics of the 44 Hz fundamental, vibrational deflections are not significant enough to affect electrical or structural performance of the antenna.

2.1.10 Environmental Design Considerations

The open array antenna is structurally designed and analyzed to operate at 15 rpm atop the ASR-7 in wind velocities up to 75 knots in all manners of precipitation, including encasement in 1-1/2-inch thick radial ice. The antenna is also designed to survive 130-knot winds in all types of precipitation including encasement in radial ice up to 1-1/2 inches thick. The open array antenna has been successfully tested to be within the maximum allowable deflection under a simulation of the worst combination of operating conditions. These are 1-1/2 inches of radial ice (0.9 specific gravity), 15 rpm and 85-knot winds striking at the worst angle. The loads imposed by these conditions are shown in figure 2-6. A wind load analysis, performed by a consulting firm, Applied Technology Associates, formed the basis for determining these loads. The deflection of the open array antenna under simulated worst-case environmental conditions was measured at the facilities of Long Island Metal, Inc., the fabricators of the open array structure. Detailed results of this test are presented in paragraph 2.4.1. Other major environmental parameters that the antenna is designed to meet are operating temperatures ranging from -50 C to +70 C, relative humidity from 5% to 100% including condensation due to temperature changes, altitudes to 12,000 feet above MSL and a maximum barometric pressure of 30.5 inches of mercury.

The design philosophy followed to accomplish this protection is to prevent moisture accumulation in the antenna and its enclosure. In addition, all components are coated to seal them against moisture. Each seam in the open array antenna is completely welded, thus assuring watertight integrity between the 3-inch diameter tubes, 2-inch diameter tubes, and the 4-inch structural channel. Aluminum alloy 6061-T6 is used for all structural members and exhibits excellent corrosion resistance. The enclosure located at the bottom of the antenna is also constructed of aluminum alloy 6061 sheet, with riveted interfaces sealed with Devcon F Adhesive Sealant. The removable access panels at the bottom of the antenna

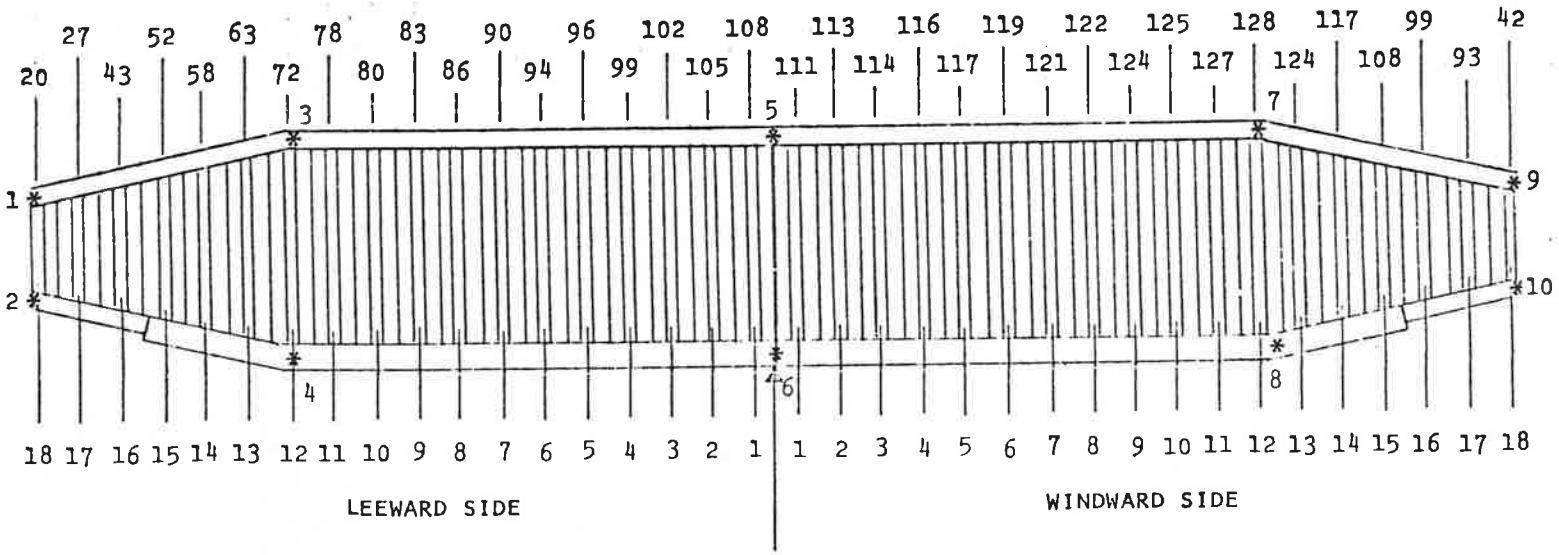

NOTES:

1. LOADS ARE IN POUNDS AND INCLUDE THE EFFECTS OF 15 RPM ROTATION AND ANTENNA ORIENTATION DURING MAXIMUM OPERATING CONDITIONS OF 1 1/2 IN. RADIAL ICE (SP=0.9) AND 85 KNOT WINDS.

2. (*) DENOTES 1-10 POINTS AT WHICH DEFLECTION MEASUREMENTS SHOULD BE MADE.

Figure 2-6. Open Array Antenna, Loads Under Worst Case Operating Conditions

are installed with silicone rubber gaskets to prevent moisture entry. Drain holes are provided in the bottom of the access panels to allow any condensation to escape. The entire exterior of the structure is primed with zinc chromate and painted in accordance with FAA-STD-003 Paint System BE-9, Color No. 17875 White Gloss per FED-STD-595.

The support structures necessary for ASR mounting, as well as all mounting flanges, are also finished in accordance with the above specification. The dipole mounting flanges are sealed against the 2-inch diameter tubes with silicone rubber gaskets. The networks are finished with RTV 3145, which is a white silicone sealant. This finish is very effective in sealing against moisture, and was humidity tested on a sample network. All cable connections made to the networks and dipoles are brush coated with MIL-V-173 varnish to ensure sealing and to supply a locking feature against vibration-induced loosening of connections. The outer dielectric shield of the tuned reflectors is constructed of glass-reinforced polyester resin. The exterior surface is primed and painted using white enamel. Color is Lusterless White No. 37875 per FED-STD-595. The tuned reflectors also have an epoxy filler at each end of the rod to prevent moisture from entering.

2.1.11 Load Analysis

One of the objectives of the design phase of the program was to minimize the structural impact of the open array antenna on the ASR antenna by duplicating as nearly as possible the wind loads and weight of the beacon antenna in the open array antenna design. Ideally this would result in only a marginal increase in total load as seen by the ASR antenna reflector, bearing and motor drive. Structurally, it became apparent that the critical environmental specification required of the 4-foot by 26-foot antenna was the maximum operating level of 85-knot winds, while rotating at 15 rpm with 1-1/2 inches radial ice covering the entire surface, even though the survival condition creates a much higher load situation.

The extreme environmental condition of a 1-1/2-inch thick radially iced antenna results in effectively closing the open structure to the wind. This greatly increases the total wind force on the antenna. Also, since the open array antenna has a greater surface area than the existing beacon antenna, there is an increase in the total weight of the ice load over the FA-7202 beacon antenna. To best distribute these increased loads, an extremely stiff backup structure and rigid interface mounting brackets are employed, although at a weight penalty. To determine the loads which the wind applies on the existing FA-7202 Beacon and ASR antenna pair and on the open array and ASR antenna pair in both

the iced and non-iced conditions, a detailed wind loading analysis was performed by Applied Technology Associates. The results of the wind load analysis are presented in tables 2-2, 2-3 and 2-4. From the results of the analysis it can be concluded that for the maximum survival and operating conditions, the total loads applied at the antenna's interface and the ASR pedestal bearing are greater for the 4-foot by 26-foot open array antenna. The effect of these increased loads on the ASR drive system and reflector are discussed in the interface analysis (paragraph 2.1.13) and structural analysis (paragraph 2.1.12), respectively. For the non-iced conditions, the loads are approximately the same, except for the overturning moment of the open array antenna, which has to be greater due to the longer moment arm to the center of pressure where the loads are applied on the 4-foot antenna aperture.

TABLE 2-2. SUMMARY OF WIND LOADS (Pounds)

Condition	7202 Beacon	4' x 26' Open Array	ASR Antenna
Survival Condition	3670	7257	9100
Maximum Operating (Iced)	1618	3215	5000
Maximum Operating (Non-iced)	1618	1691	3940

TABLE 2-3. SUMMARY OF OVERTURNING MOMENTS AT ANTENNA INTERFACE AND ASR BEARING (Foot-Pounds)

Condition	7202 at ASR Interface	7202 & ASR at Bearing	4' x 26' at ASR Interface	4' x 26' & ASR at Bearing
Survival Condition	3670	90,700	14,514	136,000
Maximum Operating (Iced)	1618	45,500	6,430	65,800
Maximum Operating (Non-iced)	1618	39,900	3,389	42,000

TABLE 2-4. SUMMARY OF AZIMUTH TORQUE BECAUSE OF WIND LOADS (Foot-Pounds)

Condition	7202 Beacon	4' x 26' Open Array	ASR Antenna
Maximum Operating (Iced)	2070	7700	4750
Maximum Operating (Non-iced)	2070	2060	2130

2.1.12 Structural Analysis

The design of the 4-foot by 26-foot open array antenna has been structurally analyzed and has been shown to have sufficient strength and rigidity to meet the survival and operational requirements. This analysis was performed by R. F. Systems Inc. in an early contract phase. The ASR-7 structure has also been treated in this analysis to determine the impact of the loads presented by the open array antenna for the operating and survival conditions. The results of this structural analysis, along with the design approach, are presented here for the open array and ASR antennas.

The material used throughout the welded open array antenna and mounting structures is aluminum alloy 6061-T6 which has yielded strength of 35,000 psi. However, annealing occurs in the welded zones causing a decrease in this yield strength. In these areas, 15,000 psi is used in the analysis. This number is conservative, since the American Welding Society Text Volume IV records a 22,000 psi yield strength for 6061-T6 heli-arc weld, using 4043 weld rod. The highest stresses occur during the survival conditions of 130-knot winds with 1-1/2 inches radial ice (specific gravity = 0.9) covering the entire 4-foot by 26-foot antenna and ASR antenna. Under these conditions a minimum margin of safety of 1.21 occurs in the open array antenna. (A margin of safety of 1.2 using 15KSI yield strength is effectively a margin of safety of 1.75 using the documented 22 KSI yield strength noted above.) This condition exists in the 3-inch diameter tube running horizontally across the top of the open array antenna. The minimum margins of safety for the ASR and open array antennas' support structures are 1.34 and 1.65, respectively. The minimum margin of safety for the ASR occurs in the lowermost rear vertical member in the second vertical truss section from the centerline of the antenna. The open array antenna support structure members with the 1.65 margin of safety are the long diagonal tubes supporting the top of the outer ends of the 4-foot by 26-foot structure.

The critical design condition, however, was to withstand the maximum operating conditions and still remain within allowable antenna deflection. This combination of conditions consists of 85-knot winds striking the antenna system rotating at 15 rpm with 1-1/2 inches of radial ice formation. The approach selected was to design a mounting structure that would minimize weight and wind resistance at the expense of allowing some deflections in the open array antenna. This structure has previously been described in paragraph 2.1.1. Under the maximum environmental operating conditions, the open array antenna and support structure were calculated and tested to be within the deflection specification requirements. The deflections experienced under the simulated loads, although within the specification requirements established by electrical performance parameters, are close to the acceptable limits. This indicates that under the given loading conditions, the open array antenna's designed strength-to-weight ratio is efficiently accomplished. This is not to say that weight reduction cannot take place at the sacrifice of strength, but rather that the antenna is not overdesigned at the penalty of weight for the required loading. It is expected that in production some areas can be reduced in weight without significantly decreasing the antenna's strength. Those areas include, but are not limited to, the backup structure, joint design, interface brackets, and adjustable struts. The antenna itself can be somewhat reduced in weight in areas of component design and the use of special extrusions, where quantities and conservative safety margins exist.

A simplified analysis was made of the ASR reflector structure to evaluate the effect of the loads imposed by the open array antenna under all environmental conditions. The conclusion reached was that under the worst-case operating conditions of 85-knot winds and 1-1/2 inches of ice on the open array antenna and ASR reflector, bending from the loads imposed on the reflector may result in marginal operation; with 85-knot winds and 1/2 inch of radial ice satisfactory operation is predicted. The analysis of the reflector consisted of two specific tasks. First, the stresses on specific structural members, under the survival conditions of 130-knot winds and 1-1/2 inches of radial ice on both the open array and ASR antennas, were calculated to determine margins of safety. These results were stated earlier (paragraph 2.1.11). Second, the deflections of the reflector tips under the maximum operating conditions were calculated. Figure 2-7 illustrates the structural model employed to compute margins of safety and deflection. This model is a conservative simplification of the actual structure. The model chosen ignores the rigidity normally provided by the missing portions of the structure, particularly the horizontal trusses and the diagonal members between these trusses.

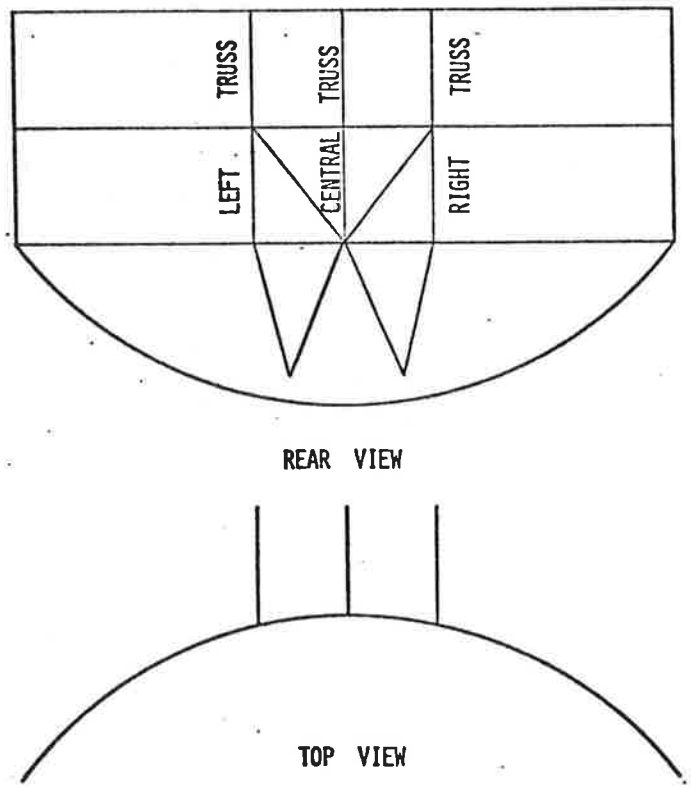

Figure 2-7. ASR Reflector, Simplified Structural Model

In addition, the analysis assumes pinned joints at all intersections, whereas in reality, stiff frame members are used. This latter assumption ignores the transfer of moments exhibited by the frame members, which contributes to the deflection. However, an analysis based on pinned joints yields a greater deflection than an analysis based on stiffened intersections, so that this approach is felt to be a conservative one.

The analysis of the simplified model led to the conclusion that the performance of the ASR antenna would be marginal when 85-knot winds occur on the 15 rpm rotating system encased in 1-1/2 inches of radial ice. Under these conditions the upper corner of the ASR reflector is conservatively analyzed to deflect 0.90 inch, whereas the ASR specification requirement is 0.75 inch. Since it is highly unlikely in most locations that the antennas will be subjected to ice accumulations of 1-1/2 inches, a non-iced condition for the operating condition of 85-knot winds and 15 rpm antenna rotation was analyzed. In this case, the centerline deflection is 0.266 inch, whereas 0.375 inch maximum is specified for the ASR. In the azimuth plane, deflection is 0.618 inch, the maximum allowable is 0.750 inch.

In summary, the structural analysis has included the effects of both operating and non-operating conditions on the 4-foot by 26-foot open array antenna on top of the existing ASR. For the non-operating requirement of 130-knot winds and 1-1/2 inches of ice, studies show that both the open array and ASR antennas would survive without permanent deformation under conditions of full icing on both antennas. For the operating requirement of 85-knot winds during 15 rpm rotation and 1-1/2 inches radial ice, our study indicates that most combinations of ice and wind are acceptable except for some extreme conditions involving a combination of ice and wind. In the marginal condition of 85-knot winds and ice accumulations greater than 1/2 inch, the conservative estimates indicate that the ASR reflector deflections would exceed specifications. It should be noted that the open array antenna will perform with no degradation to the ASR in operating conditions of zero to 1/2 inch radial ice and 85-knot winds. This conclusion is reached in the following manner: without any ice coating at all, the open array antenna is almost equivalent in loads to the FA-7202 antenna. With as much as 1/2 inch of ice, the additional cross section of the open array antenna is small enough so that additional wind and weight loads can be accepted by the present system. With ice loads greater than 1/2 inch and extending beyond 1 inch of ice, the exposed area of the open array antenna to wind loading will be significantly greater. Consequently, loads will exceed those which exist in the present system.

2.1.13 ASR Interface Analysis

As previously described, the non-iced loads imposed on the ASR reflector are approximately the same for the open array and for the FA-7202 antennas. However, when icing is included, the wind loads on the open array antenna are greater than for the FA-7202 antenna. Due to these increased loads, there was a need to study key portions of the ASR antenna, to ensure the achievement of the performance requirements of the open array and ASR pair, and to assess the long term effects on the operational capabilities of the ASR system.

The components of the ASR which would be affected with any increase in loads are the reflector, bearing, and drive system. The effects on the reflector under the maximum operating and survival conditions have previously been discussed in the structural analysis portion of this report.

and azimuth aperture illuminations. Figure 2-8 shows a schematic diagram of the open array antenna. The sum beam is formed by feeding a single coaxial hybrid, which in turn feeds a series line of couplers in two stripline boards. Each output of the stripline azimuth network is connected to an elevation network by a semi-rigid cable. The open array antenna also forms a simultaneous difference pattern for monopulse operation. For this mode, both coaxial hybrids are fed by a 6-dB coaxial coupler. The two hybrids then feed both lines of the stripline azimuth networks. The same elevation networks are used for both the sum and the difference pattern, thus providing identical elevation patterns.

2.2.2 Dipole Design

A dipole was chosen for the radiating element in the open array antenna. The design criteria were that it be matched to within 1.5:1 VSWR over the band, that cross-polarized radiation be suppressed, and that it be operable when exposed to an FAA Class III environment. An existing Hazeltine design that has been used extensively in a rigorous environment was adapted in order to meet the requirements. This design consisted of a two post balun type dipole encapsulated in a rigid epoxy potting. The potting provided protection against adverse climatic conditions, while the balanced two post balun made this an ideal array element because of the inherent cancellation of stem currents, which greatly reduces cross-polarized radiation caused by mutual coupling effects. The mechanical layout is shown in figure 2-9(A). Its electrical equivalent is shown in figure 2-9(B). The dipole has an impedance Z_d which is dependent on its length L. Z_d is transformed through a length of transmission line K to the feed point. The length K is chosen so that the impedance level at the feed point is 50 ohms. The reactive part of the impedance is tuned out by the shorted stub of length d.

The array environment has a slight effect on the impedance level. In order to test the dipole in an array environment without fabricating many dipoles, it was necessary to design an array simulator. A conventional single element waveguide array simulator could not be used because of the wide horizontal element spacing used in the array. The scan angle of a single element waveguide simulator was great enough to introduce grating lobes. The simulator used (figure 2-10) consists of two large ground planes separated by the vertical element spacing of 5.63 inches, with the dipole mounted between the two ground planes. The images of the dipole above and below the ground planes simulate an infinite vertical array with uniform illumination. Dipoles may be placed on either side of the test dipole to give an approximate correction for horizontal mutual coupling effects. Slight errors are introduced because the actual array is of finite dimension and non-uniformly

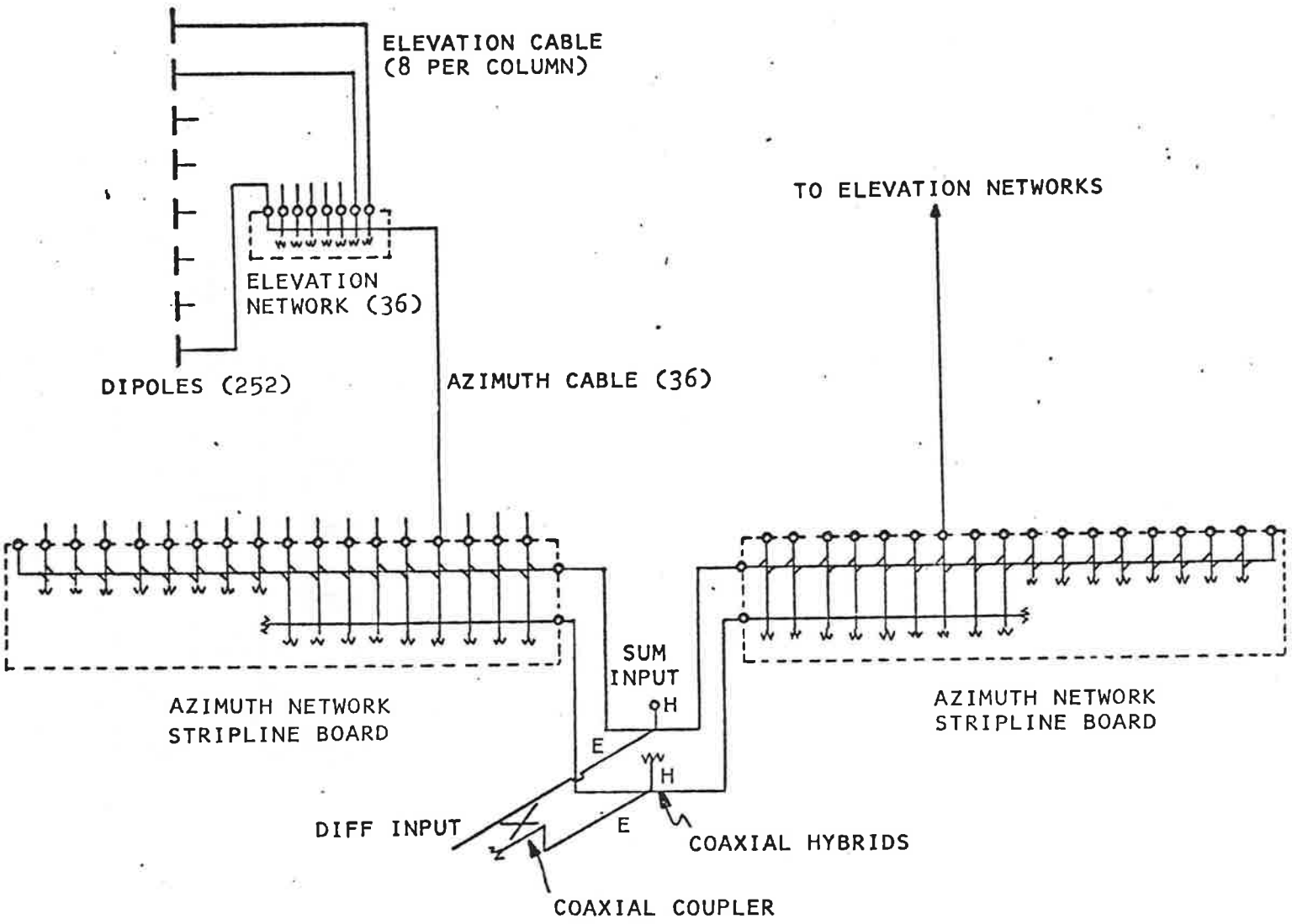

Figure 2-8. Open Array Antenna, Schematic Diagram

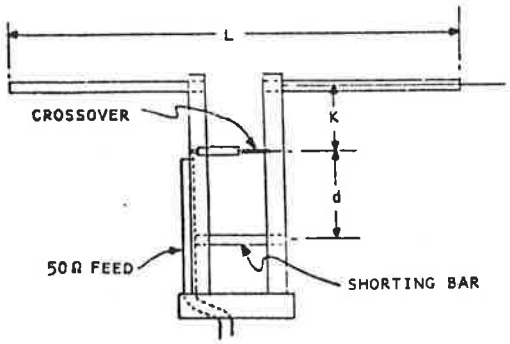

A. MECHANICAL LAYOUT

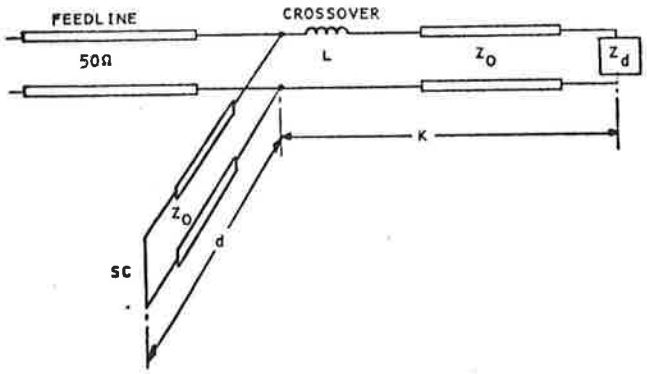

B. ELECTRICAL EQUIVALENT

Figure 2-9. Open Array Dipole and Equivalent Circuit

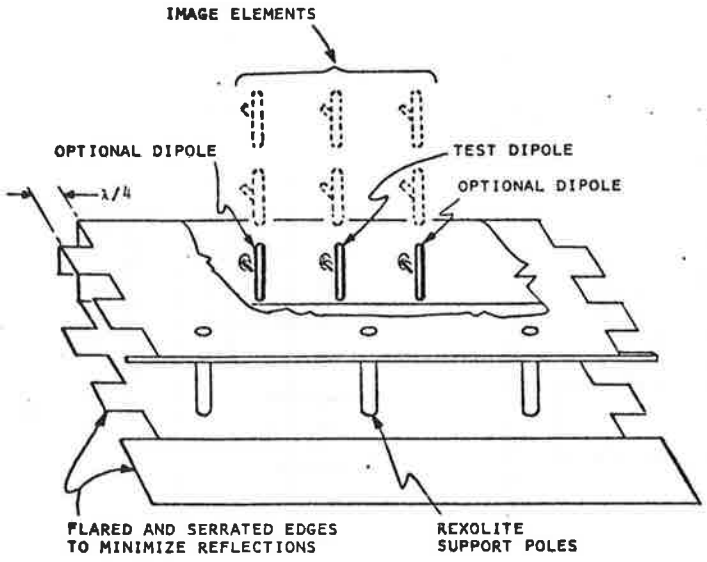

Figure 2-10. Dipole Array Simulator

illuminated. A first order correction for these effects was made in the dipole design, using a computer model of the array. A preliminary dipole was fabricated using RTV as a potting substance. This rubber material has a dielectric constant approximately equal to the rigid epoxy. It proved to be an invaluable aid in the adjustment procedure, because of the ease with which it can be peeled away. The dipole was fabricated with longer than predicted arms, which were then gradually shortened until the dipole was matched. All impedance measurements were made in the simulator.

The first test models resulted in the bandwidth being too narrow. The armlength for these dipoles after adjustment was about 3 inches. When the dipole was redesigned for 4-inch long arms, the required bandwidth was achieved. The final design was matched to within 1.5:1 VSWR over the band. An impedance plot for the prototype model is shown in figure 2-11. All dipoles were potted by the injection molding process. Prior to potting, a fiberglass tube was placed in the mold around the arms of the dipole. This stiffener guards against breakage in the final product. Finally, a silver conductive coating was painted around the stem of the dipoles. This shield, whose height was adjusted for an optimum match, is used to further suppress cross-polarized radiation. Two tests were performed on the production models. The first was a continuity check of the silver paint from the base of the dipole to the top of the shield. If the shield were grounded well, the dipole was painted and a final electrical check was performed in the simulator. The electrical characteristics of all the production models were found to be very repeatable. All the dipoles that were used in the array had a VSWR between 1.06:1 and 1.35:1 at 1030 MHz, and between 1.26:1 and 1.6:1 at 1090 MHz.

2.2.3 Dipole Array Excitation

Each dipole in the 36 dipole columns is fed by a length of 0.141-inch diameter semi-rigid cable connecting the radiating element to its associated elevation network. The semi-rigid cable and stripline elevation network together supply suitable excitations to each dipole in the column such that the desired elevation pattern is radiated. The electrical path length through the elevation network and cable is the same for each cable, except for a phase length of less than $\pm$90 degrees. This phase difference, in conjunction with a 180-degree phase shift achieved by physically rotating the dipole 180 degrees, is used to obtain the desired phase at each element. The result of this equal line length design is that the elevation pattern will not scan with frequency. The pattern will remain at the same level at the horizon over the 1030-1090 MHz band, and only the upper roll-off will vary with frequency. The 36 elevation networks receive their inputs via

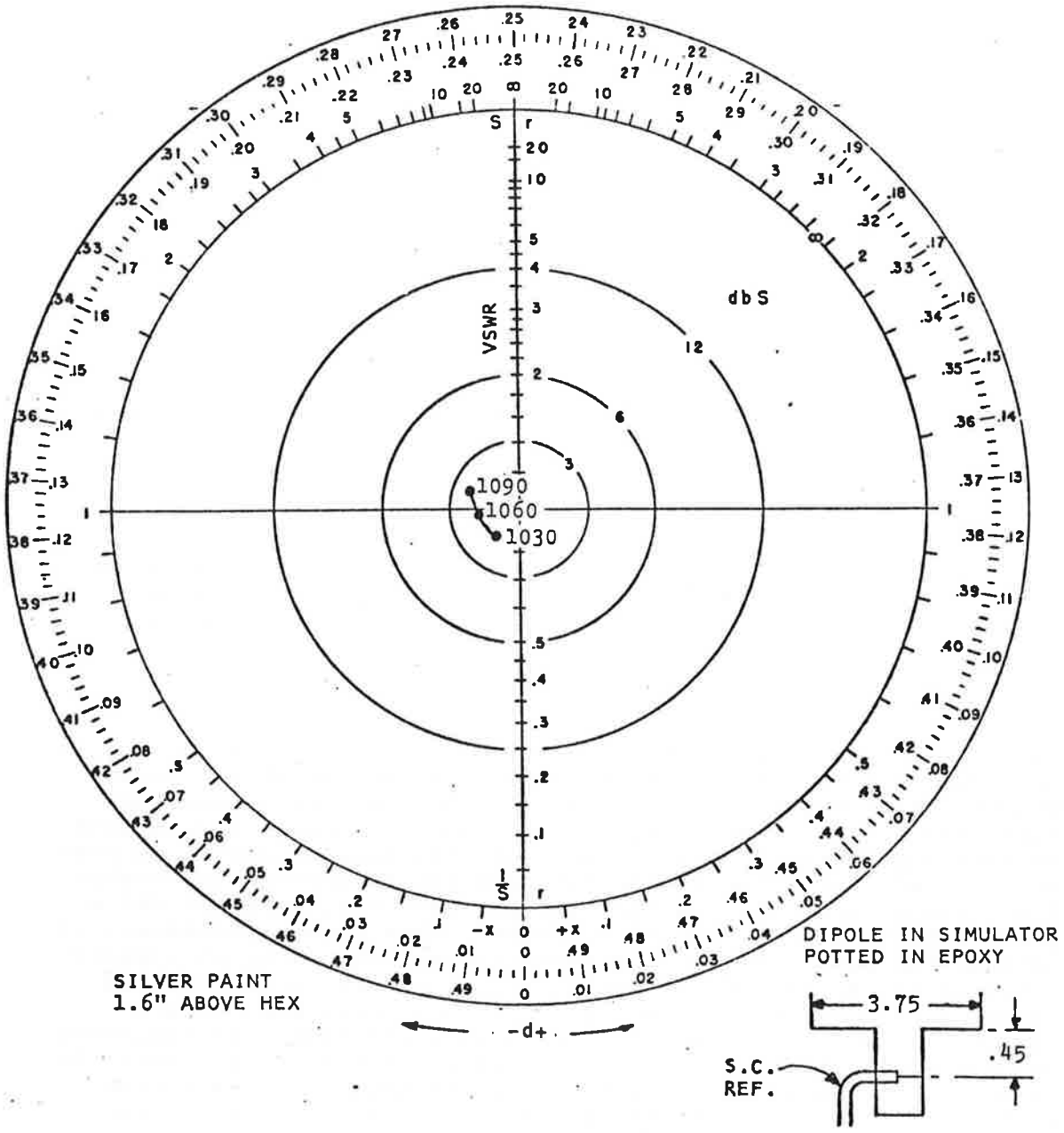

Figure 2-11. Final Dipole Impedance

0.250-inch diameter aluminum shielded foamflex semi-rigid cables connecting the elevation networks to the azimuth network assembly, which consists of two stripline networks, two hybrids and one coupler.

The azimuth network forms both a sum illumination and a simultaneous independent difference illumination. To accomplish this, a two-line ladder network is used. The forward line of stripline networks, fed by the in-phase output of the first hybrid, forms the sum illumination. A series of 17 couplers in each stripline network form the desired azimuth amplitude taper. The difference illumination is obtained by feeding both lines of the stripline networks via both of the coaxial hybrids. The hybrids in turn are fed with a single power divider and phase correcting cables. As shown in the simplified diagram in figure 2-12(A), a complete two-line network is needed to achieve completely independent sum and difference illuminations. However, when low sidelobe sum and difference patterns are desired, it is possible to modify the illuminations so that the edge portion of both illuminations is the same (figure 2-12(B)). This permitted the elimination of 7 couplers in the secondary line of couplers in the actual azimuth network.

2.2.4 Effect of Tapered Structure

A further modification to the azimuth and elevation illuminations was required because of the taper that exists at each end of the array structure to reduce the wind load. To correct for the effect of the tapered structure, the azimuth illumination was increased by 1 dB in the outermost 3 columns and by 0.5 dB in the adjacent 3 columns. The elevation illumination was increased by 1 dB for the top and bottom rows. This correction yields exactly the desired azimuth pattern at certain elevation angles, with slightly degraded sidelobe performance at other angles. However, this effect is so small as to be unnoticeable in the measured azimuth patterns. A slight difference in the elevation sidelobe levels as measured at the peaks of the sum and difference azimuth patterns can also be attributed to the tapered structure. A loss in gain also results, but the strength of illumination is very weak in the area of the taper, and the loss is insignificant (0.02 dB). Antenna patterns showing measured performance at various frequencies and angles are presented in Appendix A.

2.2.5 Elevation Network Design

Each elevation network consists of a series of seven printed circuit couplers on a stripline board. The purpose of the network is to couple the required power to each dipole element in a column. The desired phase is obtained by selecting the correct cable lengths between the elevation network and the dipoles. The stripline network is constructed in three layers, with the photo etched

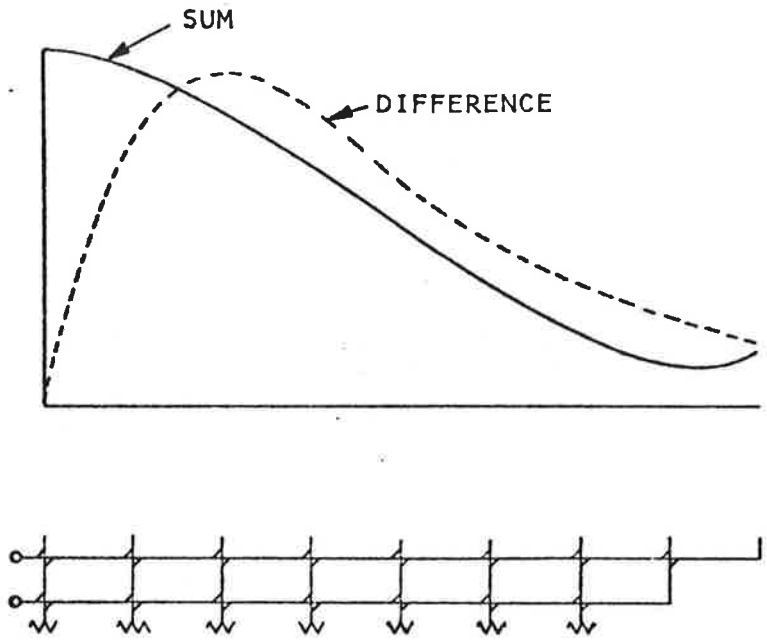

A. NOMINAL APERTURE ILLUMINATION AND NETWORK

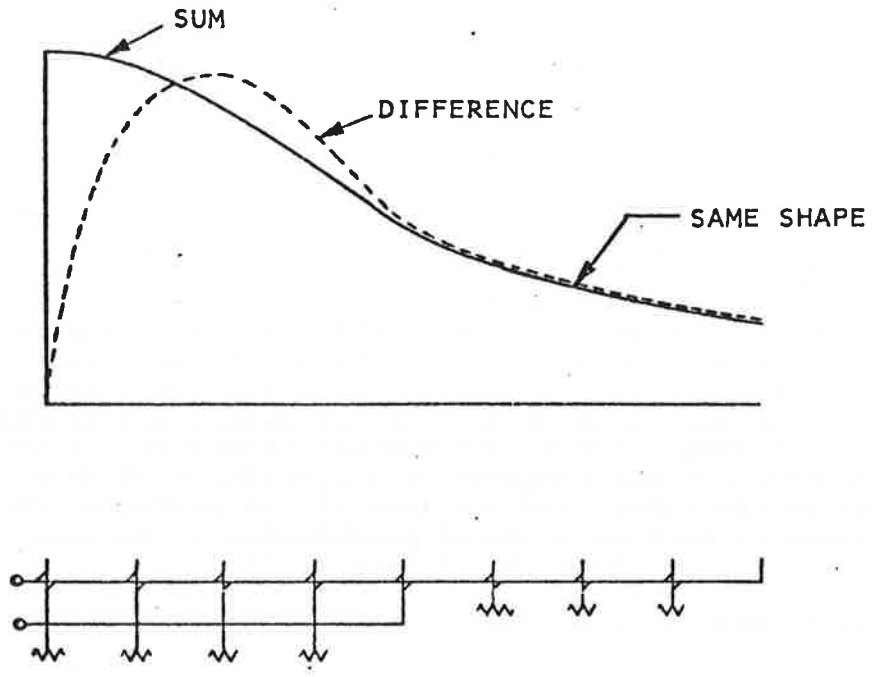

B. MODIFIED APERTURE ILLUMINATION AND NETWORK

Figure 2-12. Simplification of Azimuth Network

circuit on the center board. The seven printed couplers are quarter-wave long, backward wave designs, and coupled line spacing is used to vary the coupling. Because the couplers are spaced nearly one-quarter wave apart, the network is well matched.

Once the network outputs were calculated from the desired elevation excitation and corrections calculated for mutual coupling, the stripline coupler dimensions were derived. A prototype network was fabricated and trimmed to the desired output voltages. The total quantity of networks was then released for fabrication. After assembly, each unit was tested for transmission amplitude and phase to two outputs. A percentage of the networks were completely tested. Table 2-5 shows the measured results. The average insertion loss through the networks was 0.2 dB, and the maximum input VSWR measured was 1.2:1.

TABLE 2-5. MEASURED ELEVATION NETWORK AMPLITUDES AT 1060 MHz

Output No.	Design Goal (dB)	Measured Average (dB)	Range of Measured Values (dB)
8	-17.5	-17.3	±1.0
7	-33.5	-33.4	±1.0
6	- 8.4	- 8.9	±1.0
5	- 4.0	- 4.1	±0.5
4	- 4.8	- 4.7	±0.5
3	-11.1	-11.6	±1.0
2	-33.5	-34.5	±1.0
1	-17.8	-17.9	±1.0

NOTE: Output No. 8 is associated with the top dipole in the dipole column, output No. 1 with the bottom dipole.

2.2.6 Azimuth Network Design

The azimuth network includes two stripline networks, two coaxial hybrids, one coupler, and the cables required to connect these components. The two azimuth stripline networks feed the 36 elevation networks and are used in forming the simultaneous sum and difference patterns. Before the network components could be designed, the azimuth sum and difference illuminations had to be finalized. As described in paragraphs 2.2.3 and 2.2.4 the theoretical optimum sum and difference patterns had to be modified to correct for reduction in the number of couplers in the stripline boards and for the tapered ends of the antenna structure. The taper was accounted for by increasing the amplitude of the outermost columns slightly, thus approximately correcting for the missing dipole elements.

The modification to the azimuth stripline boards was accomplished by choosing a compromise taper (for both the sum and difference illuminations) for the outer seven columns. No correction was made to the azimuth illuminations to account for mutual coupling. This was because the azimuth illuminations change slowly compared to the dipole spacing. In addition, measurements have shown that, because the horizontal spacing of the dipoles is much larger than $\lambda/2$, the azimuth coupling is almost negligible. The final azimuth network illuminations are listed in table 2-6. These illuminations yield patterns with peak sidelobe levels of -32 dB.

TABLE 2-6. AZIMUTH NETWORK OUTPUTS

Output	Sum Design Amplitude (volts)	Diff Design Amplitude (volts)
1	1.00	0.10
2	0.99	0.30
3	0.97	0.49
4	0.94	0.65
5	0.89	0.78
6	0.85	0.88
7	0.79	0.95
8	0.73	0.97
9	0.67	0.96
10	0.60	0.92
11	0.54	0.83
12	0.48	0.73
13	0.47	0.72
14	0.39	0.59
15	0.31	0.48
16	0.25	0.38
17	0.22	0.34
18	0.21	0.33

NOTE: Output number 1 is at the center of the antenna, number 18 is at the outer edge. The two illuminations are normalized for equal power.

Once the final illumination was achieved, the stripline boards were designed. As shown schematically in figure 2-8, the stripline boards have two lines of couplers printed on them, with the two lines interconnected. Two identical boards are used in the antenna. The long row of couplers is used to form one-half of the sum illumination. The two stripline boards are then fed in-phase by one hybrid to form the complete sum illumination. To achieve an independent difference illumination, both lines of couplers on the board must be fed in the correct amplitude and phase ratio. An existing computer program was used to calculate the coupler values for the two lines and the required amplitude and phase ratio between the two lines. Fortunately, the desired ratio turned out to be exactly satisfied by a 6-dB coupler, which was readily available. In order to keep the stripline coupler values realizable, it was necessary to terminate the short rear line of couplers. This resulted in an additional gain loss in the difference channel of less than 0.1 dB. The azimuth stripline boards are the same three-layer construction as the elevation networks. The couplers and interconnecting lines are printed on the center board, which is then sandwiched between the two outer dielectric boards. All input and output connectors are type TNC. The semi-rigid cables which connect the hybrids, coupler and stripline boards were trimmed to provide equal phase at all 36 columns.

2.3 RANGE TESTS

2.3.1 General

Two antenna test ranges were utilized in evaluating the antennas: a 1,000-foot range at Hazeltine's Smithtown facility and a 2,000-foot range at ESSCO Corporation in West Concord, Mass. The longer range was required to accurately evaluate the 26-foot open array antenna which has a far-field distance of 1,500 feet. The omni antenna measurements and certain open array antenna measurements not requiring a long range were performed at Smithtown. In addition, a focusing technique was used to measure the far-field performance of the open array antenna at Smithtown. This technique proved successful, as can be seen from the comparison of the Smithtown and the ESSCO measurements discussed in paragraph 2.3.11.

The following tests were performed on the open array antenna at the Smithtown test range:

Azimuth patterns (sidelobes, backlobes, beamwidth)
Elevation patterns
Gain
Setup of boresight telescope
Skew and squint
Monopulse performance (null depth, sum/diff. linearity)

The following tests were performed on the open array antenna at the ESSCO test range:

Azimuth patterns (sidelobes, backlobes, beamwidths)
Elevation patterns

2.3.2 Assembly and Alignment

The open array antenna was assembled and aligned prior to range tests at Smithtown as follows:

a) The elevation networks and cables, which had been previously tested, were installed.

b) The dipoles were mounted and attached to the ends of the elevation cables and the tuned reflectors were mounted between the columns.

c) The azimuth networks and cables were installed.

d) The two halves of the antenna structure were assembled.

e) The input hybrids and interconnecting cables were installed. The input and azimuth network assembly had been pre-aligned and tested as a unit on the bench prior to installation. However, as a final check the entire assembly from the input connectors to the ends of the elevation cables was measured for transmission amplitude and phase. Measurements were taken across the entire azimuth aperture for elevation output port numbers 4 and 5 from the sum and difference inputs at 1030 and 1090 MHz. Computer calculated patterns were obtained from the recorded data. Three azimuth cables were trimmed to more exactly equalize the phase front.

f) The backup structure and mounting brackets were attached to the antenna structure. A testing fixture, used to adapt the antenna to the existing antenna mount, was fabricated and fitted to the antenna structure at this time.

2.3.3. Smithtown Test Facility

A photograph of the Smithtown antenna range is shown in figure 2-13. This facility consists of a 1,000-foot valley-type range. A source tower, located at one end of the range, can be seen in the upper right-hand corner of the photograph. The lower and upper roof areas of the main building provide the antenna testing area. These roof levels contain 7 antenna mounts. The mount selected for the open array antenna is located on the upper roof level. An L-band 30-foot reflector-type antenna was chosen for the source. In order to provide a flat illumination across the aperture of the open array antenna, it was necessary to modify the highly directive source so that it would radiate a wider beam. This was accomplished by replacing the wide beam feed horn on the source by a more directive 2-dipole feed. This new feed widened the beam of the source by illuminating less of the reflector dish. The wide aperture of the open array (26 ft) on the relatively short range also caused phase defocusing across the array. The difference in electrical distance from the source to the center and to the ends of the open array antenna was compensated for by placing short focusing cables in series with the cables leading to the elevation networks from the azimuth network. These cables were longer for the center elements and made the array appear to have a flat phase front incident on it. The focusing cables were not necessary on the longer ESSCO range and were removed for those tests. The beam of the source antenna was aligned with the test position by making illumination measurements before the open array antenna was placed on the mount. These measurements were made using an illumination test fixture which consisted of a corner reflector antenna, moveable over the 26-foot aperture both horizontally and vertically. The source antenna was steered until the illumination measurements showed a relatively uniform amplitude variation. The final measured illumination had a ± 1 dB ripple over the vertical aperture of the open array antenna. Over the horizontal aperture, the illumination had a ± 0.1 dB ripple with a gradual taper in amplitude to an average of -0.8 dB at the ends of the antenna.

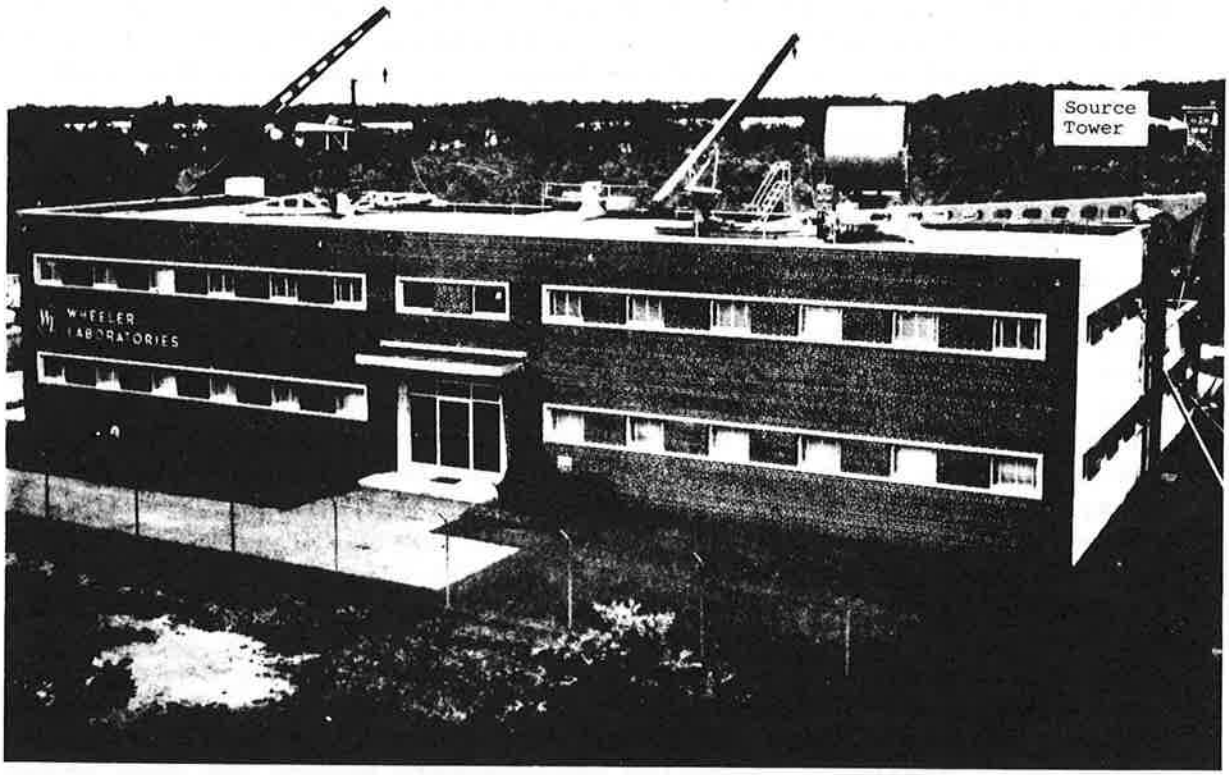

Figure 2-13. Aerial Photo of Smithtown Antenna Test Range

2.3.4 Smithtown Range Pattern Tests

A photograph of the open array on its test fixture is shown in figure 2-14. It consists of an upper AZ/EL table upon which the antenna and adapter assembly were mounted. The AZ/EL table was attached to a 10-foot tower which rested on the lower azimuth table. The AZ/EL/AZ combination permits three axes of rotation of the antenna under test. The uppermost azimuth mount, in conjunction with the elevation mount, was used for all of the conical cut azimuth patterns. For elevation pattern measurements, the two upper mounts were set so that the long axis of the array was vertical, then the lower azimuth table was rotated. The azimuth patterns were taken in a full 360° circle by rotating the upper azimuth table. Conical azimuth cuts were taken at elevation angles ranging from -2° to +40°. The correct elevation angle was obtained through rotation of the elevation mount. Several elevation patterns were also recorded at azimuth angles within the vicinity of the peak of the main beam. Elevation patterns were taken with the antenna in the vertical orientation described above. This position permits 360° elevation pattern cuts and, more importantly, minimizes the illumination of the ground, thereby increasing the accuracy of the measurements. Patterns were taken at 1030 and 1090 MHz. Azimuth sum and difference patterns were recorded at various elevation angles with the source polarization both aligned and crossed with that of the open array antenna. The sum and difference patterns are shown in Appendix A. Elevation patterns were measured for both the sum and difference patterns at 1030 and 1090 MHz. These patterns are also shown in Appendix A. All patterns exhibited the desired sharp cut-off at the horizon, and low sidelobes (less than -20dB) below the horizon. As expected, the tapered ends of the array caused the difference pattern elevation sidelobes to be 1 to 2 dB lower than the corresponding sum pattern sidelobes. One discrepancy was noted between the specified performance and the measurements; the slope of the elevation pattern at the horizon was 1.0 to 1.1 dB per degree instead of 1.25 dB per degree. It was concluded that errors in the vertical excitation caused the discrepancy and that it should be possible to improve the performance in future antennas.

2.3.5 Gain Tests

The gain of the open array antenna was measured by the substitution method, using a standard gain horn antenna. Without the EMI filter installed, the gain of the antenna on the sum peak was 23.5 dB at 1030 MHz and 23.9 dB at 1090 MHz. The measurement was made at the

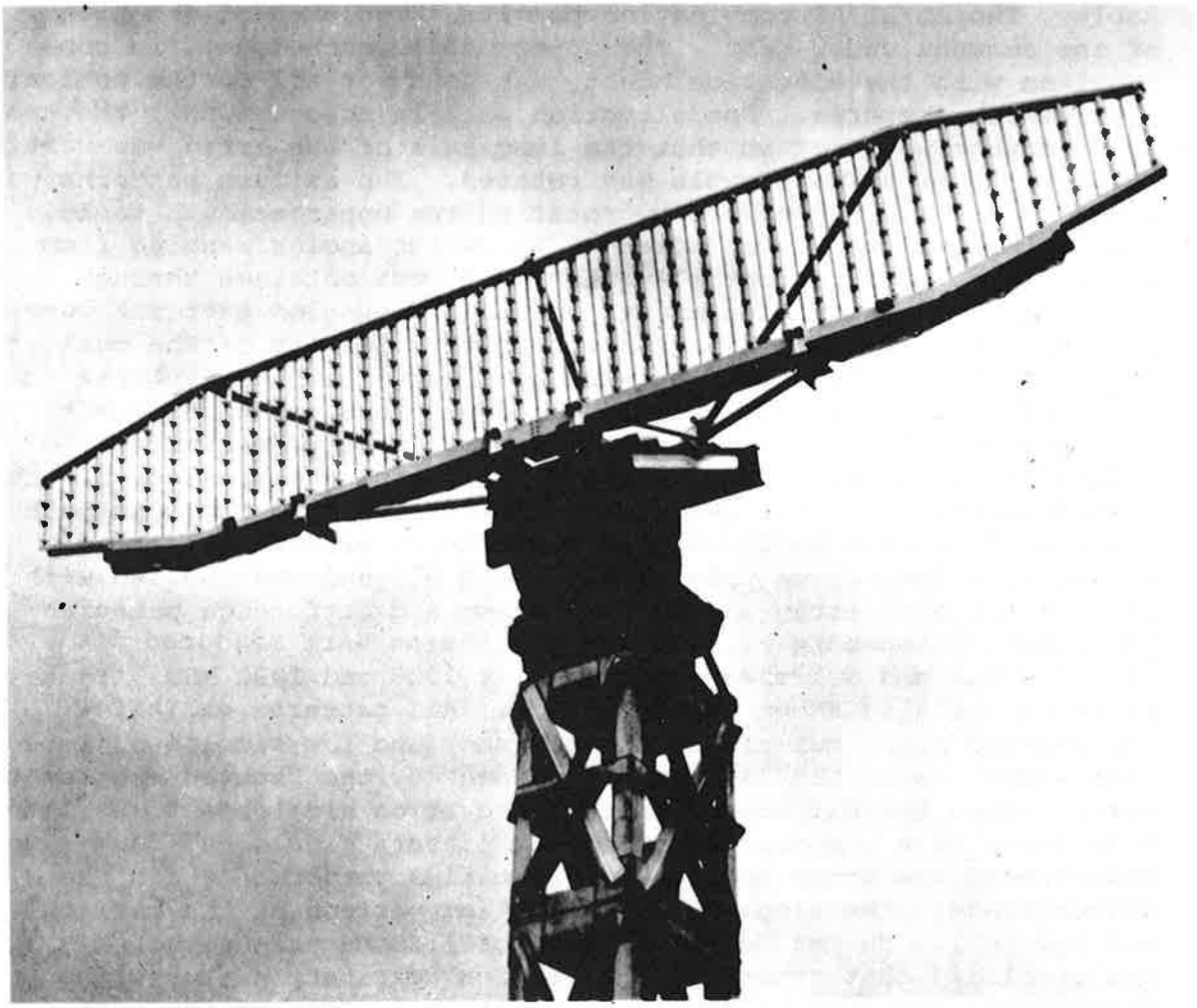

Figure 2-14. Open Array Antenna on Test Mount

peak of the elevation pattern. The peak difference pattern gain is approximately 2.7 dB below the sum pattern gain. The EMI filter will reduce the gain between 0.5 and 0.9 dB, depending on frequency.

2.3.6 Setup of Boresight Telescope

A boresight telescope was mounted on the open array antenna at Smithtown. The telescope was mounted on the top of the component box and to one side of the centerline of the antenna. The telescope is removable and is fitted with precision alignment pins to facilitate accurate remounting. The crosshairs of the telescope are aligned with the nominal horizon of the array in elevation, and with the null of the 1090 MHz difference pattern in azimuth. The telescope alignment was checked on the ESSCO test range; the azimuth pointing angle was within 0.03 degree of the measured pattern null.

2.3.7 Skew and Squint Tests

The skew and squint of the open array antenna were also measured on the Smithtown range. To accomplish this, the array was carefully leveled and aligned in azimuth with the source antenna. Sum and difference patterns were measured at 1030 and 1090 MHz. The center of the sum patterns was taken as halfway between the 10 dB points; the center of the difference patterns was taken as halfway between the 10 dB points in the null. Figure 2-15 presents the results of the measurements. Skew is defined as the variation in pointing angle as a function of elevation angle, while squint is defined as the difference in pointing angle between 1030 and 1090 MHz for a given elevation angle. Both measured parameters are well within the specification limits.

2.3.8 Monopulse Performance Tests

The ability of the open array antenna to direction-find off axis using monopulse techniques was also investigated. Sum and difference patterns were measured at various elevation angles; then the difference/sum ratio was calculated at 0.1 degree intervals in azimuth out to the half-power points of the sum pattern. Two characteristics of the difference/sum ratio are of interest: one is the linearity of the ratio with azimuth angle, while the other is the variation in the best linear fit with elevation angle. Good linearity simplifies the processing required to derive the aircraft direction. A small variation of the best linear fit with elevation

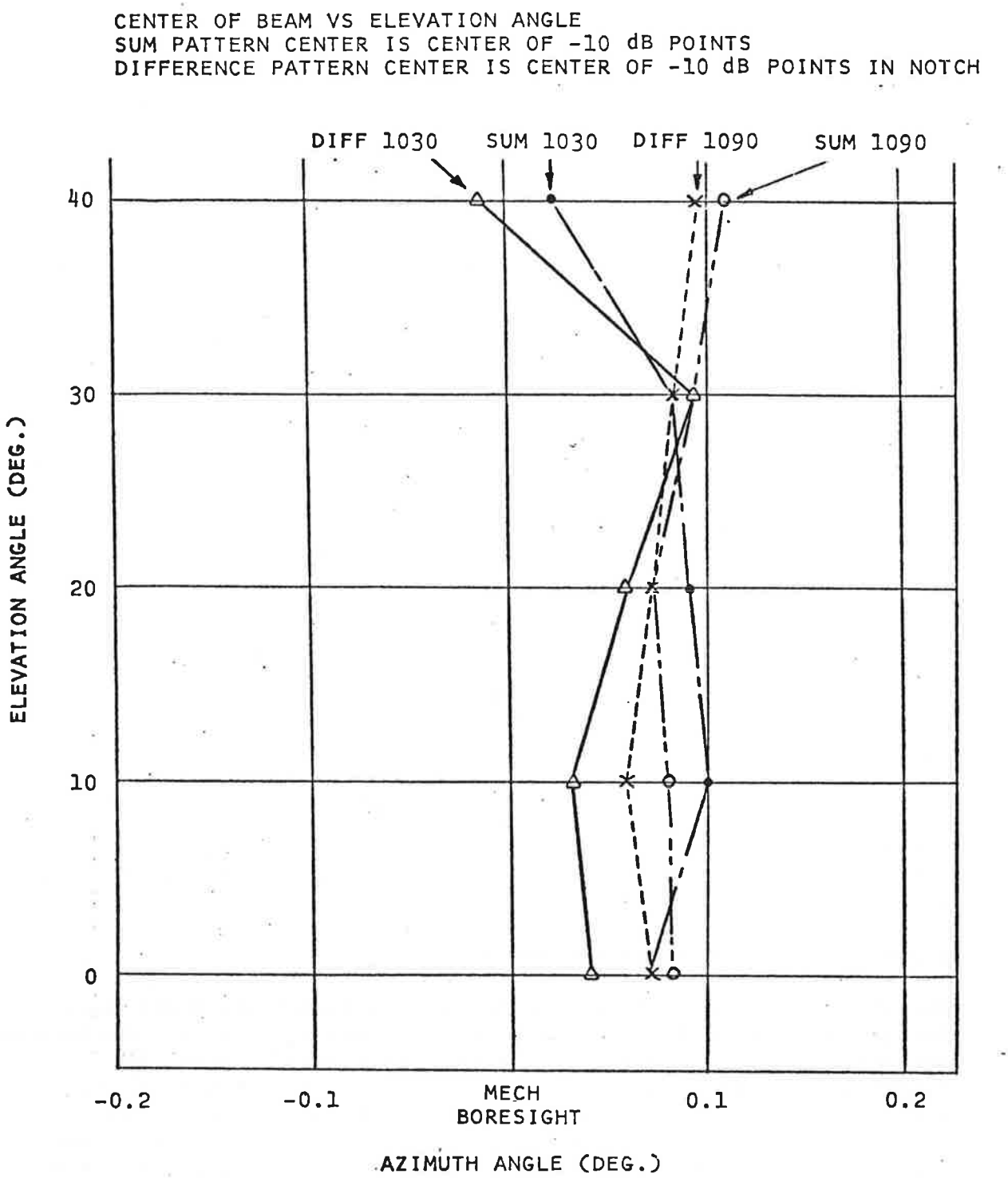

Figure 2-15. Beam Skew and Squint Measurements

angle would permit accurate direction-finding without a prior knowledge of the aircraft elevation angle. Δ/Σ linearity was determined by obtaining points from an expanded sum-difference pattern. Points were sampled at 0.1^{o} increments to the 3 dB beamwidth. Plots of the sample data were made at 1090 MHz and for 0^{o}, 10^{o}, 20^{o} and 30^{o} elevation. One such plot at 0^{o} elevation is shown in figure 2-16. The best linear fit to the sampled points was found by a least-mean-square fit to the data. A plot of the slope of the best linear fit versus elevation angle is shown in figure 2-17. The best linear fit slope variation was $\pm$2.6% for $0\text{-}10^{o}$ elevation and $\pm$7.6% from $0\text{-}30^{o}$. Δ/Σ linearity was determined by comparing the true slope at each point to the slope of the best linear fit. A plot of the percent difference in slopes at 0^{o} elevation is shown in figure 2-18. Points could only be read to $\pm$0.25 dB, which corresponds to a true slope error of $\pm$2.5%. Thus the true errors may be less than indicated on the graph. It should be noted that the worst-case azimuth error for the data plotted in figure 2-18 is 0.08 degree.

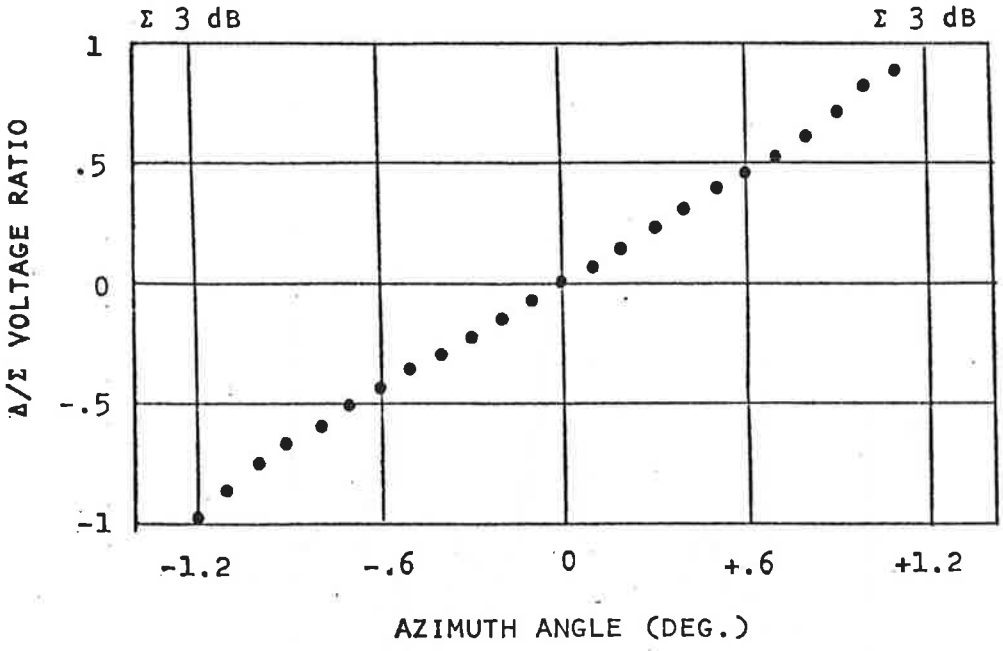

Figure 2-16. Δ/Σ Ratio Versus Azimuth Angle

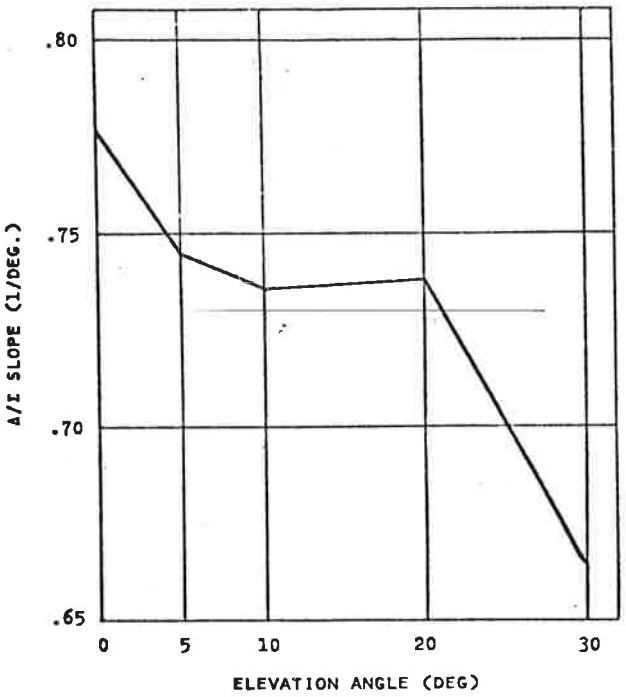

Figure 2-17. Δ/Σ Slope Versus Elevation Angle

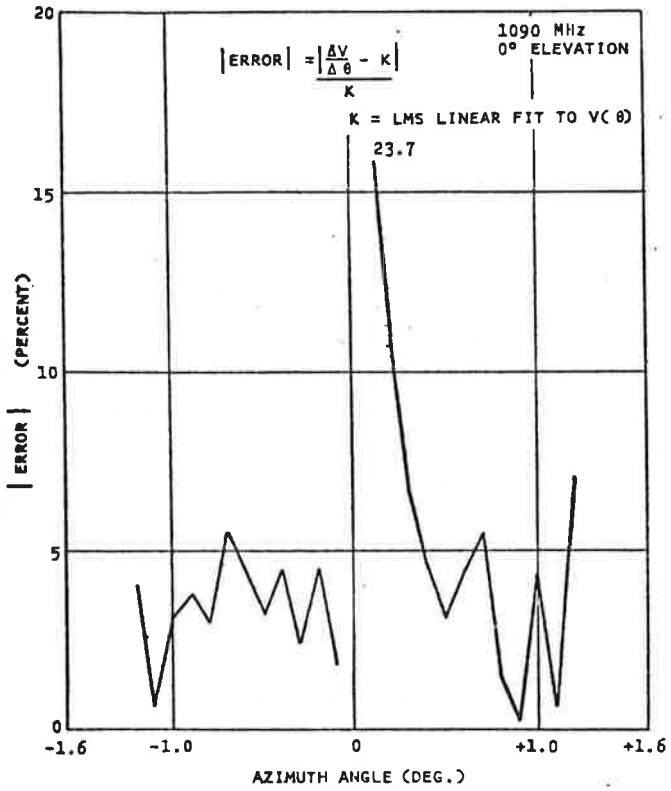

Figure 2-18. True Slope Versus Best Linear Fit

2.3.9 ESSCO Test Facility

The antenna test range located at ESSCO, Inc., in West Concord, Mass., is a reflection type range. The range, shown in the diagram of figure 2-19, is 2000 feet long, and is graded flat to within 4 inches. An 80-foot test tower is located at one end of the range and a source building is located at the other end. An 8-foot diameter dish antenna was used for a source antenna. Because the range is a reflection type, the antenna under test must be positioned at a maximum of the combined direct and reflected signal. The open array antenna was mounted on the same tower and antenna mount used at Smithtown. The entire assembly was then mounted on an azimuth mount atop the 80-foot test tower. Antenna mount control cables and receiver cables were run down to a shelter located in the tower underneath the azimuth mount. The illumination of the range was tested by probing the fields in the area where the open array antenna was to be mounted. The probe was a standard gain horn mounted on a mechanical structure which permitted continuous recording of the signal level. The illuminations were very good, both in horizontal and vertical measurements. Typical ripples were $\pm$0.1 dB and typical amplitude taper of the illumination was less than 0.5 dB.

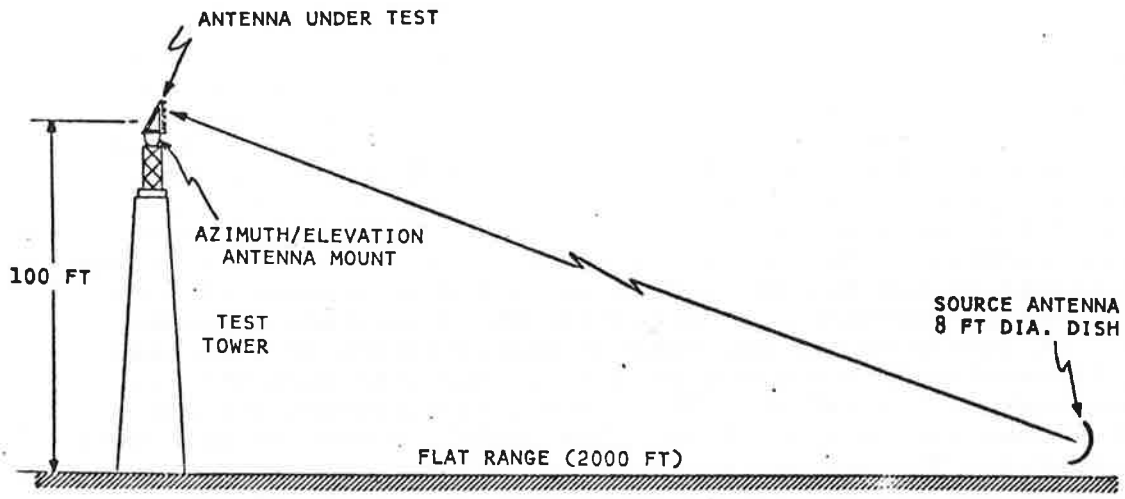

Figure 2-19. ESSCO Antenna Test Range

2.3.10 ESSCO Range Pattern Tests

A complete set of azimuth patterns was measured for 1030 and 1090 MHz, sum and difference, and for various elevation angles. A typical azimuth sum pattern is shown in figure 2-20. Note that the near-in sidelobes are between -25 and -30 dB, with the far-out sidelobes below -40 dB. A sharp backlobe at a level between -21 and -30 dB exists on all patterns. This backlobe structure is caused by residual leakage through the open ground plane. All of the measured patterns were evaluated and the measured pattern performance was tabulated. Figures 2-21 and 2-22 show the peak sidelobe level relative to the main beam peak at the same elevation angle plotted as a function of elevation angle for the sum and difference patterns at 1030 and 1090 MHz, respectively. It should be noted that typically only one or two of the sidelobes reach the peak level. Figures 2-23 and 2-24 show the peak backlobe level relative to the peak of the forward signal of the antenna at the same elevation angle.

Another parameter of interest is the azimuth beamwidth of the antenna as a function of elevation angle. Figure 2-25 shows the -3 dB and -10 dB beamwidths as a function of frequency and elevation angle. Because of the coordinates used in measuring the beamwidths, the measured beamwidth will increase as 1/cos (elev. angle).

2.3.11 Comparison of ESSCO and Smithtown Range Results

The measurements of the open array antenna made on both the Smithtown and ESSCO test ranges showed excellent agreement. Beamwidths were measured on both ranges. The average disagreement on 3 dB beamwidths (measured at nine elevation angles) was 1.5 percent of the nominal beamwidth, with a maximum deviation of 6 percent for one measurement. For the 10 dB beamwidths, the average disagreement was 2.5 percent of the average beamwidth, with a maximum deviation of 4 percent on two measurements. Backlobe measurements were also compared. Most measurements with backlobe levels around -22 dB agreed within 0.5 dB, with a maximum disagreement of 1 dB. As the backlobe decreased in amplitude, the disagreement became larger. At levels of -25 dB, maximum disagreements of 2 dB were noted, increasing to a maximum of 3 dB in one case when the backlobe was weaker than -30 dB. The average disagreement for all backlobe measurements was 0.8 dB. Peak sidelobe measurements were also compared. The average disagreement between the two sidelobe measurements was 1.2 dB, with a worst-case of 3.5 dB for one measurement. As with the backlobe, the repeatability was better for the stronger peak sidelobes.

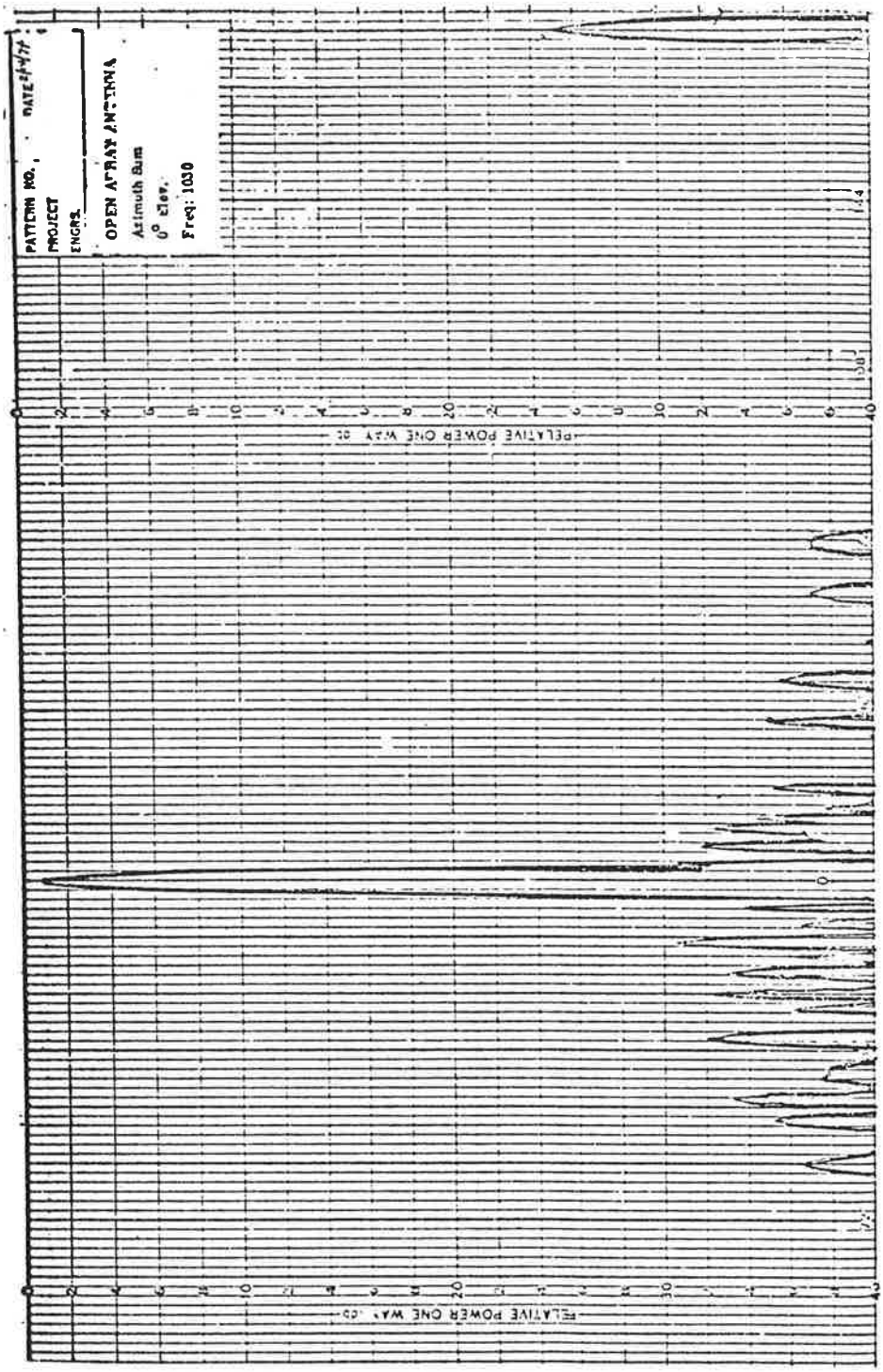

Figure 2-20. Typical 360° Azimuth Sum Pattern

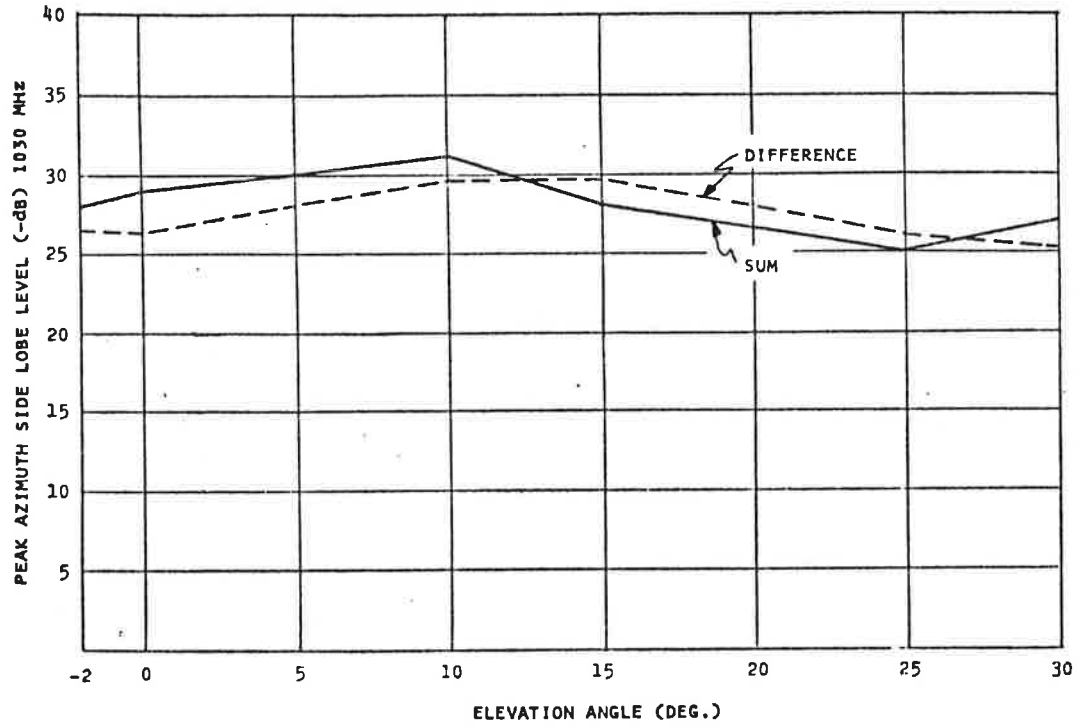

Figure 2-21. Peak Sidelobe Level Relative to Directional Beam Peak at the Same Elevation Angle, 1030 MHz

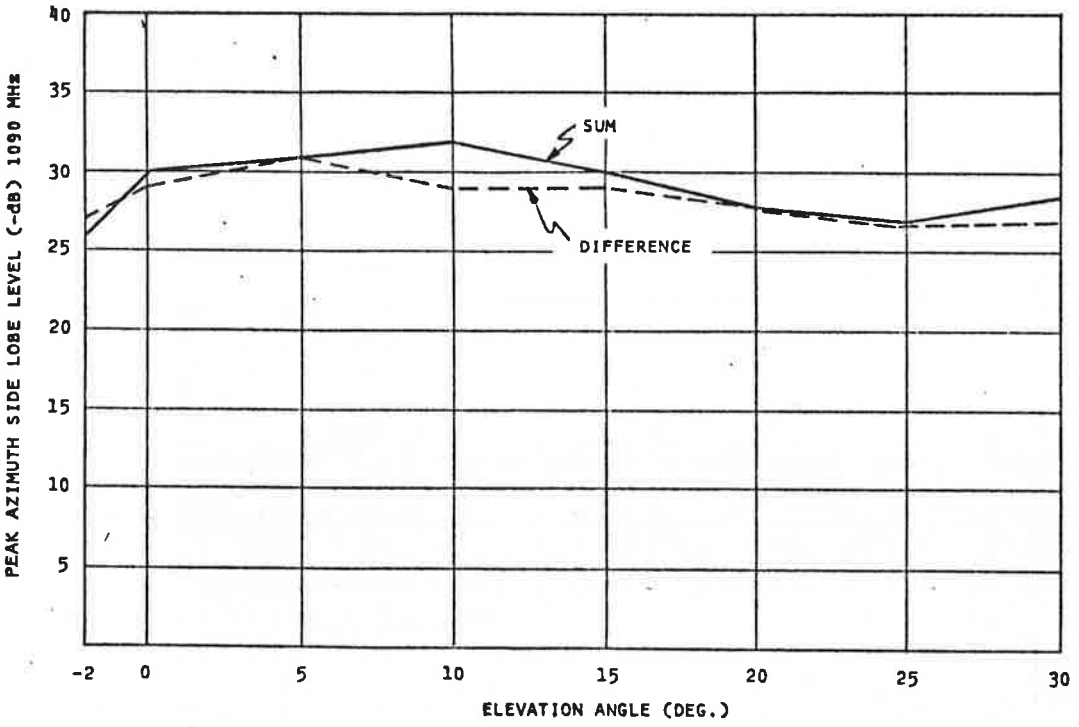

Figure 2-22. Peak Sidelobe Level Relative to Directional Beam Peak at the Same Elevation Angle, 1090 MHz

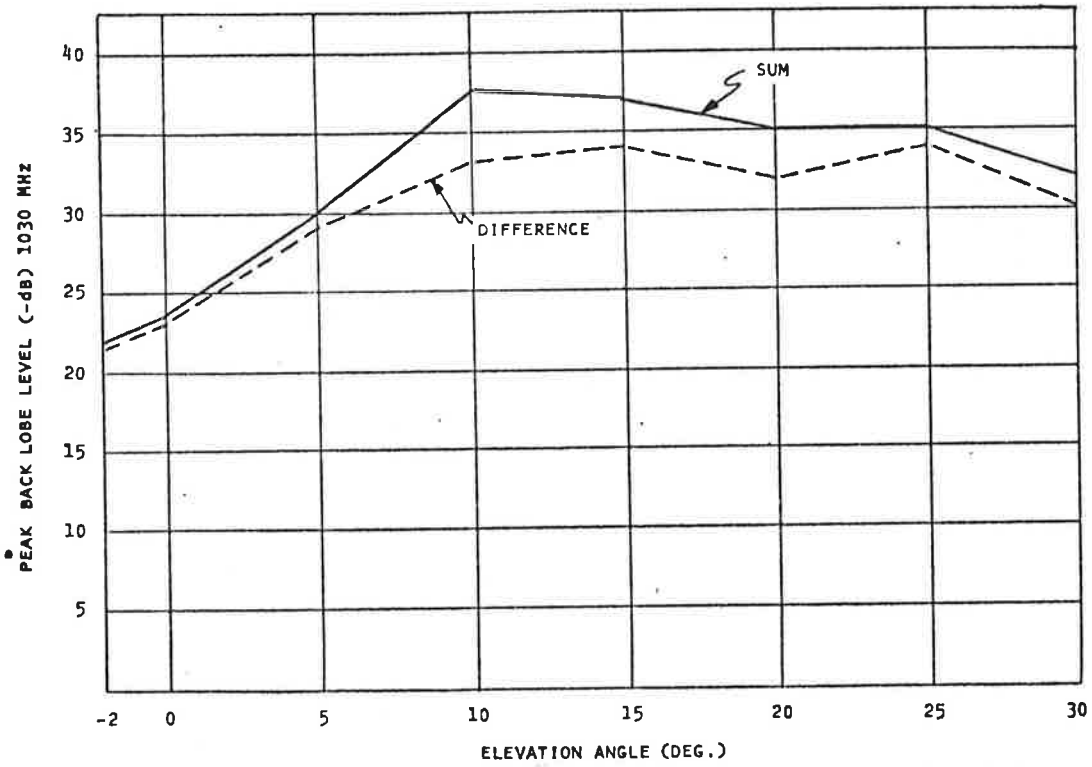

Figure 2-23. Peak Backlobe Level Relative to Directional Beam Peak at the Same Elevation Angle, 1030 MHz

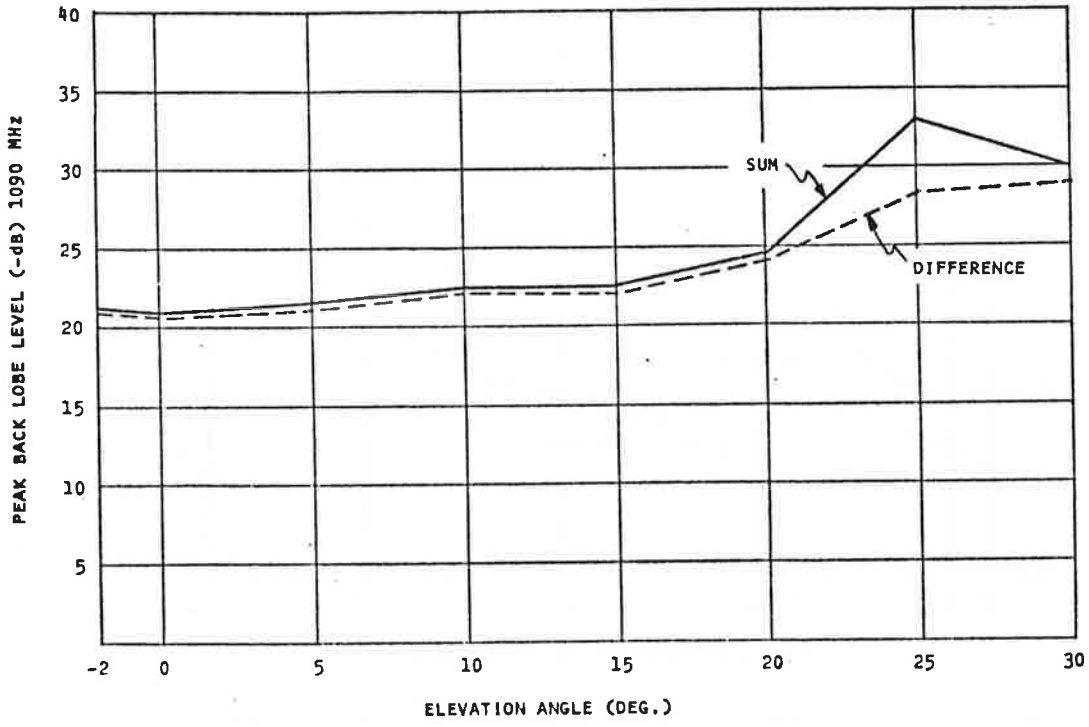

Figure 2-24. Peak Backlobe Level Relative to Directional Beam Peak at the Same Elevation Angle, 1090 MHz

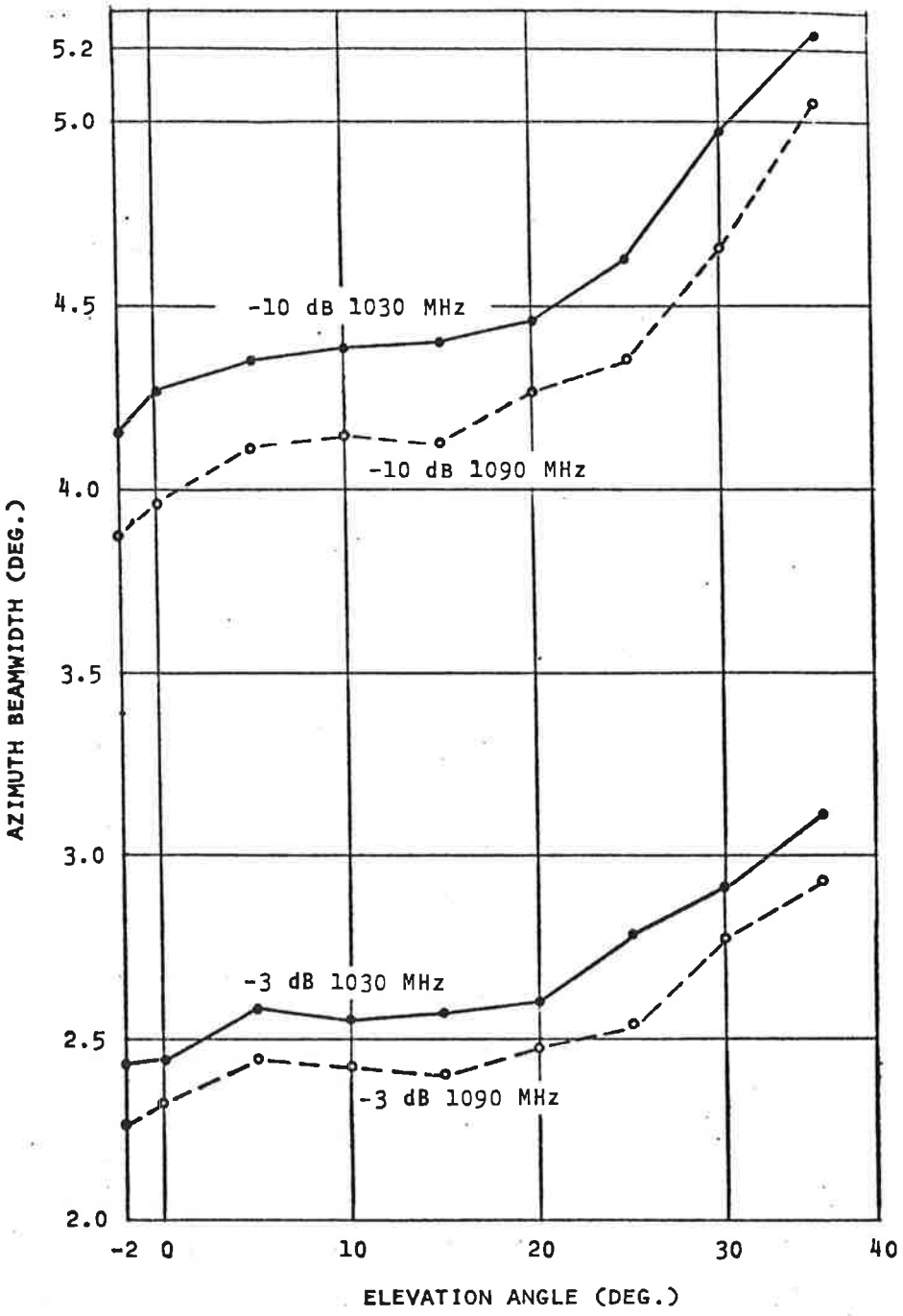

Figure 2-25. Plot of Sum Azimuth Beamwidths Versus Elevation Angle

2.4 TYPE TESTS

2.4.1 Deflection Tests

The antenna structure and backup structure were tested under simulated conditions of wind, ice and antenna rotation. To accomplish this, the loads imposed on the antenna were calculated for the case of 1.5 inches of radial ice, 85-knot wind and 15 rpm rotation rate. Figure 2-6 shows the worst-case loading on a column-by-column basis. To perform the measurement, the antenna and backup structures were mounted as shown in figure 2-26. The six bottom mounting feet were bolted to the upright steel "I" beams and the three struts were bolted to a cross-member at the bottom of the "I" beams. A reference set of measurements of the antenna deflection was made using a transit. These measurements are tabulated in figure 2-27. Next, sandbags were hung from each column in accordance with figure 2-6. The weight was applied to at least two points on each column. After loading, the deflection of the end points was measured. The deflection measurements with load are also tabulated in figure 2-27. The loading was then removed, and the deflection remeasured to determine if any permanent deformation of the array had occurred.

The flatness of the array was measured after loading. The rms flatness of the array was still within the 0.055-inch specification required in Hazeltine Specification S6906.

2.4.2 Electrical Component Tests

The following components were subjected to the type tests:

1 dipole
1 azimuth network
1 elevation network

All components were tested in accordance with MIL-STD-810B, method 501, procedure II - high temperature, and method 502, procedure I - low temperature. The dipole was also tested according to method 506 - rain, and the divider networks were tested according to method 507, procedure I - humidity. Finally, the dipole was tested while being encased in 1-1/2 inches of radial ice. All tests except the ice test were performed in Hazeltine's environmental chambers; the ice test was performed in the array simulator. The three components were placed simultaneously in the chamber for temperature testing. The temperature tests consisted of a cyclic exposure of the items under test to high and low temperatures. The dipole and networks were

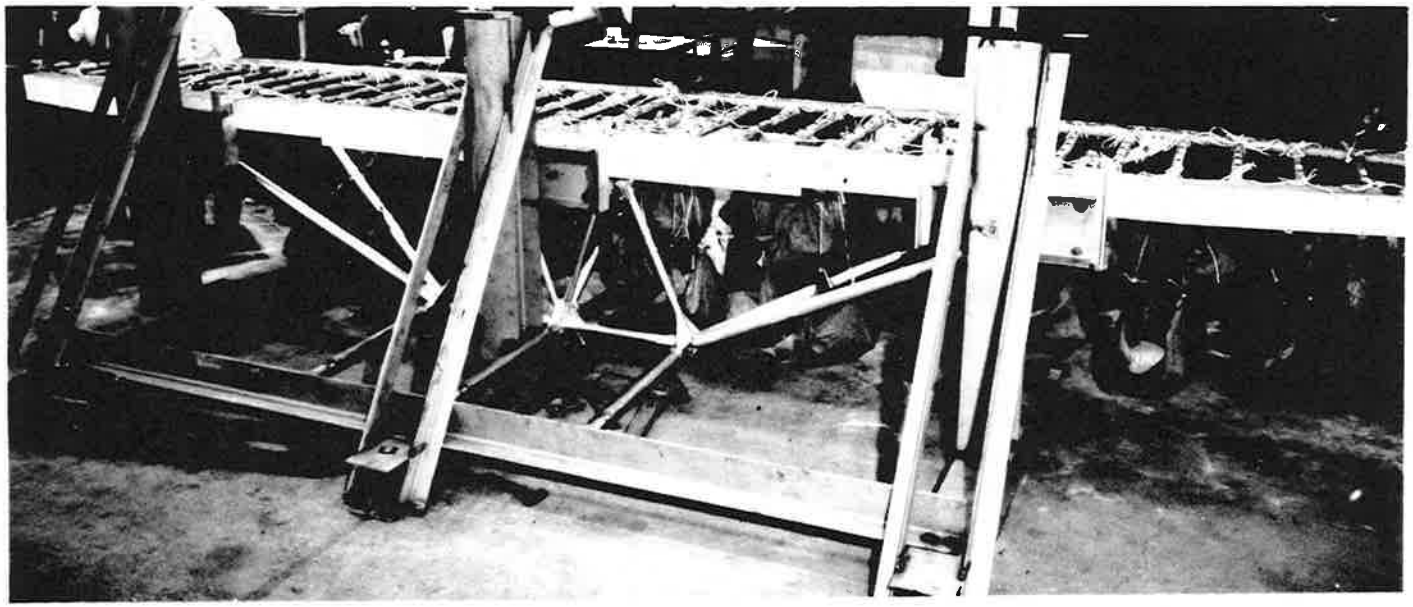

Figure 2-26. Deflection Test Setup

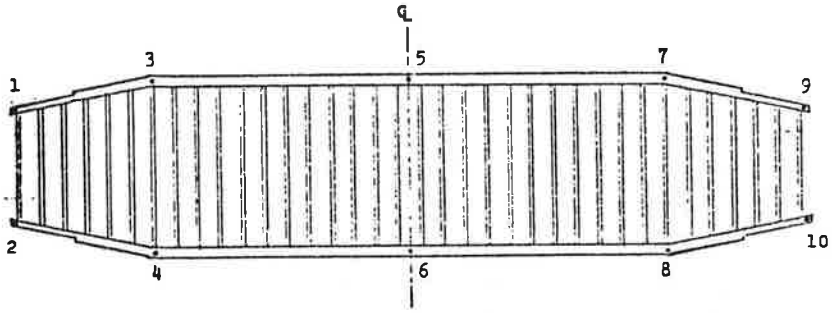

PT	BEFORE LOAD	WITH LOAD	REMOVED LOAD
1	10 5/16	10 9/16	10 5/16
2	10 1/4	10 9/16	10 7/16
3	10 3/16	10 15/32	10 11/32
4	10 3/16	10 1/8	10 1/8
5	10	10 3/16	10
6	10 1/16	10 3/16	10 1/8
7	9 7/8	10 17/32	10 1/16
8	9 3/4	9 15/16	9 25/32
9	9 11/16	10 23/32	9 3/4
10	9 5/8	10 11/16	9 3/4

Figure 2-27. Deflection Test Measurements

measured before, during, and after the imposition of the extreme temperatures. The divider networks were measured before exposure to the humidity and immediately after. The dipole rain test was not performed strictly according to method 506. This was due to a deficiency of equipment. The dipole was placed in a chamber and water was sprinkled on it for 1 hour. The rain rate was measured to be 20 inches per hour. Method 506 calls for rates of 5 and 12 inches per hour. Since the dipole functioned within specifications during the 20 in./hr. rainfall, it can be concluded that it would function during lighter rainfalls. The dipole performance was evaluated by examining changes in its VSWR. The divider networks were judged on a sampling of output port measurements. Transmission amplitude and phase readings were taken. A network analyzer operating with a phase gain indicator was used to measure amplitude and phase of the network outputs. The analyzer with a polar display was used to measure dipole impedance for the temperature tests, and a slotted line was used for rain and ice measurements. The dipole VSWR was high for the temperature and rain measurements. The readings taken

ranged from 1.5:1 to 3.2:1 VSWR, compared to normal 1.1:1 to 1.5:1 VSWR. The high reflection is attributable to the testing environment, which is a small reflective chamber. Also, a single dipole was tested, whereas the dipole was designed for use in an array. However, valid conclusions can be drawn, as the main objective of these tests was to note changes in VSWR with the imposition of extreme climatic conditions. The small metallic chamber also accounts for a disparity of measurements from test to test. The direction of radiation is highly critical in the reflective environment, and a repositioning of the dipole which occurred during the changing of the test setup caused a change in VSWR level from the temperature to rain tests. It should be noted, however, that during each of the tests, the dipole was mounted rigidly and care was taken not to jostle it.

A complete set of measurements was taken before the imposition of any environmental conditions, and immediately thereafter. These measurements included dipole VSWR and a complete set of output amplitudes and phases for the divider networks. Only two network output ports were sampled for the temperature tests, whereas a complete set of measurements was taken for the humidity tests. Before all network measurements were made, a reference cable placed outside the test chamber was measured. These reference measurements were used to compensate for any equipment drift. An analysis of the various test results is given below.

2.4.3 Analysis of Type Test Results

The deflection test resulted in an asymmetrical deformation of the antenna structure, indicating that, under conditions of 85-knot wind and 1.5 inches of radial ice during 15 rpm rotation, the pattern will be slightly distorted. This effect is evaluated in the following manner. The deflection is plotted in figure 2-28 in terms of equivalent electrical phase in degrees. The asymmetrical measurements may be resolved as shown into a linear phase tilt component, causing beam pointing error, and a defocusing component, causing null fill-in and increased sidelobes.

The beam pointing error (θ) is related to the aperture width and the edge-to-edge phase tilt as follows:

$$\text{Sin } \theta = \frac{\text{Edge-to-edge phase tilt (deg)}}{\text{Aperture width (deg)}}$$

For small angles, θ(rad) $\sim$ Sin θ, so that the pointing error in degrees may be calculated as:

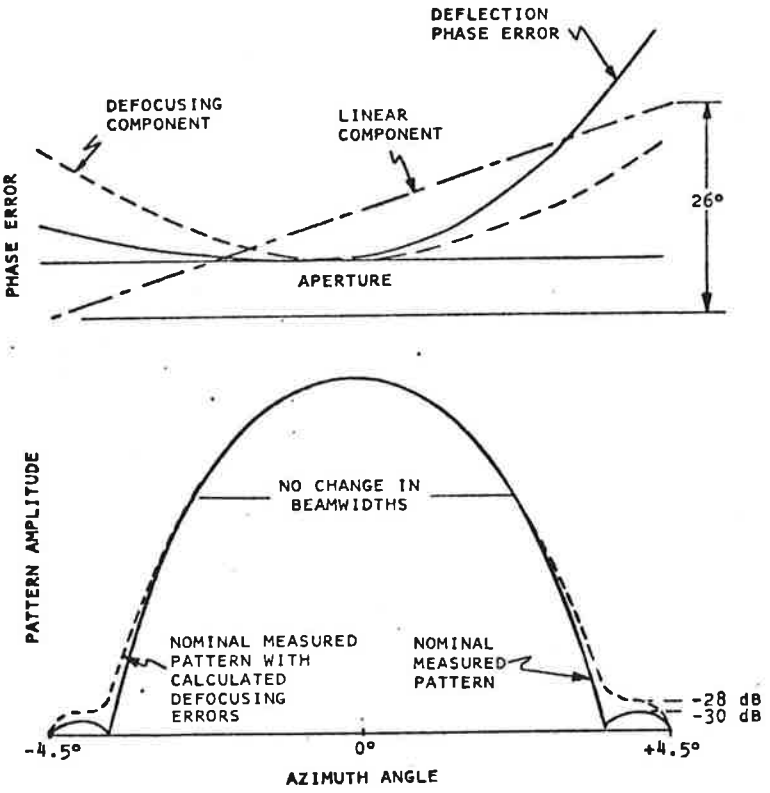

Figure 2-28. Effect of Deflection on Array Patterns

$$\text{Pointing error (deg)} = \frac{\text{Edge-to-edge phase tilt (deg)}}{\text{Aperture width (deg)}} \times 57.3 \text{ (deg/rad)}$$

Thus,

$$\text{Pointing error} = \frac{26 \times 57.3}{9720} = 0.15^{\circ}$$

The defocusing effect can be evaluated by assuming that the phase error has the form $(1-\cos \frac{2\pi x}{d})$ where x is the aperture variable and d is the period of the error. For this case the pattern error is simply a small quadrature pattern slightly shifted away from the main beam (1). The total pattern is the sum of the nominal pattern and the error pattern. Using measured nominal patterns, the effect of defocusing has been calculated and the result is plotted along

(1) J. Brown, "The Effect of a Periodic Variation in the Field Intensity Across a Radiating Aperture," Proc. IEE, Vol 97, Part III, 1950.

with the nominal pattern in figure 2-28. The effect of defocusing is essentially confined to the region between -4.5 degrees and +4.5 degrees in azimuth. The wind loading on the array also results in a small tilt of the array which will move the elevation pattern upward by approximately 0.3 degree. This will not result in any significant change in elevation pattern coverage.

The dipole was evaluated under exposure to temperature, rain and ice. Over the range of temperatures from -60°F to +155°F, the dipole showed an insignificant variation in VSWR. In addition, this effect should be common to all dipoles, thus eliminating all pattern effects. The small variation in VSWR may result in a gain variation with temperature of 0.1 to 0.2 dB. The dipole again showed a small variation in reflection during the rain tests. The impedance variation may at any instant fluctuate from dipole to dipole and so it is assumed that some effect on the sidelobes could be observed. The pattern error can be calculated from the RMS aperture error using the formula:

$$Ve = \frac{Va}{\sqrt{N\eta}}$$

Ve = RMS pattern error voltage
Va = RMS aperture error voltage
N = number of elements
η = aperture efficiency

The dipole impedance variation could result in an amplitude or phase error, depending on the impedance change; if we assume only the greatest possible phase error, an RMS random error of 1.8 degrees is obtained on the aperture. Thus the pattern error voltage (converting 1.8 degrees to radians) is:

$$Ve = 0.03/\sqrt{252 \times 0.4} = 0.003$$

This amplitude error voltage will increase a 28 dB design sidelobe level to not more than 27 dB. Because the present antenna has only a few sidelobes above -30 dB, there is even less likelihood of raising a sidelobe out of specification. Measurements made at the Smithtown test range during a light rain indicated no significant increase in sidelobes. The effect of ice on the dipole is greater than the effect of rain. The ice tends to act as a shunt capacitance across the dipole, thereby detuning it from resonance. The nominal 1.5:1 VSWR of the dipole in the array environment increased to approximately 2.5:1 with 1.5 inches of radial ice. The effect of ice on the antenna patterns is highly dependent on the distribution of ice on the array. If the ice is distributed uniformly on all of the dipole elements,

then no pattern distortion will occur, and the only result will be a loss in gain of approximately 0.8 dB caused by reflection loss. This additional reflection will be absorbed by the networks and will not cause a significant increase in the VSWR presented to the transmitter. If the ice is not uniformly distributed, then the errors introduced may cause beam pointing errors and increased sibelobes.

To evaluate these pattern errors, first let us assume that the error contributed by the ice is predominantly a phase error. Because the ice behaves as a shunt capacitance in detuning the dipole element, this is a reasonable assumption. The measured element impedance with and without 1.5 inches of ice yields a maximum phase error of 25^{o}. If the ice builds up in an uneven manner so that a random thickness of ice is coated onto each dipole, the worst-case result will be a random error on the aperture, which will increase the sidelobes. If we assume the maximum error is uniformly distributed between 0 and 25 degrees, the rms phase error is 7 degrees and the mean phase is 12.5 degrees. Using the equation for rms pattern error voltage presented previously, the computation shows that the peak sidelobe level will be less than -25.4 dB 95 percent of the time, assuming the array has a uniform sidelobe level of -28 dB.

Because of the open nature of the array structure, it is not likely that the variation in ice thickness will be as great as that assumed above. Thus, there is even less possibility that the array will operate out of specification. If it is assumed that the thickness of ice deposited on the antenna varies across the aperture because of rotation (the ice builds up on the leading side of the rotating antenna), then a beam pointing error will occur. A very simple error estimate can be made by assuming that the varying ice thickness imposes a linear phase tilt across the aperture with a maximum error of 25 degrees on the leading edge of the array and no error at the trailing edge. Then the beam pointing error, calculated in the same manner as before, is:

$$\text{Pointing error } (25 \times 57.3)/9720 = 0.15^{o}$$

It should be noted that this pointing error will also occur with the present ATCRBS antenna because of the transmission phase error caused by ice on the radome of the antenna. Under conditions of 85-knot wind and 1-1/2 inches of ice, the beam pointing errors resulting from deflection and from dipole detuning will add, resulting in a total pointing error of 0.3 degree. This is entirely acceptable for the present ATCRBS system.

The environmental tests on the elevation and azimuth networks indicate no significant change with temperature. A total insertion phase change of 10 degrees was measured on the networks, with variation from output to output of only 1 to 2 degrees. The

change in average insertion phase is common to all networks and will not affect array performance. The humidity test resulted in a 15° phase tilt along the length of the azimuth network, and was the most significant error noted. It was concluded that the error was caused by moisture between the layers of the stripline board; the moisture entering through the TNC connectors. To prevent this problem in the final array, each connector pair was coated with Dow-Corning DC4 dielectric grease before assembly. The phase error resulting from the humidity test is nearly identical to the defocusing error caused by mechanical deflection of the structure. Using the same analysis, the pattern error is the same as shown in figure 2-28.

In summary, it can be concluded from the type tests that the antenna should yield satisfactory performance under the required range of environmental conditions.

3. OMNI ANTENNA

3.1 MECHANICAL DESIGN

3.1.1 General Description

The omni antenna (figures 1-5 and 1-6) consists basically of a column of six dipoles covered by a 4-foot high by 6.5-inch diameter radome. The dipoles are mounted to a support mast/reflector which is approximately 4 inches wide and 1 inch thick. The entire radome and support mast assembly are bolted to a main mounting plate. The elevation network is enclosed in a 6.5-inch diameter by 10.3-inch deep circular housing located below the main mounting plate. The method of mounting the dipoles to the support mast/reflector enables the dipole feed cables to be routed through the support mast to the elevation network.

3.1.2 Mounting Arrangement

The mounting arrangement of the omni antenna calls for a 3-inch diameter, 0.375-inch wall thick aluminum mast, which bolts directly to the omni antenna base. The antenna input connector projects out of the network enclosure at the bottom of the antenna, and connects to a feed cable routed through the mast. The omni antenna and mast are of a straightforward mounting configuration with three attachment points to the ASR tower. Any suitable location on the tower can be utilized provided that the open array antenna has sufficient rotational clearance. In the mounting at NAFEC, New Jersey, a lightning rod was removed and its position taken by the omni mast.

3.1.3 Weight Breakdown

The final weight breakdown of the omni antenna and its components is presented in table 3-1.

TABLE 3-1. WEIGHT BREAKDOWN, OMNI ANTENNA (Pounds)

Omni Antenna Dipoles	1.5
Cables for Elevation Network	2
Radome	8.5
Support Structure and Network	20
Total	32

3.1.4 Dipole Construction

Details of the electrical design of the omni antenna dipoles are presented in paragraph 3.2.2. Each individual dipole is printed on a single stripline board with a "T" junction at the central feedpoint. The stripline material is copper clad styrene copolymer, reinforced with fiberglass. The individual dipoles are connected to the elevation network by semi-rigid cables which are routed through the support mast/ground plane.

3.1.5 Elevation Network

The elevation beam forming network used in the omni antenna is similar to that used in the open array antenna. Refer to paragraph 2.1.5 for construction details.

3.1.6 Environmental Design Considerations

The omni antenna was designed to meet the same environmental conditions as the open array antenna (paragraph 2.1.10), except for the 15 rpm rotational requirement, which does not apply. As in the case of the open array antenna, lightweight materials were used throughout. The omni antenna structure is fabricated of aluminum alloy 6061. The entire structure is finished per MIL-C-5541 Chemical Film CL3. This is a gold irridescent finish offering excellent corrosion protection. The exterior surfaces are finished in accordance with FAA-STD-003 Paint System BE-9 Color No. 17875 White Gloss per FED-STD-595. The printed stripline dipoles are protected with a coating of PT-207. This is a polyvinyl fluoride compound often used to seal printed wiring boards against moisture and dirt, and offers adequate protection against moisture in the radome. The radome is constructed of glass-reinforced polyester resins. The exterior surface is primed and painted using white enamel. The color is Lusterless White No. 37875 per FED-STD-595. The elevation network and all cable connections were sealed in the same manner as in the open array antenna.

3.1.7 Load Analysis

Due to the relatively small loads and inherently high strength of the omni antenna, no special structural tests were required.

3.2 ELECTRICAL DESIGN

3.2.1 General

The omni antenna was designed for use in conjunction with the open array antenna. It is intended to produce an approximately omnidirectional azimuth pattern and a shaped elevation pattern. The

omni antenna elevation pattern should match closely the open array elevation pattern in order to minimize differential lobing which could result in lost replies. The design chosen to accomplish these goals is shown schematically in figure 3-1. Each pair of printed-circuit dipoles is fed in-phase and spaced from the ground plane such that an omnidirectional pattern is radiated in azimuth. The elevation pattern is shaped using the same elevation network used in the open array antenna. Design corrections required due to the differences between the dipole types used in the omni and open array antennas are described below. Figure 3-2 shows a typical omni elevation pattern plotted against an open array elevation pattern to demonstrate the close agreement of the two patterns. A set of omni antenna patterns is provided in Appendix A.

3.2.2 Printed Dipole Design

A printed circuit design was used for the omni antenna dipoles. This approach was used because printed circuit elements offer versatility in design and low cost in fabrication. The dipole design was accomplished in two steps. First, a dipole pair was designed in a simulator which approximates an infinite vertical array of dipoles with uniform excitations. Figure 3-3 shows a dipole pair mounted in the parallel plate simulator. After the dipole pair had been impedance-matched in the simulator, a small correction was made to each dipole matching. This correction was necessary because the mutual coupling environment is different for the omni antenna than for the open array antenna. This would normally require different elevation networks for each antenna. Since the same elevation network was intended to be used for both antennas, the matching in the printed dipoles was adjusted to correct for the given network illumination outputs. The modification to the dipole matching results in less than 0.5 dB loss in the omni antenna gain.

3.2.3 Elevation Network Design

The elevation network used in the omni antenna is identical to the elevation network used in the open array antenna, with one exception: a type HN connector is used for the input connector in lieu of the type TNC connector in the open array antenna. Connections from the elevation network to the dipole elements are made by 0.141-inch diameter semi-rigid cables.

3.3. RANGE TESTS

The omni antenna was measured at the Smithtown test facility using the 1,000-foot range. The antenna was mounted vertically on the

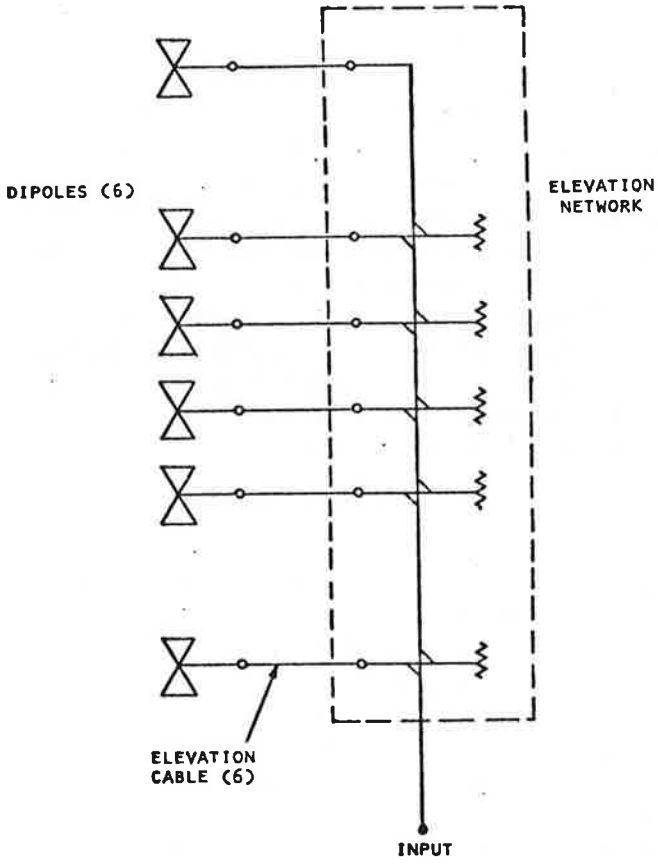

Figure 3-1. Omni Antenna, Schematic Diagram

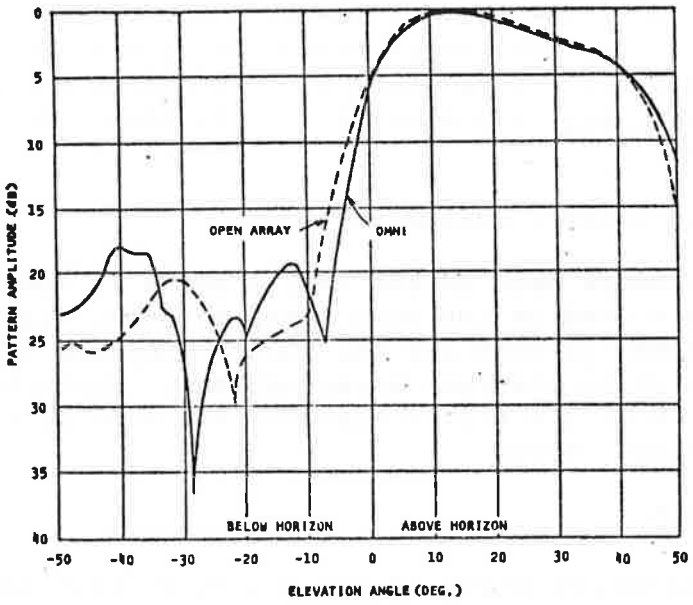

Figure 3-2. Comparison of Omni and Open Array Elevation Patterns

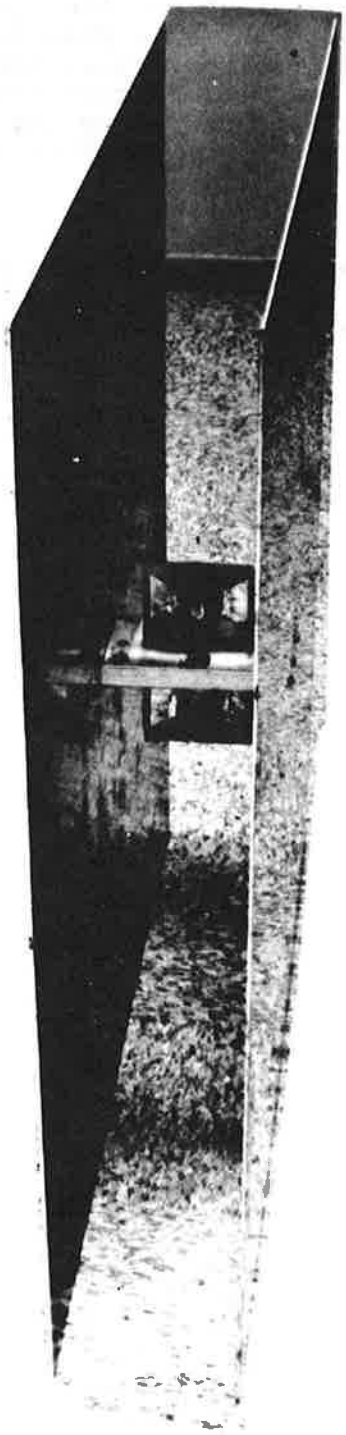

Figure 3-3. Omni Simulator for Impedance Matching

same test pedestal that was used for the open array antenna (paragraph 2.3.4). Azimuth patterns were measured by tilting the antenna to the required elevation angle, then rotating the upper azimuth mount to take a "conical pattern cut". Elevation patterns were measured by tilting the antenna by use of the elevation mount. The omni antenna patterns are presented in Appendix A.

3.4 TYPE TESTS

Type tests were performed on the elevation network, which is common to both the omni antenna and the open array antenna. These tests are described in paragraphs 2.4.2 and 2.4.3.

APPENDIX A. ANTENNA PATTERNS

A.1 OPEN ARRAY ANTENNA

A set of test patterns for the open array antenna is presented in figures A-1 through A-80. The patterns in figures A-1 through A-6 were taken on the Smithtown range, the remaining patterns on the ESSCO range.

A.2 OMNI ANTENNA

A set of test patterns for the omni antenna is presented in figures A-81 through A-96. All omni antenna patterns were taken on the Smithtown range.

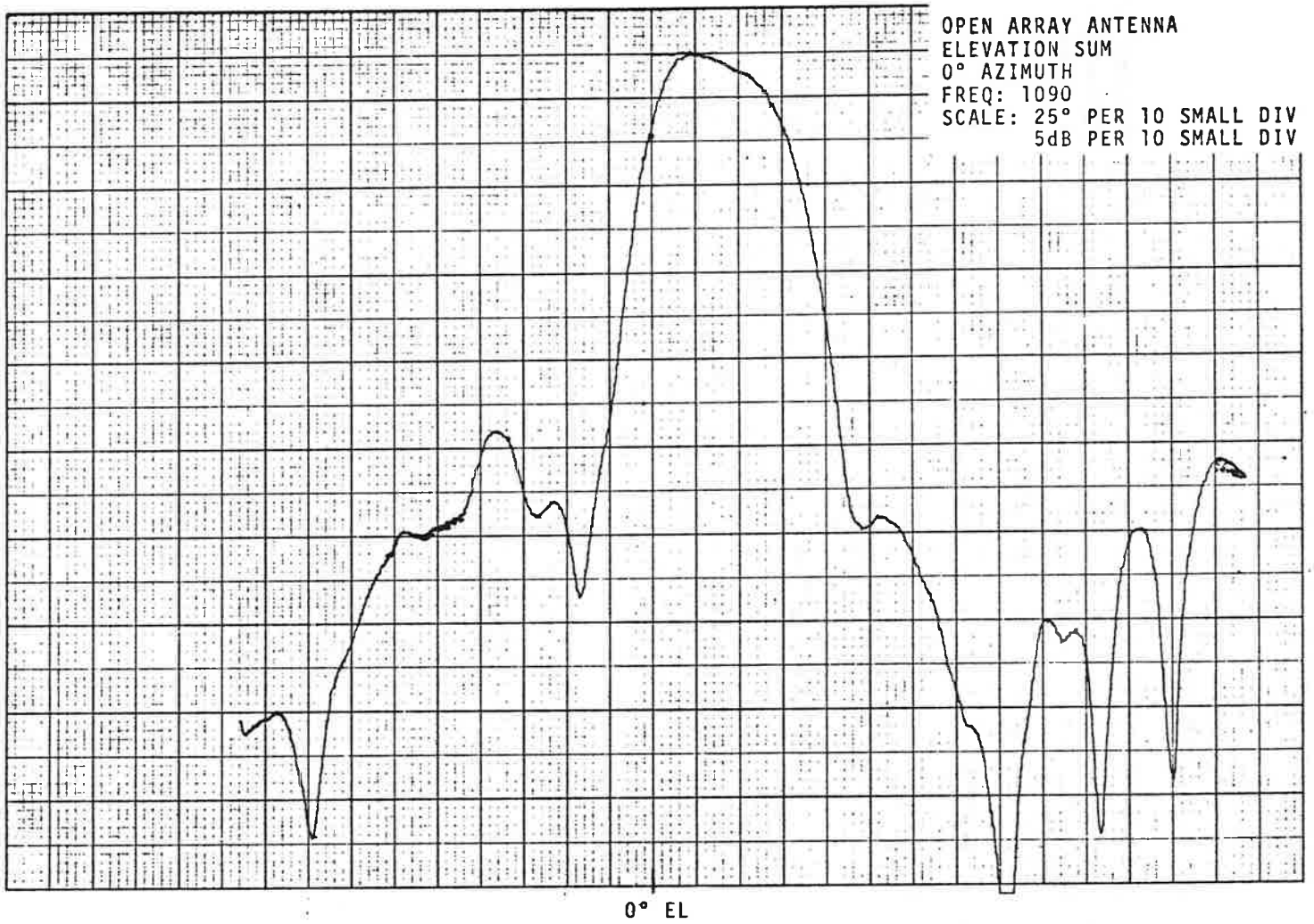

Figure A-1. Open Array Elevation Sum Pattern, 0° Azimuth, 1090 MHz

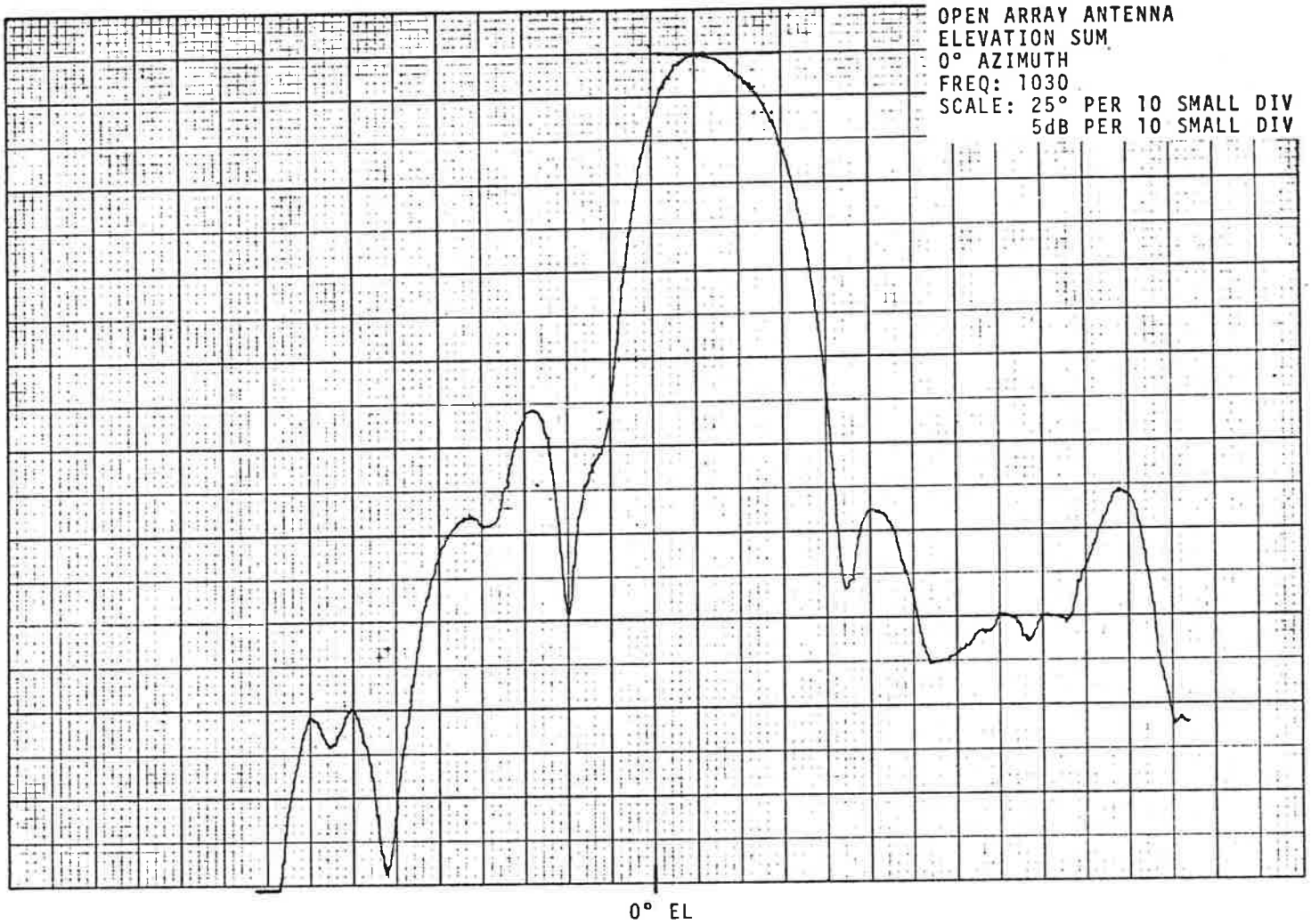

Figure A-2. Open Array Elevation Sum Pattern, 0° Azimuth, 1030 MHz

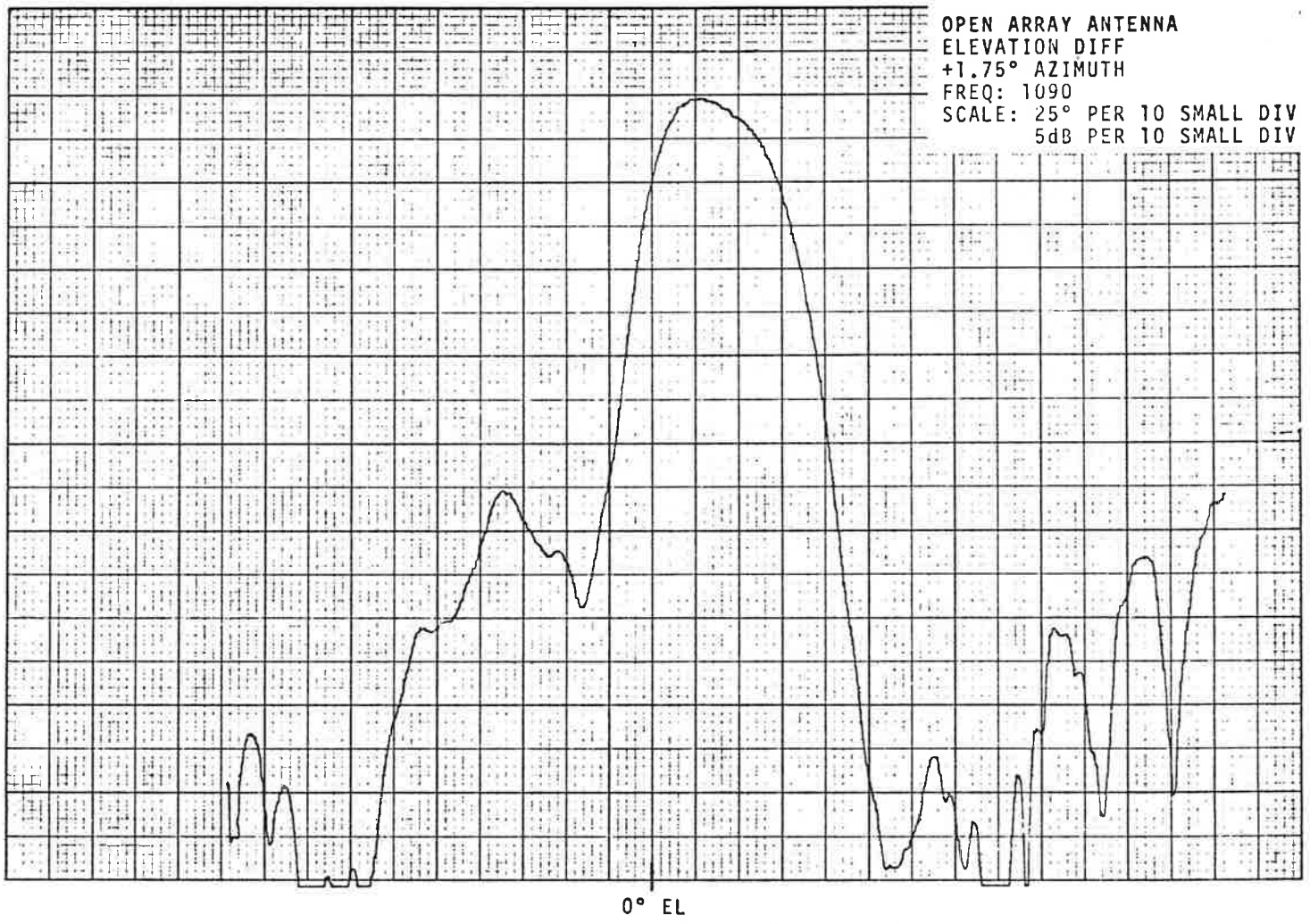

Figure A-3. Open Array Elevation Difference Pattern, +1.75° Azimuth, 1090 MHz

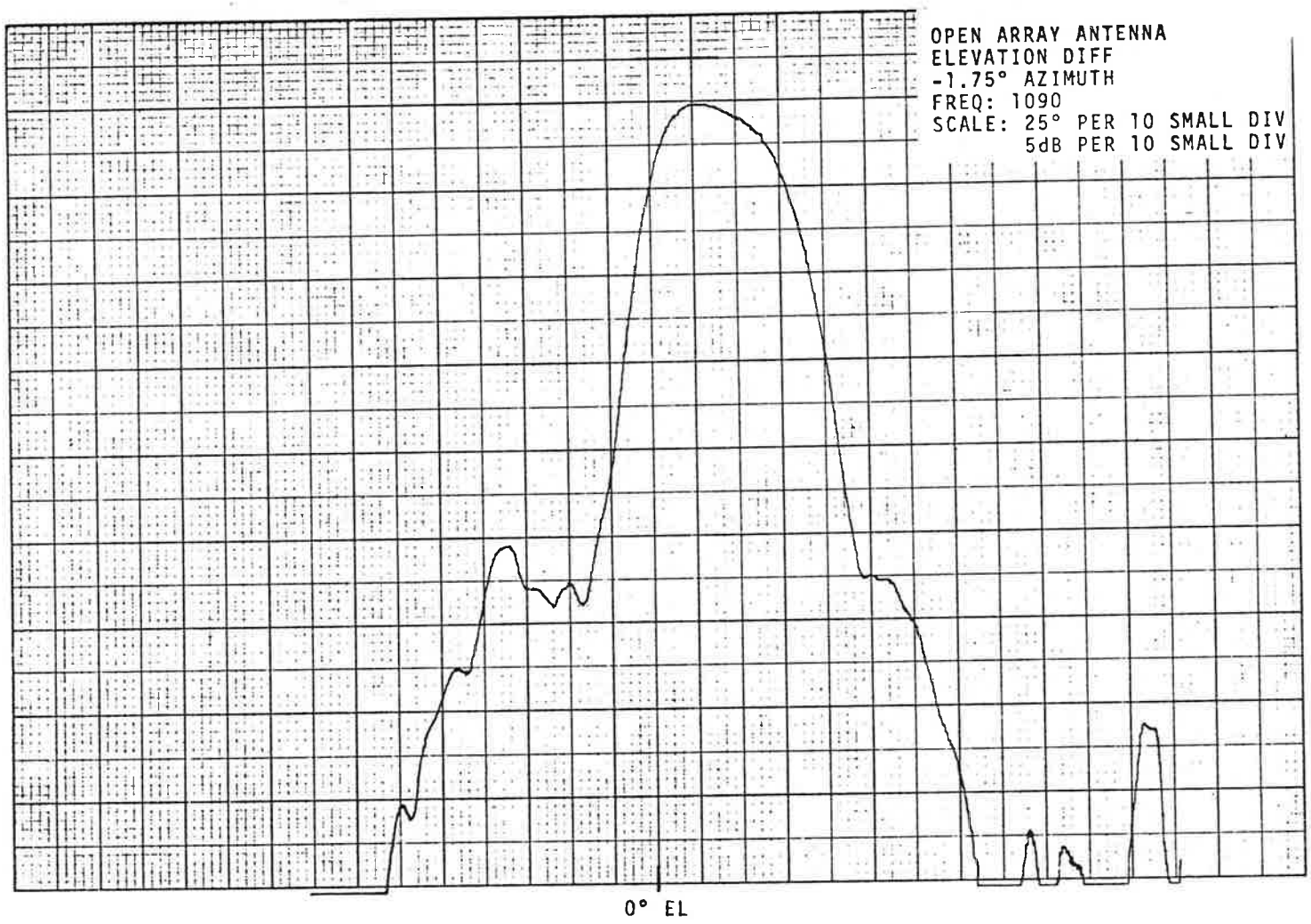

Figure A-4. Open Array Elevation Difference Pattern, -1.75° Azimuth, 1090 MHz

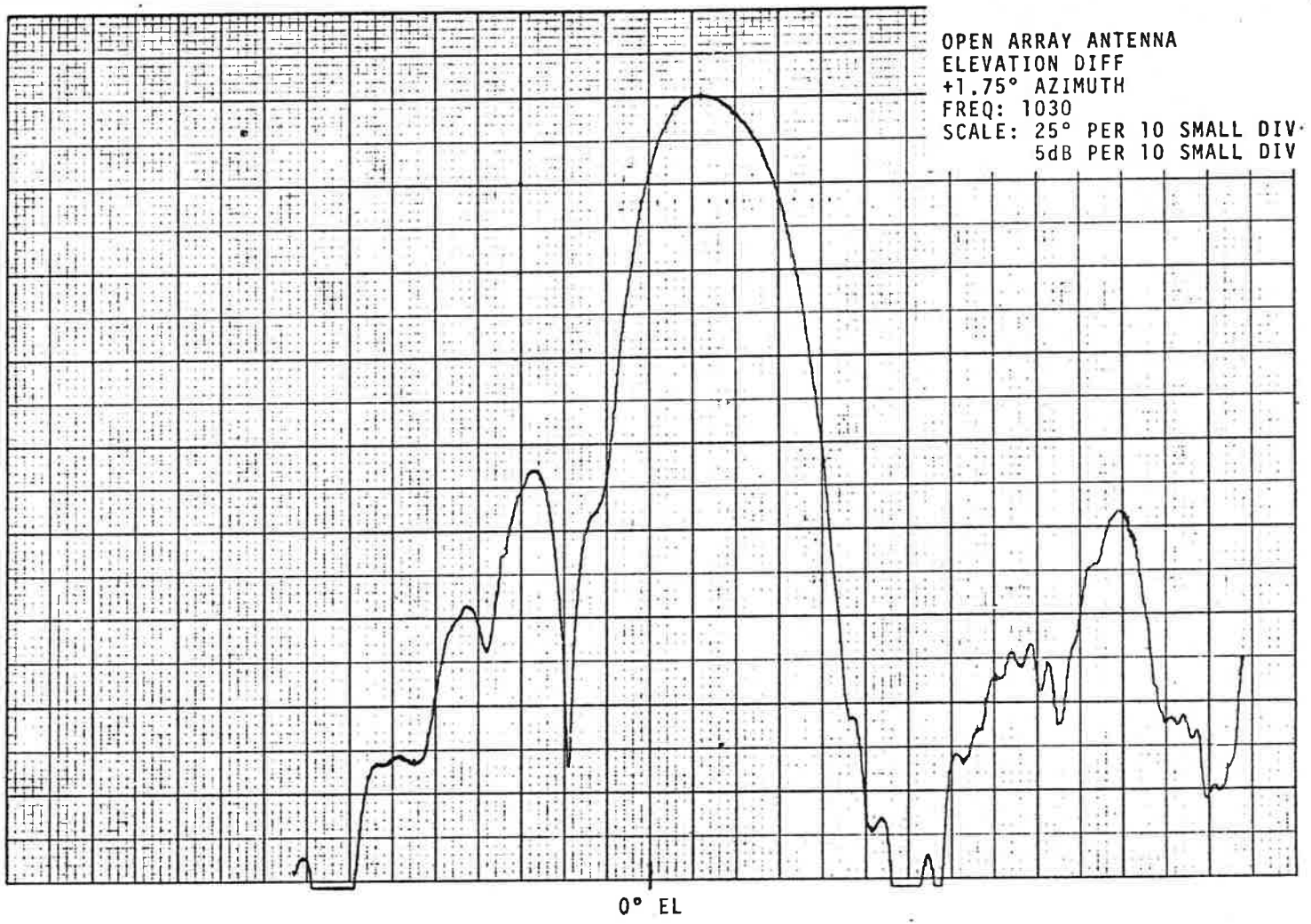

Figure A-5. Open Array Elevation Difference Pattern, +1.75° Azimuth, 1030 MHz

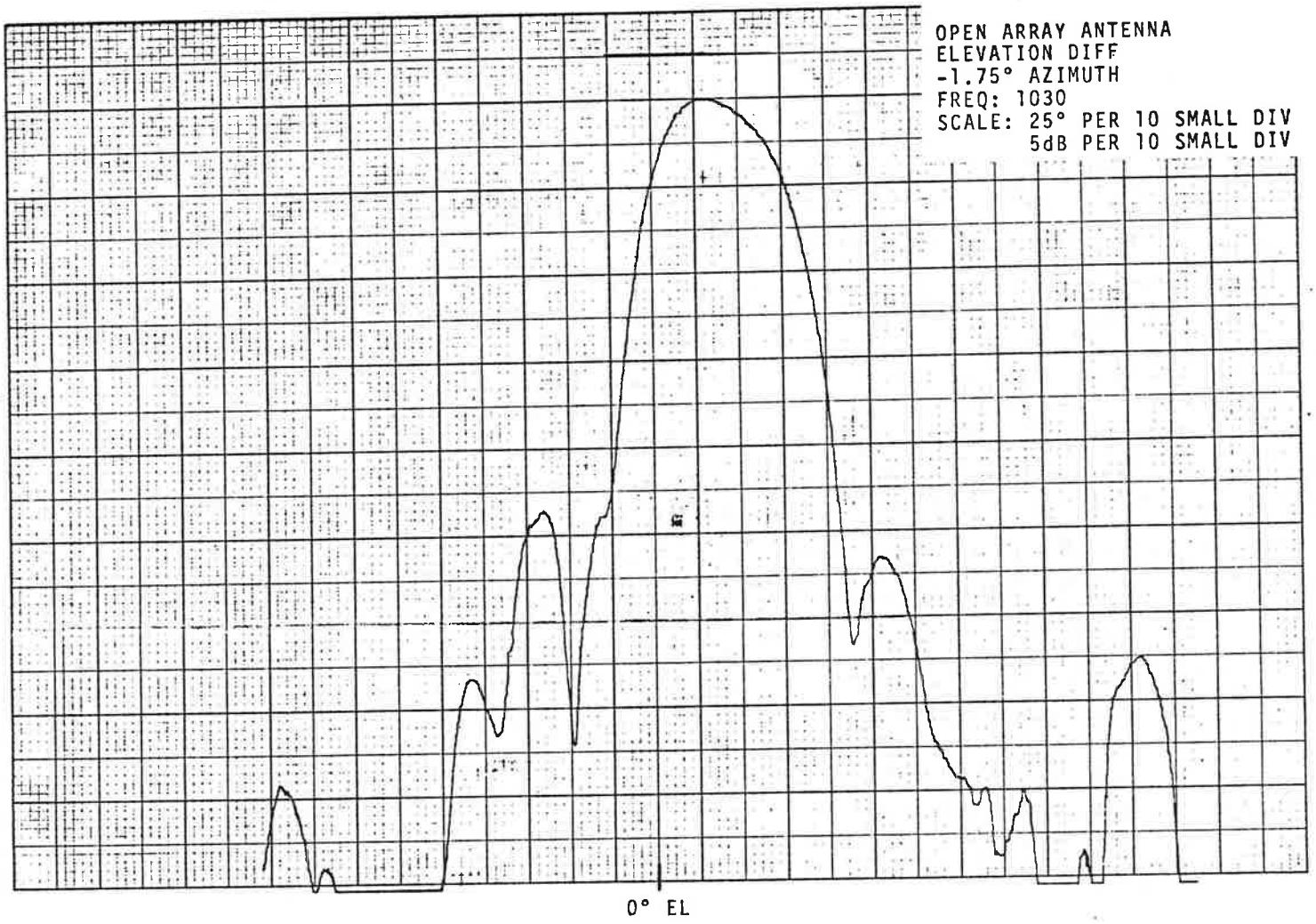

Figure A-6. Open Array Elevation Difference Pattern, -1.75° Azimuth, 1030 MHz

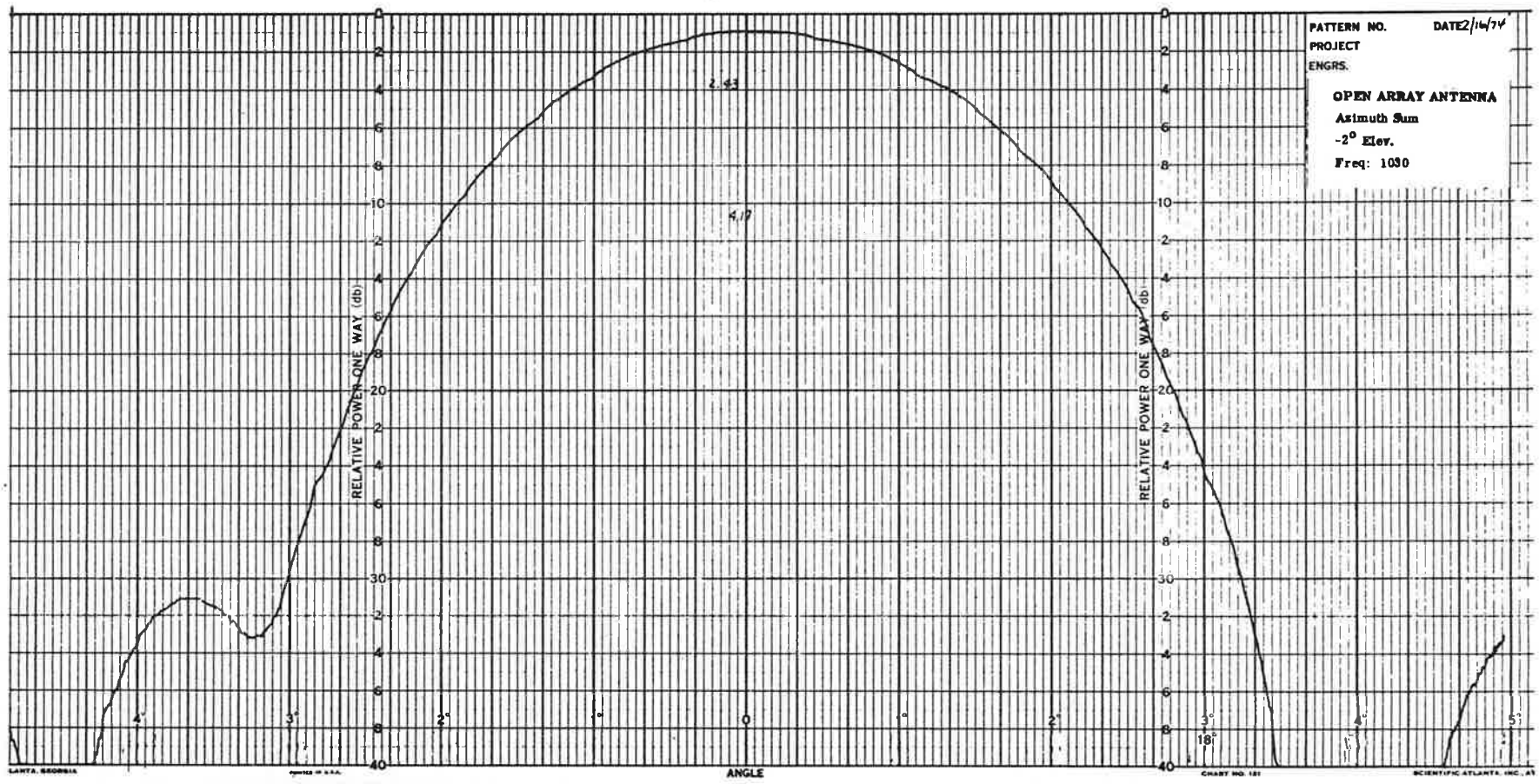

Figure A-7. Open Array Azimuth Sum Pattern, -2° Elevation, 1030 MHz, Narrow Angle

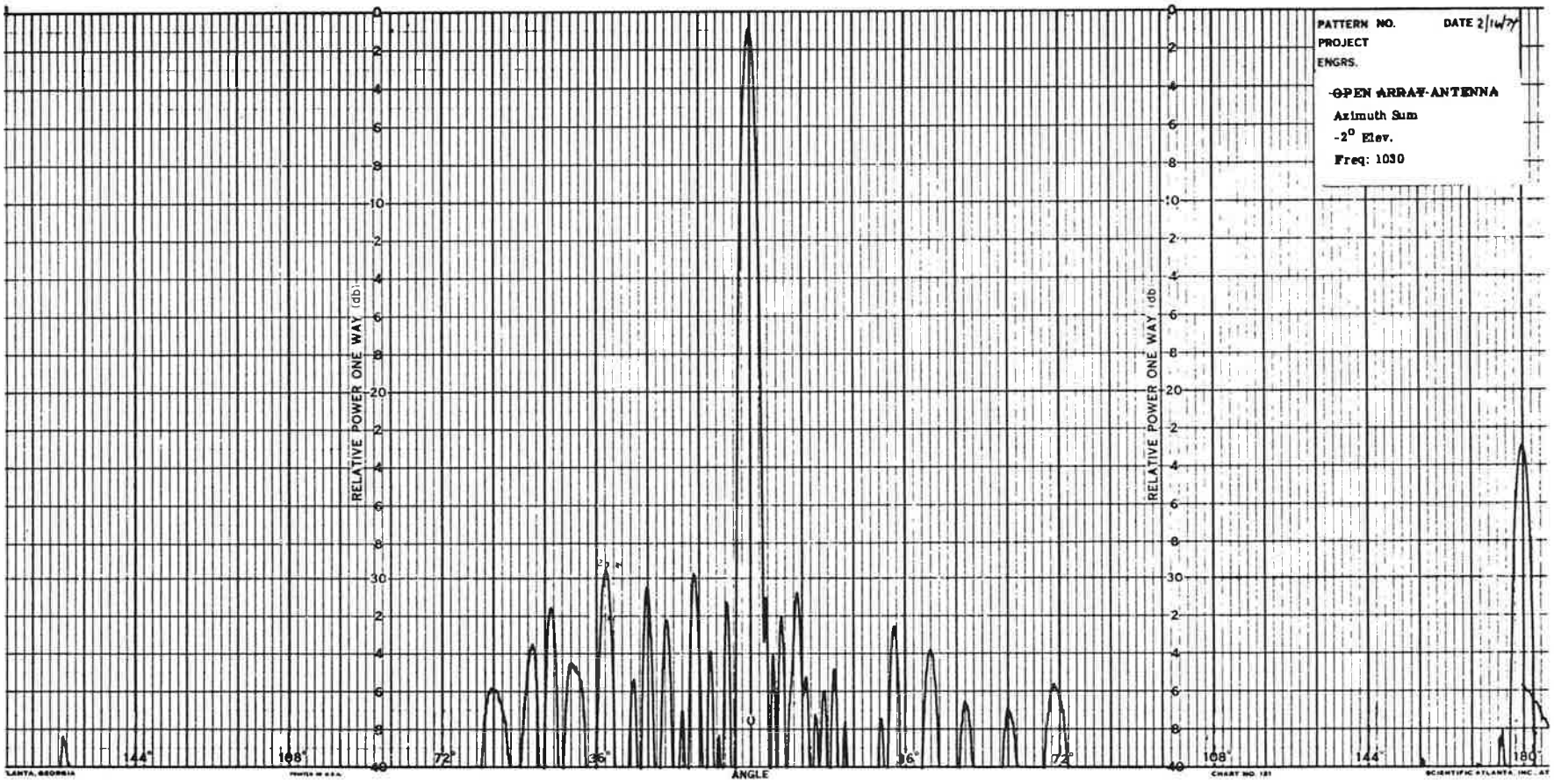

Figure A-8. Open Array Azimuth Sum Pattern, -2° Elevation, 1030 MHz, Wide Angle

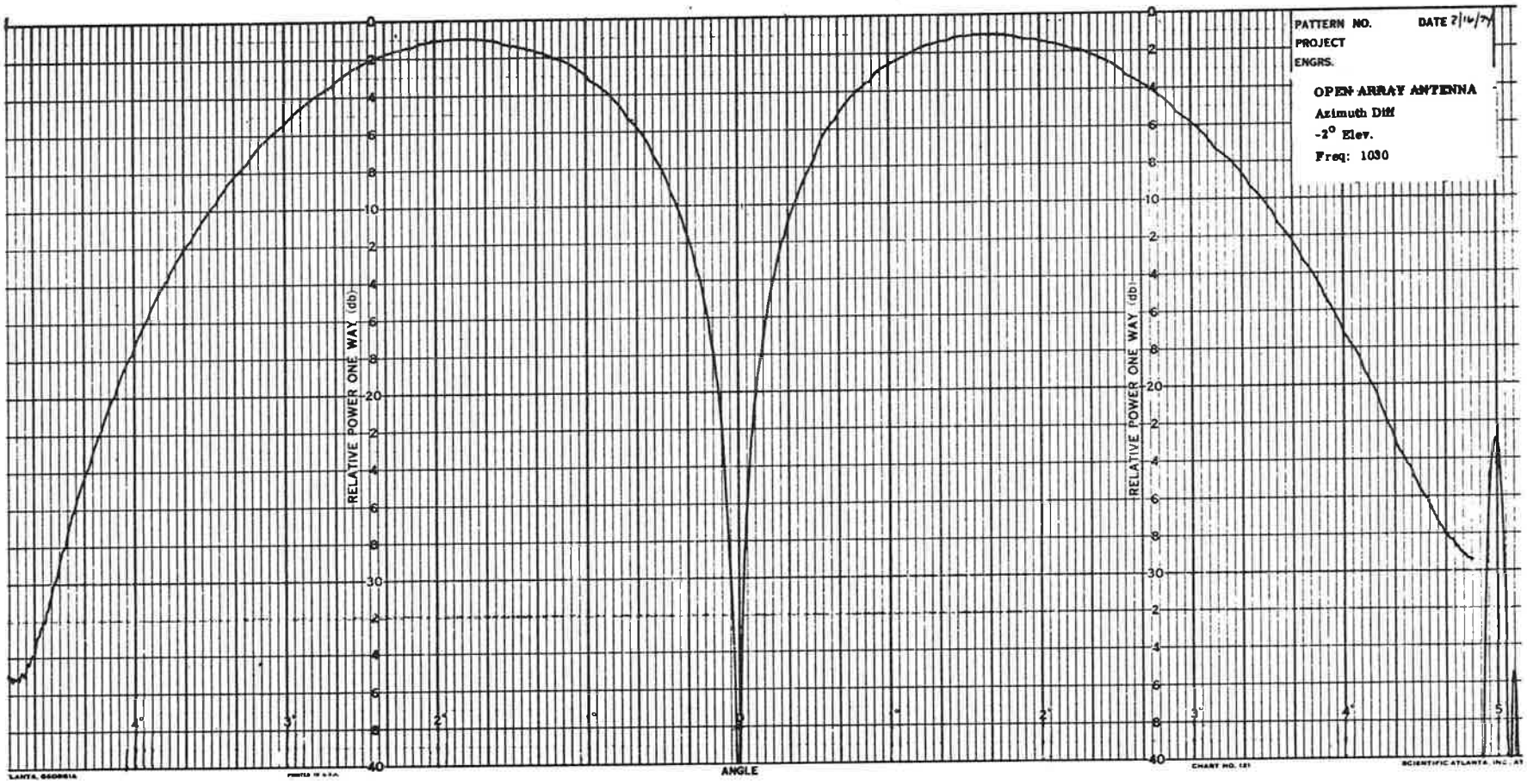

Figure A-9. Open Array Azimuth Difference Pattern, -2° Elevation, 1030 MHz, Narrow Angle

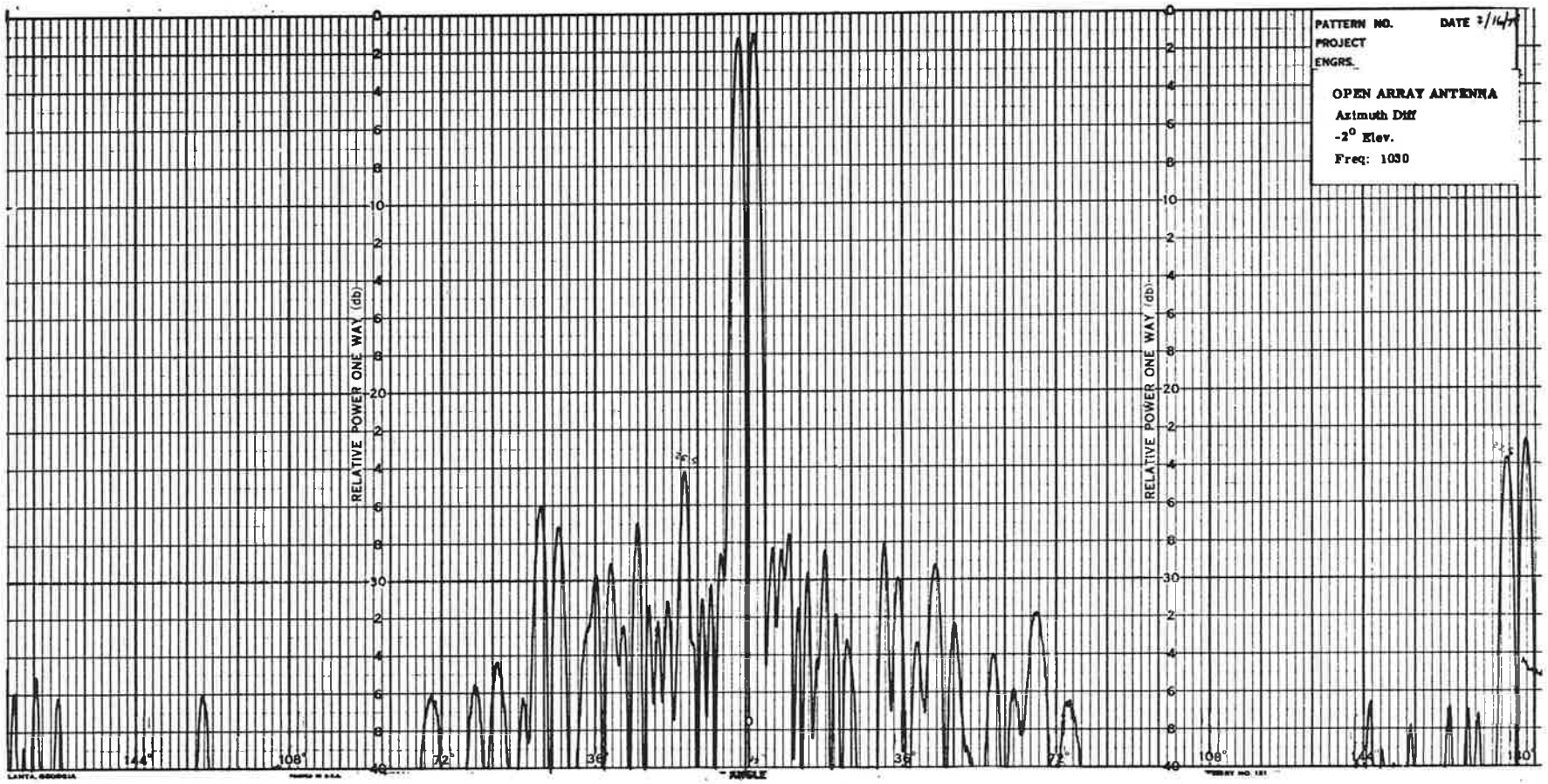

Figure A-10. Open Array Azimuth Difference Pattern, -2° Elevation, 1030 MHz, Wide Angle

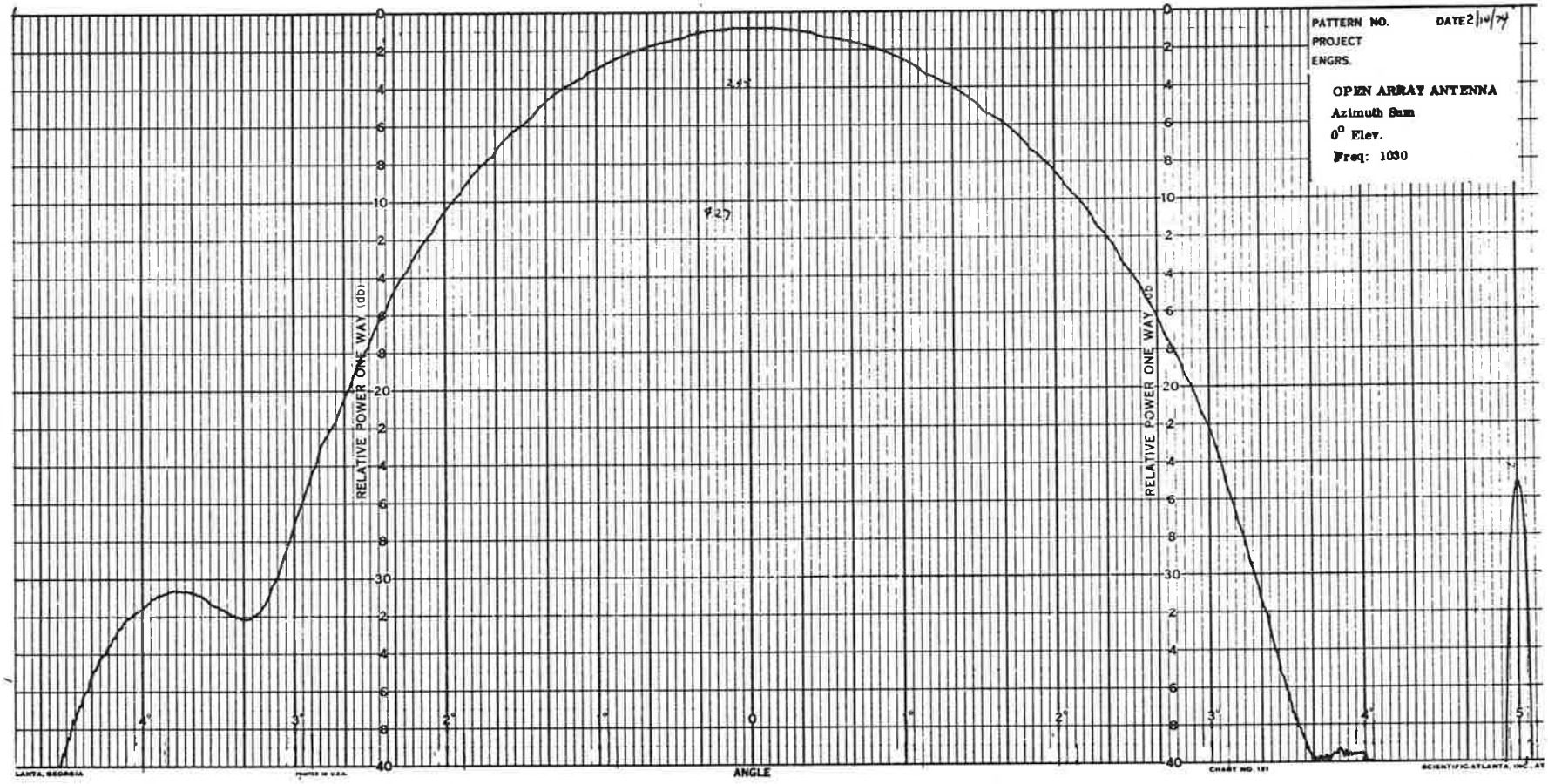

Figure A-11. Open Array Azimuth Sum Pattern, 0° Elevation, 1030 MHz, Narrow Angle

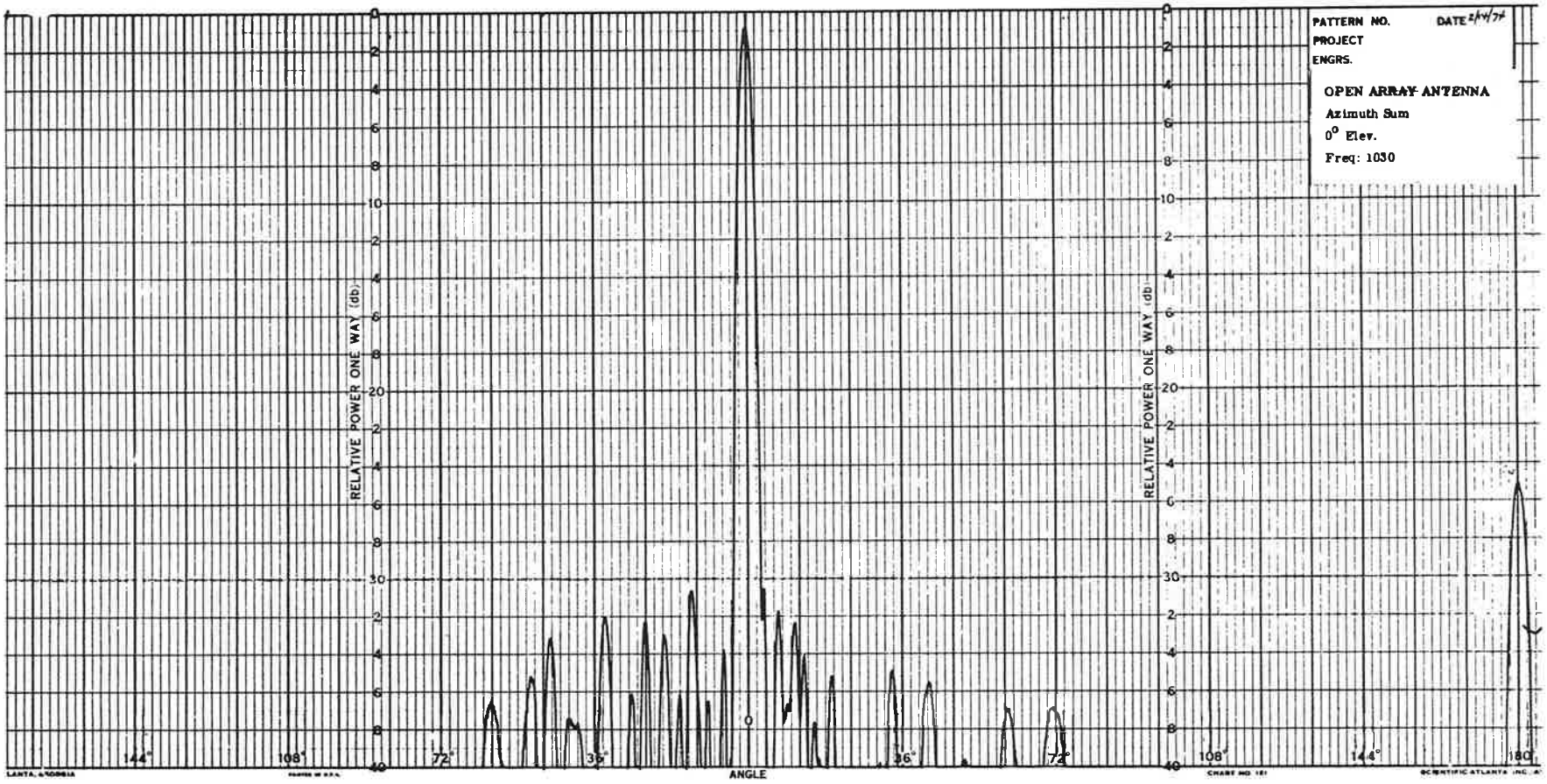

Figure A-12. Open Array Azimuth Sum Pattern, 0° Elevation, 1030 MHz, Wide Angle

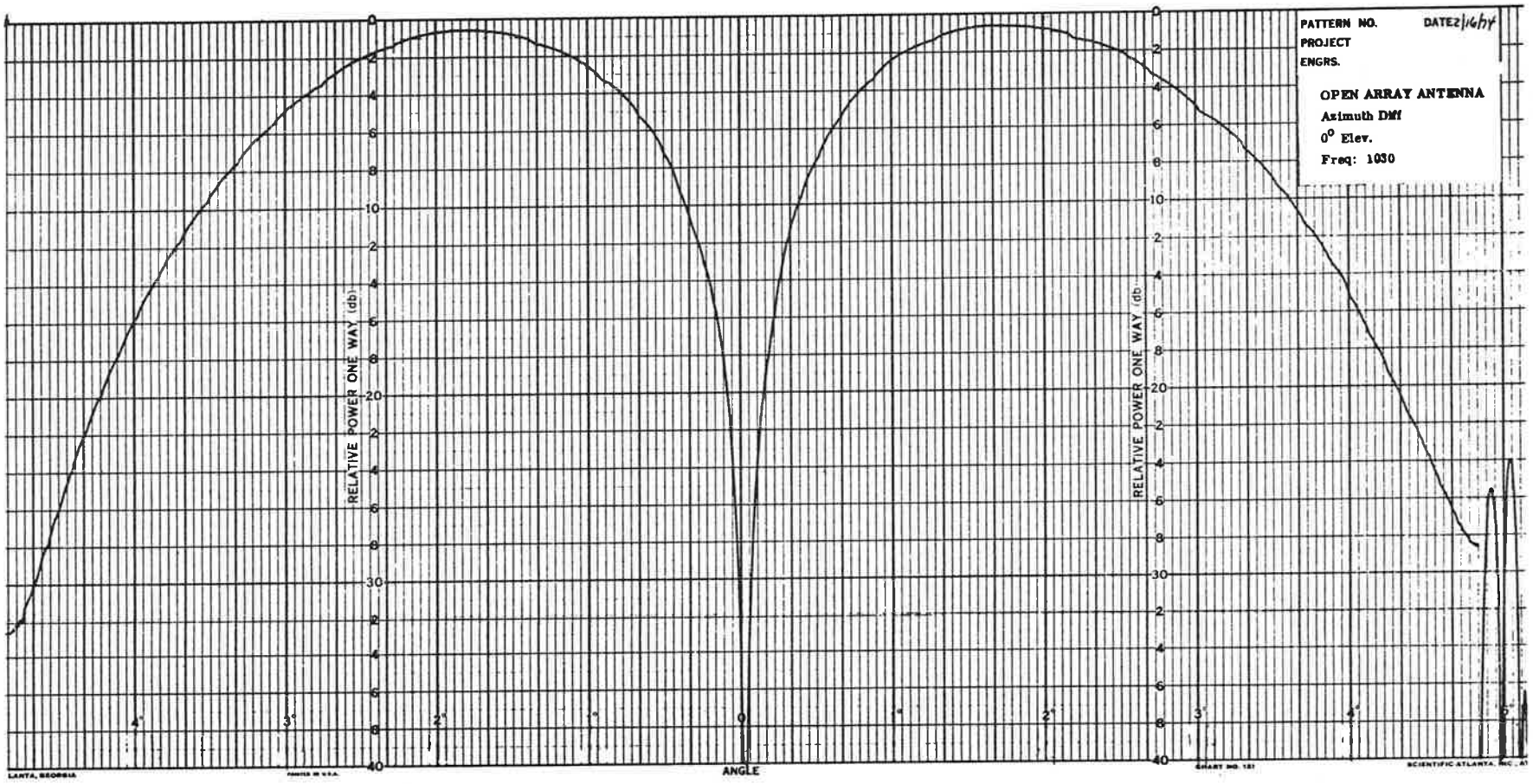

Figure A-13. Open Array Azimuth Difference Pattern, 0° Elevation, 1030 MHz, Narrow Angle

Figure A-14. Open Array Azimuth Difference Pattern, 0° Elevation, 1030 MHz, Wide Angle

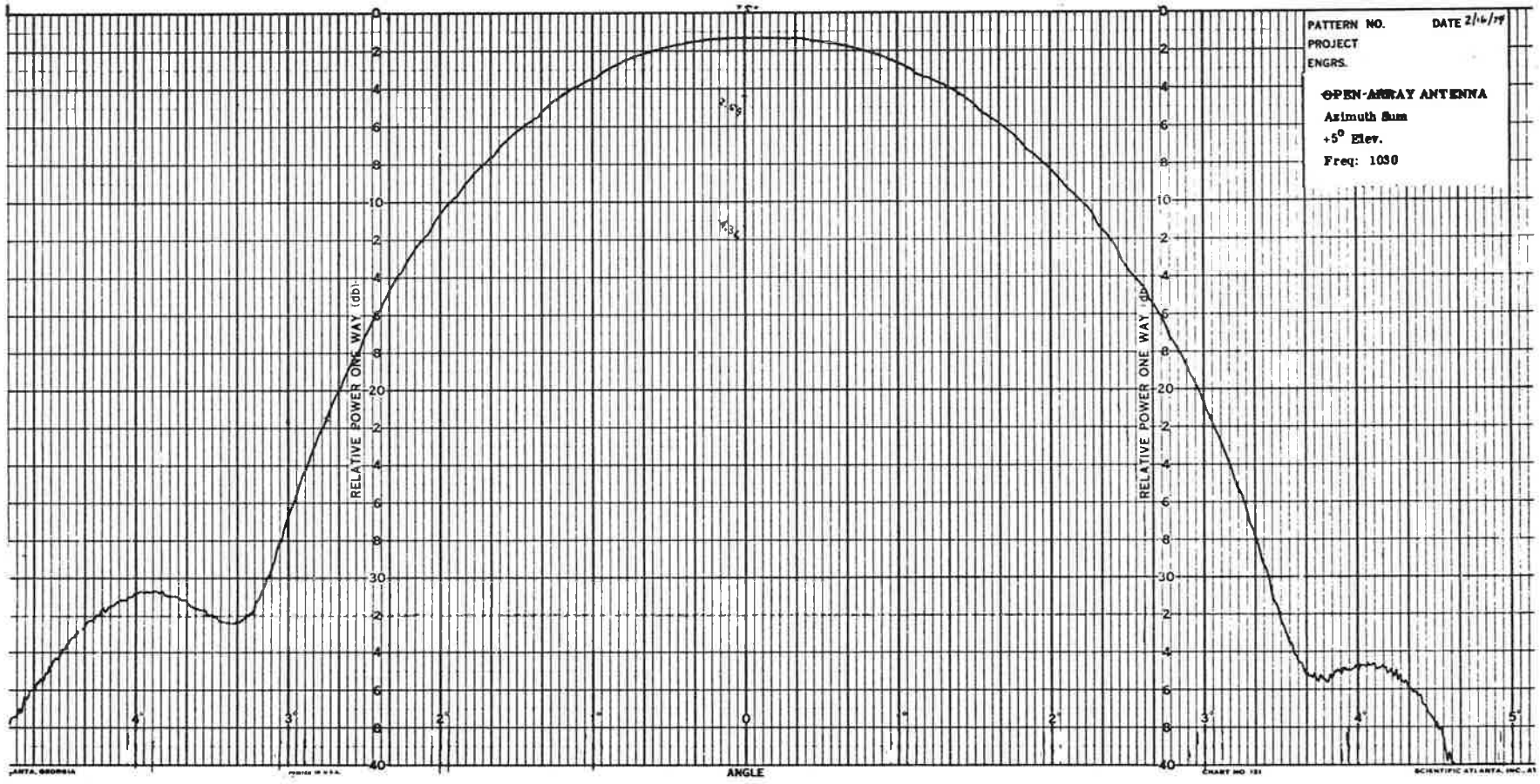

Figure A-15. Open Array Azimuth Sum Pattern, 5° Elevation, 1030 MHz, Narrow Angle

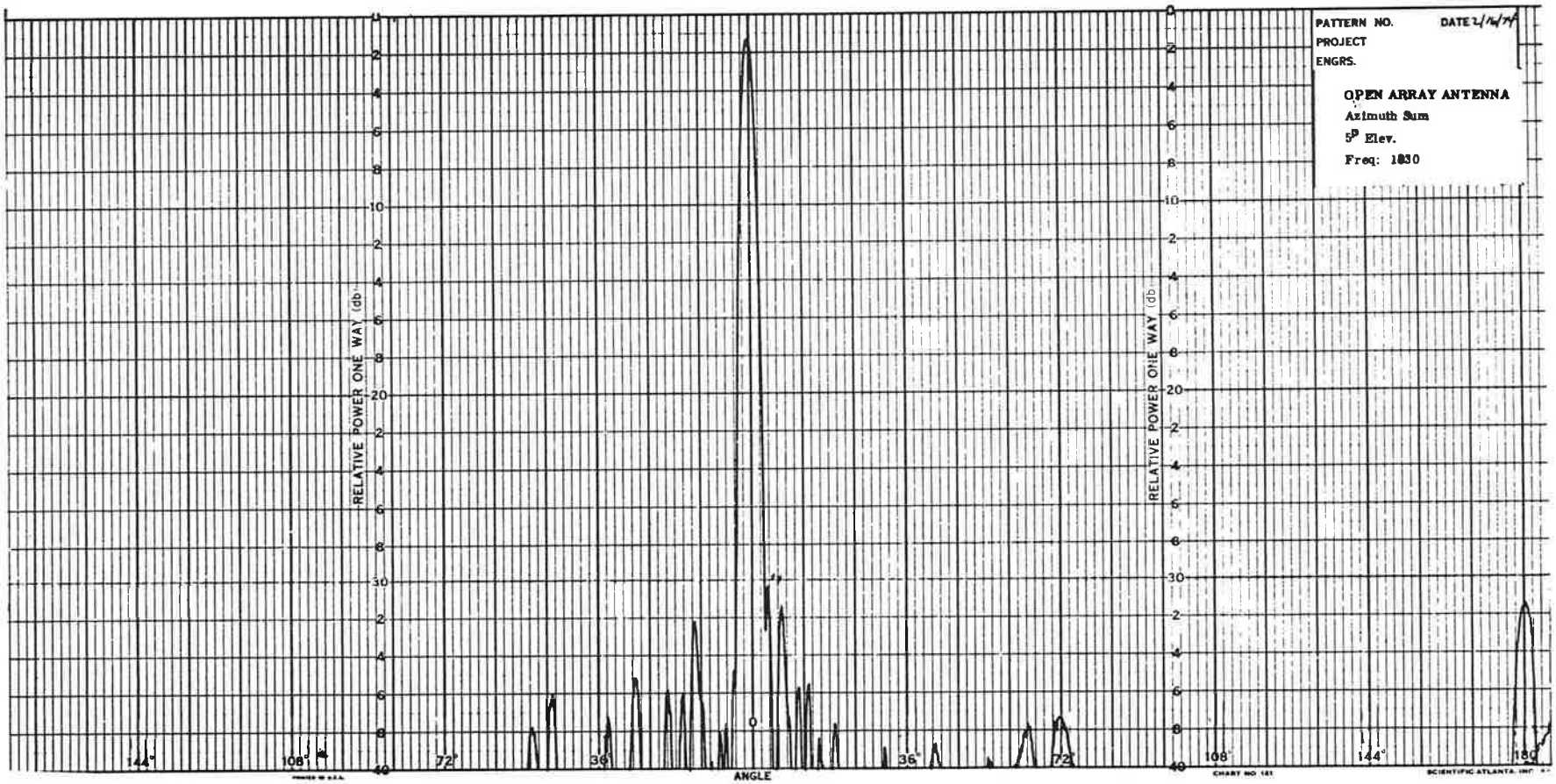

Figure A-16. Open Array Azimuth Sum Pattern, 5° Elevation, 1030 MHz, Wide Angle

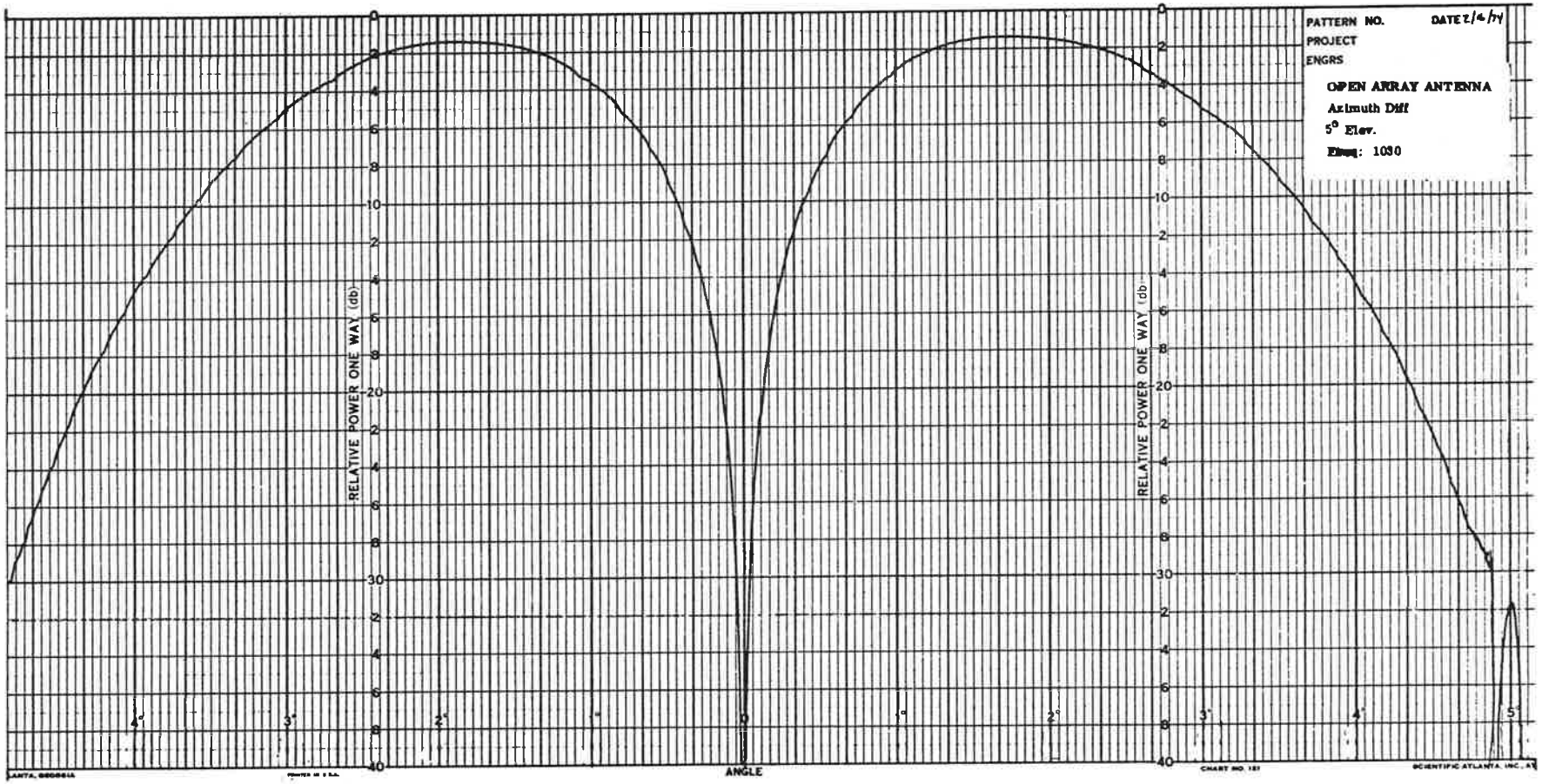

Figure A-17. Open Array Azimuth Difference Pattern, 5° Elevation, 1030 MHz, Narrow Angle

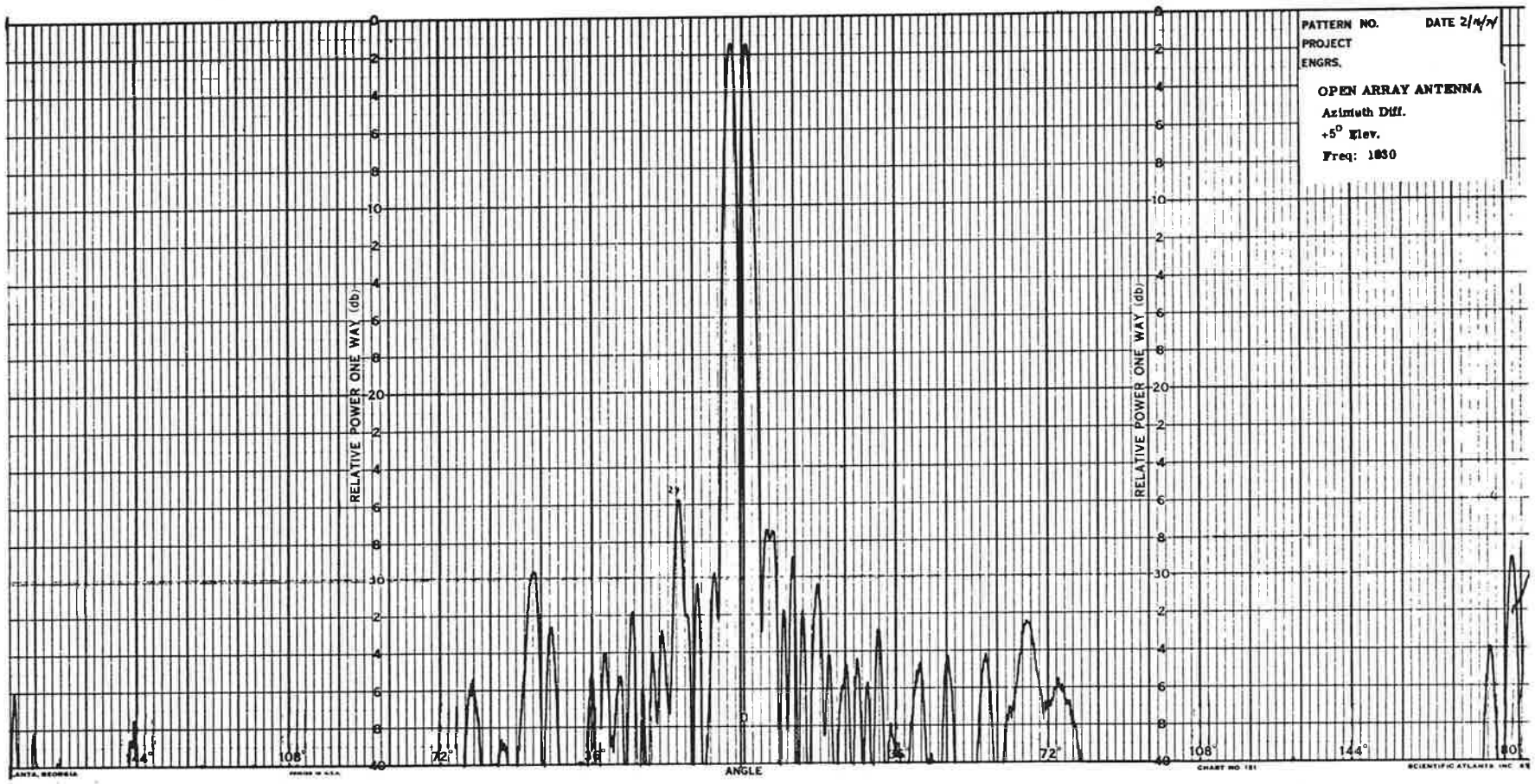

Figure A-18. Open Array Azimuth Difference Pattern, 5° Elevation, 1030 MHz, Wide Angle

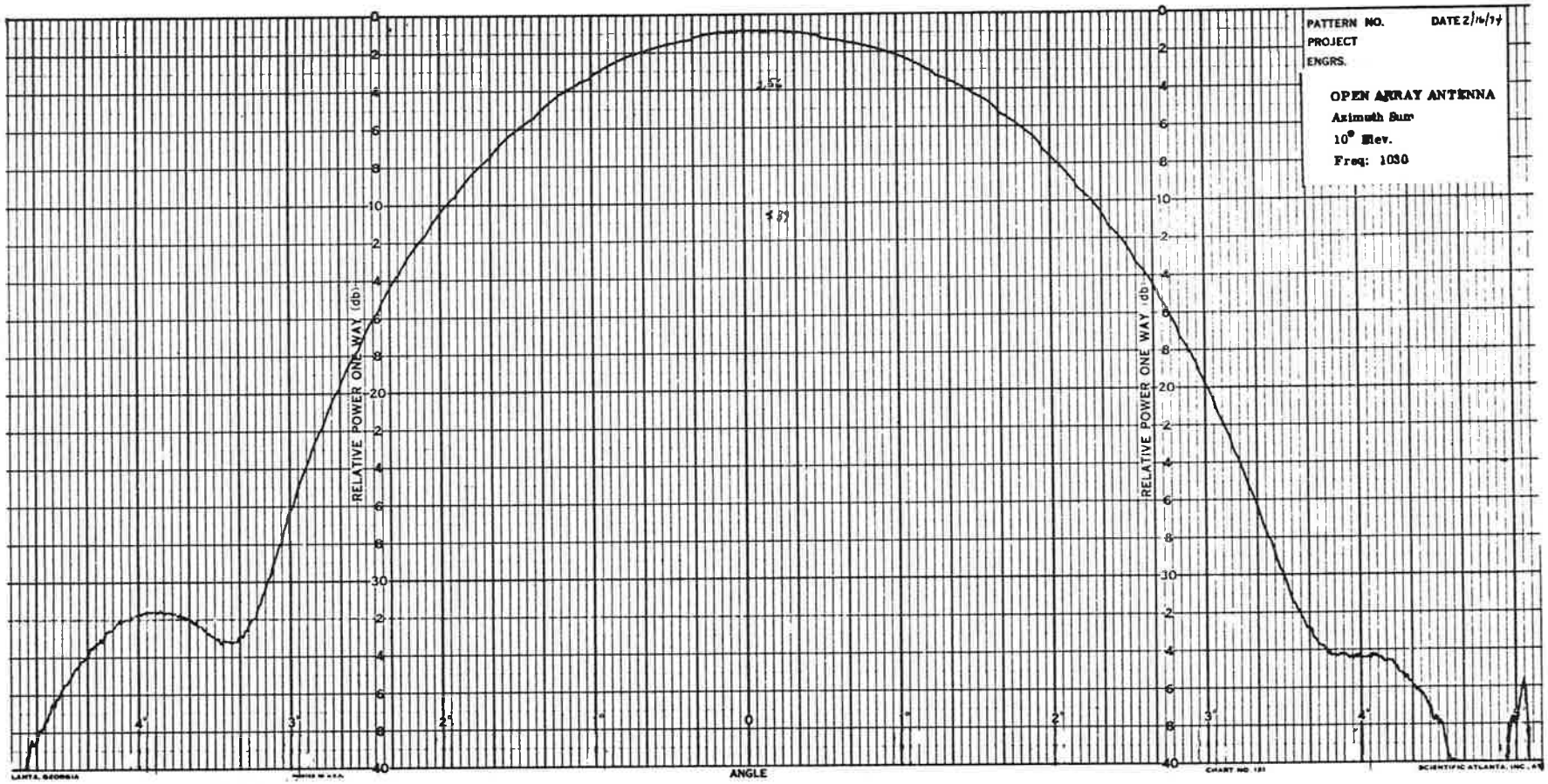

Figure A-19. Open Array Azimuth Sum Pattern, 10° Elevation, 1030 MHz, Narrow Angle

Figure A-20. Open Array Azimuth Sum Pattern, 10° Elevation, 1030 MHz, Wide Angle

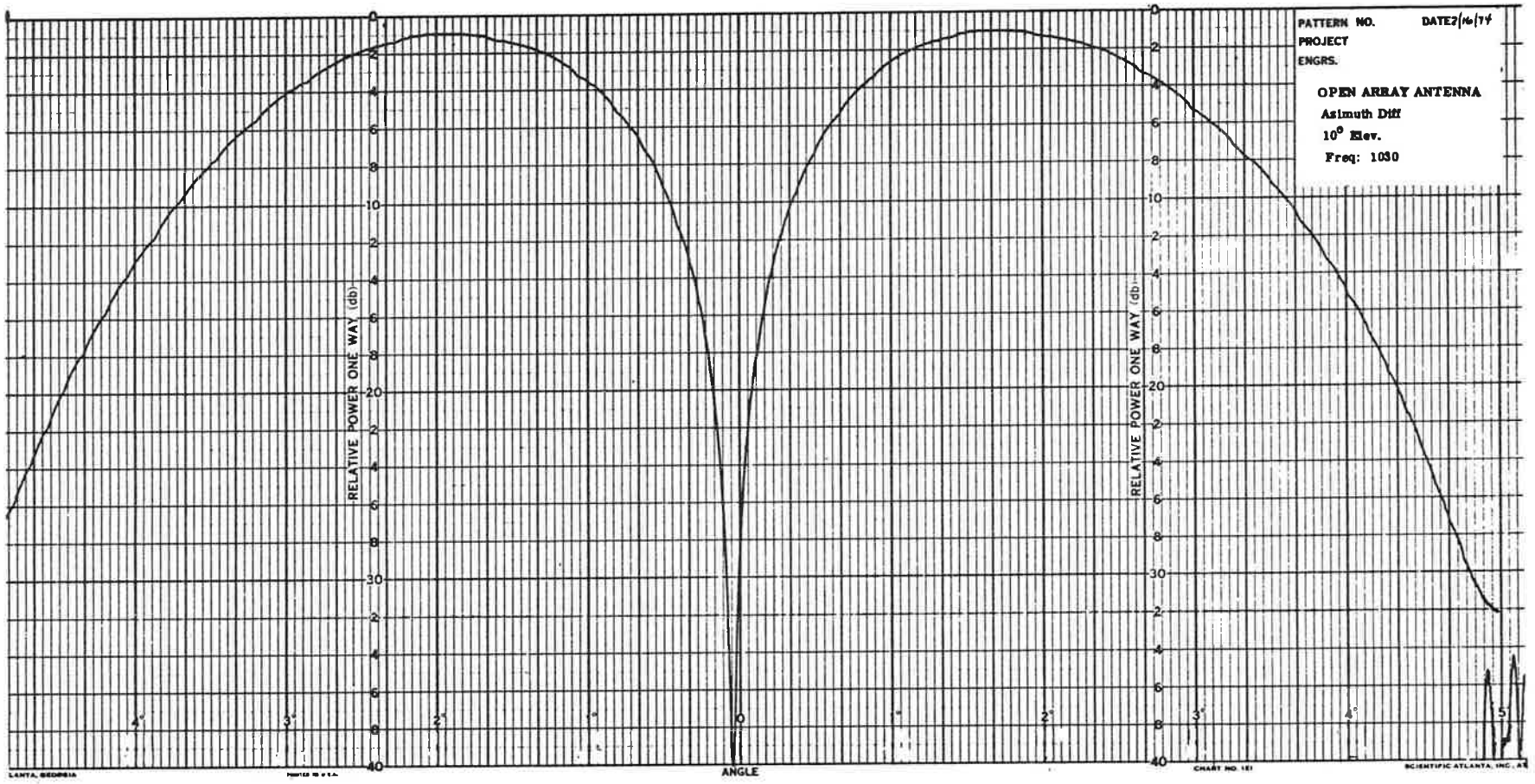

Figure A-21. Open Array Azimuth Difference Pattern, 10° Elevation, 1030 MHz, Narrow Angle

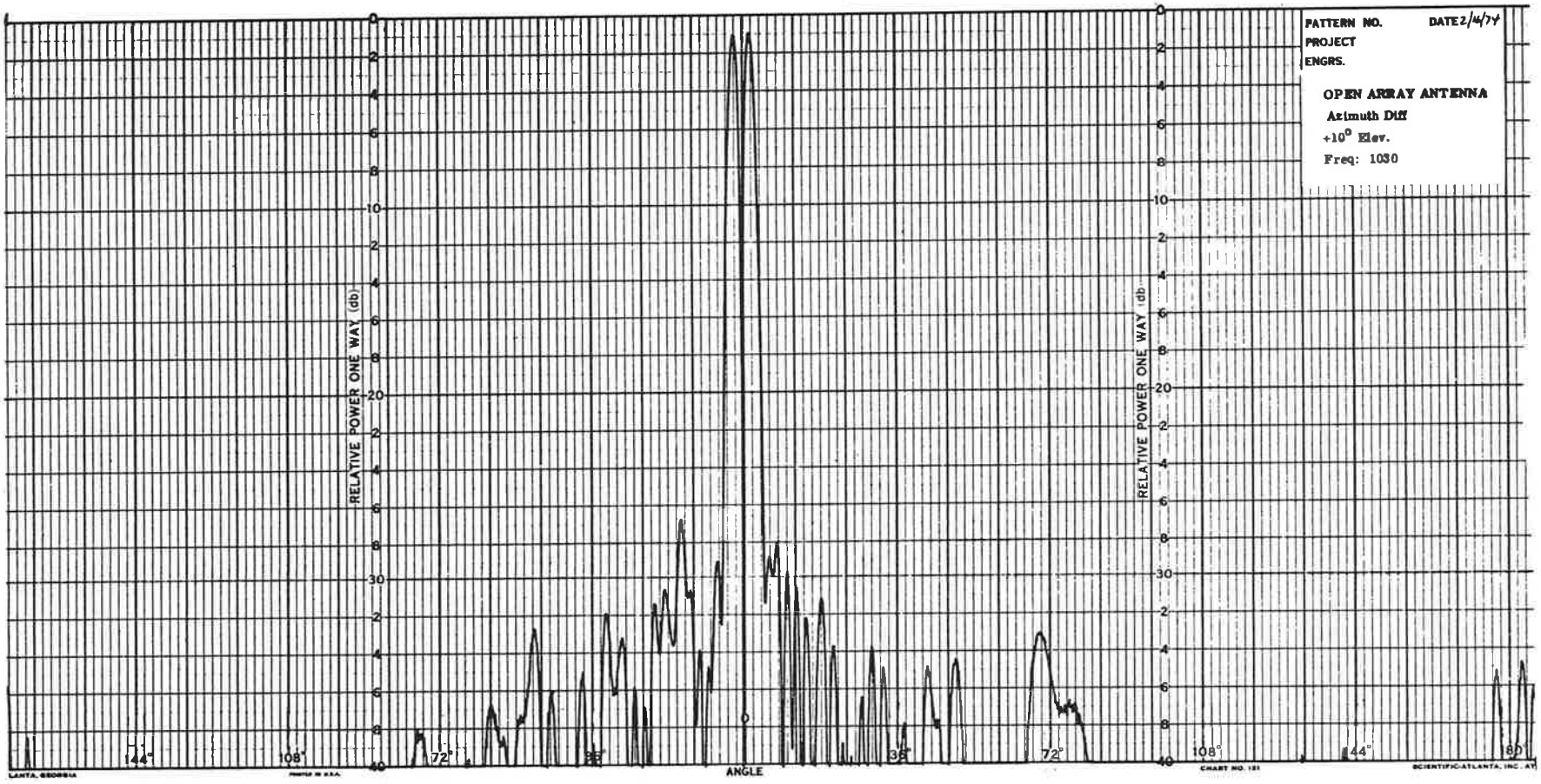

Figure A-22. Open Array Azimuth Difference Pattern, 10° Elevation, 1030 MHz, Wide Angle

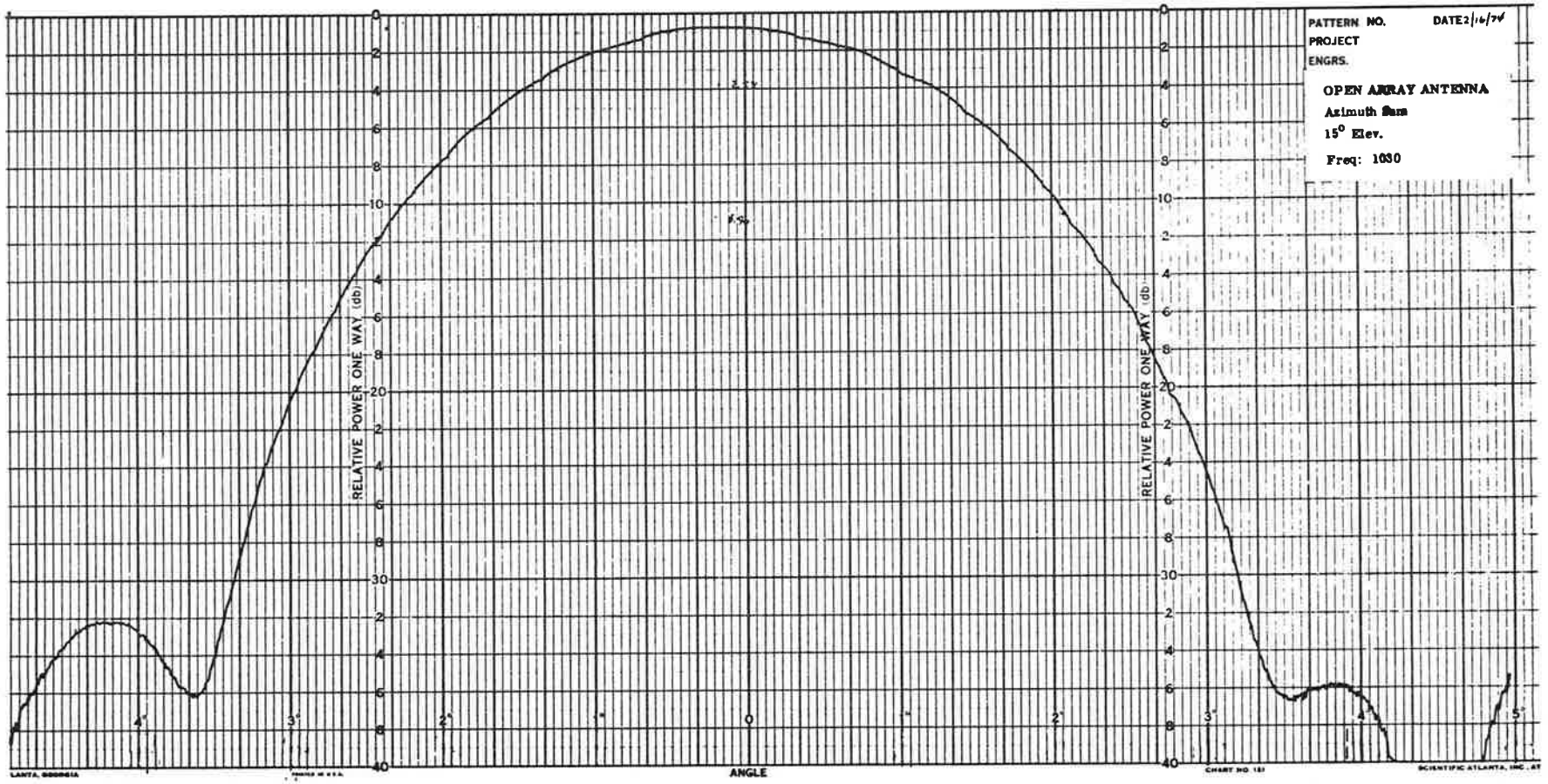

Figure A-23. Open Array Azimuth Sum Pattern, 15° Elevation, 1030 MHz, Narrow Angle

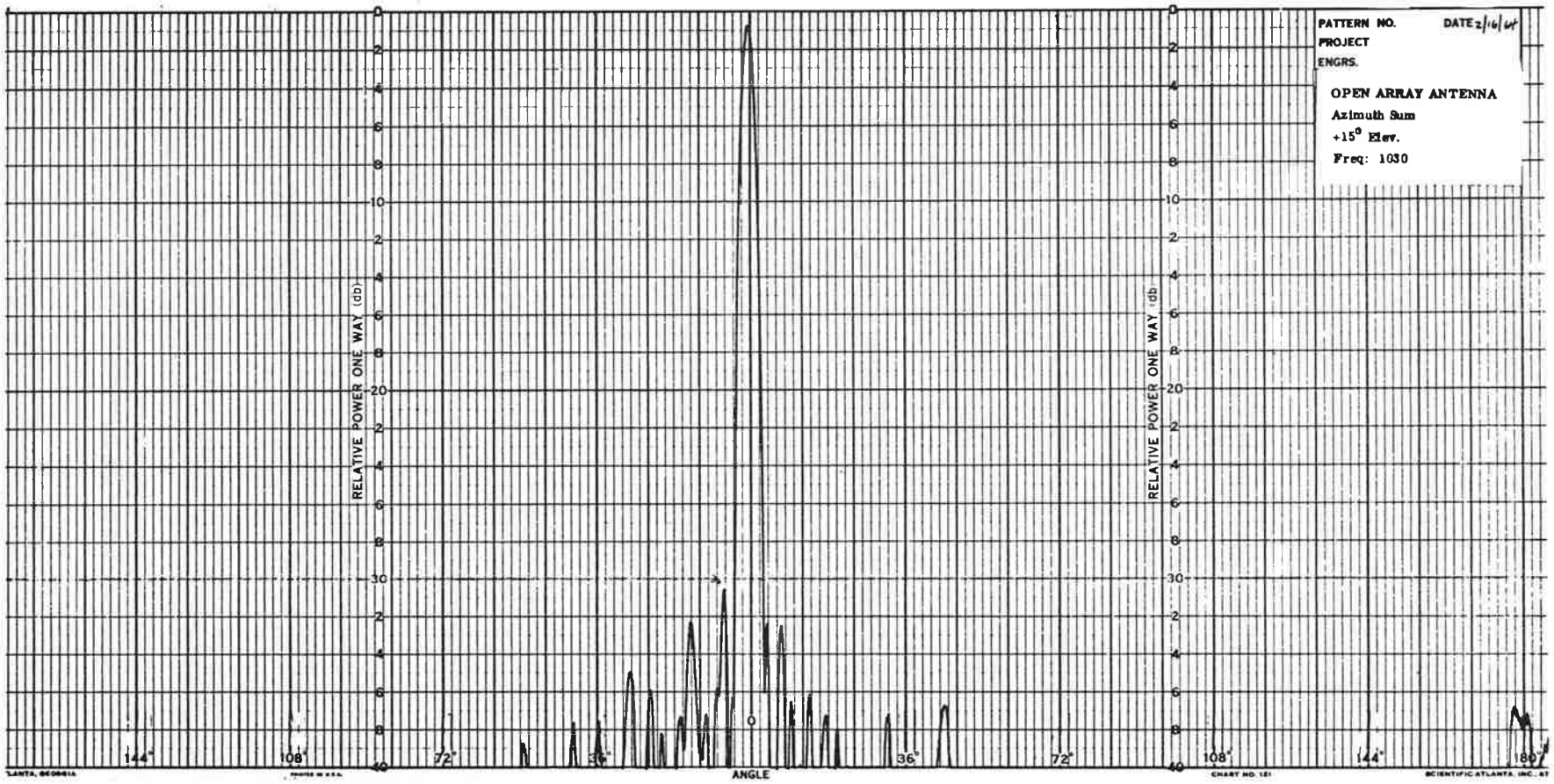

Figure A-24. Open Array Azimuth Sum Pattern, 15° Elevation, 1030 MHz, Wide Angle

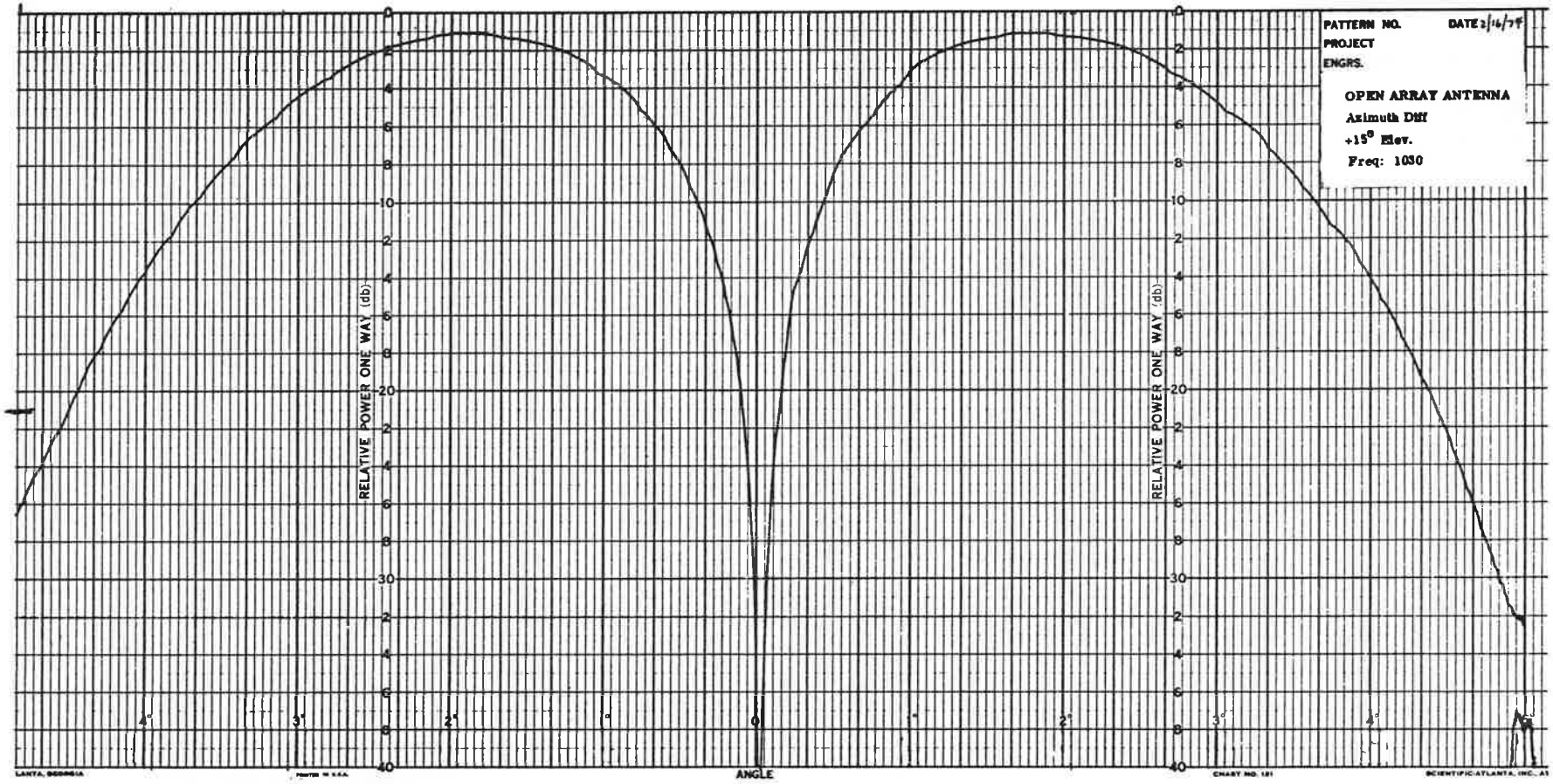

Figure A-25. Open Array Azimuth Difference Pattern, 15° Elevation, 1030 MHz, Narrow Angle

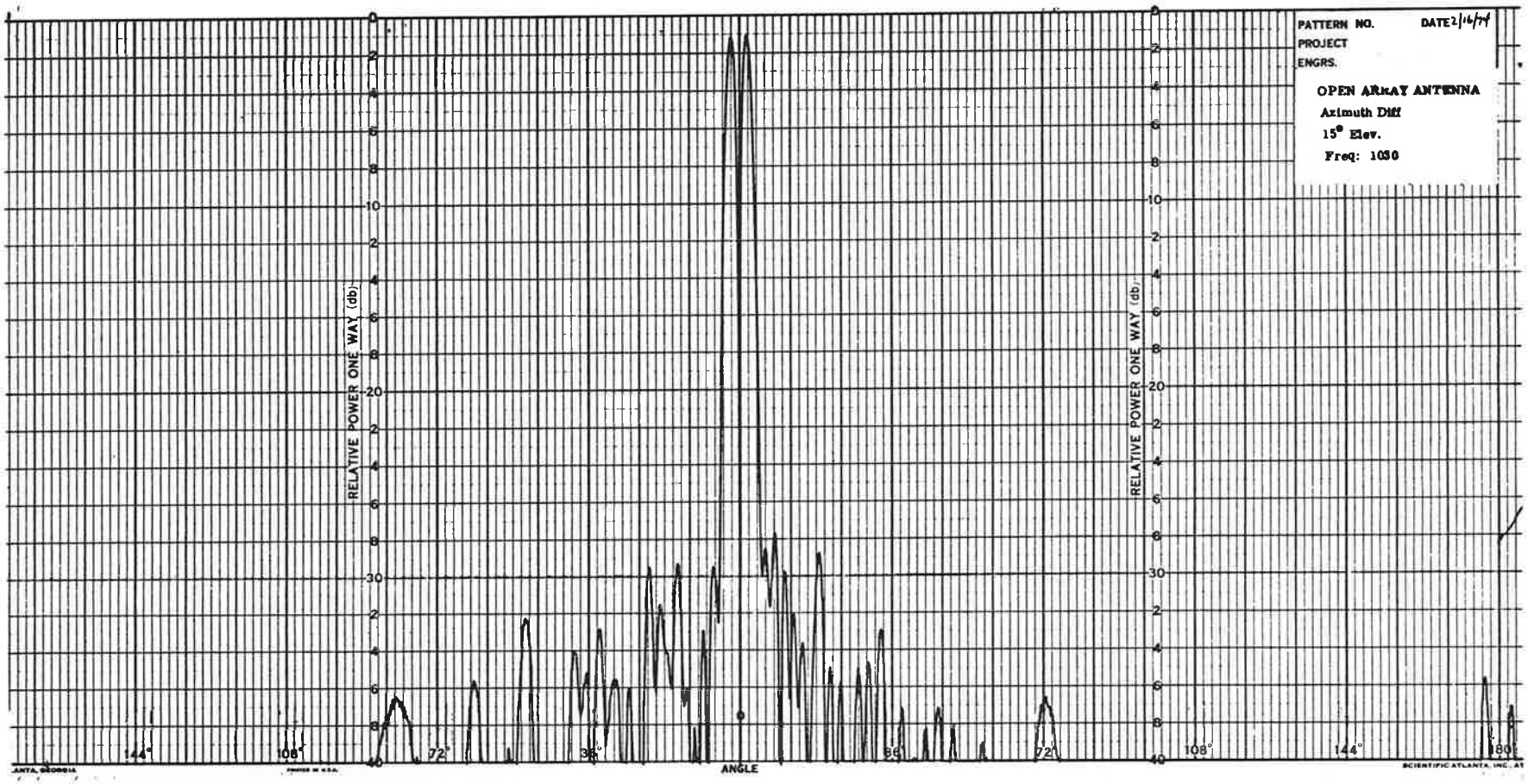

Figure A-26. Open Array Azimuth Difference Pattern, 15° Elevation, 1030 MHz, Wide Angle

Figure A-27. Open Array Azimuth Sum Pattern, 20° Elevation, 1030 MHz, Narrow Angle

Figure A-28. Open Array Azimuth Sum Pattern, 20° Elevation, 1030 MHz, Wide Angle

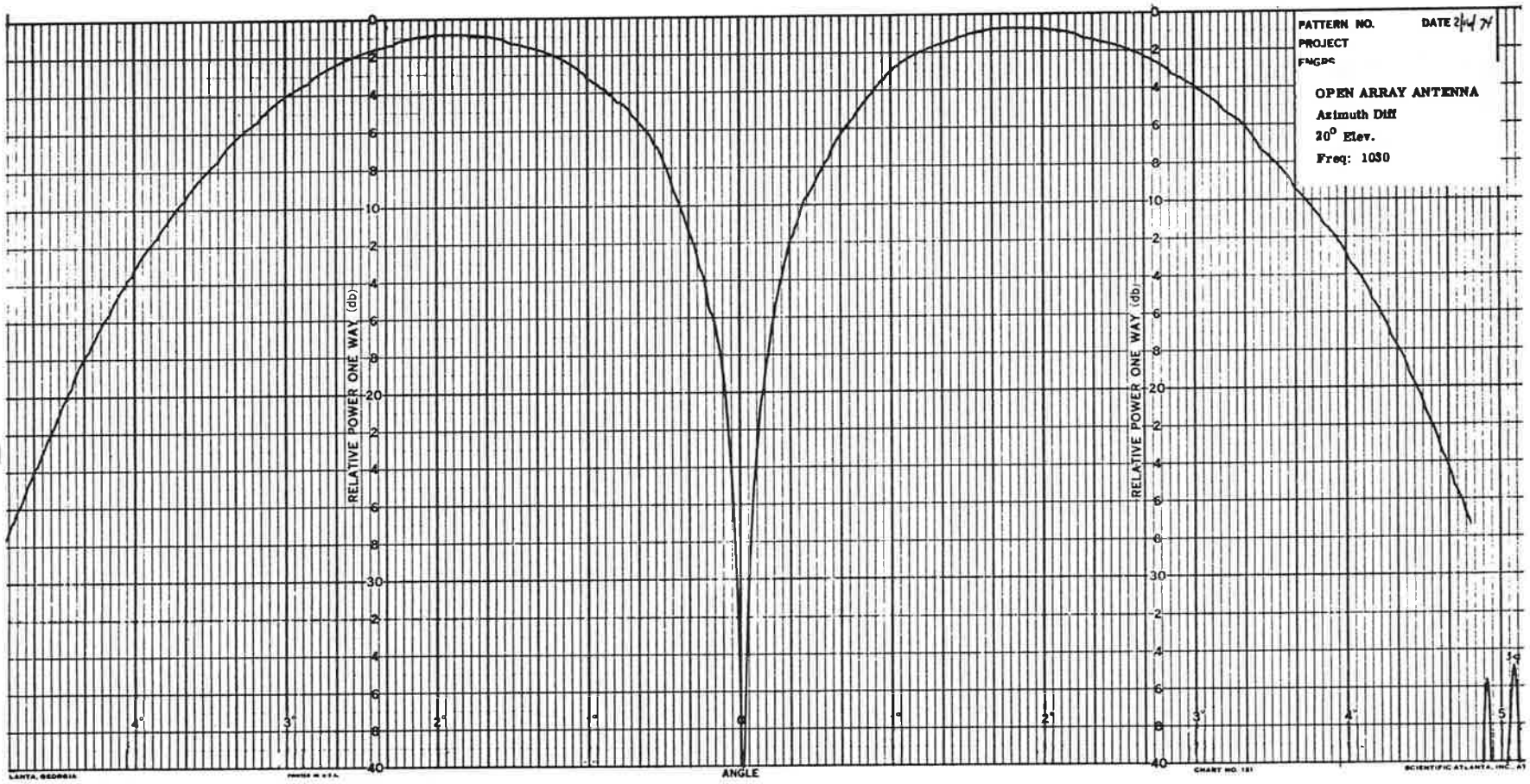

Figure A-29. Open Array Azimuth Difference Pattern, 20° Elevation, 1030 MHz, Narrow Angle

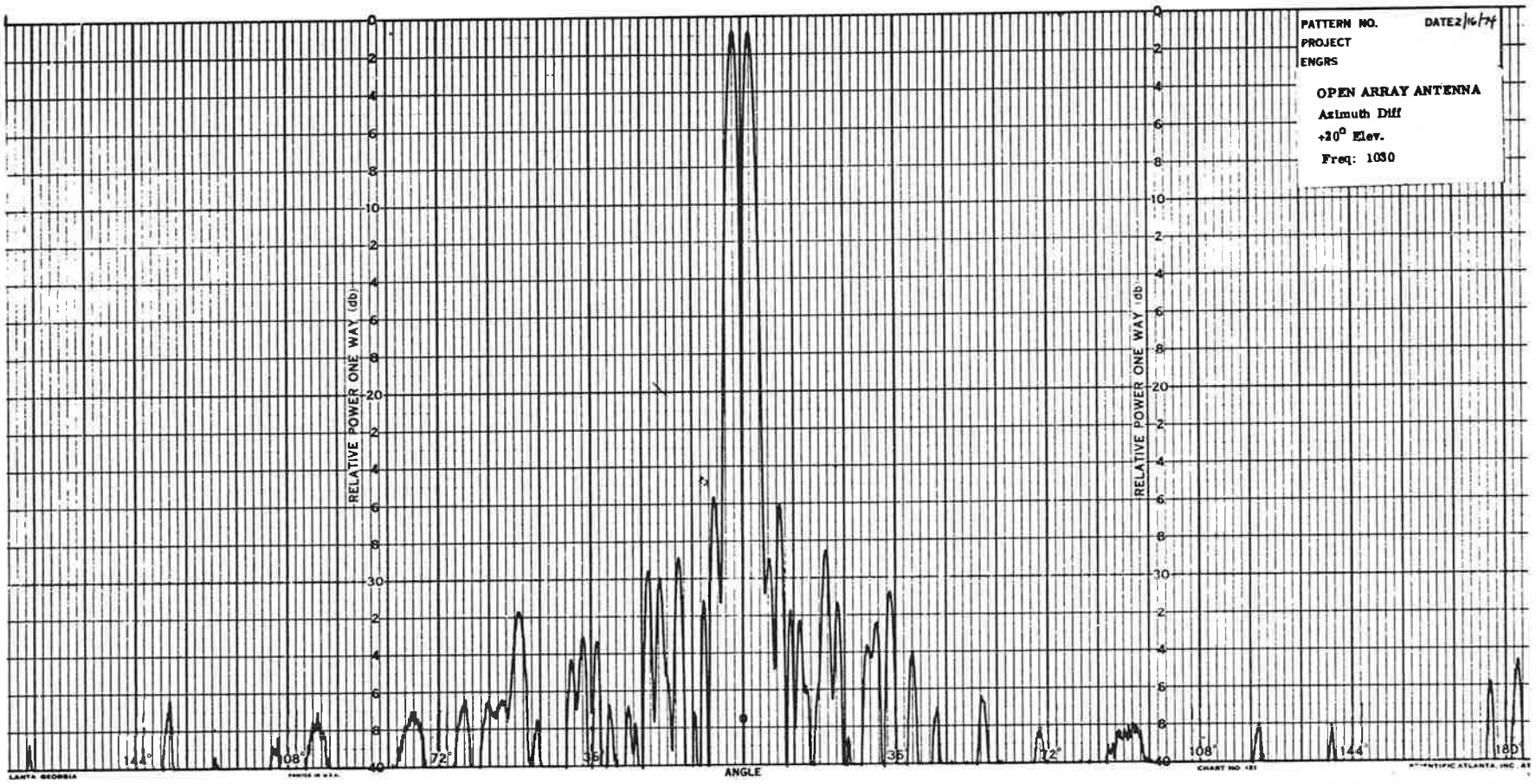

Figure A-30. Open Array Azimuth Difference Pattern, 20° Elevation, 1030 MHz, Wide Angle

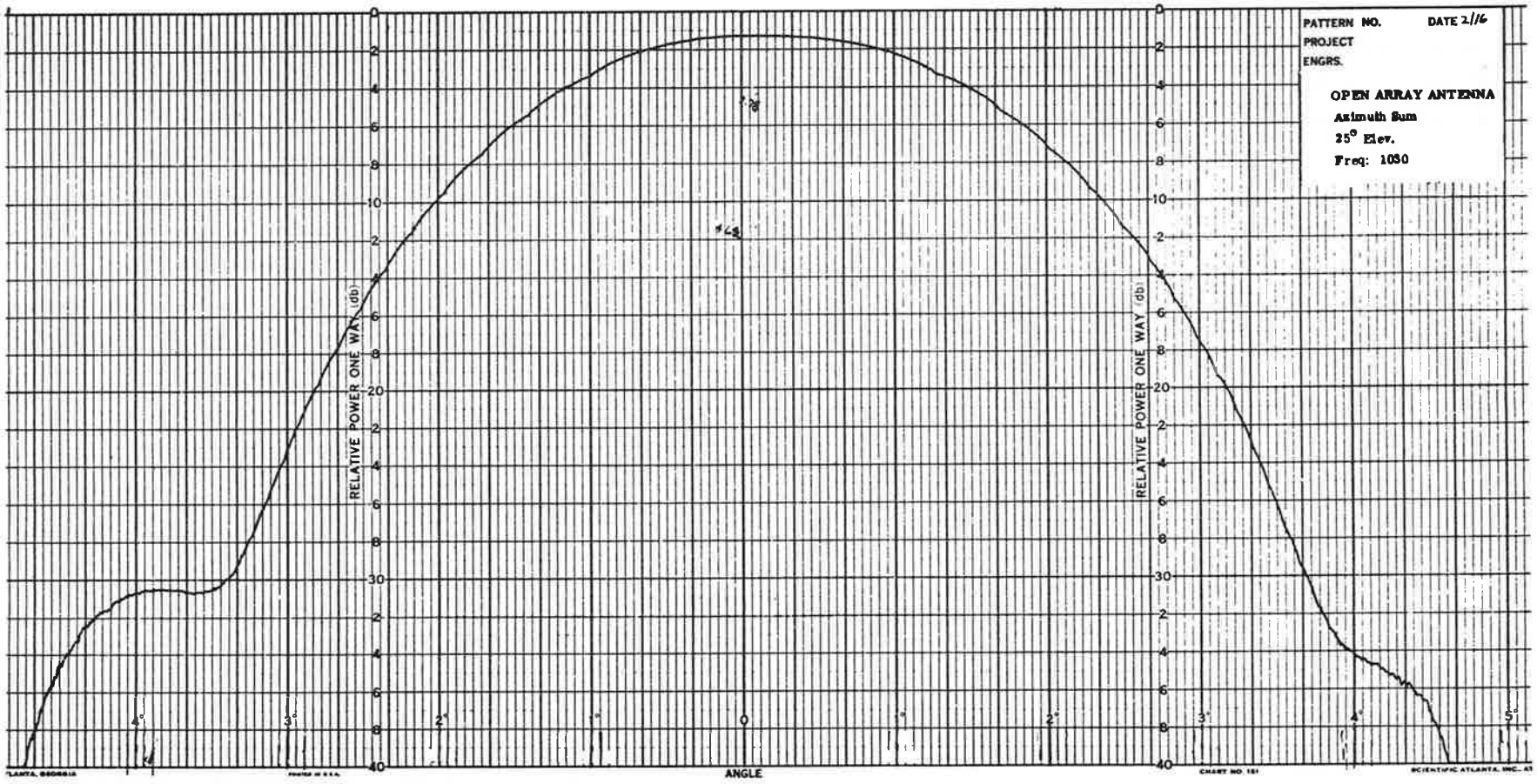

Figure A-31. Open Array Azimuth Sum Pattern, 25° Elevation, 1030 MHz, Narrow Angle

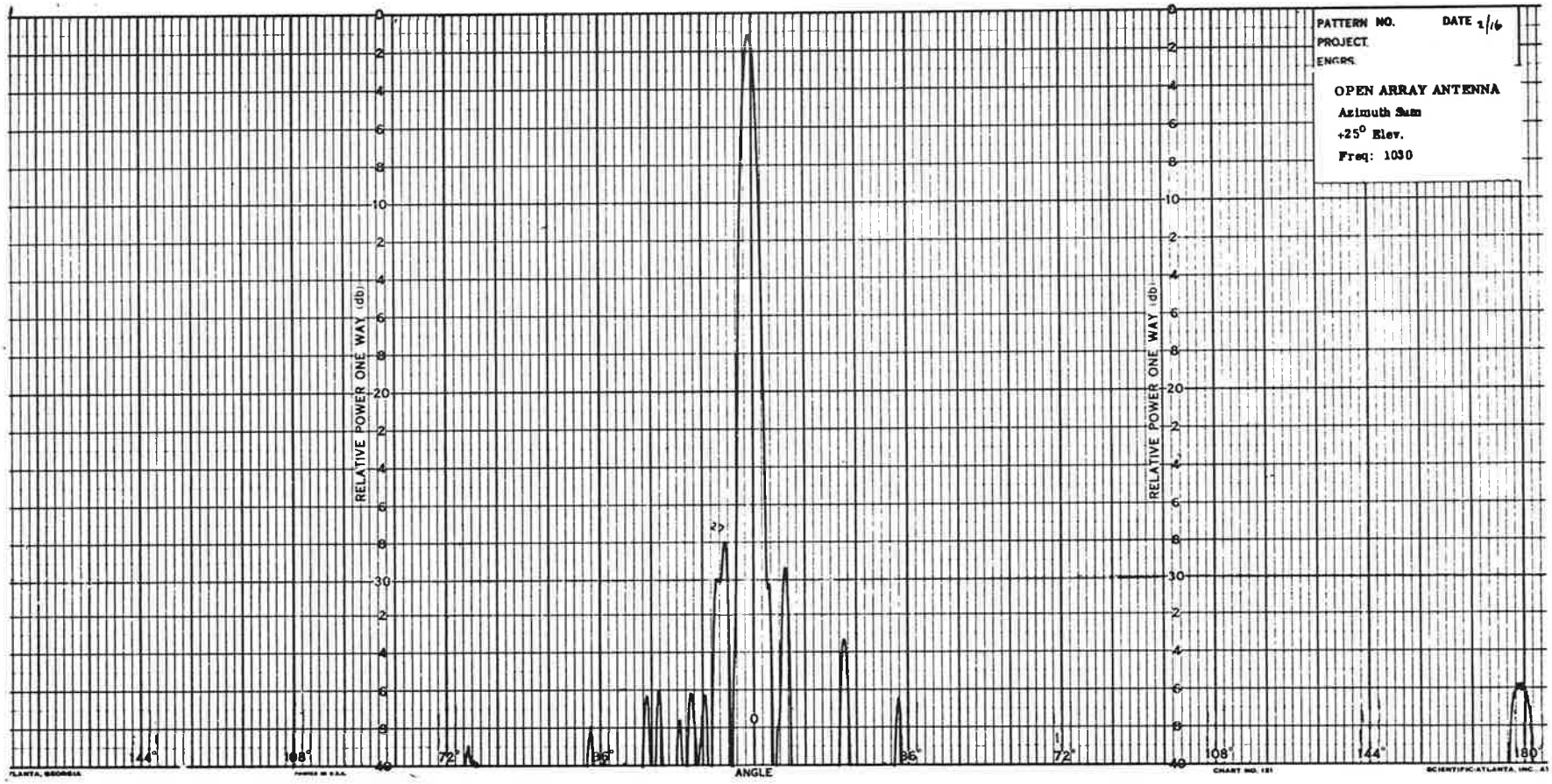

Figure A-32. Open Array Azimuth Sum Pattern, 25° Elevation, 1030 MHz, Wide Angle

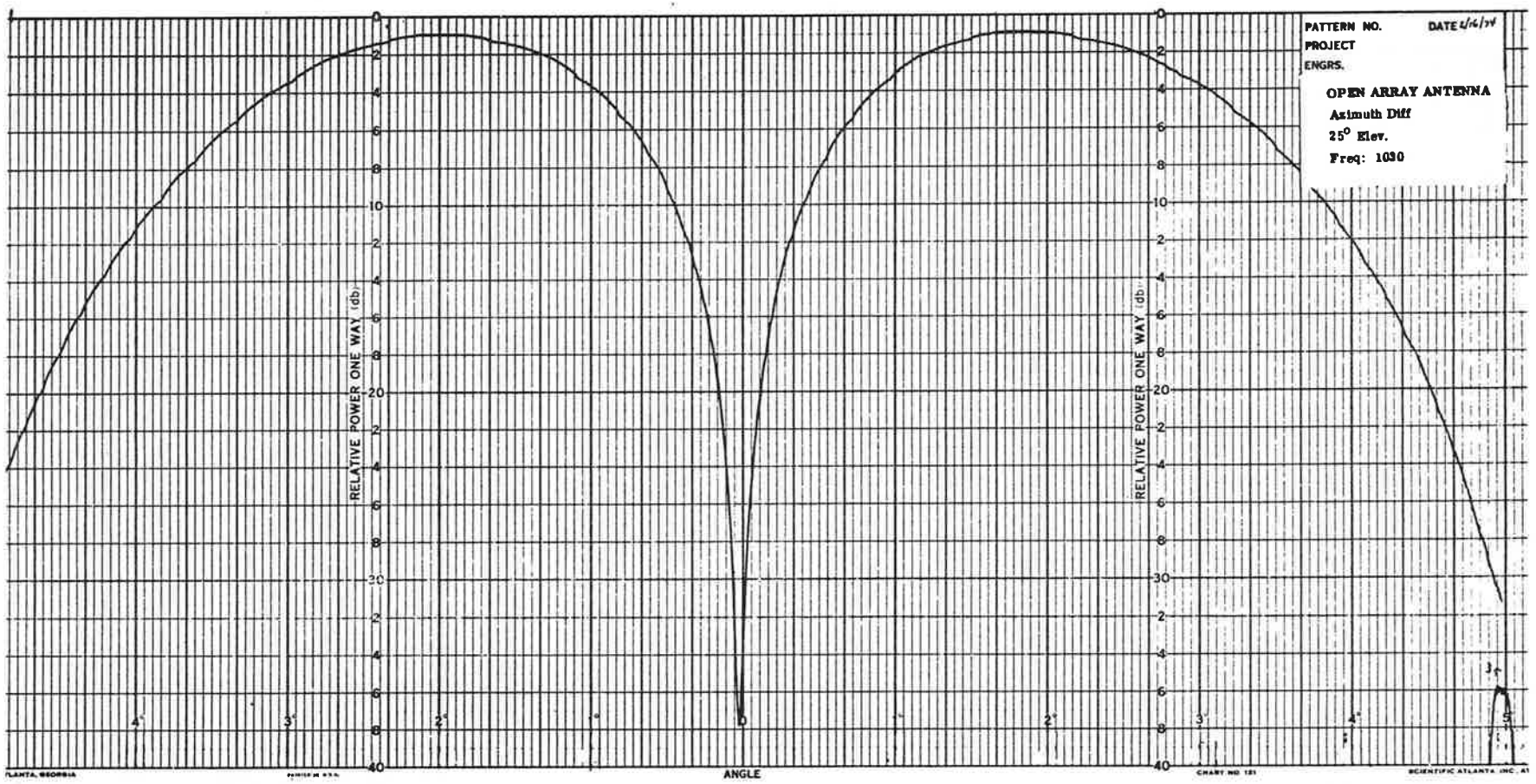

Figure A-33. Open Array Azimuth Difference Pattern, 25° Elevation, 1030 MHz, Narrow Angle

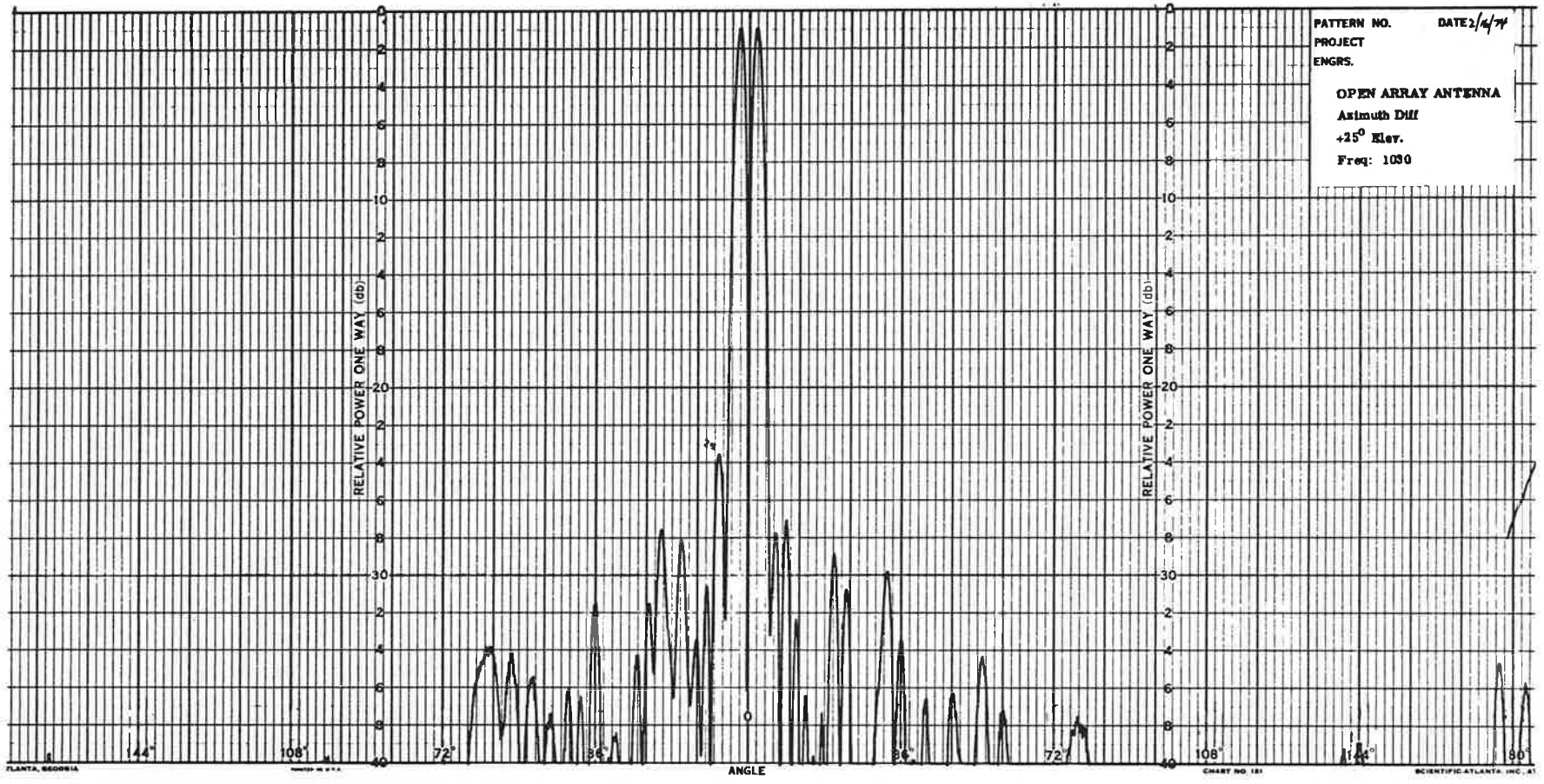

Figure A-34. Open Array Azimuth Difference Pattern, 25° Elevation, 1030 MHz, Wide Angle

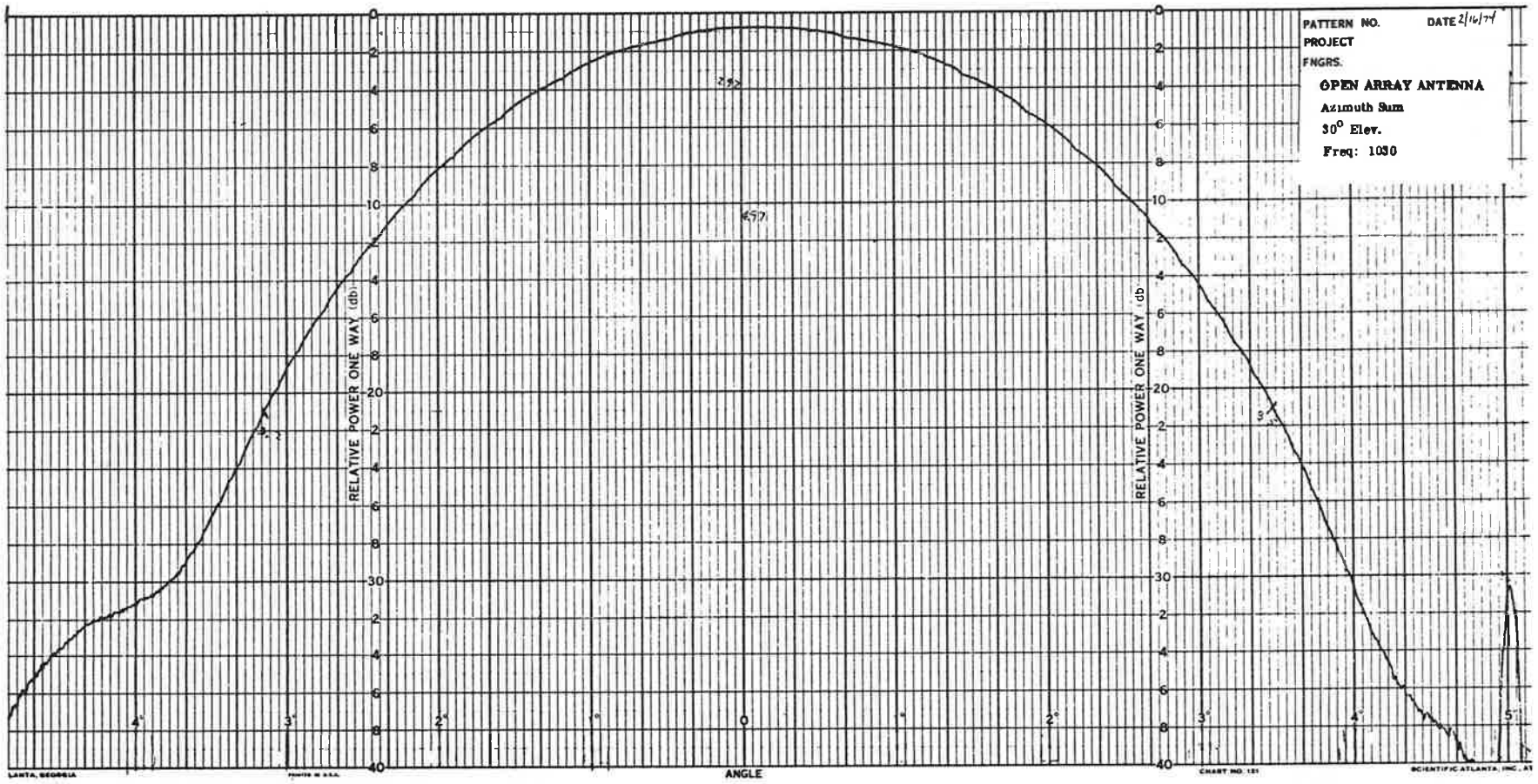

Figure A-35. Open Array Azimuth Sum Pattern, 30° Elevation, 1030 MHz, Narrow Angle

Figure A-36. Open Array Azimuth Sum Pattern, 30° Elevation, 1030 MHz, Wide Angle

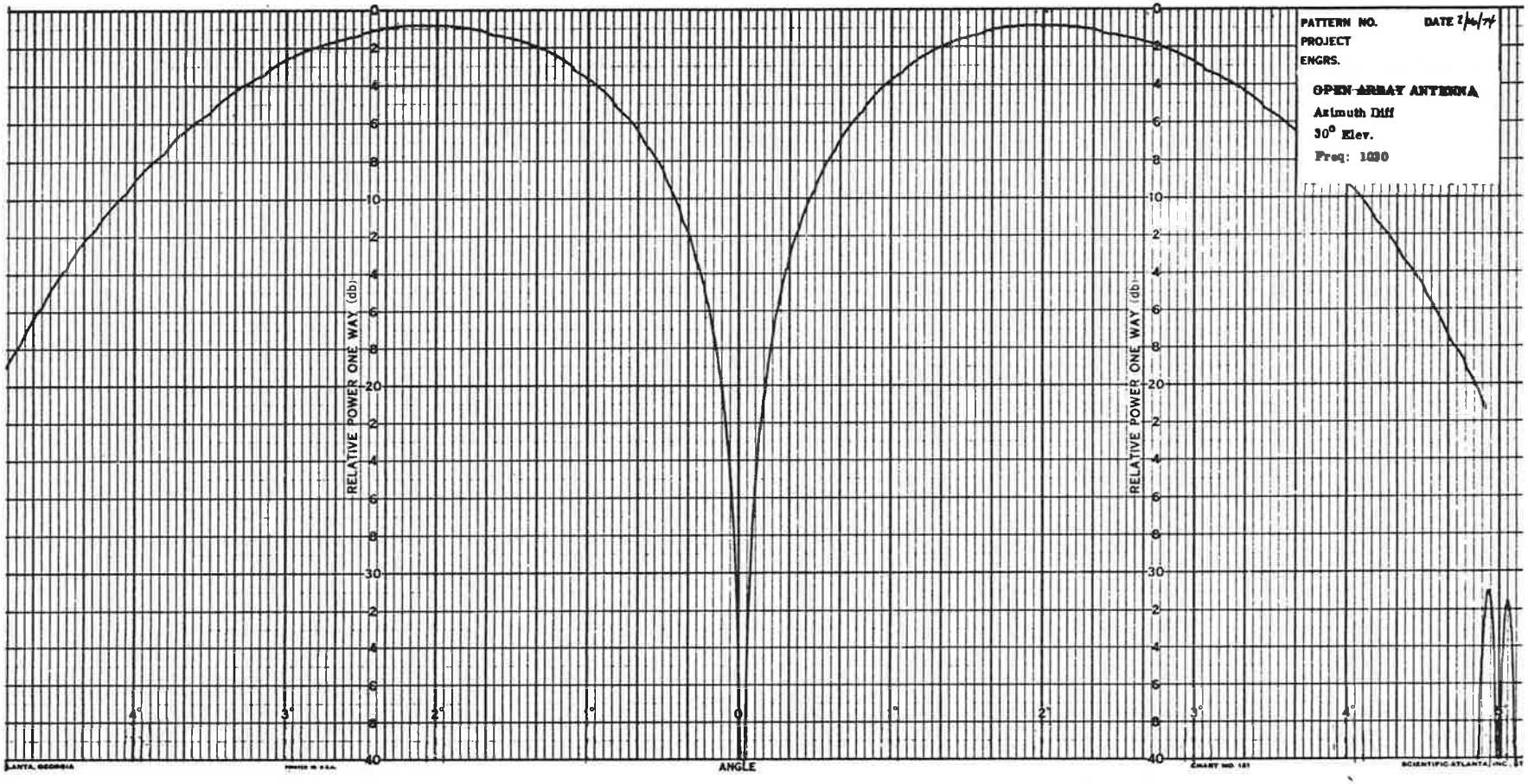

Figure A-37. Open Array Azimuth Difference Pattern, 30° Elevation, 1030 MHz, Narrow Angle

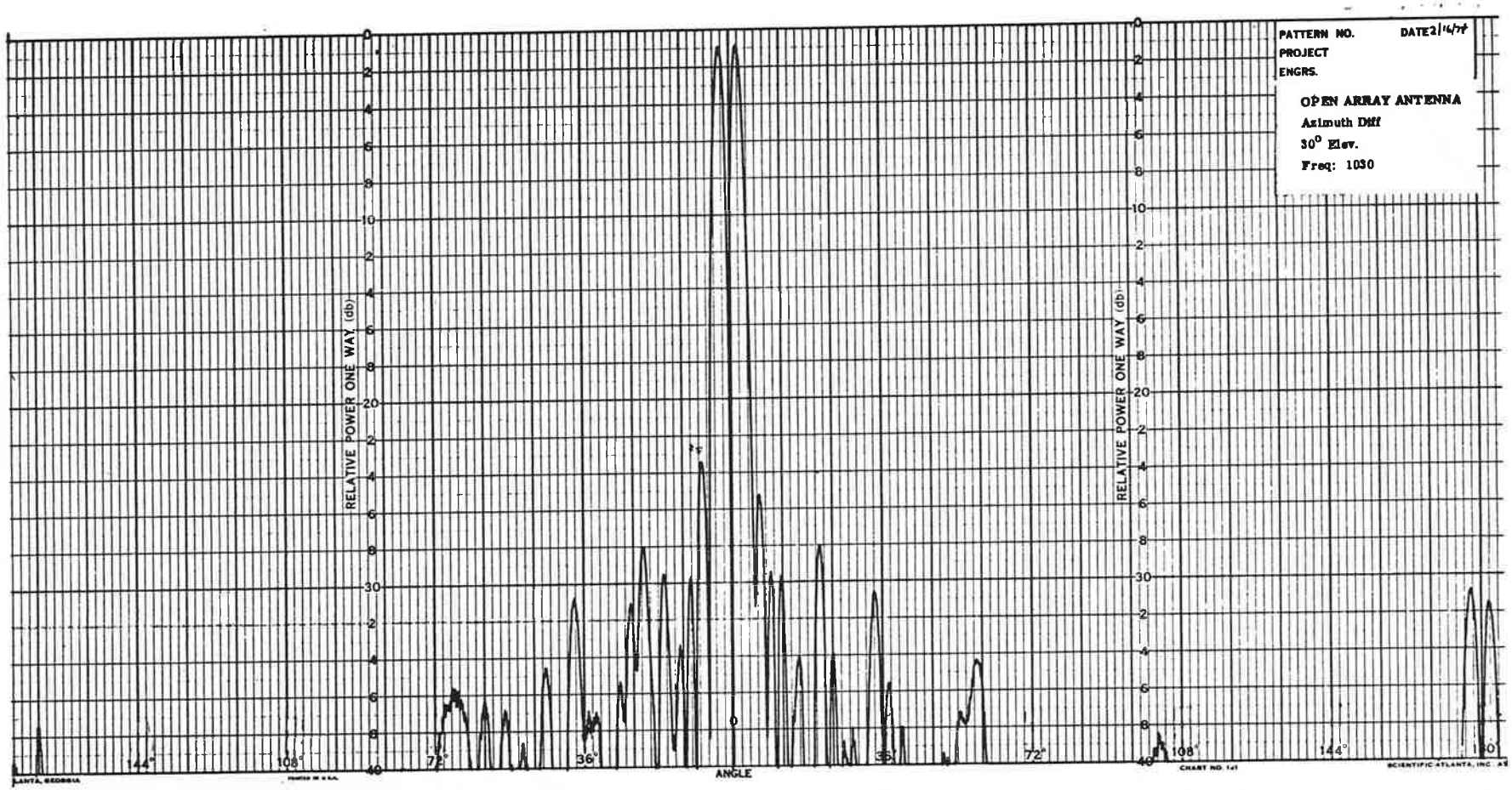

Figure A-38. Open Array Azimuth Difference Pattern, 30° Elevation, 1030 MHz, Wide Angle

Figure A-39. Open Array Azimuth Sum Pattern, 35° Elevation, 1030 MHz, Narrow Angle

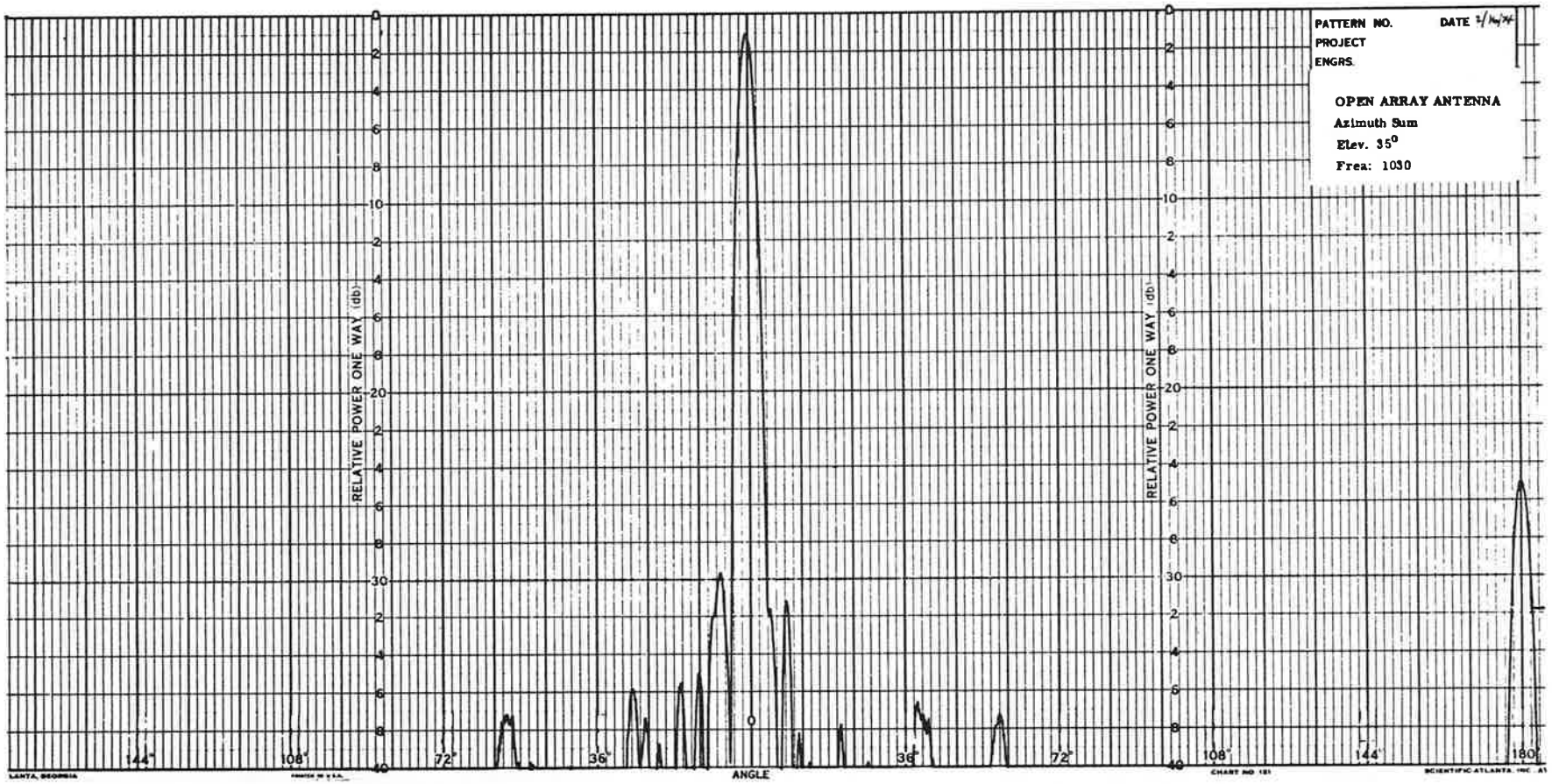

Figure A-40. Open Array Azimuth Sum Pattern, 35° Elevation, 1030 MHz, Wide Angle

Figure A-41. Open Array Azimuth Difference Pattern, 35° Elevation, 1030 MHz, Narrow Angle

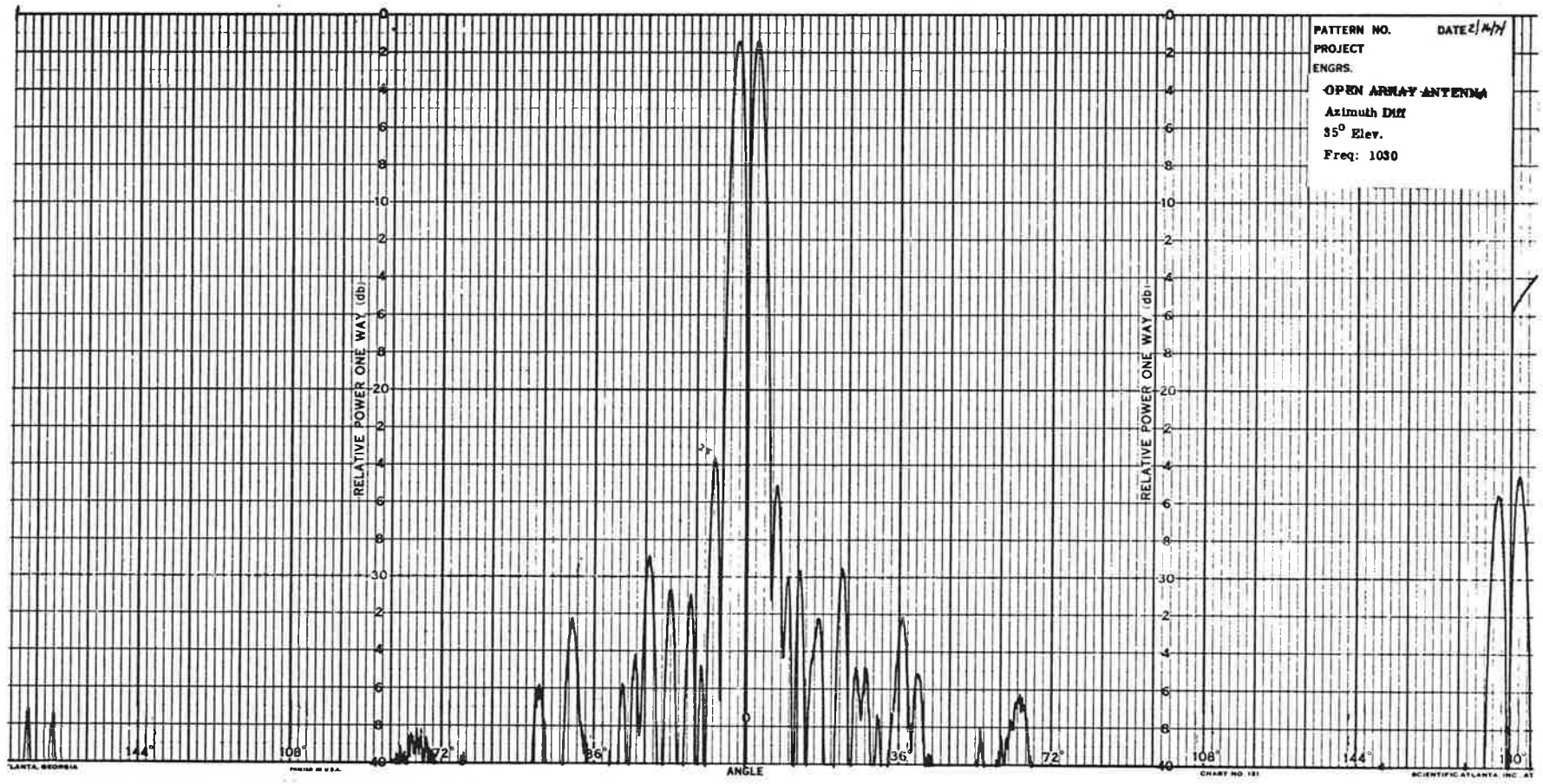

Figure A-42. Open Array Azimuth Difference Pattern, 35° Elevation, 1030 MHz, Wide Angle

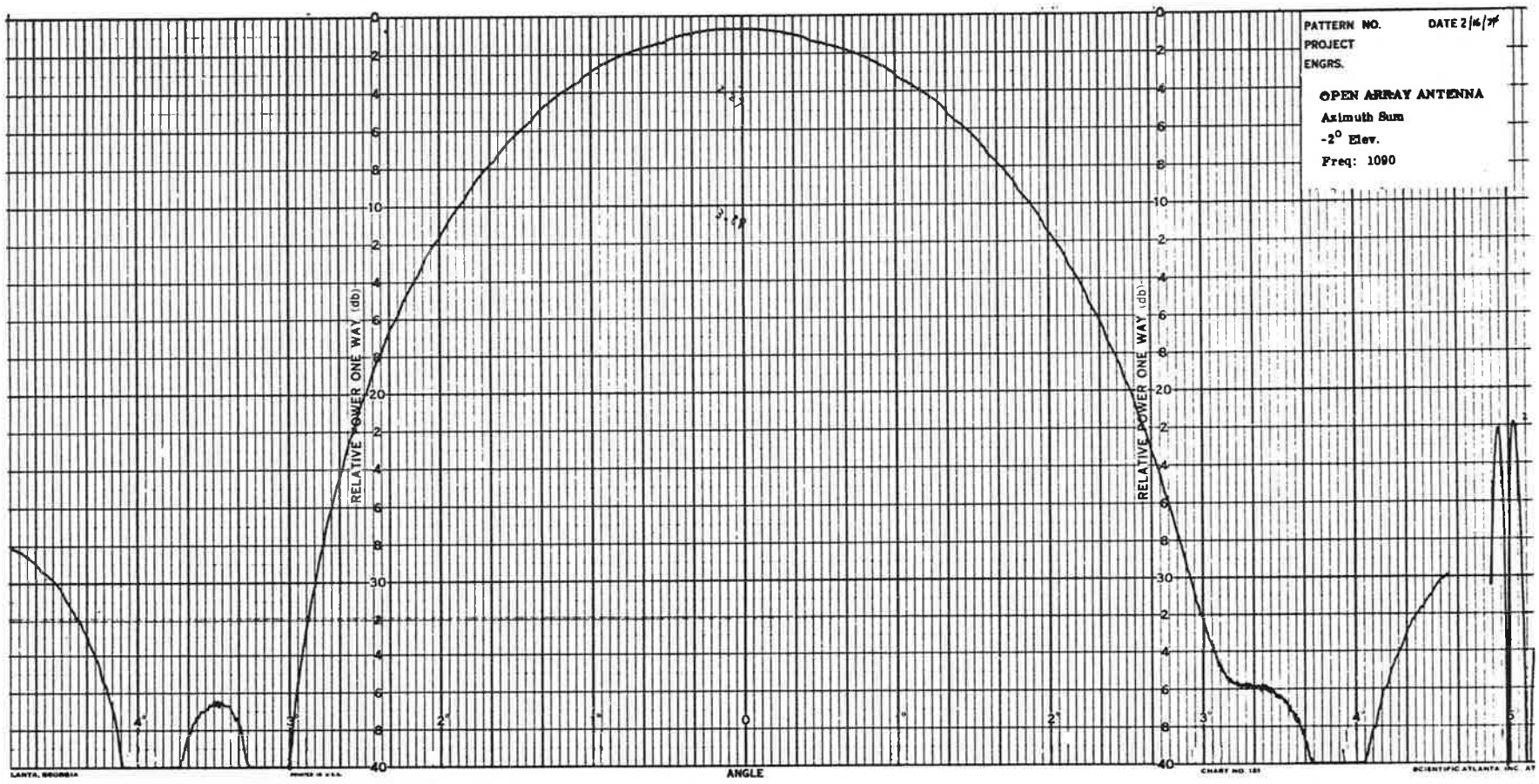

Figure A-43. Open Array Azimuth Sum Pattern, -2° Elevation, 1090 MHz, Narrow Angle

Figure A-44. Open Array Azimuth Sum Pattern, -2° Elevation, 1090 MHz, Wide Angle

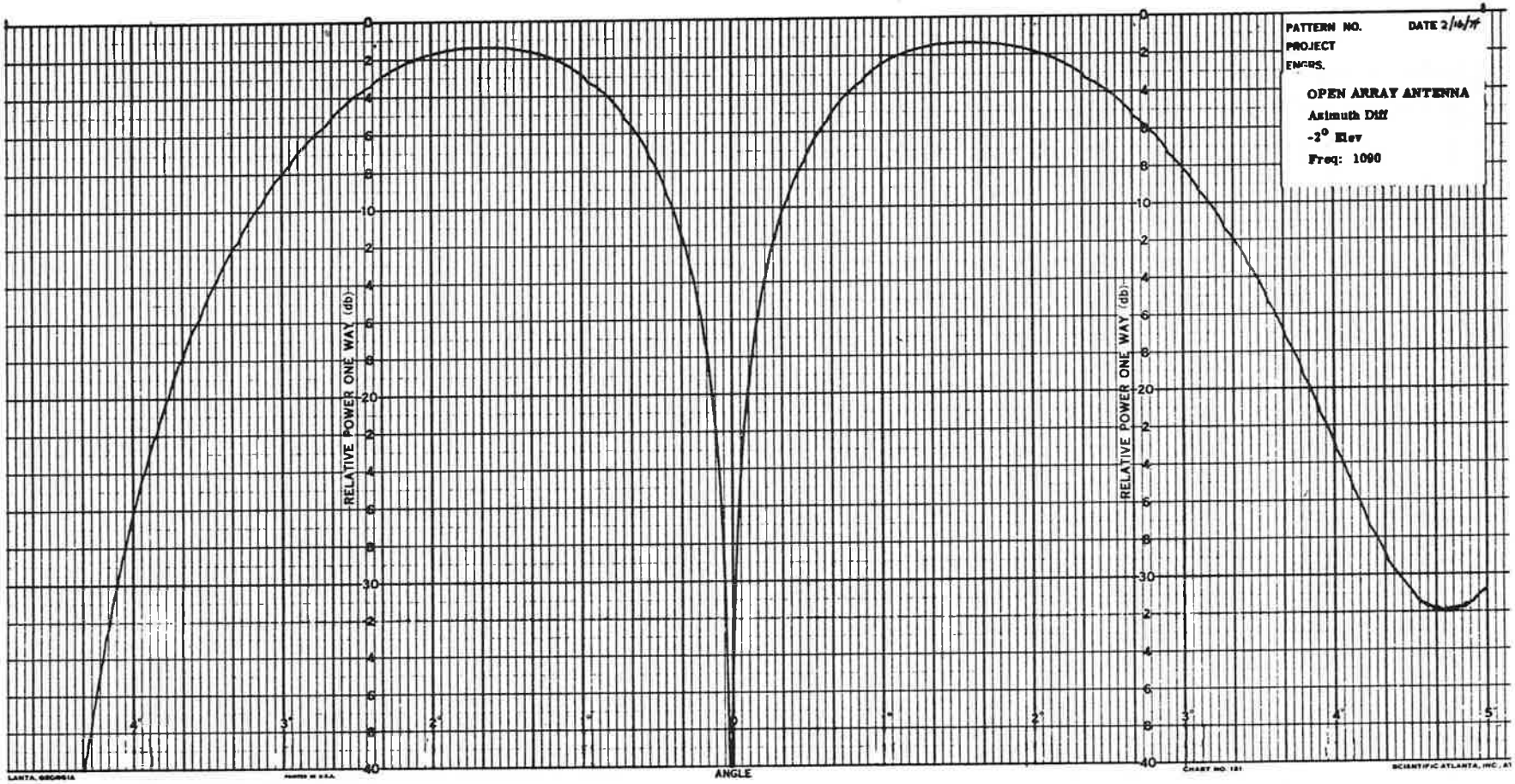

Figure A-45. Open Array Azimuth Difference Pattern, -2° Elevation, 1090 MHz, Narrow Angle

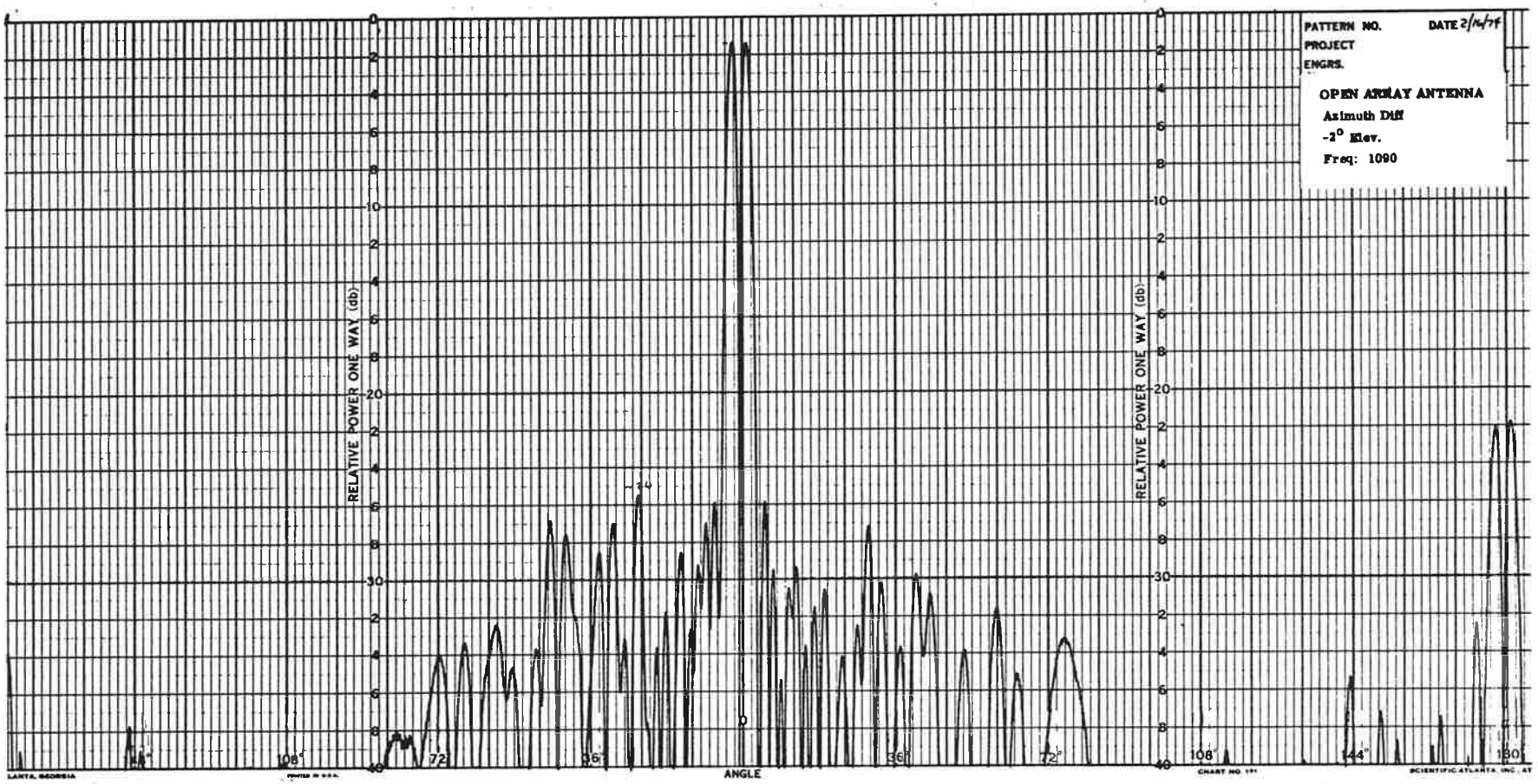

Figure A-46. Open Array Azimuth Difference Pattern, -2° Elevation, 1090 MHz, Narrow Angle

Figure A-47. Open Array Azimuth Sum Pattern, 0° Elevation, 1090 MHz, Narrow Angle

Figure A-48. Open Array Azimuth Sum Pattern, 0° Elevation, 1090 MHz, Wide Angle

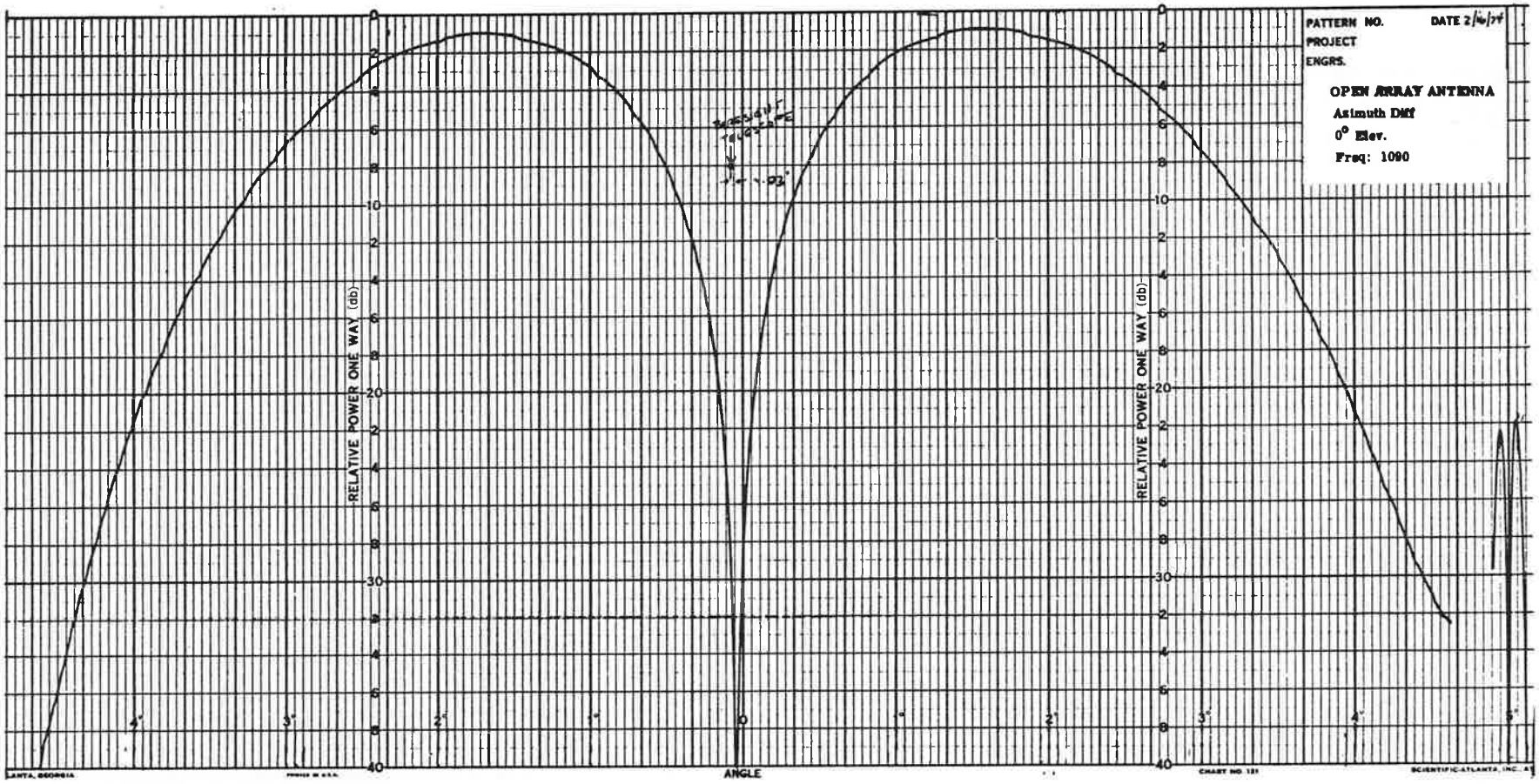

Figure A-49. Open Array Azimuth Difference Pattern, 0° Elevation, 1090 MHz, Narrow Angle

Figure A-50. Open Array Azimuth Difference Pattern, 0° Elevation, 1090 MHz, Wide Angle

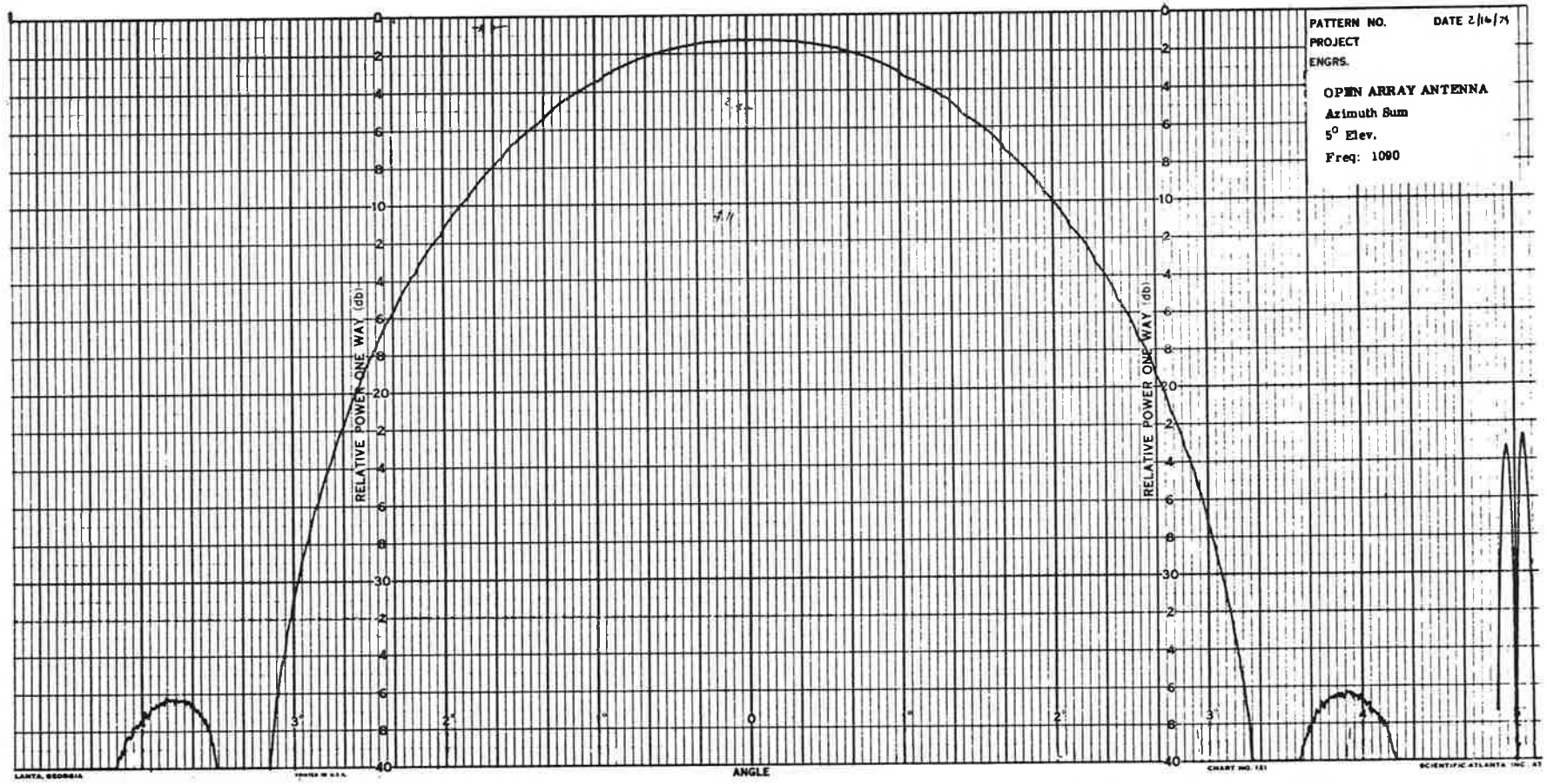

Figure A-51. Open Array Azimuth Sum Pattern, 5° Elevation, 1090 MHz, Narrow Angle

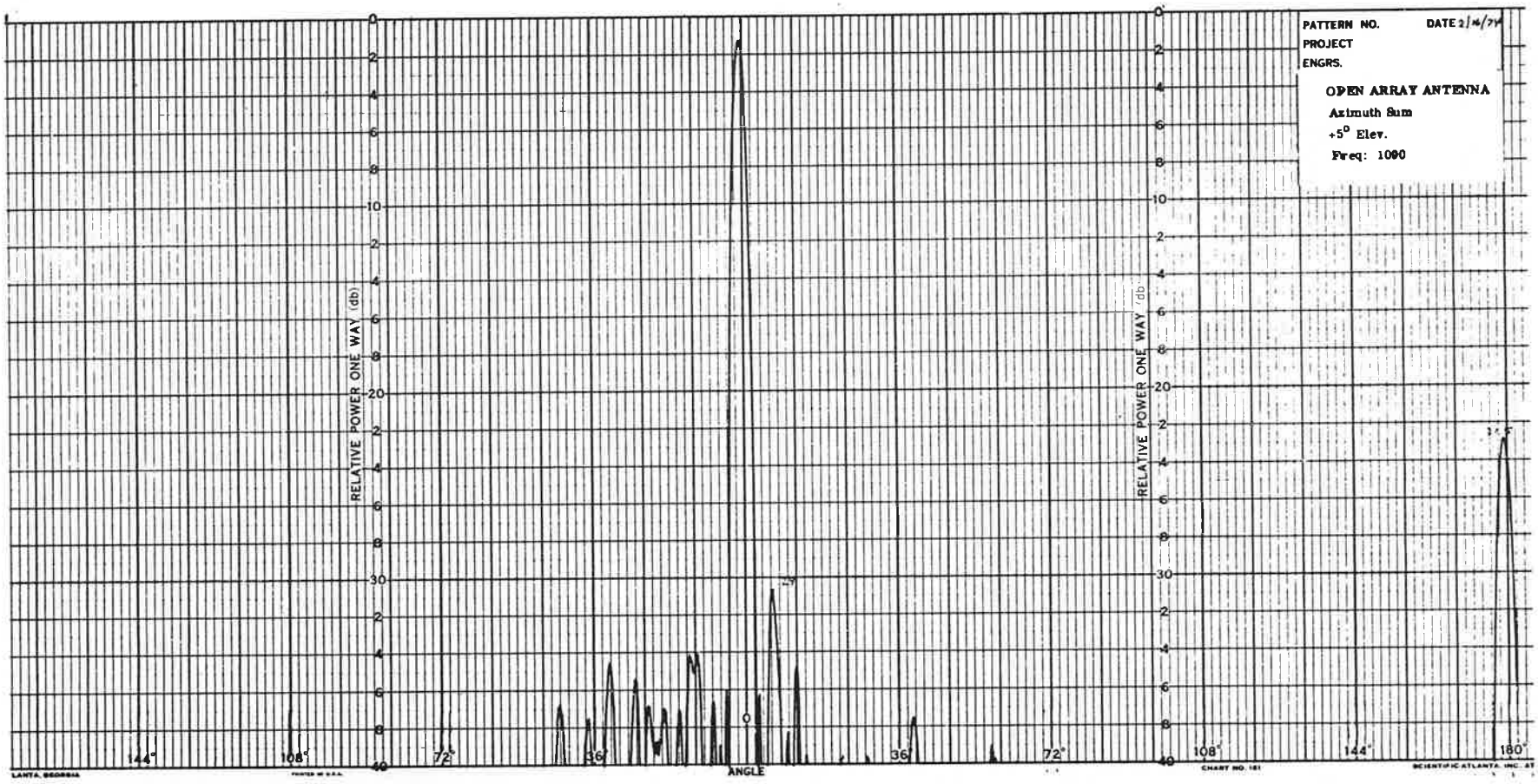

Figure A-52. Open Array Azimuth Sum Pattern, 5° Elevation, 1090 MHz, Wide Angle

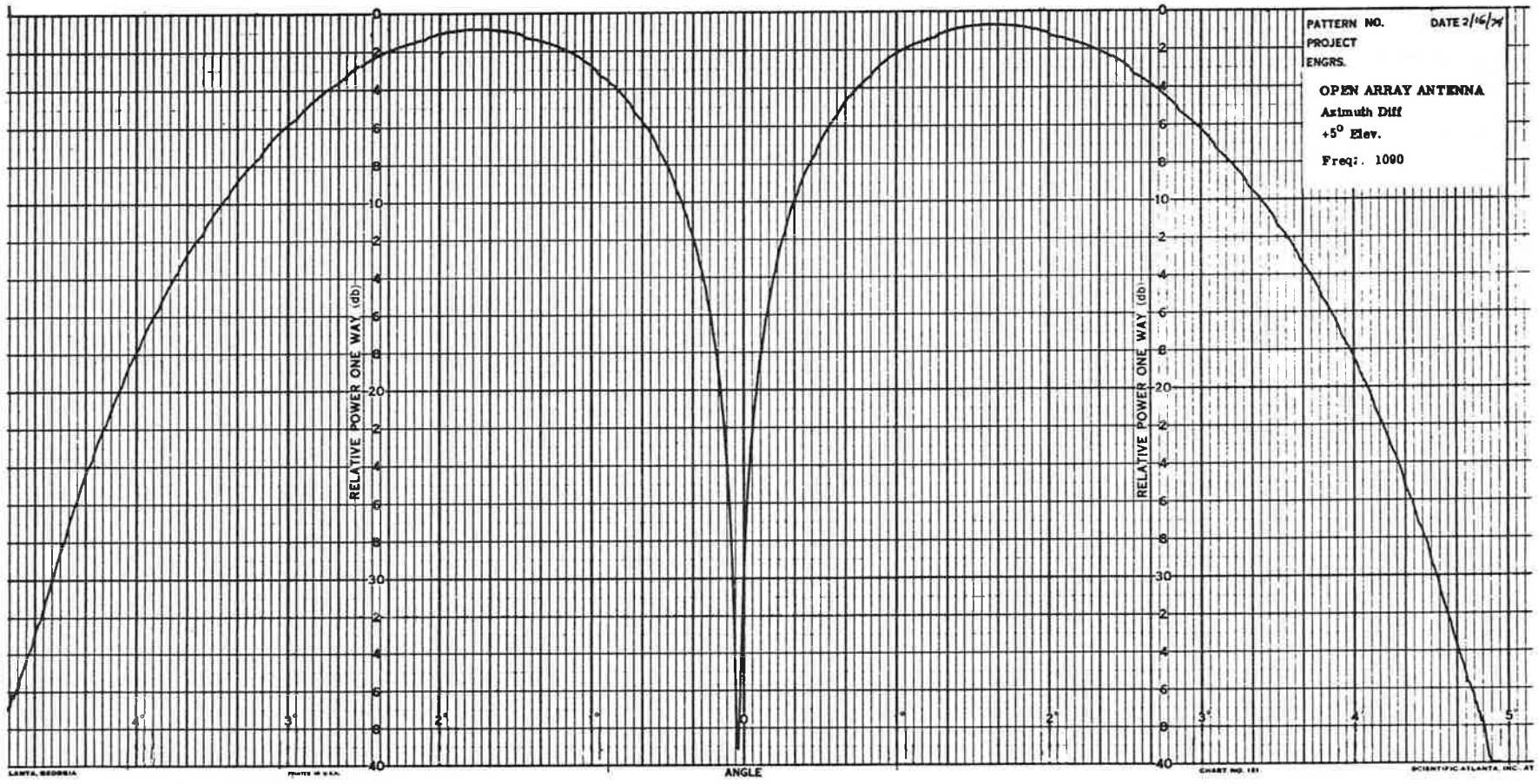

Figure A-53. Open Array Azimuth Difference Pattern, 5° Elevation, 1090 MHz, Narrow Angle

Figure A-54. Open Array Azimuth Difference Pattern, 5° Elevation, 1090 MHz, Wide Angle

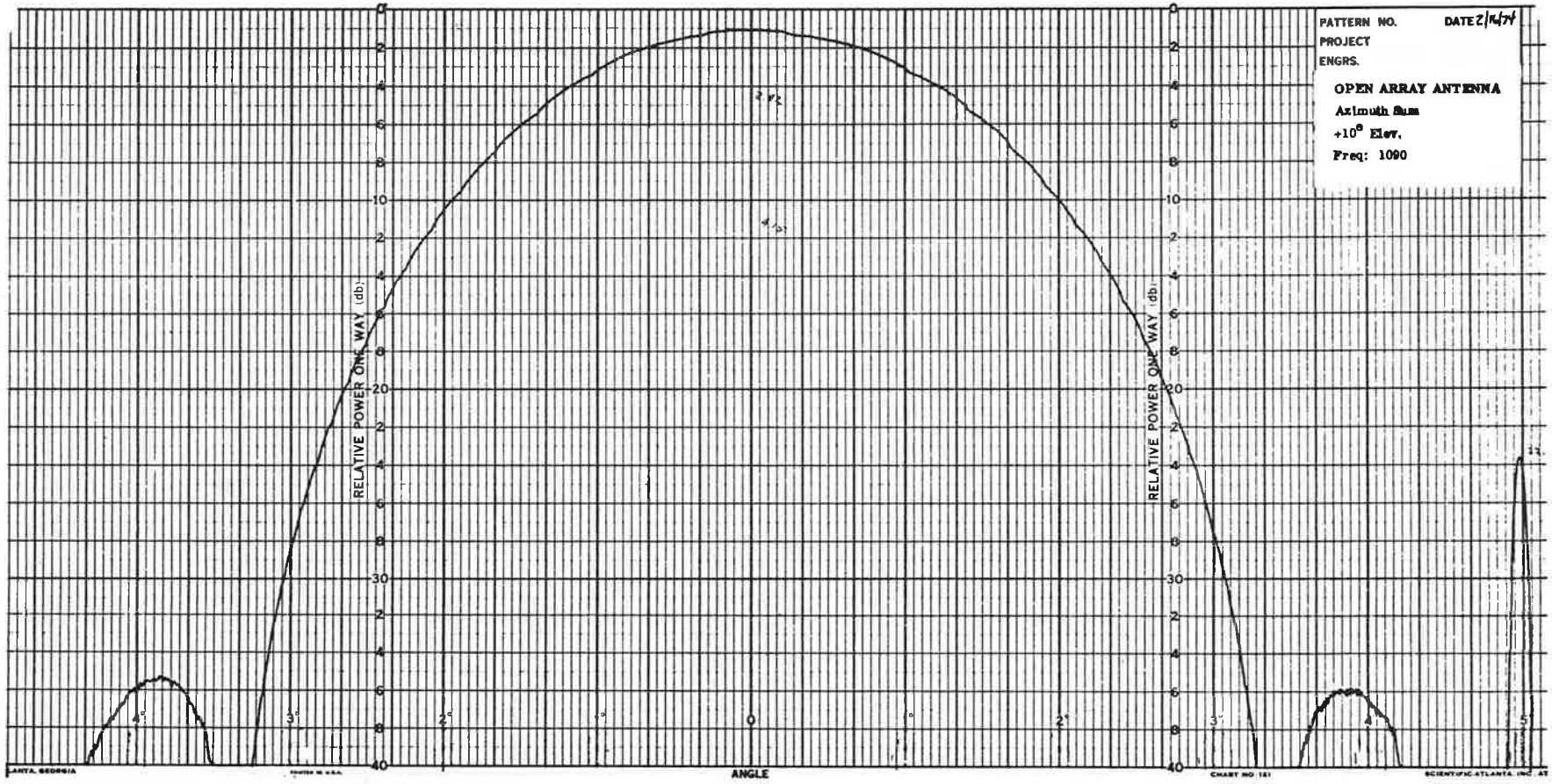

Figure A-55. Open Array Azimuth Sum Pattern, 10° Elevation, 1090 MHz, Narrow Angle

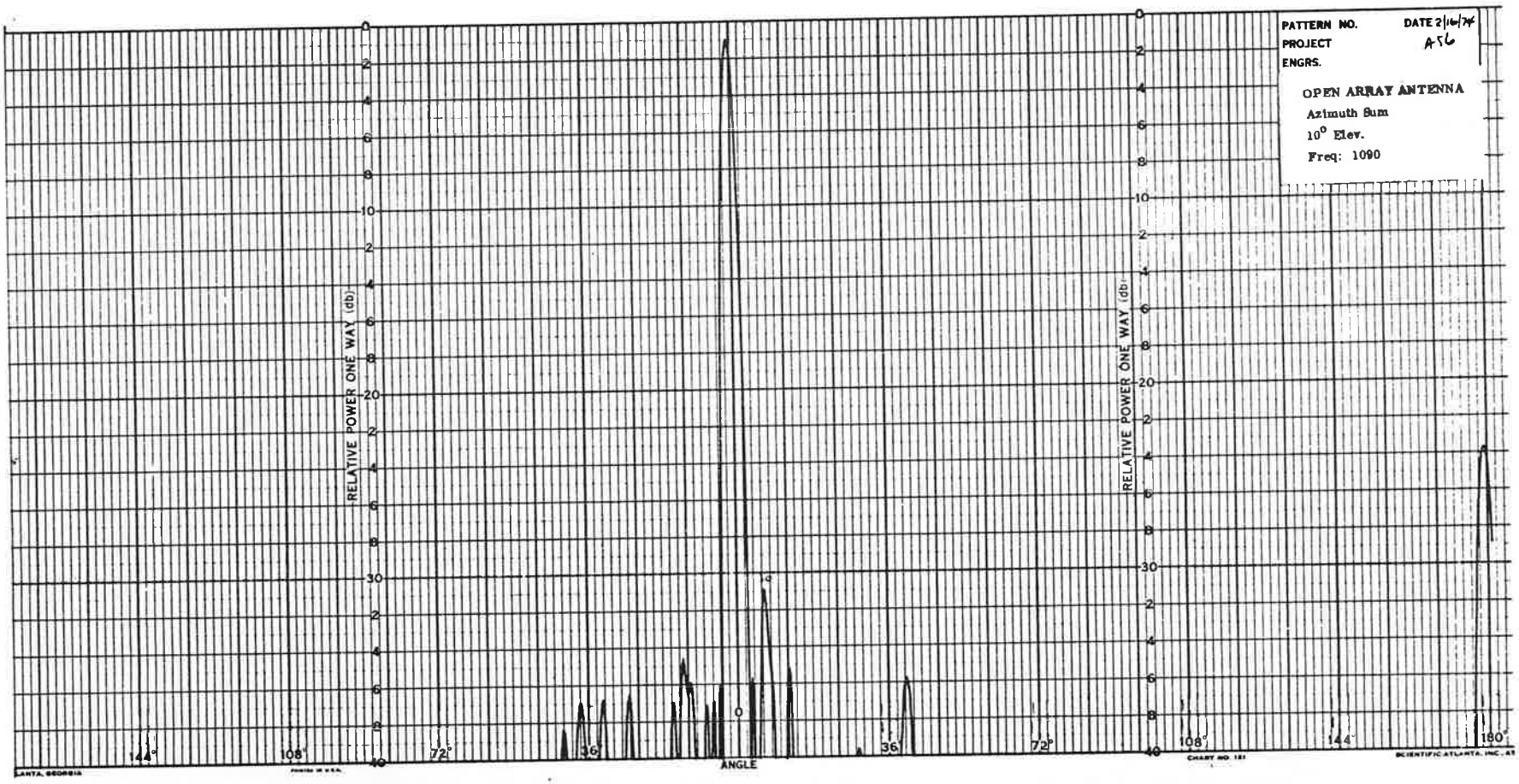

Figure A-56. Open Array Azimuth Sum Pattern, 10° Elevation, 1090 MHz, Wide Angle

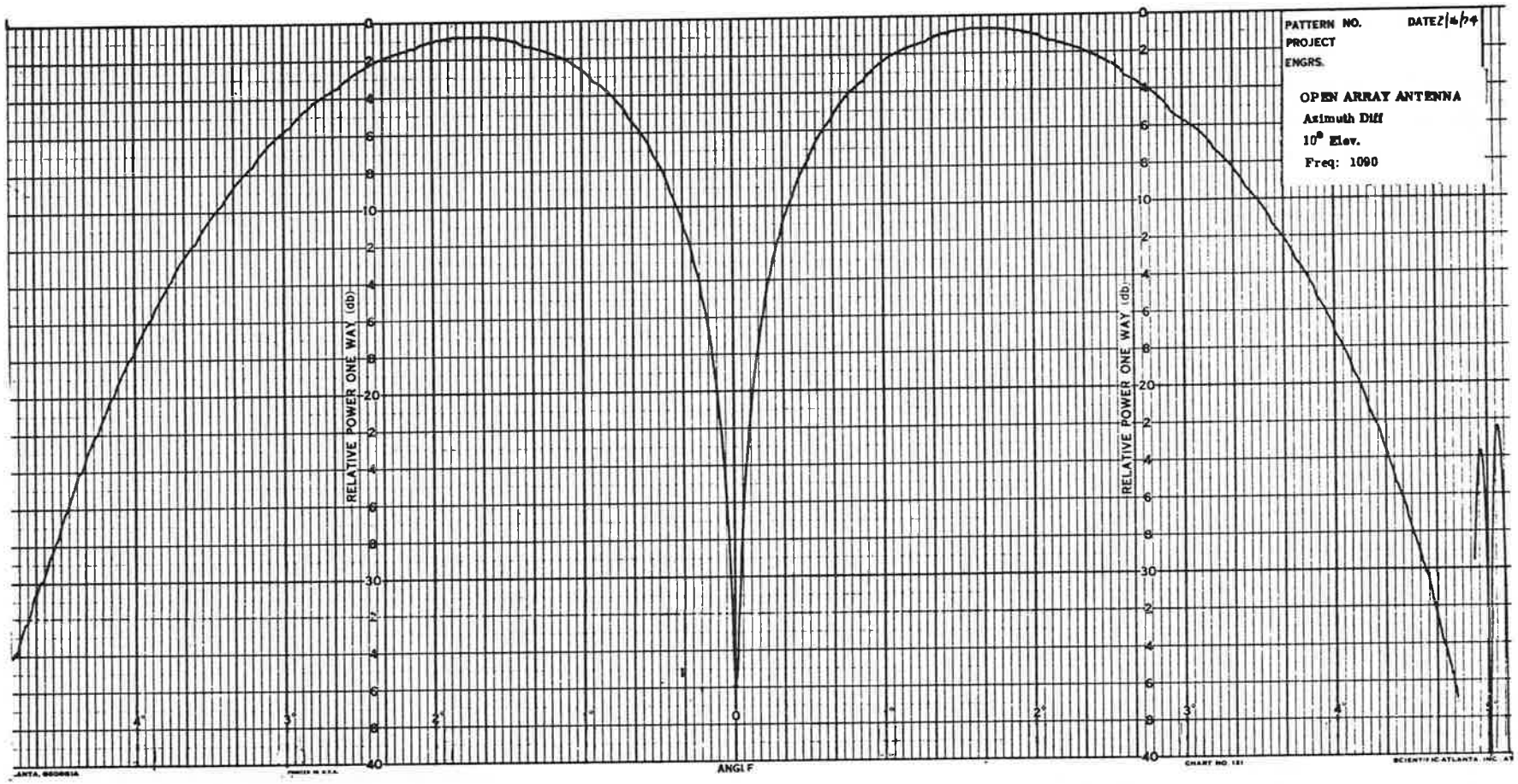

Figure A-57. Open Array Azimuth Difference Pattern, 10° Elevation, 1090 MHz, Narrow Angle

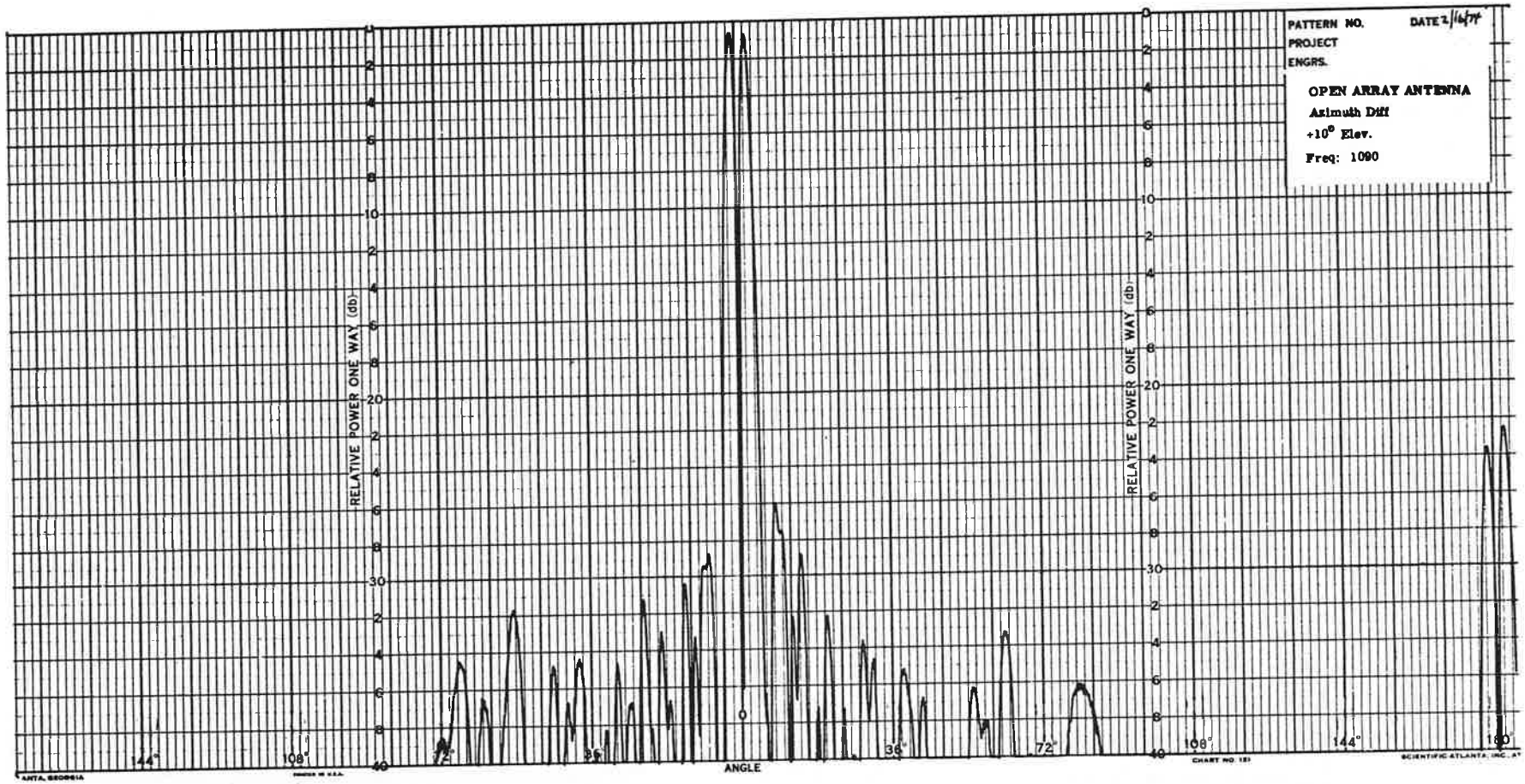

Figure A-58. Open Array Azimuth Difference Pattern, 10° Elevation, 1090 MHz, Wide Angle

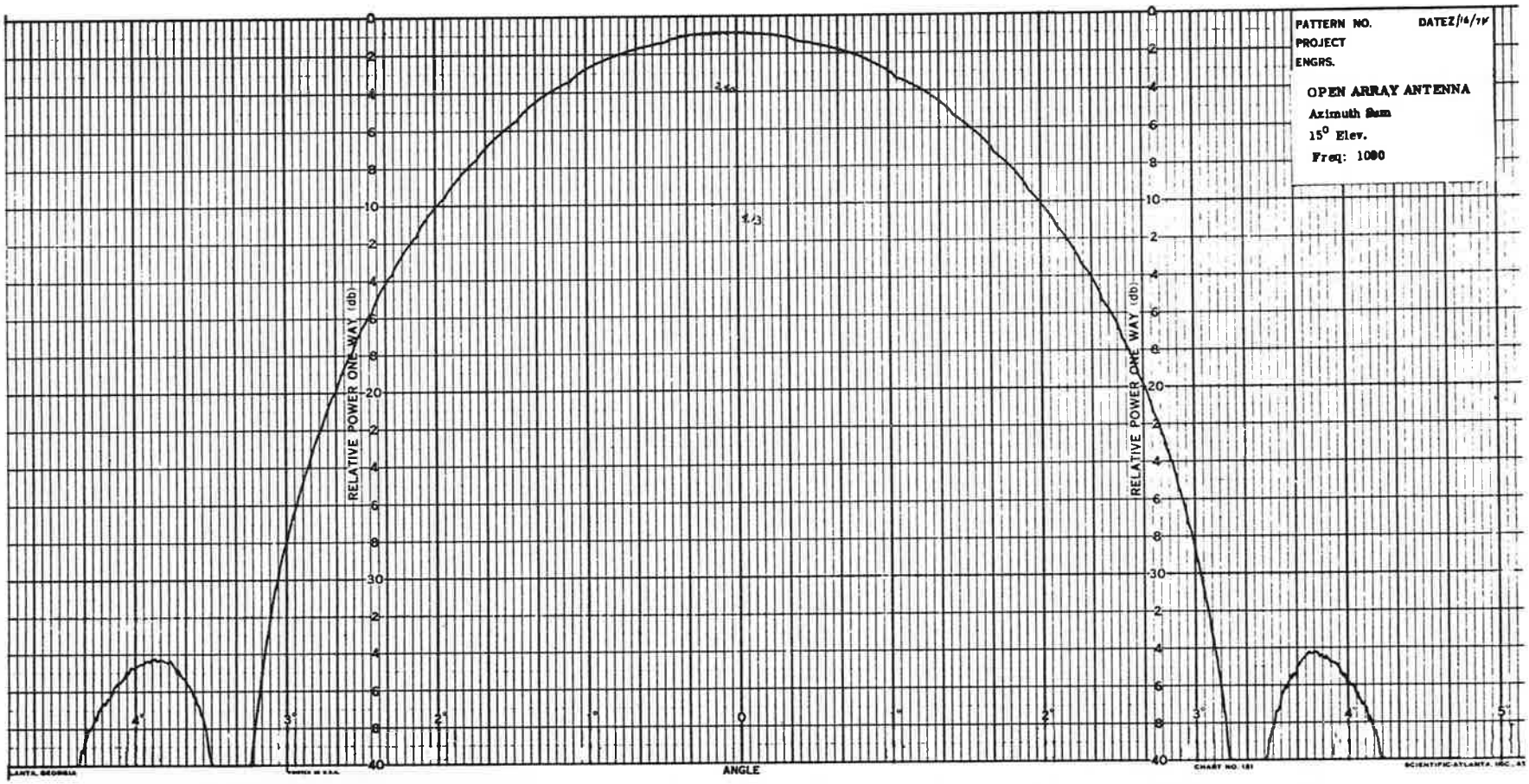

Figure A-59. Open Array Azimuth Sum Pattern, 15° Elevation, 1090 MHz, Narrow Angle

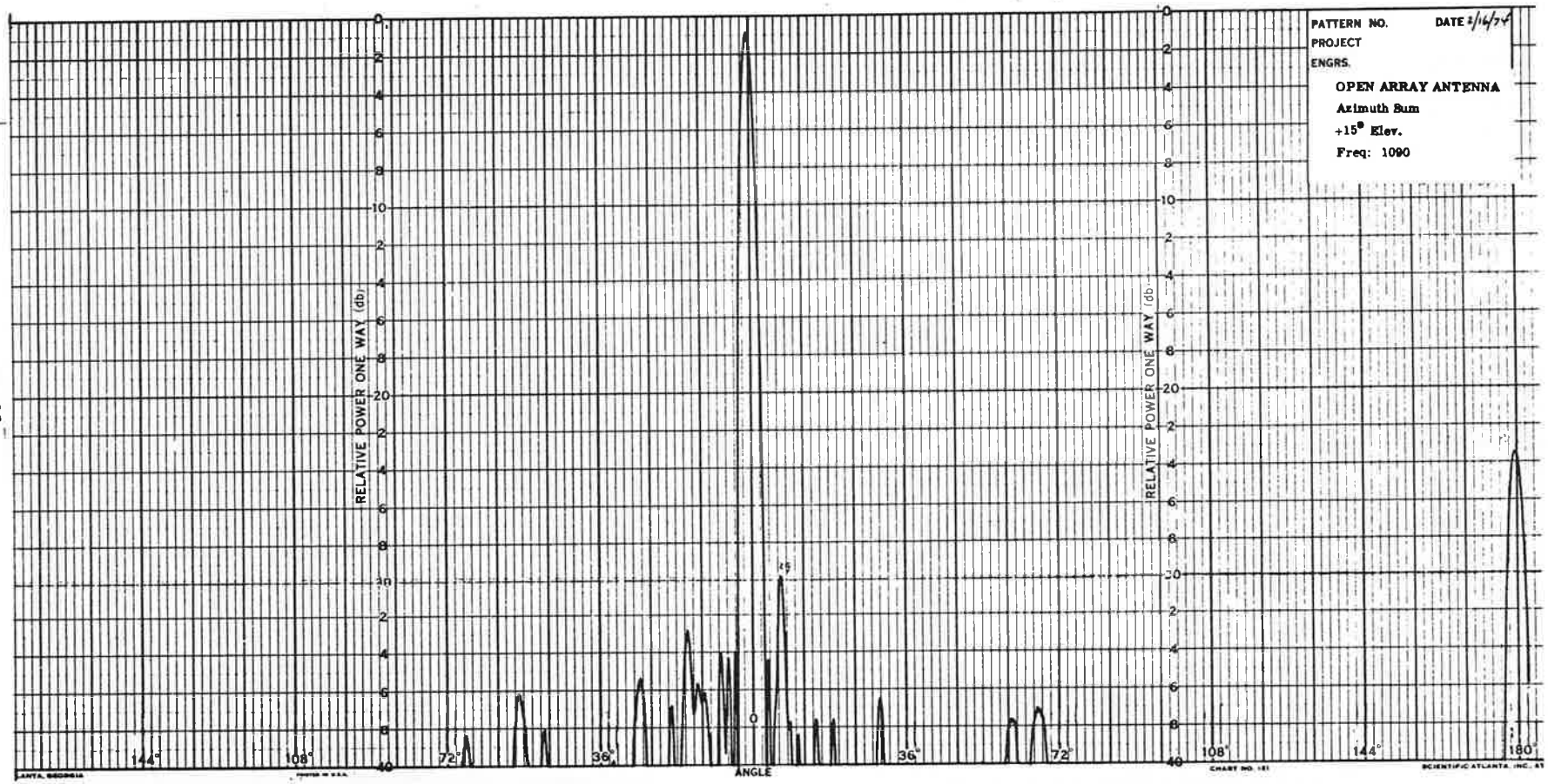

Figure A-60. Open Array Azimuth Sum Pattern, 15° Elevation, 1090 MHz, Wide Angle

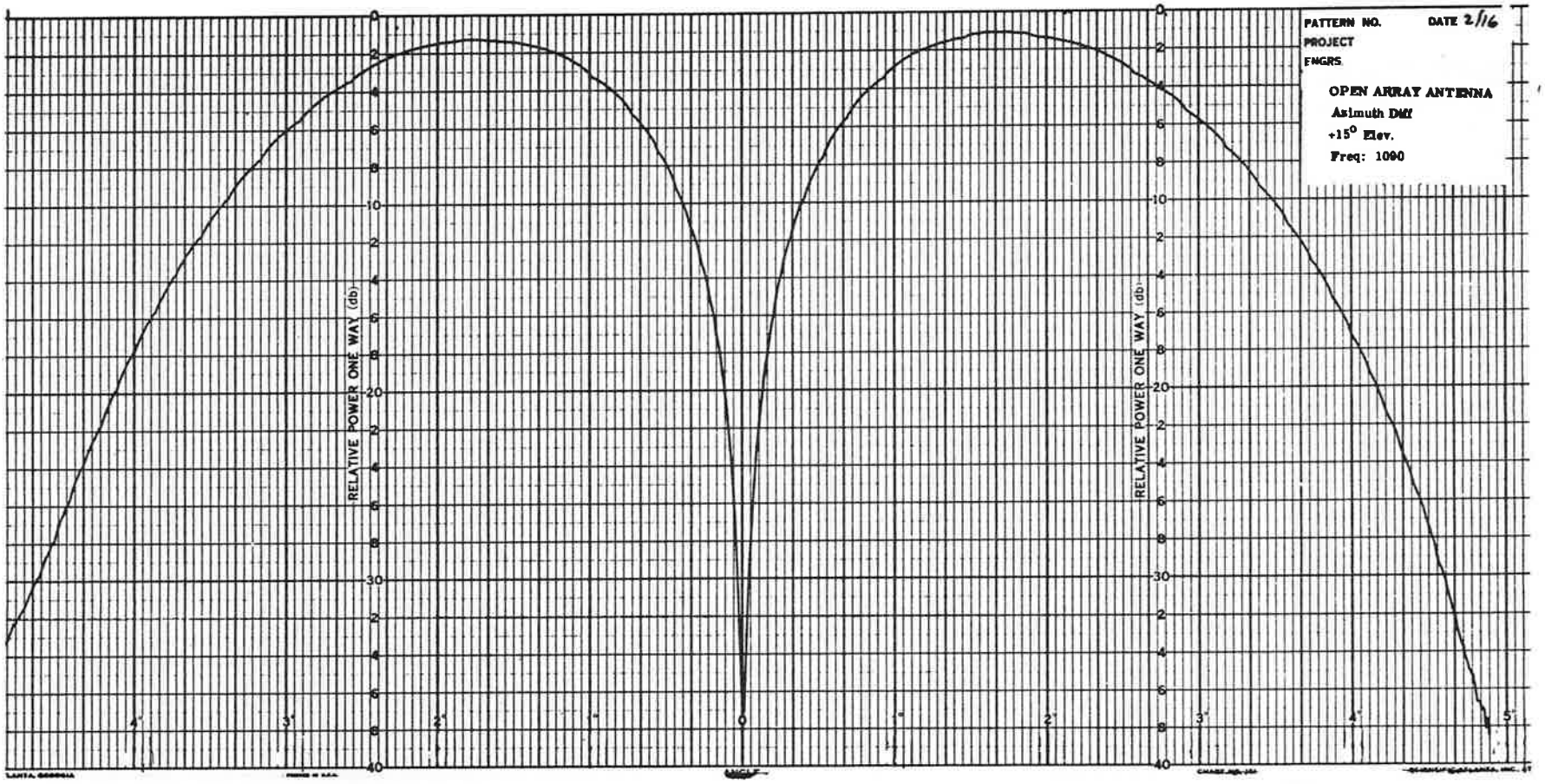

Figure A-61. Open Array Azimuth Difference Pattern, 15° Elevation, 1090 MHz, Narrow Angle

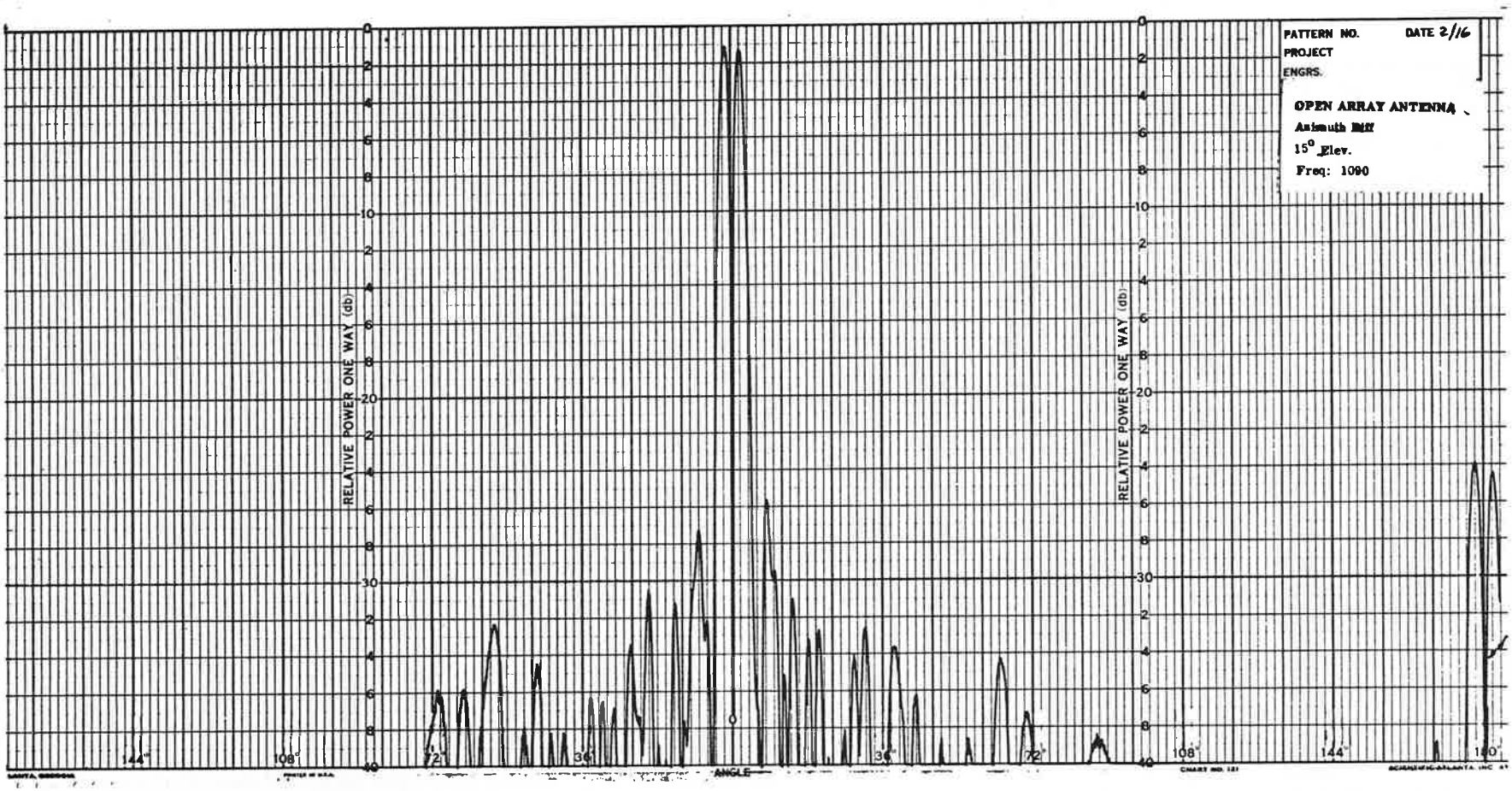

Figure A-62. Open Array Azimuth Difference Pattern, 15° Elevation, 1090 MHz, Wide Angle

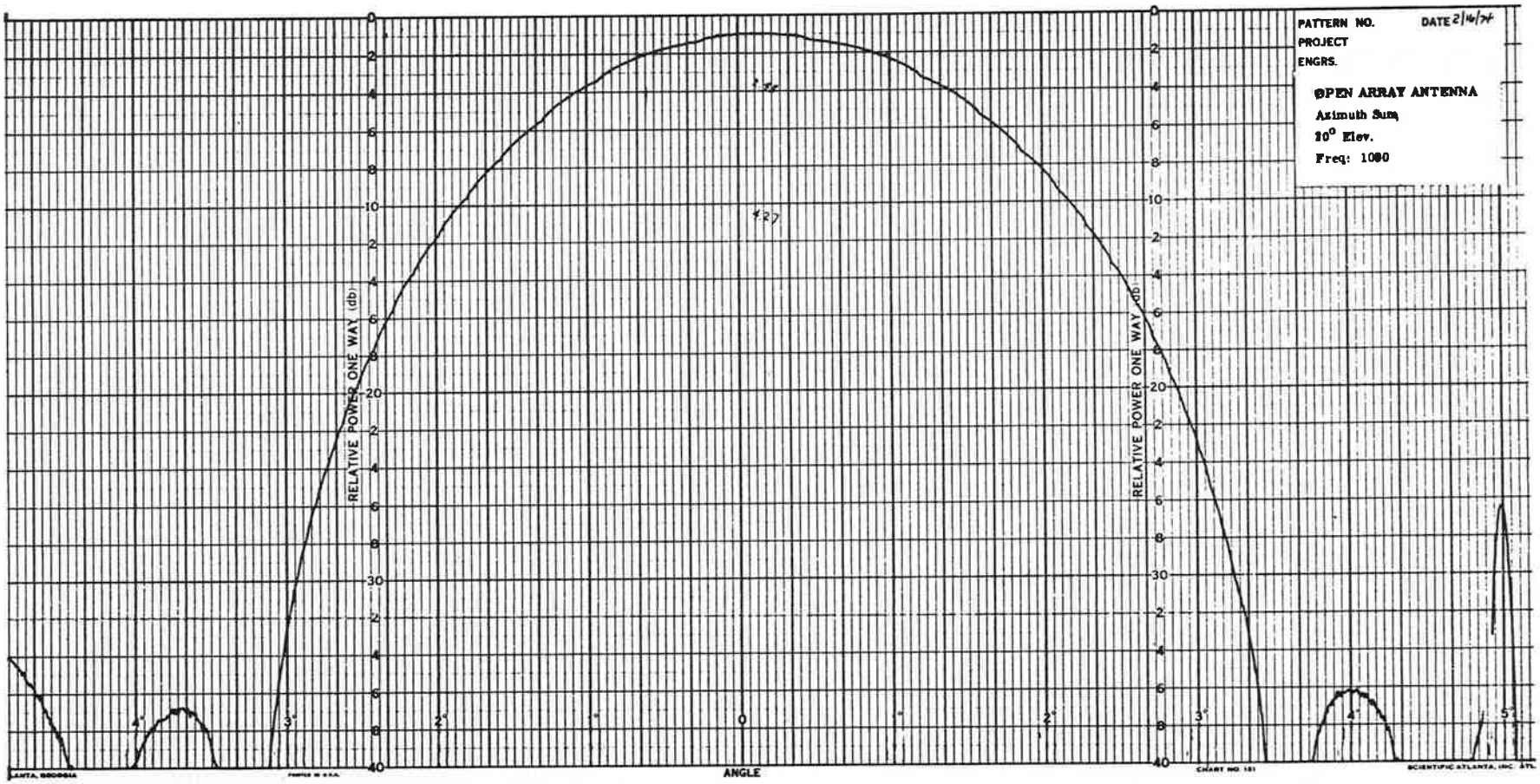

Figure A-63. Open Array Azimuth Sum Pattern, 20° Elevation, 1090 MHz, Narrow Angle

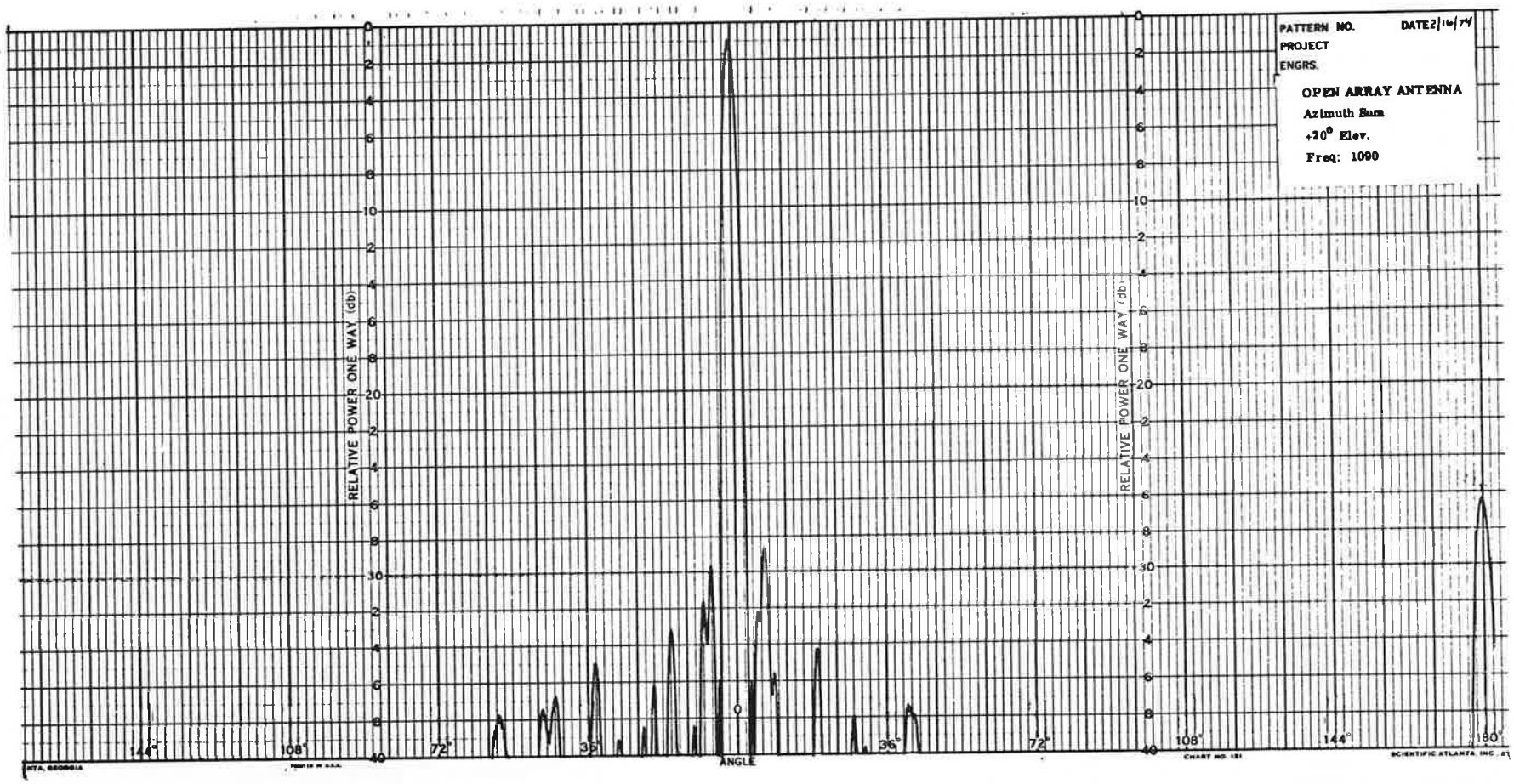

Figure A-64. Open Array Azimuth Sum Pattern, 20° Elevation, 1090 MHz, Wide Angle

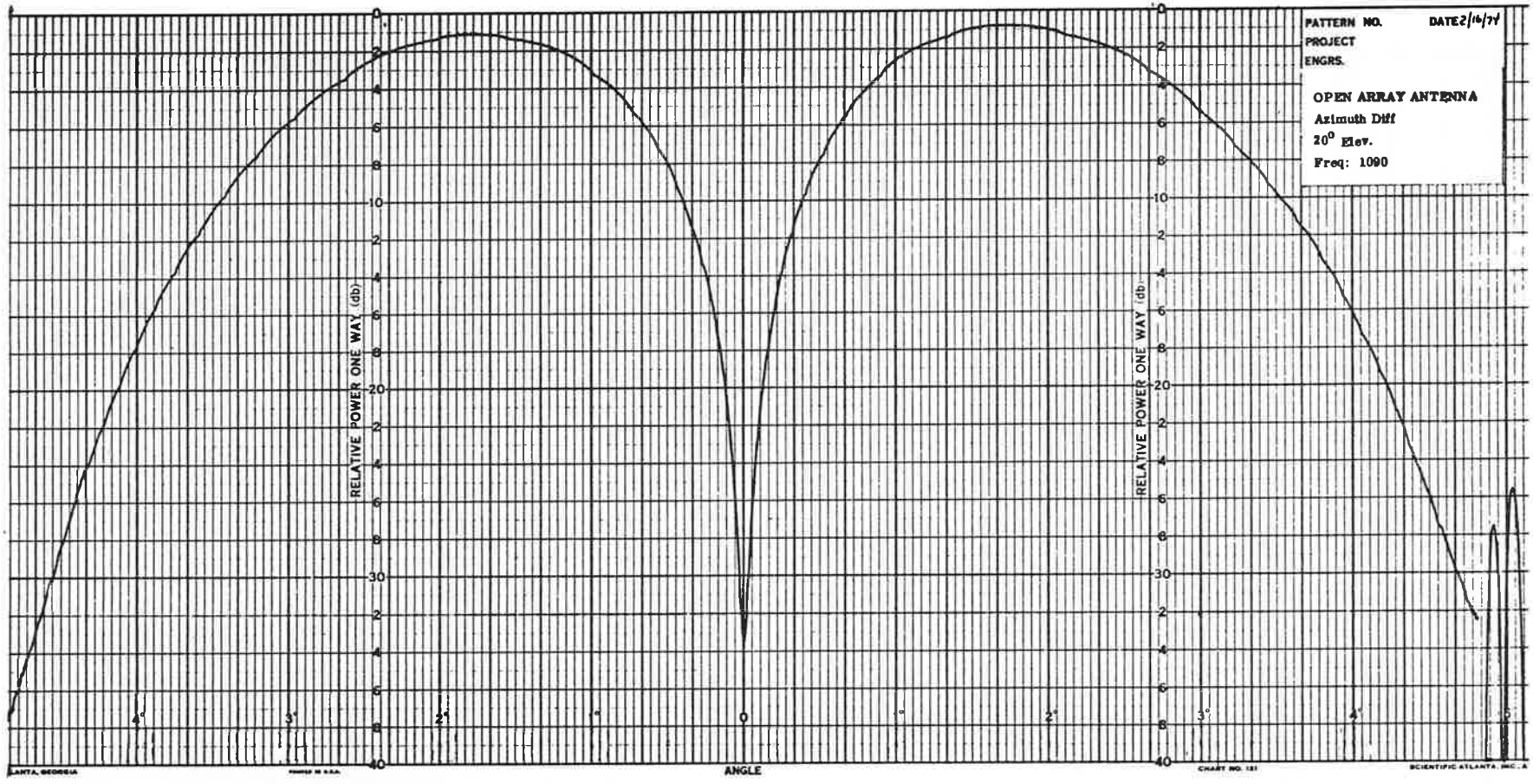

Figure A-65. Open Array Azimuth Difference Pattern, 20° Elevation, 1090 MHz, Narrow Angle

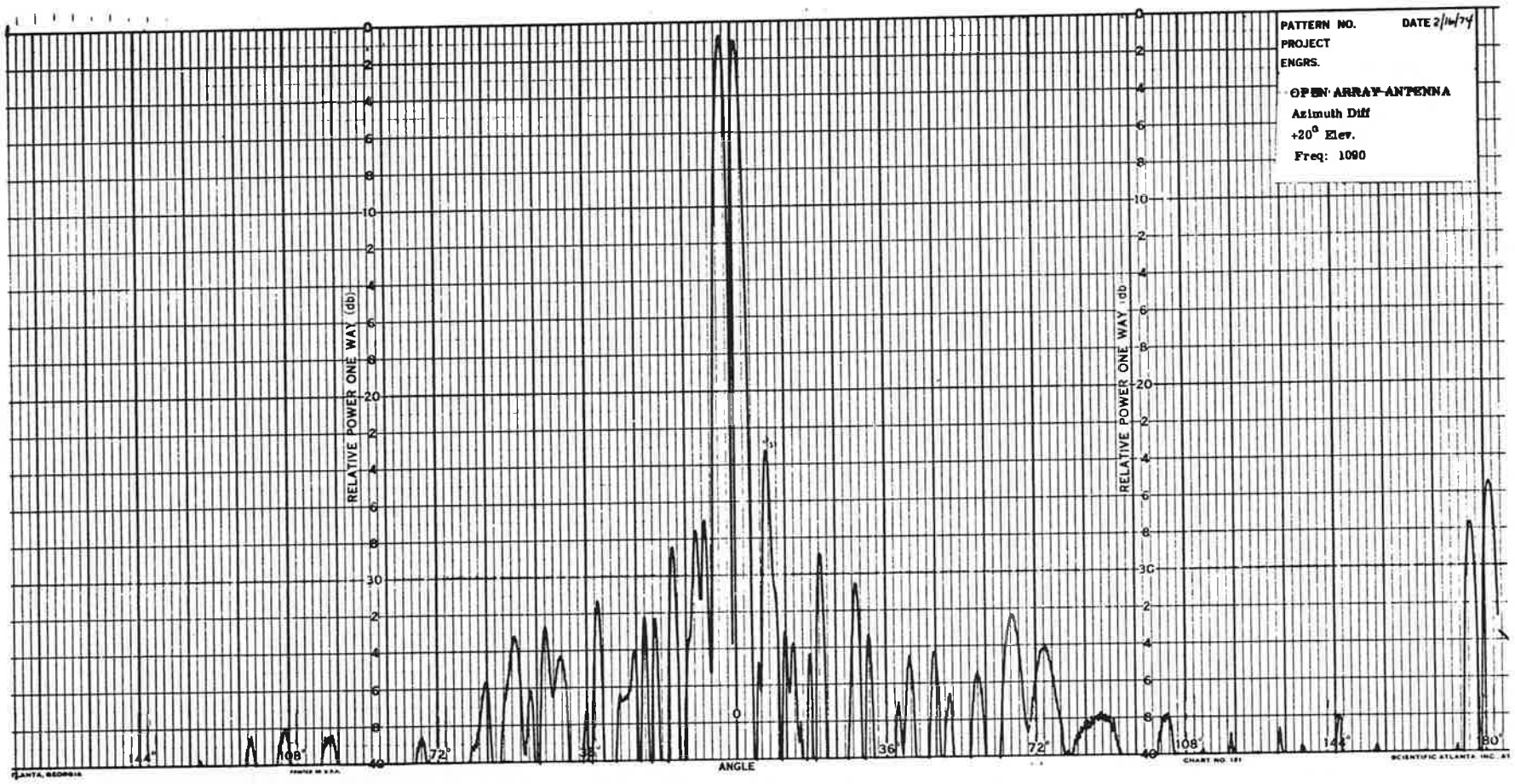

Figure A-66. Open Array Azimuth Difference Pattern, 20° Elevation, 1090 MHz, Wide Angle

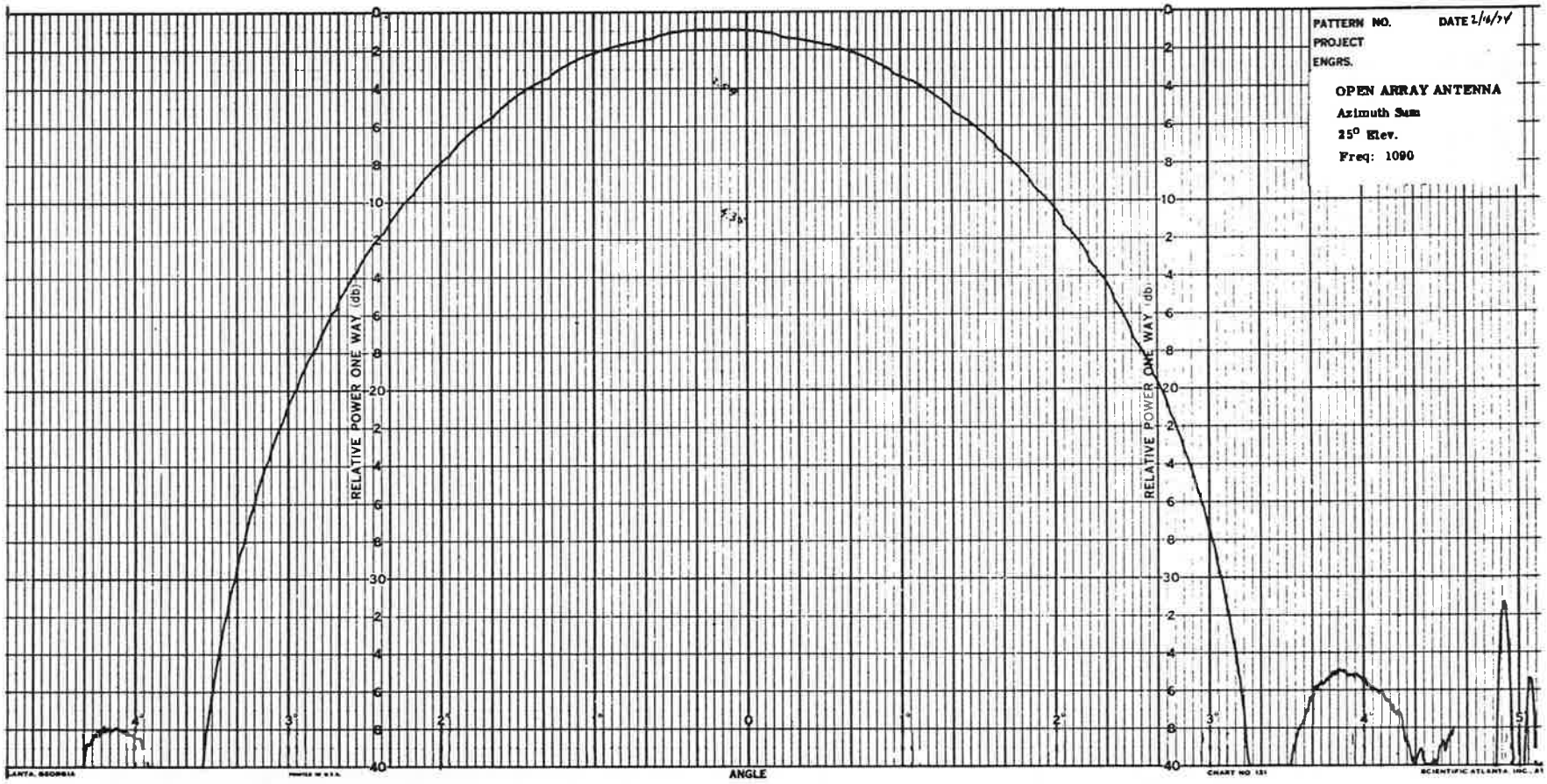

Figure A-67. Open Array Azimuth Sum Pattern, 25° Elevation, 1090 MHz, Narrow Angle

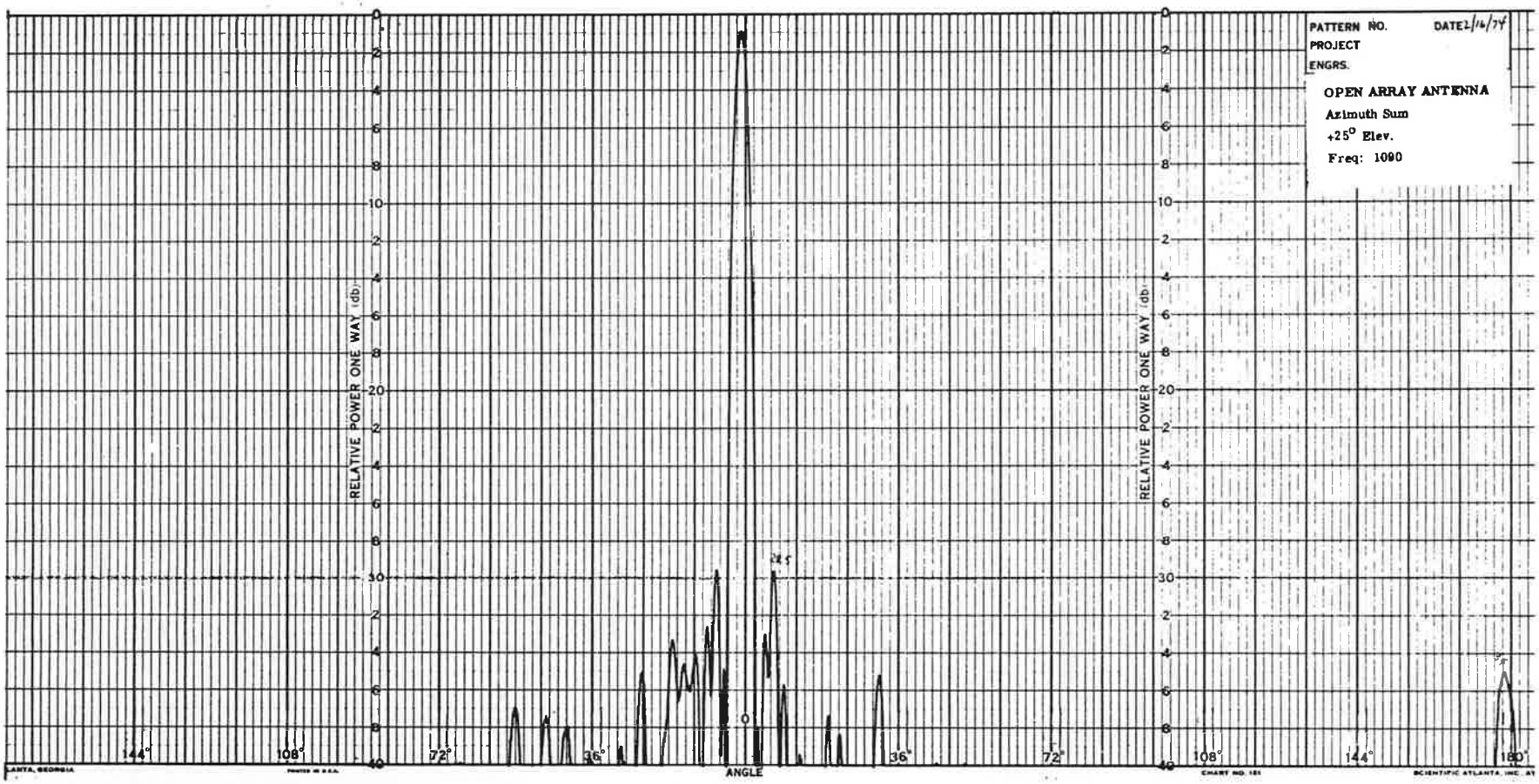

Figure A-68. Open Array Azimuth Sum Pattern, 25° Elevation, 1090 MHz, Wide Angle

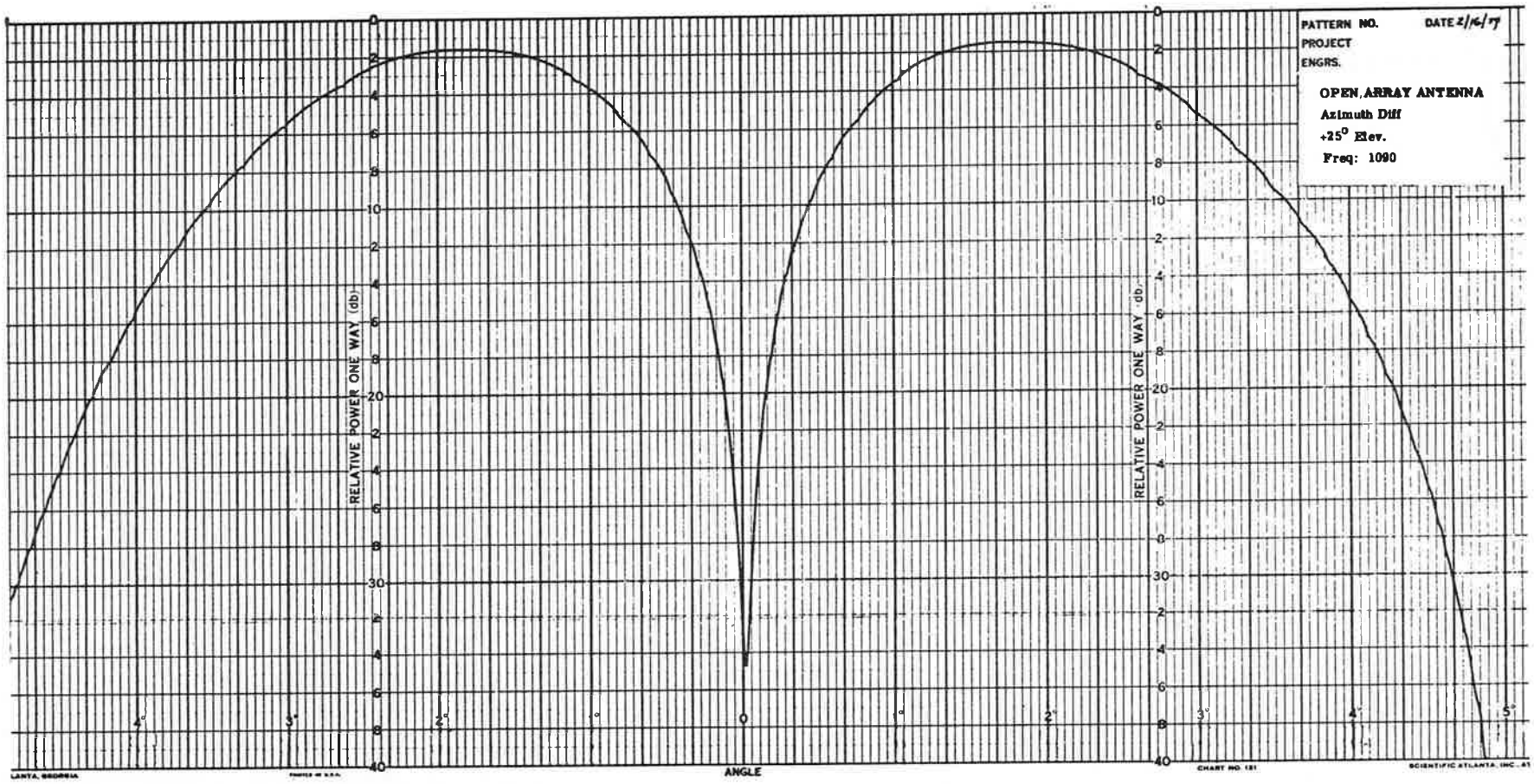

Figure A-69. Open Array Azimuth Difference Pattern, 25° Elevation, 1090 MHz, Narrow Angle

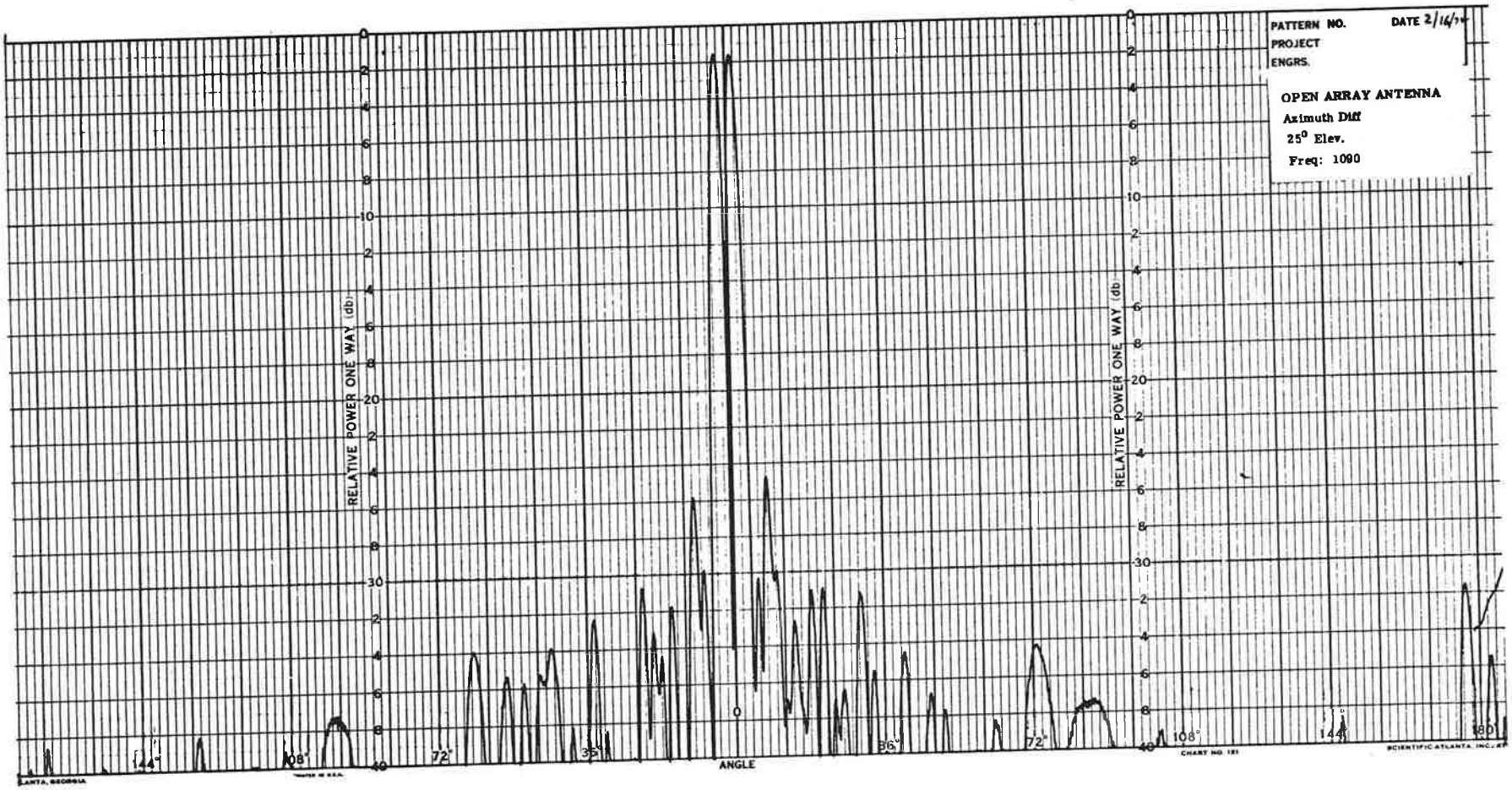

Figure A-70. Open Array Azimuth Difference Pattern, 25° Elevation, 1090 MHz, Wide Angle

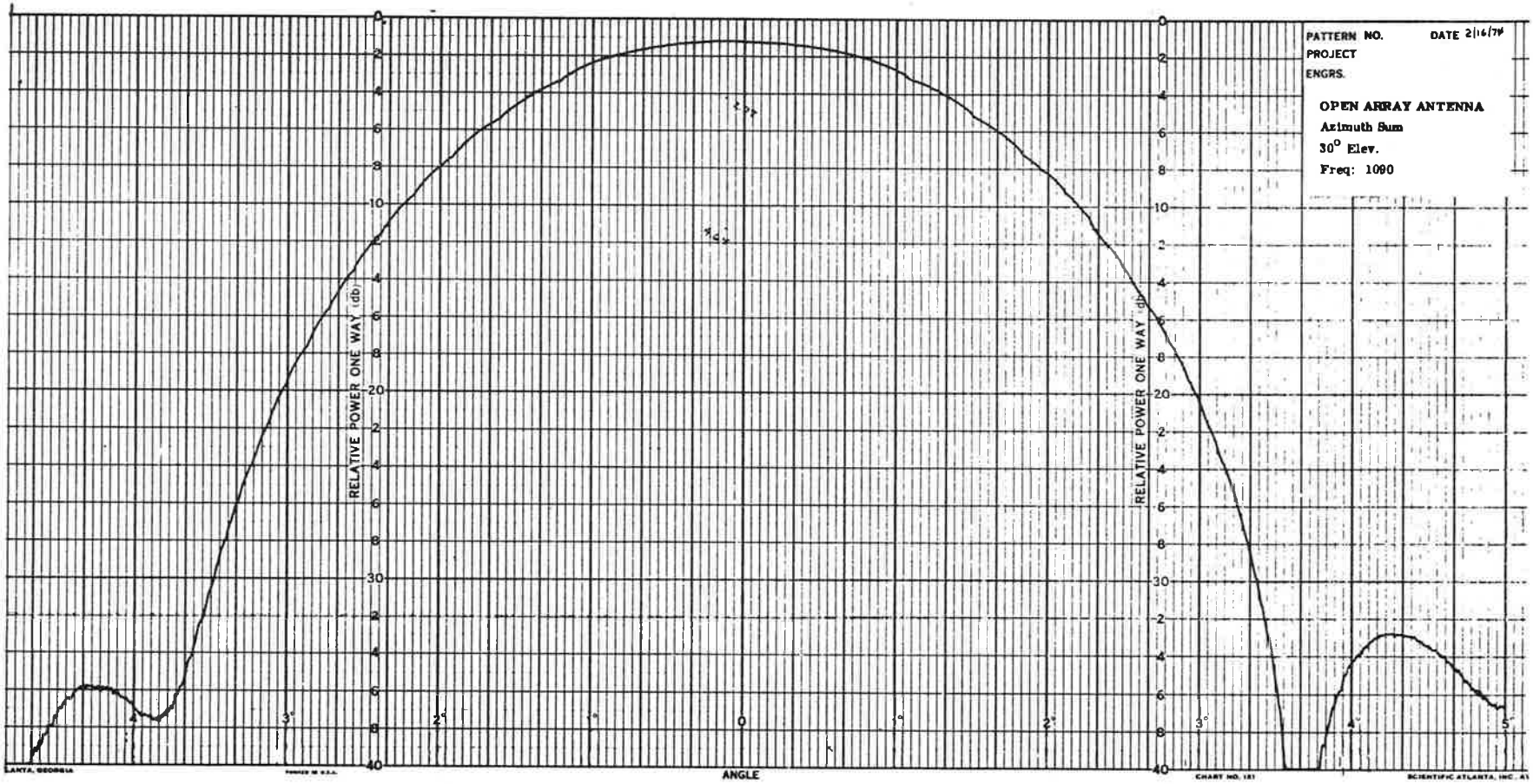

Figure A-71. Open Array Azimuth Sum Pattern, 30° Elevation, 1090 MHz, Narrow Angle

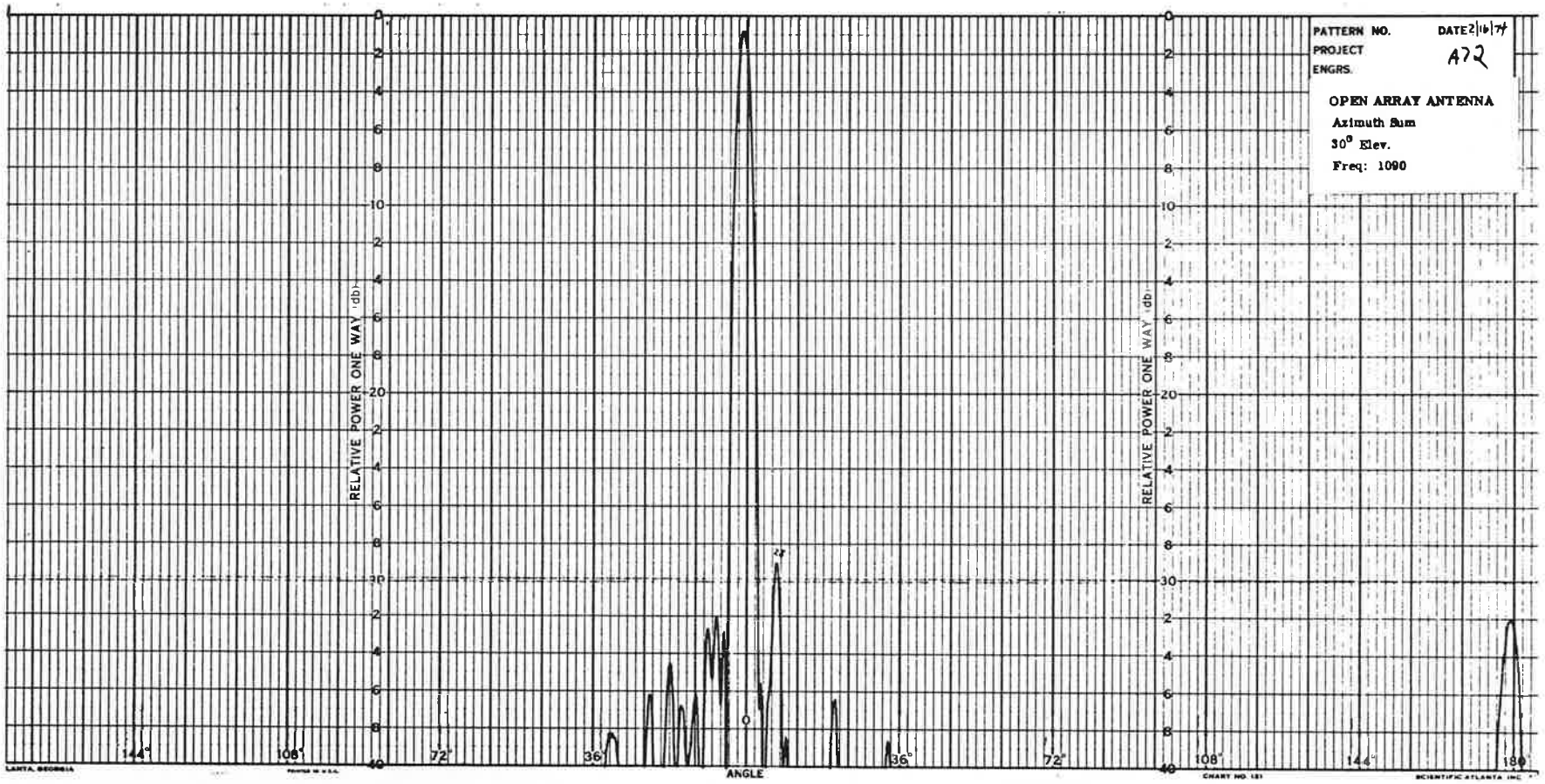

Figure A-72. Open Array Azimuth Sum Pattern, 30° Elevation, 1090 MHz, Wide Angle

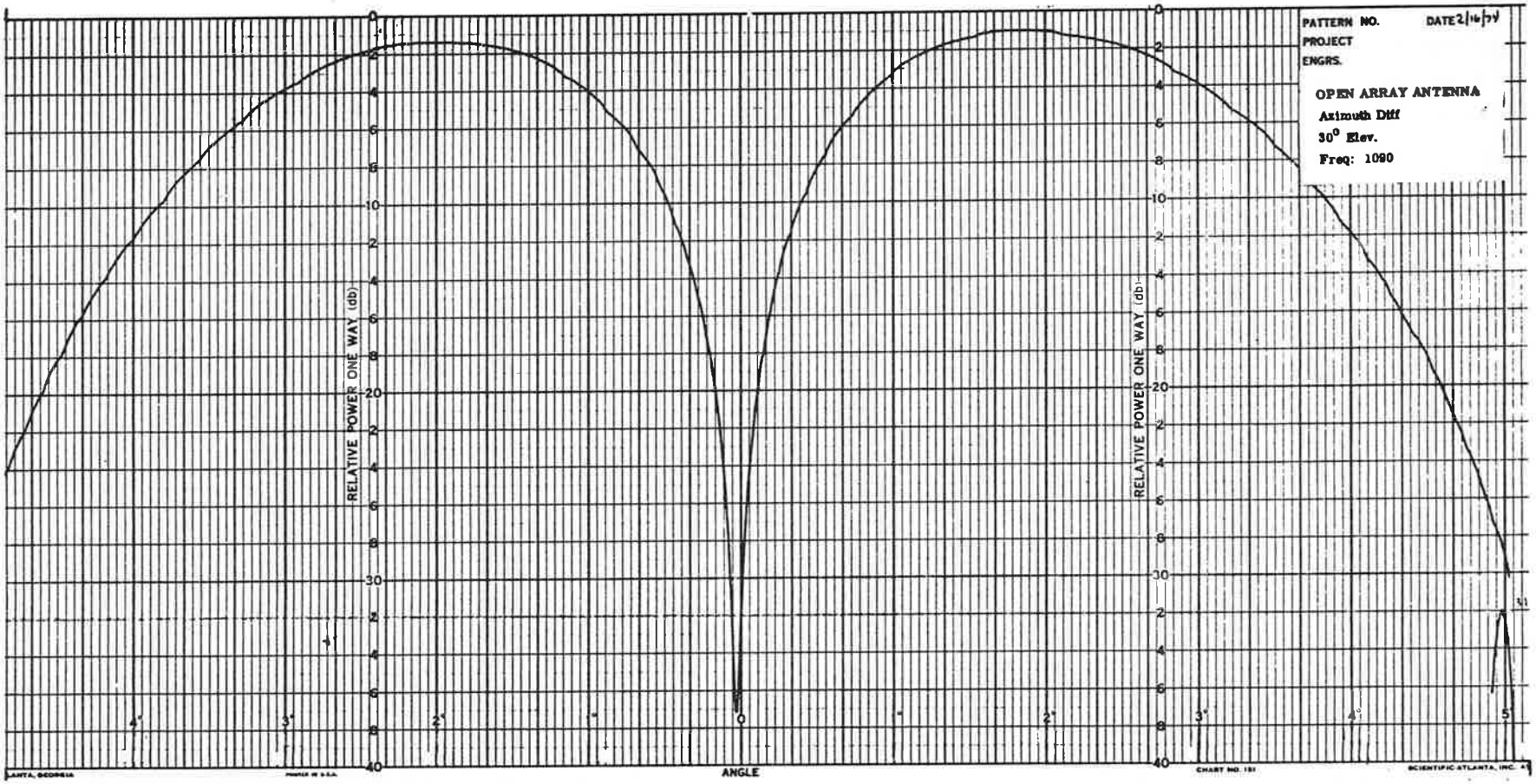

Figure A-73. Open Array Azimuth Difference Pattern, 30° Elevation, 1090 MHz, Narrow Angle

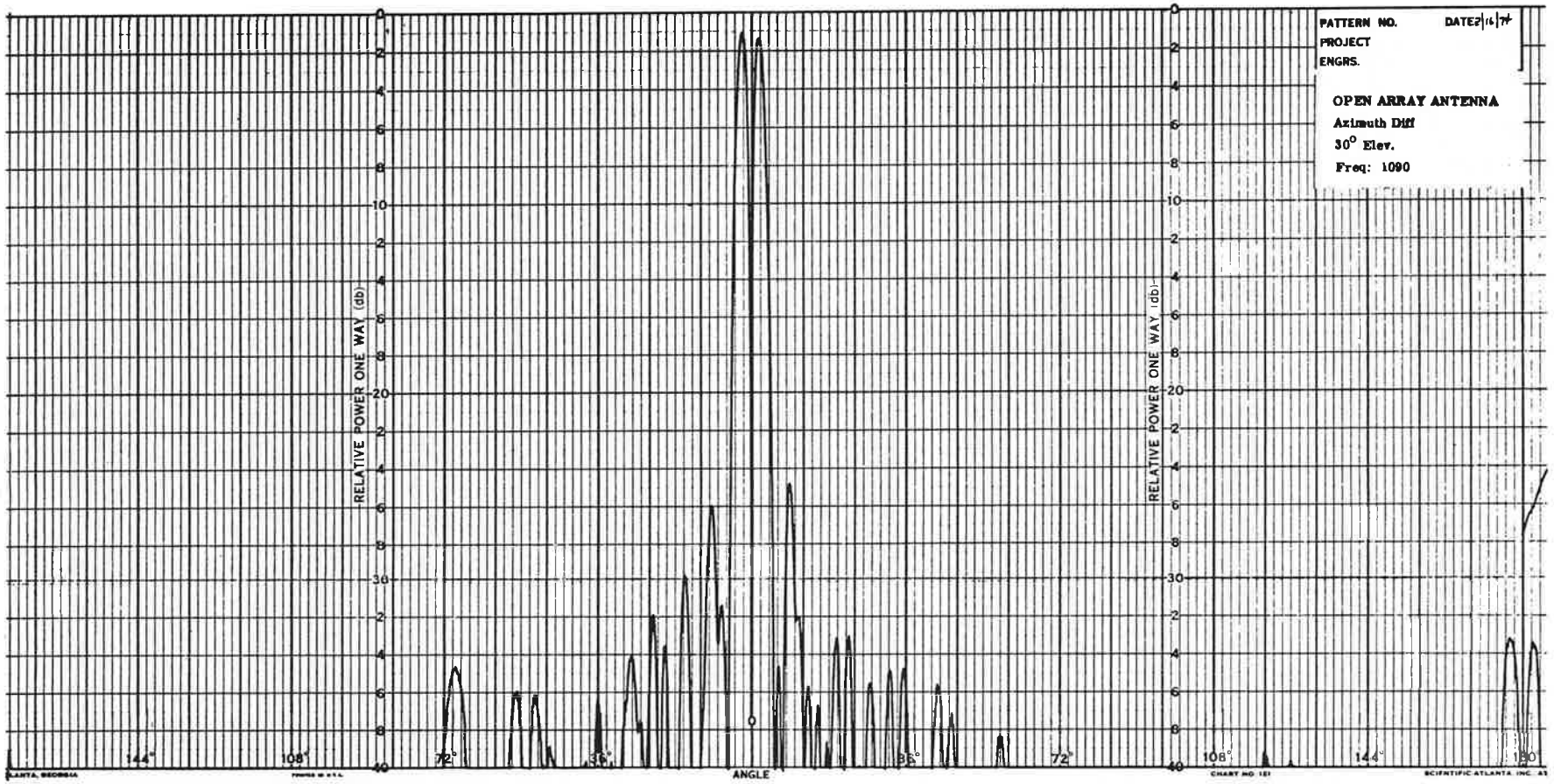

Figure A-74. Open Array Azimuth Difference Pattern, 30° Elevation, 1090 MHz, Wide Angle

Figure A-75. Open Array Azimuth Sum Pattern, 35° Elevation, 1090 MHz, Narrow Angle

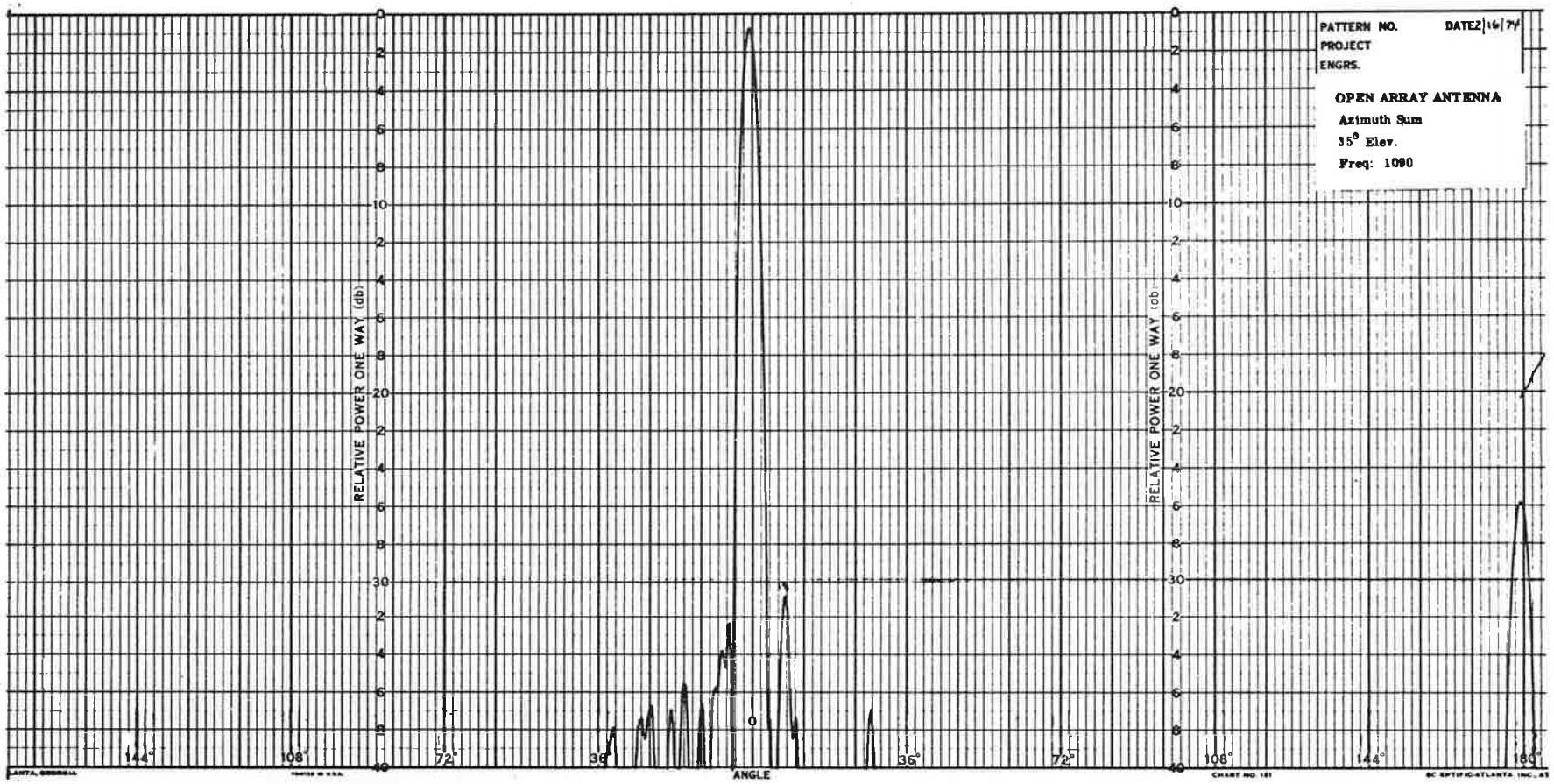

Figure A-76. Open Array Azimuth Sum Pattern, 35° Elevation, 1090 MHz, Wide Angle

Figure A-77. Open Array Azimuth Difference Pattern, 35° Elevation, 1090 MHz, Narrow Angle

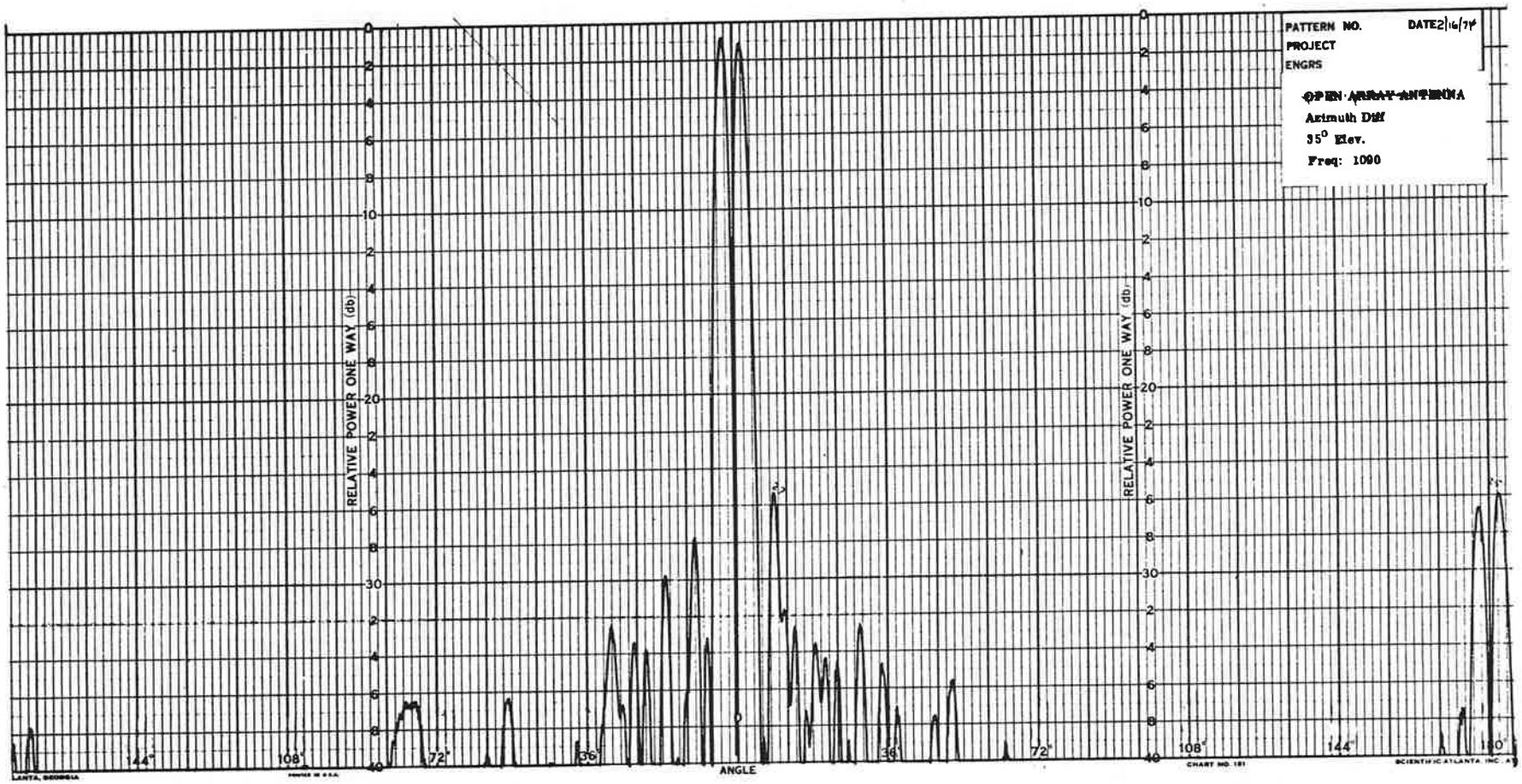

Figure A-78. Open Array Azimuth Difference Pattern, 35° Elevation, 1090 MHz, Wide Angle

Figure A-79. Open Array Elevation Pattern 1090 MHz

Figure A-80. Open Array Elevation Pattern 1030 MHz

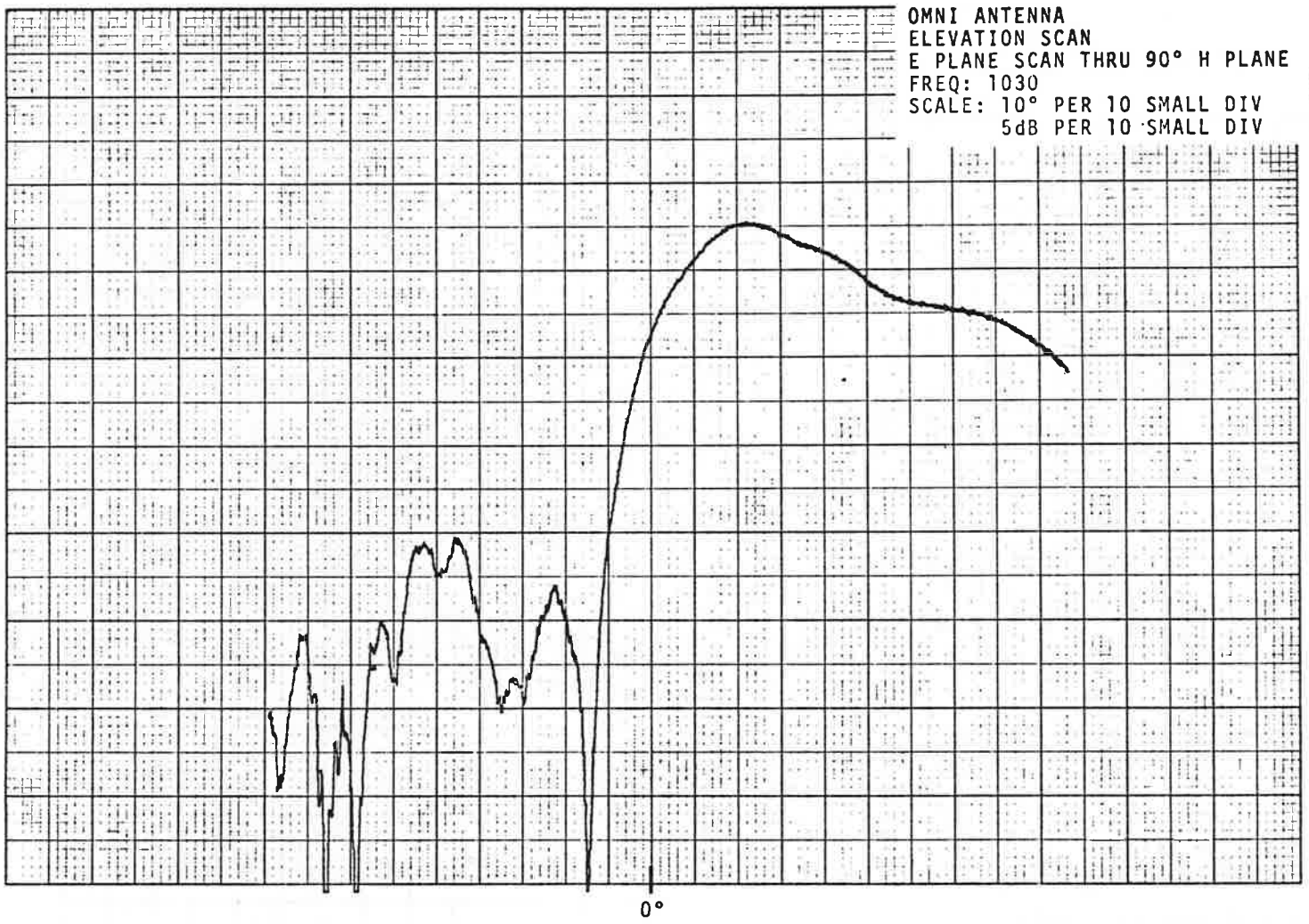

Figure A-83. Omni Antenna Elevation Pattern, 1030 MHz, E Plane Scan Through 90° H Plane

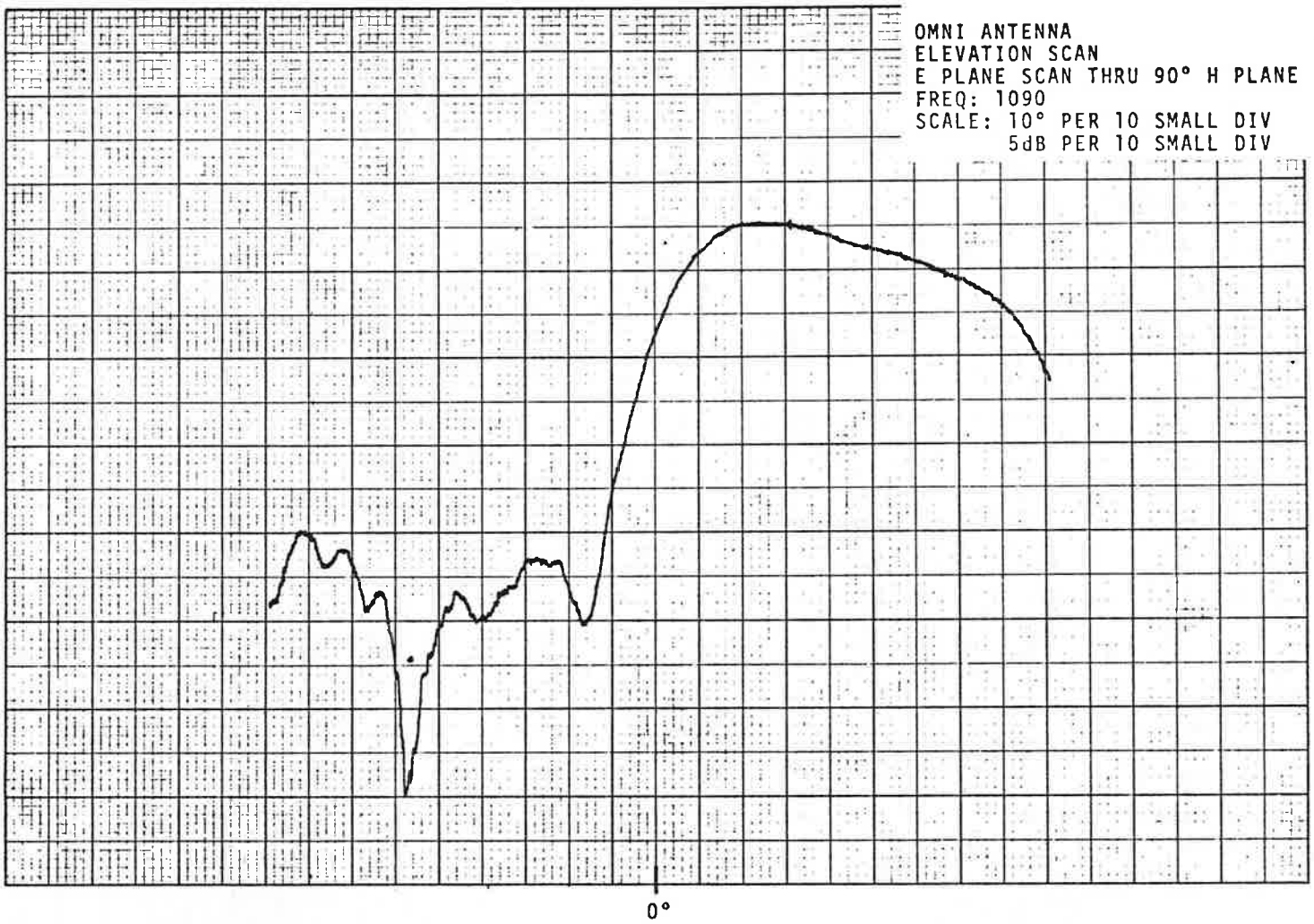

Figure A-84. Omni Antenna Elevation Pattern, 1090 MHz, E Plane Scan Through 90° H Plane

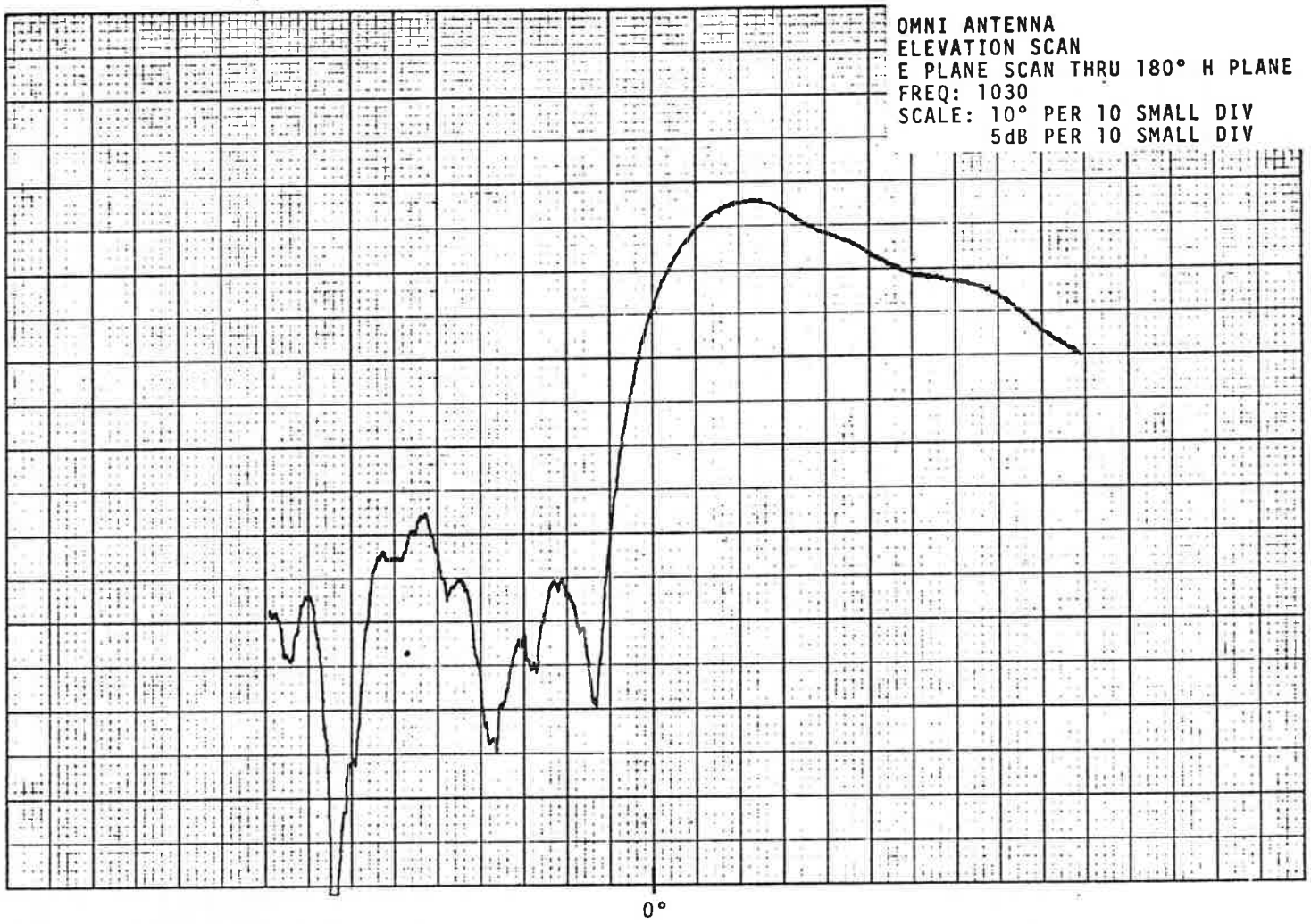

Figure A-85. Omni Antenna Elevation Pattern, 1030 MHz, E Plane Scan Through 180° H Plane

Figure A-86. Omni Antenna Elevation Pattern, 1090 MHz, E Plane Scan Through 180° H Plane

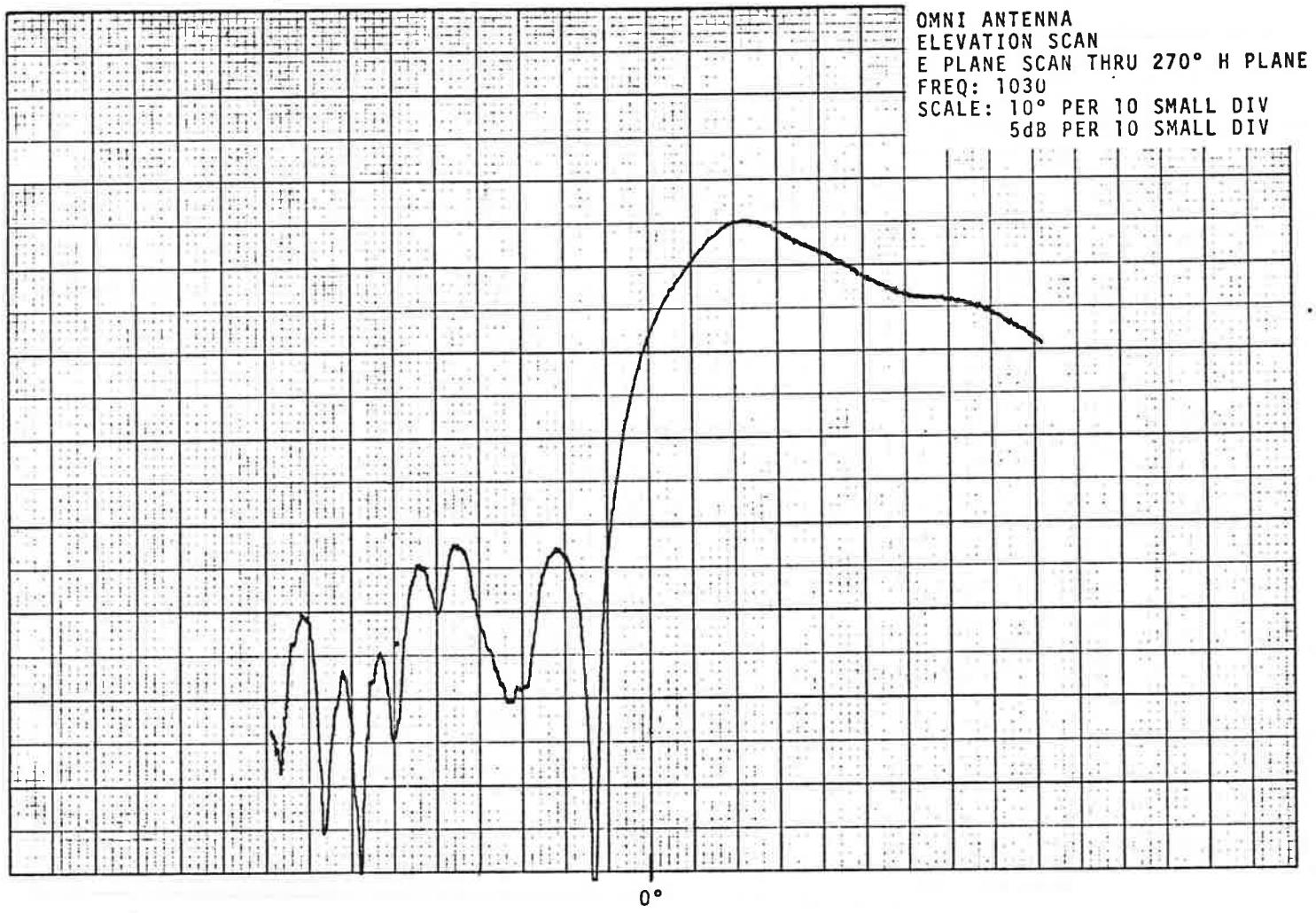

Figure A-87. Omni Antenna Elevation Pattern, 1030 MHz, E Plane Scan Through 270° H Plane

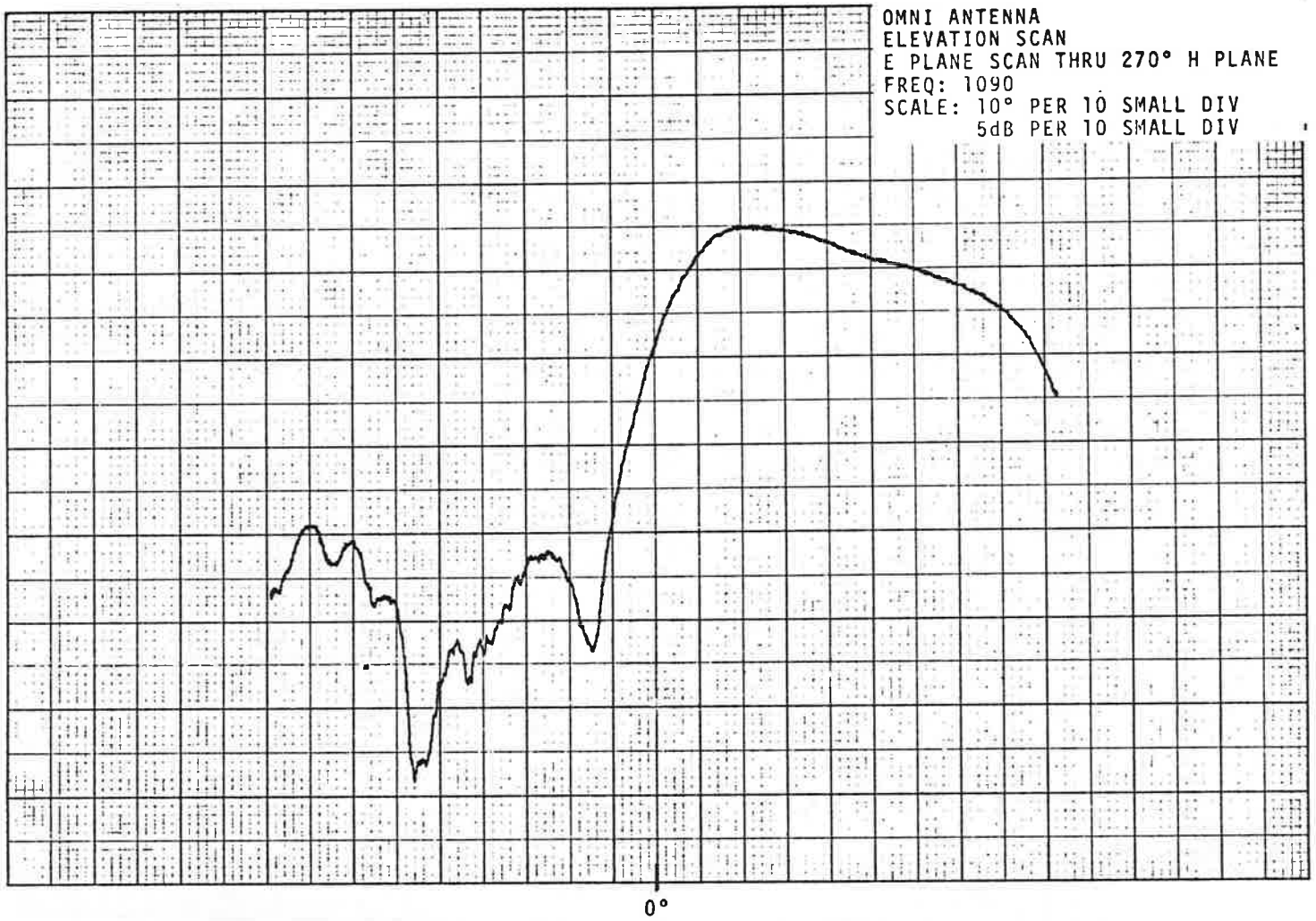

Figure A-88. Omni Antenna Elevation Pattern, 1090 MHz, E Plane Scan Through 270° H Plane

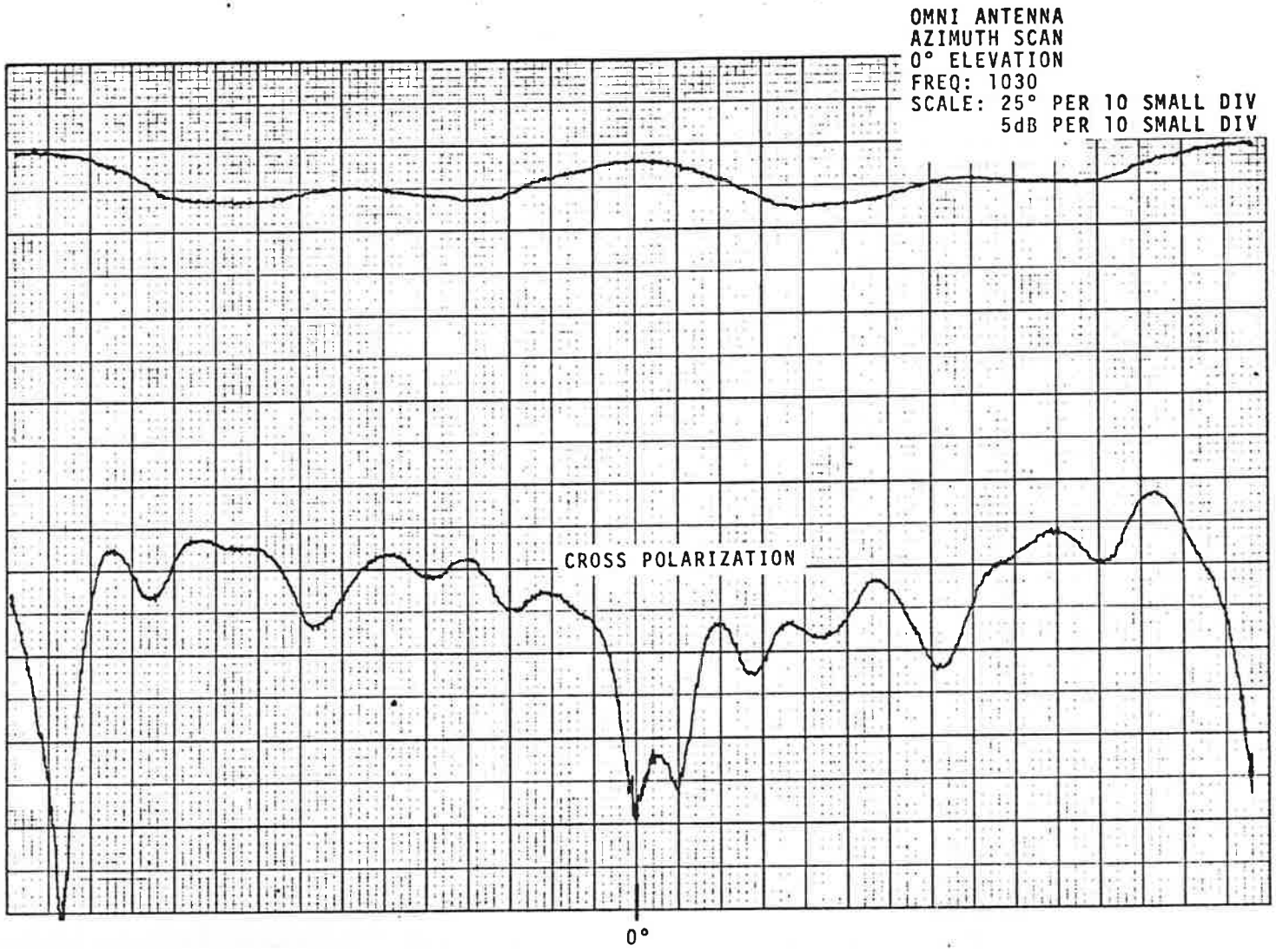

Figure A-89. Omni Antenna Azimuth Pattern, 1030 MHz, 0° Elevation

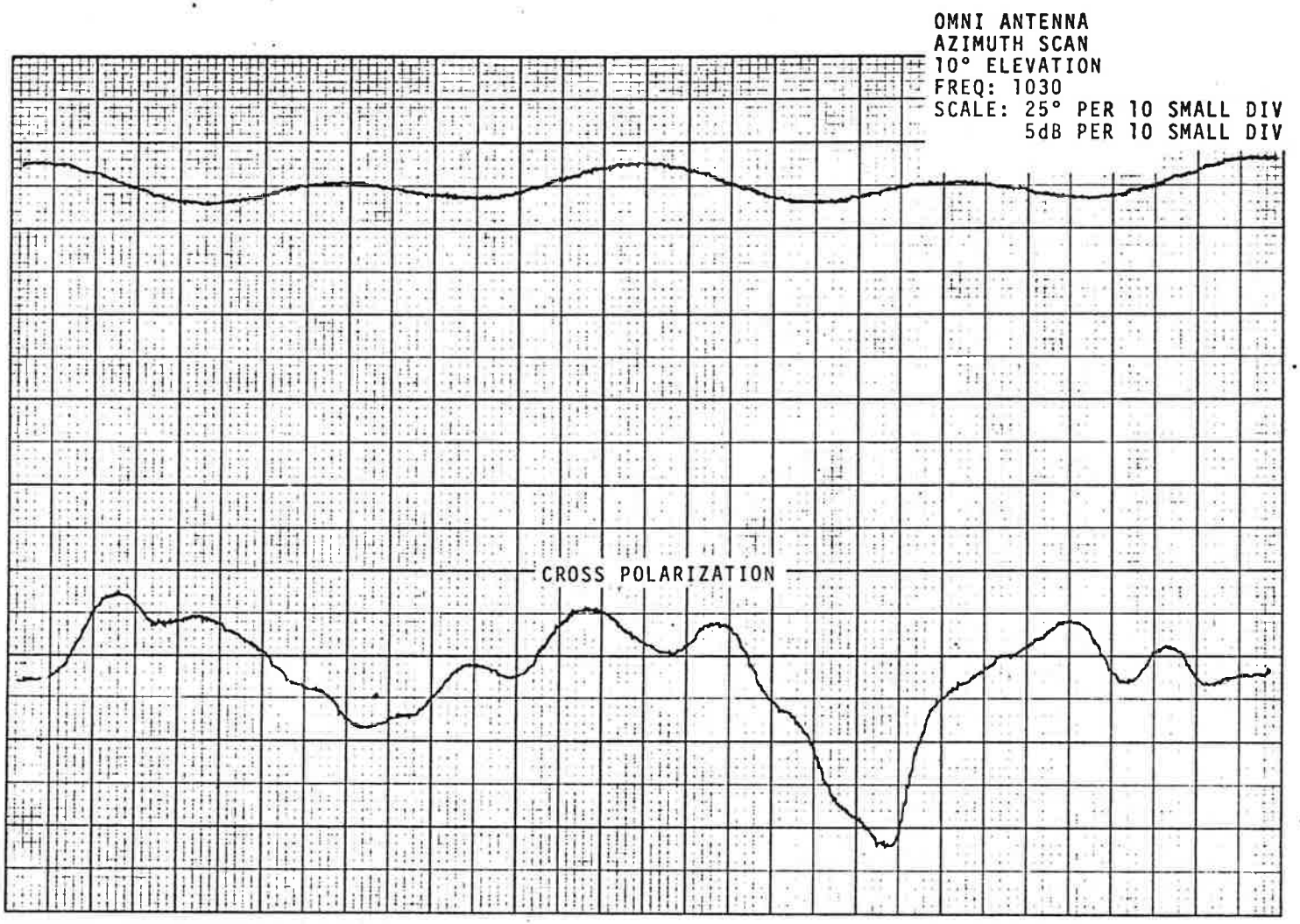

Figure A-90. Omni Antenna Azimuth Pattern, 1030 MHz, 10° Elevation

Figure A-91. Omni Antenna Azimuth Pattern, 1030 MHz, 20° Elevation

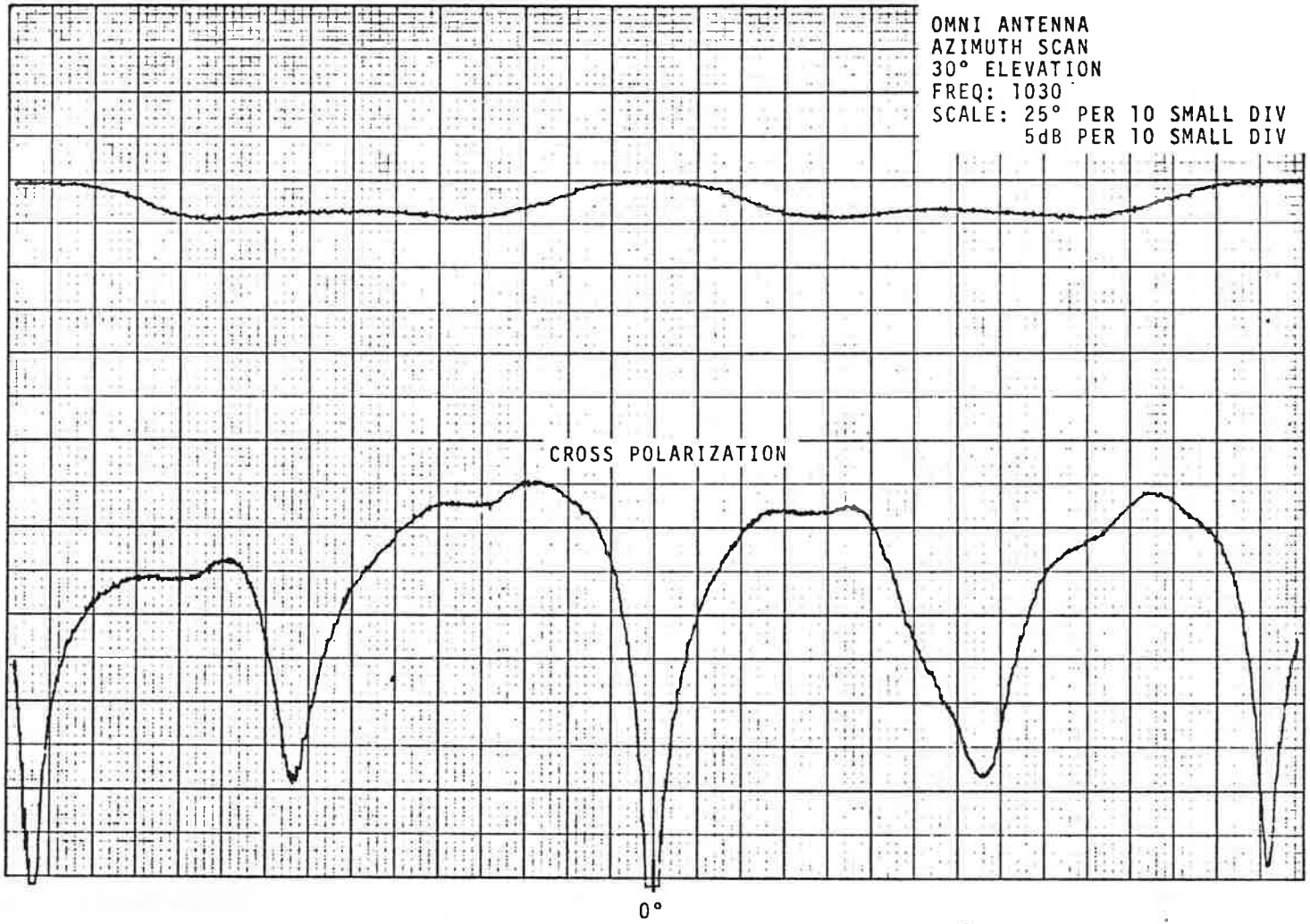

Figure A-92. Omni Antenna Azimuth Pattern, 1030 MHz, 30° Elevation

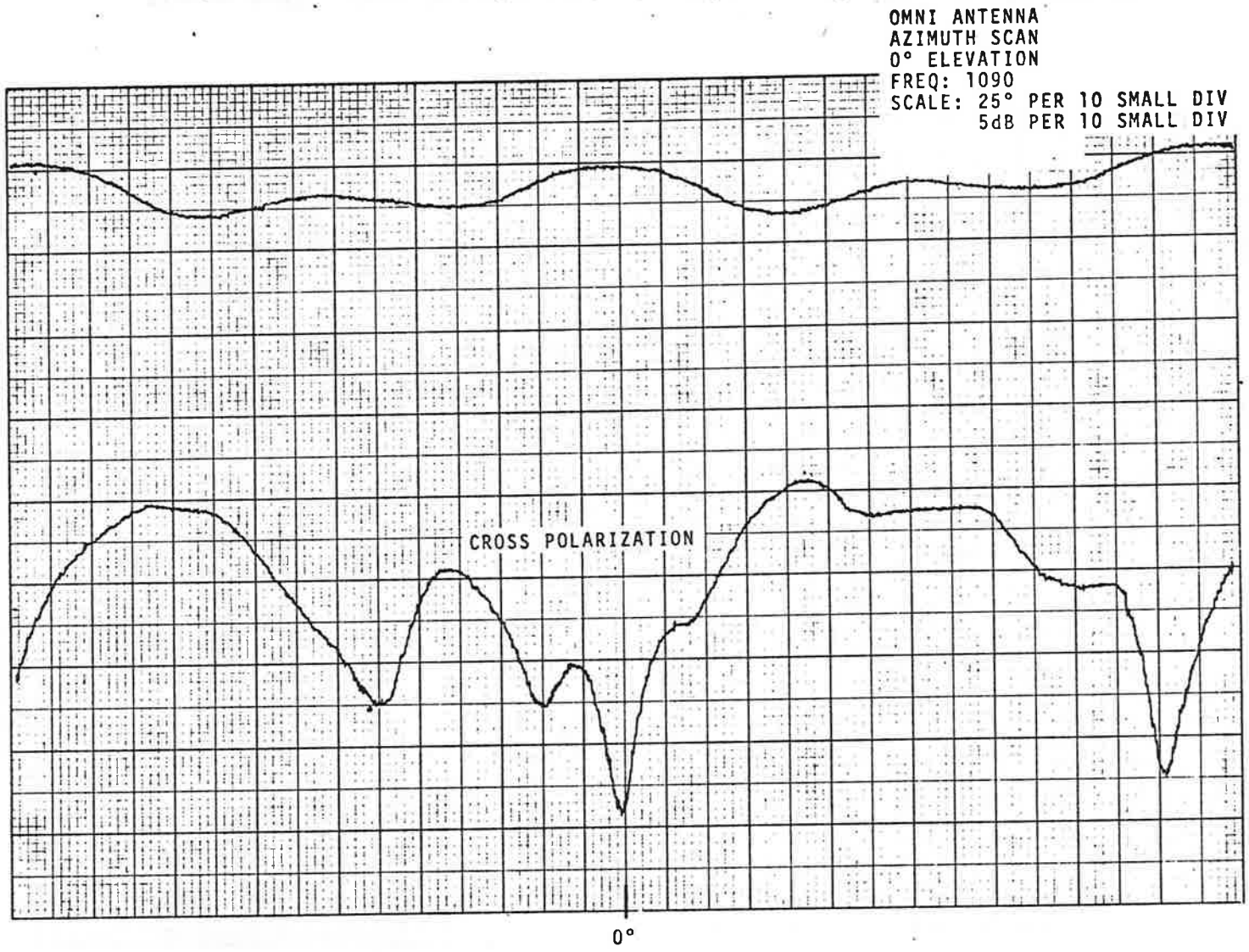

Figure A-93. Omni Antenna Azimuth Pattern, 1090 MHz, 0° Elevation

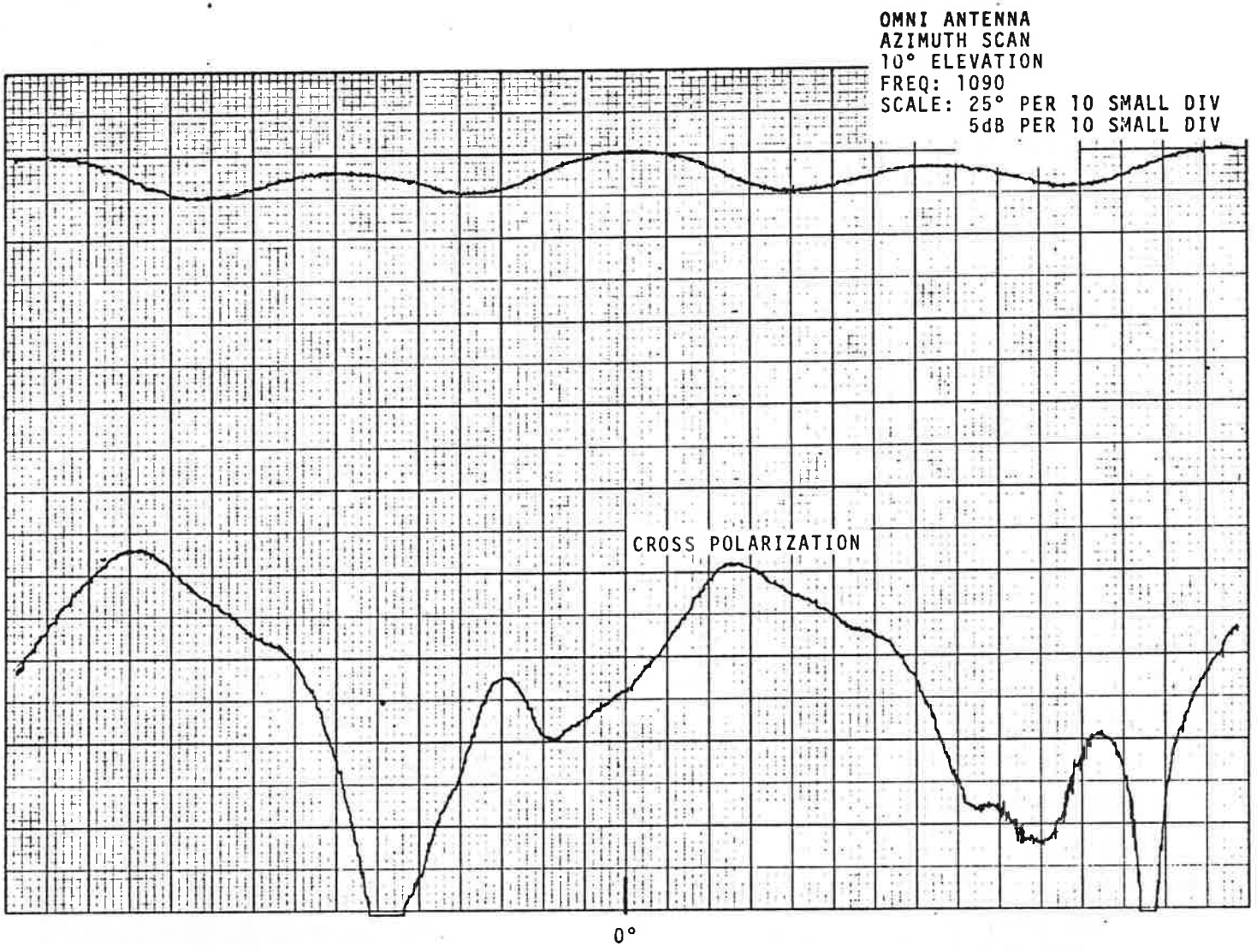

Figure A-94. Omni Antenna Azimuth Pattern, 1090 MHz, 10° Elevation

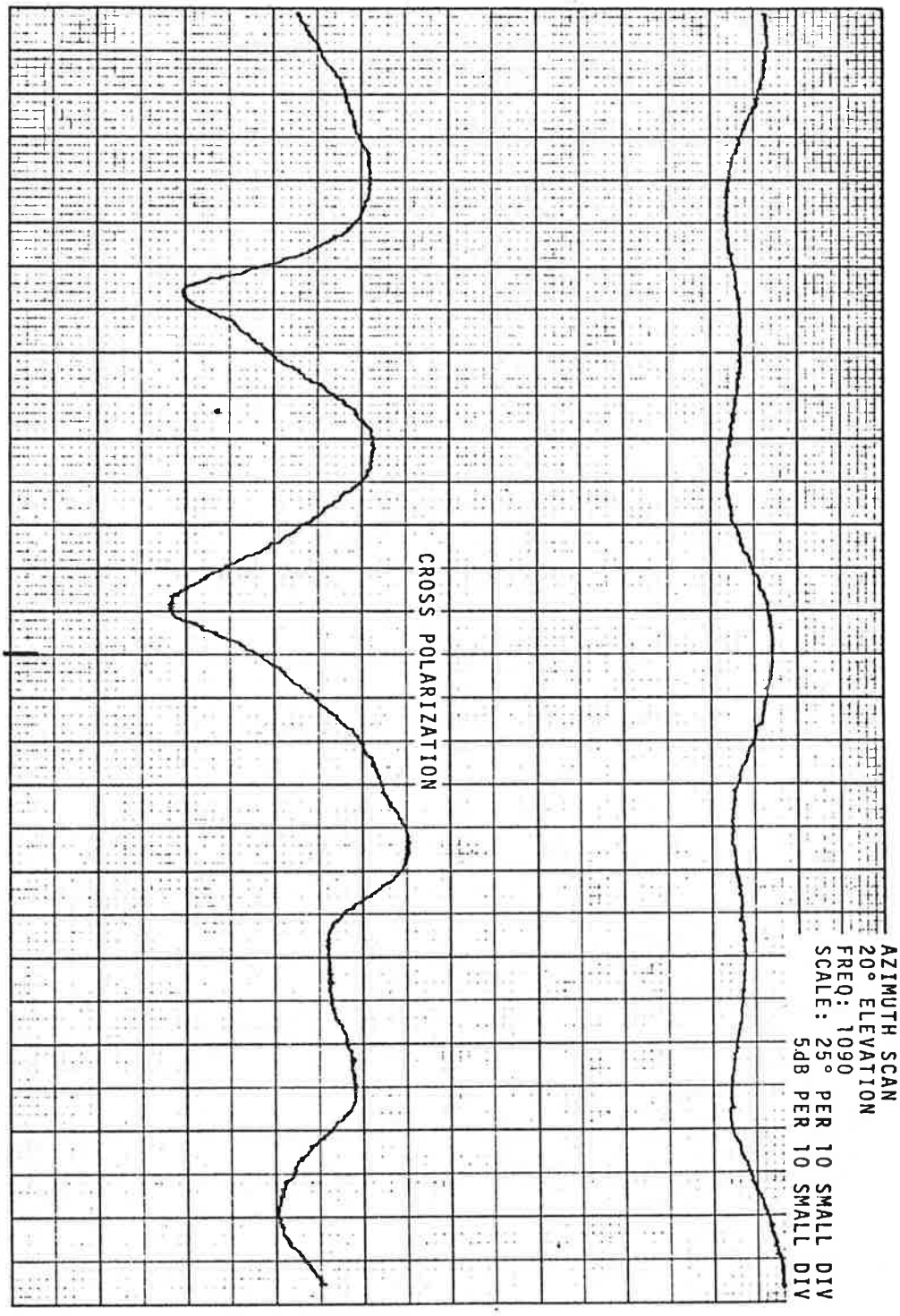

Figure A-95. Omni Antenna Azimuth Pattern, 1090 MHz, 20° Elevation

Figure A-96. Omni Antenna Azimuth Pattern, 1090 MHz, 30° Elevation

APPENDIX B. SPECIFICATION

DESIGN CONSTRAINTS FOR ATCRBS ANTENNA IMPROVEMENT KIT

1.1 ASR ANTENNA PERFORMANCE

The modifications to the ASR antenna shall not cause degradation of any ASR antenna electrical characteristics described below:

a. Frequency range: 2700 MHz to 2900 MHz
b. VSWR: 1.4 to 1 at net average power
c. Power handling capacity: 1250 kilowatt peak at 0.002 duty cycle
d. Power gain: Minimum of 34 dB over an isotropic source
e. Beamwidths of azimuthal radiation pattern:

Elevation Angle	Power Point	Beamwidth
positive 4 degrees (principal plane)	minus 3 dB	1.5 ±0.15 degrees
minus 3 to positive 30 degrees	minus 3 dB	1.5 ±0.3 degrees
positive 4 degrees	minus 10 dB	3 degrees maximum
positive 4 degrees	minus 17 dB	4 degrees maximum

f. Side lobes:

Elevation Angle	Side Lobe Level
positive 4 degrees (principal plane)	minus 20 dB
minus 3 to positive 10 degrees	minus 18 dB
positive 10 to positive 30 degrees	minus 15 dB

g. Back radiation: Minus 30 dB, from 90 degrees to 270 degrees
h. Elevation radiation pattern: Cosecant squared from the upper half-power point to positive 30 degrees; half-power beamwidth is approximately 5 degrees.
i. At minus 3-1/2 degrees (7-1/2 degrees below the principal plane) the power is at least 20 dB down from that at the nose of the beam.
j. The Integrated Cancellation Ratio (ICR) in elevation equals 20 dB.
k. ICR in azimuth at positive 4 degrees elevation equals 20 dB; at positive 2 to positive 10 degrees elevation equals 14 dB; at zero degrees to positive 2 degrees and at positive 10 to positive 20 degrees equals 10 dB; and at positive 20 to positive 30 degrees equals 8 dB.

1.4.6. Antenna Receive Pattern

The antenna receive patterns at 1087 MHz through 1093 MHz achieved by means of the modification shall conform to the limits stated for the azimuthal and elevation radiation patterns.

1.4.7. Response to Cross Polarized Returns

The response to horizontally polarized returns at frequencies between 1087 MHz and 1093 MHz shall be at least 15 dB below the level of the azimuth vertically polarized beam peak at the particular elevation angle being examined.

1.4.8. Directional Beam Squint, Frequency

The azimuthal center of the directional beam as measured at 1030 MHz at any elevation angle between the lower half power point of the vertical pattern and positive 25 degrees above the horizon shall not vary more than $\pm$0.20 degrees in azimuth from that measured from 1087 MHz through 1093 MHz.

1.4.9. Replacement Dipole

The interrogator radiation pattern achieved by the modification will no longer be matched in vertical profile with the omnidirectional pattern of the SLS dipole. A radiator with vertical aperture and resulting lobe structure approximating that of the ASR directional antenna shall be substituted for the presently used SLS omnidirectional dipole.

1.5 ANTENNA ISOLATION

Not applicable.

1.6 ELECTROMAGNETIC RADIATION ENVIRONMENT

Any beacon antenna system modification designed in conformance with this engineering requirement shall contain protective devices capable of attenuating spurious rf energy from 1280 MHz to 11,000 MHz, a minimum of 50 dB. The attenuation by such protective devices to signals at frequencies 1015 MHz to 1045 MHz and 1075 MHz to 1105 MHz shall not exceed 1.0 dB. Such protective devices or filters provided as part of the modification kit shall be installed at a location in the antenna system so that they can be removed easily prior to installation at a facility where such protective devices are already included in the interrogator/receiver. All circuitry used in the antenna modification kits shall be capable of operating satisfactorily in the environment of the ASR radar operating the frequency range from 2700 MHz to 2900 MHz at a peak power of one megawatt.

1.7 ANTENNA STRUCTURE

Components to be installed on the ASR beacon antenna system as part of the modification kit shall be designed to recognize the environmental operational requirements.

1.8 INSTALLATION OF MODIFICATION

The modification kit supplied in conformance with this engineering study shall be capable of being completely installed, adjusted and checked out at an operational field site. The installation of the modification must be accomplished with the minimum of radar system down-time if this modification is to gain widespread application.

1.9 SEPARATE ROTATING ANTENNA DESIGN FOR ASR INSTALLATIONS

Not applicable.

1.10 INTERROGATOR CHARACTERISTICS

This antenna system will operate with an interrogator/receiver having the following characteristics:

a)	Interrogation transmitter	32 dB above one watt with facilities for adjustment to any value between 32 dB and 17 dB above one watt as measured across a 52-ohm resistive load
b)	Receiver sensitivity	See U.S. National Standard for ATCRBS paragraph 2.8.3
c)	Receiver sensitivity time control (STC)	See U.S. National Standard for ATCRBS paragraph 2.8.4
d)	Transponder characteristics	See U.S. National Standard for ATCRBS paragraph 2.7
e)	Interrogator modes	Modes 2, 3/A and C

1.11 ANTENNA RADIATION PATTERNS

Not applicable.

1.12 PEAK POWER REQUIREMENT

Throughout the range of service conditions, the antenna system (including all r.f. paths, filter(s) shall be capable of operating, without electrical breakdown, with an input peak power of 2.3kw at a duty cycle of 8.0%.

TABLE B-1. BEACON ANTENNA PATTERN CHARACTERISTICS (continued)

Physical Quantity	ASR Modification	New Rotator
Elevation pattern at 1090 MHz:	same as 1030	
Coverage +5° to +35°		(1030) ±3 dB
Coverage -5° to +5°		(1030) ±1 dB
Directional beam skew, elevation		
From lower 3 dB point to +25°	±0.30°	
From lower 3 dB point to +30°		±0.20°
Directional beam squint, 1030/1090		
From lower 3 dB point to +25°	±0.20°	
From lower 3 dB point to +30°		± 0.10°
Cross-polarized radiation (1030 MHz)		
From -2° to +25° elev.	> 15 dB down	> 15 dB down
Cross-polarized response (1090 MHz)	> 15 dB down	> 18 dB down,
Omni pattern		
Uniformity	not specified	±1.5 dB
Max. Level		Direct.-12 dB
Min. level above directional SL		> 3 dB

APPENDIX C. REPORT OF INVENTIONS

After a thorough review of the work performed under this contract, it has been determined that no innovation, discovery, improvement or invention was made.